POLITECNICO DI MILANO

School of Civil, Environmental and Land Management Engineering
Master of Science in Civil Engineering

POLITECNICO
MILANO 1863

UNIVERSITY
OF MIAMI

CFRP Anchors for External Reinforcement:

Methodology for structural and material testing

Advisor: Prof. Carlo POGGI

Co-Advisor: Prof. Antonio NANNI

Master's Thesis by:
Lorenzo GIROTTI
838589

Academic Year: 2016/2017

POLITECNICO DI MILANO

CFRP ANCHORS FOR EXTERNAL REINFORCEMENT: METHODOLOGY FOR STRUCTURAL AND MATERIAL TESTING

By
Lorenzo Girotti

A THESIS

Submitted to
Politecnico di Milano
in partial fulfillment of the requirements for
the degree of Master of Science
in Civil Engineering

Milano, Italy
April 2017

To my family,

for always giving me strength,

for always providing a helpful advice,

for always being enthusiastic about my goals and helping me overcome my challenges,

for always encouraging me in all my pursuits, and inspiring me to follow my dreams.

ACKNOWLEDGEMENTS

Immeasurable appreciation and deepest gratitude for the help and support are extended to the following people who in one way or another have contributed in making this thesis possible.

- Dr. Carlo Poggi, my Italian advisor, for his patience in reviewing and helping me with my thesis and for giving me the chance to participate in this beautiful experience.
- Dr. Antonio Nanni, my American advisor, for giving me the opportunity to join such a professional team and for motivating us to reach bigger and bigger goals.
- Dr. Francisco De Caso, for his precious help and advice, and for making me feel an important part of this project.
- Dr. Guillermo Claure, for training and helping me on the use of laboratory instrument.
- Ed Wheatley, the producer of my anchors, for his enthusiasm and his time helping me prepare and test specimens in the lab.
- My brother Simone and my sisters Caterina and Elisabetta, for always being by my side, and providing strength throughout my journey.
- Eleonora, my "American mommy", my roommate, my friend, for sharing this amazing experience since day 1, helping me and supporting me, overcoming every difficulty we had.
- Stacy and Suri, my American roommates, for their kind welcoming me since the first day, for introducing me to Miami,and for sharing a lot of fun moments together.
- Paolo, my companion of a thousand adventures, for being my adoptive brother, for sharing best moments ever around Miami and USA.
- Alvaro, my "adoptive Spanish brother", for sharing amazing time together as a starting point of a true friendship.
- Houman, my desk mate, for sharing all the lab secrets with me, introducing and helping me using lab instruments.
- Marco and Thomas, my "predecessors", for giving me suggestions before and during my stay.
- Christian, Ming, Phil, Roger, Taïs and Thomas not only for helping me in the lab, but for being true friends, and sharing a lot of fun moments around Miami.
- All the people I was lucky to meet in USA, for their contribution to my personal growth.
- All my Italian friends, for always being worried about me, and always supporting me despite being miles and miles away.

ABSTRACT

Fiber Reinforced polymers (FRP), also known as “composites” are materials composed of fiber reinforcements and a polymer resin used for the repair and strengthening of existing concrete and masonry structures. The reinforcements impart strength and stiffness, while the resin is an adhesive matrix that bonds the fibers. The resin matrix transfers applied loads to the reinforcing fibers and protects the fibers from environmental attacks.

Research into composite for external reinforcement and rehabilitation purposes has been going on for many years up to now; the confidence in implementing such solutions has increased and reliable design procedures are now available (CNR DT-200) (ACI 440).

The efficiency of the strengthening system largely depends on adequate bond between the FRP laminate and the concrete substrate. In fact, the main issue is the premature failure due to debonding. The issue is particularly evident in flexure and severely undermine the efficiency and ductility of external reinforcement applications.

A proposed solution to counter debonding consists in mechanically anchoring the fiber sheet to the concrete substrate. The solution significantly improve the efficiency of the FRP system (Kalfat et al. 2011) and in some case to guarantee a ductile failure for the reinforced element (Grelle & Sneed, 2013).

A wide variety of anchoring devices has been proposed in order to avoid the debonding problem: U-Wrapping, spikes, staples, etc. So far, among the anchoring devices, the staple anchoring system revealed to be the most effective device. In particular, two types of staple anchoring devices were studied: flat staple anchor and round staple anchor. In a previous research, the behavior of those kind of staples acting on their dimensions was studied (Cadenazzi, 2016).

Currently, no specific criteria or guidelines exist to help the designer to choose the best anchor configuration to improve the strength of the existing concrete structure by FRP sheets avoiding the debonding problem. In order to develop a quantitative approach to anchors’ design, firstly, a reliable characterization for the single anchor’s strength and a reliable model to describe a multiple anchors joint’s behavior is required.

The following thesis wants to investigate the behavior of the staple anchor system applied to FRP sheet on a slab. The research is composed of two experimental campaigns:

- In order to study the fundamental behavior of the slab-FRP laminate-anchor system a ***first*** experimental campaign is carried out. A series of double shear tests, aimed to characterize the single anchor's strength, were performed.
- After the anchor's characterization, a series of 3-point bending (flexural) tests on slabs with different FRP anchor configurations, in order to characterize the behavior and to identify the key parameters that affect the performance of the whole system (slab-FRP laminate-Anchor) were performed in the ***second*** experimental campaign.

This investigation entered more into deep on the study of staple anchors, analyzing their performance in a larger scale than what was studied before. This thesis wants to be a step forward toward the creation of new specific design guidelines aimed to help engineers providing the necessary information to make design decision on the use of staple anchor system in effective way to enhance the bond of externally bonded FRP laminates applied on slabs.

Keywords: Experimental investigations; Carbon fiber-reinforced polymer; Composite materials; CFRP sheet; Debonding; Externally bonded; Staple anchors; Strengthened slabs; CFRP strengthening; CFRP Patch.

SINTESI

I polimeri rinforzati con fibre, meglio noti come “materiali compositi”, sono materiali formati da fibre e resina polimerica usati per la riparazione ed il rinforzo delle strutture in cemento armato e muratura già esistenti. Le fibre impartiscono robustezza e rigidità, mentre la resina è una matrice adesiva che lega le fibre. La resina trasferisce i carichi applicati alle fibre e protegge le fibre dagli attacchi degli agenti atmosferici.

La ricerca nel campo dei materiali compositi per rinforzo esterno, a scopo di riabilitazione, ha una lunga storia alle spalle; la fiducia in queste soluzioni è aumentata con il passare del tempo e affidabili codici di progettazione sono ora a disposizione dell’ingegnere (CNR DT-200) (ACI 440).

L’efficienza del Sistema di rinforzo dipende in larga misura dall’adeguato legame tra il laminato FRP ed il substrato di calcestruzzo. Infatti, il problema principale è il collasso prematuro dovuto a delaminazione del composito. Tale problema è particolarmente evidente nelle applicazioni a flessione compromettendo gravemente l’efficienza e la duttilità delle soluzioni di rinforzo esterno.

Una delle soluzioni proposte per ovviare al problema è rappresentata dall’ancoraggio meccanico della lamina di rinforzo al substrato di calcestruzzo. Tale soluzione migliora significativamente l’efficienza del Sistema FRP (Kalfat et al. 2011) garantendo in qualche caso la rottura duttile dell’elemento di rinforzo (Grelle & Sneed, 2013).

Un’ampia varietà di dispositivi di ancoraggio è stata proposta con il fine di evitare il problema della delaminazione: U-Wrapping, Spikes, Staples. Finora, tra i dispositivi di ancoraggio, il sistema di ancoraggio mediante “Staples” è quello che si è rivelato essere il dispositivo più efficace. In particolare, due tipologie di ancoraggio attraverso “Staples” sono stati studiati: ancoraggio “Flat Staples” e ancoraggio “Round Staples”. In precedenti ricerche è stato studiato il comportamento di queste tipologie di ancoraggio mediante “Staples” agendo sulle loro dimensioni geometriche (Cadenazzi, 2016).

Attualmente non esistono criteri progettuali o line guida che aiutino il progettista nello scegliere la migliore configurazione/disposizione degli ancoraggi con il fine di migliorare la resistenza della struttura applicando lamine di FRP evitando il problema della

delaminazione. Al fine di sviluppare un approccio quantitativo, prima di tutto, si richiede un'affidabile metodo di caratterizzazione della resistenza a taglio del singolo ancoraggio, cosi come un affidabile modello che consenta di descrivere il comportamento di un giunto multi-ancoraggio.

La seguente ricerca vuole testare il comportamento del sistema di ancoraggio mediante "Staples" applicato ad una lamina FRP. La ricerca è così strutturata:

- È stata effettuata una prima campagna sperimentale con lo scopo di studiare il comportamento dell'intero sistema composto da trave-lamina FRP-ancoraggio. Sono stati realizzati una serie di "double shear test" con lo scopo di investigare la resistenza del singolo ancoraggio.
- La seconda campagna sperimentale è basata su una serie di test flessionali (3-point bending tests) su travi non armate a taglio con differenti configurazioni degli ancoraggi al fine di caratterizzare il comportamento e di identificare i parametri chiave che influiscono sulle prestazioni del Sistema trave-lamina FRP-ancoraggio.

La seguente ricerca è entrata più nel dettaglio, analizzando il rendimento degli ancoraggi "Staples" in scala più ampia rispetto a quanto studiato finora. Questa tesi vuole essere un passo avanti verso la creazione di nuove linee guida per fornire agli ingegneri e progettisti le informazioni necessarie per operare in maniera corretta nella progettazione ed uso degli ancoraggi come metodo di rinforzo esterno applicati alle travi.

TABLE OF CONTENTS

LIST OF FIGURES

LIST OF TABLES

LIST OF SYMBOLS

A: average cross-sectional area.

a: FRP sheet's ends distance from supports

a': End anchors' distance from sheet's ends

as: Single rebar's area

c: Concrete Cover

CTE: coefficient of thermal expansion.

d: average diameter.

E: elastic modulus.

ε_{ult}: ultimate tensile strain.

f'c: compressive strength of the cylindrical concrete specimens.

l (anchor): anchored length, i.e. distance between end anchors

l (frp): FRP sheet's length

μ: Poisson's ratio.

σ: strength.

Pmax: maximum axial load.

ρ: density of the material.

s: Rebar horizontal spacing

Tg: glass transition temperature.

x: neutral axis

#: Rebar Number, US identification

CHAPTER 1

Introduction

1.1 Literature Review: Composite Materials

Composites are two or more distinctly different materials combined into (but not dissolved into) one structure to perform a function neither material can do independently. This is the well-known principle behind the alloying of metals and in the incorporation of chopped straw into clay for bricks by the ancient Egyptians and plant fibers into pottery by the Incas and Mayans. These ancient productions of composite materials consisted of reinforcing brittle materials with fibrous substances.

When the terms “composites” or “composite materials” are used, the definition envisioned is: *Composite materials are those solid materials composed of a binder or matrix that surrounds and holds in place reinforcements.*

Some writers have suggested an alternate definition of composites: Mixture of two or more solid materials that are mechanically separable, at least in theory, and possessing *complementary* properties. This definition emphasizes the improvements in properties possible when composites are made and, as will become clear, the complementary nature of matrix and reinforcement is the reason composites are so important commercially. However, not all properties and characteristics are advantageous when composites are made. Some of the advantages and disadvantages of composites are listed in table 1.1.

Advantages	Disadvantages
• Lightweight	• Cost of materials
• High specific stiffness	• Lack of well-proven design rules
• High specific strength	• Metal and composite designs are seldom directly interchangeable
• Tailored properties (anisotropic)	• Long development time
• Easily moldable to complex (net) shapes	• Manufacturing difficulties (manual, slow, environmentally problematic, poor reliability)
• Part consolidation leading to lower overall system cost	• Fasteners
• Easily bondable	• Low ductility (joints inefficient, stress risers more critical than in metals)
• Good fatigue resistance	• Solvent/moisture attack
• Good damping	• Temperature limits
• Crash worthiness	• Damage susceptibility
• Internal energy storage and release	• Hidden damage
• Low thermal expansion	• EMI shielding sometimes required
• Low electrical conductivity	
• Stealth (low radar visibility)	
• Thermal transport (carbon fiber only)	

Table 1.1 - Advantages and disadvantages of composites

Some important properties of composites and metals are compared in Figure 1.1. Note the low weight, low thermal expansion, high stiffness, high strength, and high fatigue resistance of composites versus steel and aluminum.

Of great value is that the separate characteristics of the matrix and reinforcements contribute synergistically to the overall properties of the composite. Moreover, because so many different matrix and reinforcement materials can be chosen, a wide range of properties is possible. Within a particular choice of matrix and reinforcement, the orientations off the reinforcements, manufacturing method, processing conditions, and combinations made with other materials all give additional variety in the properties available.

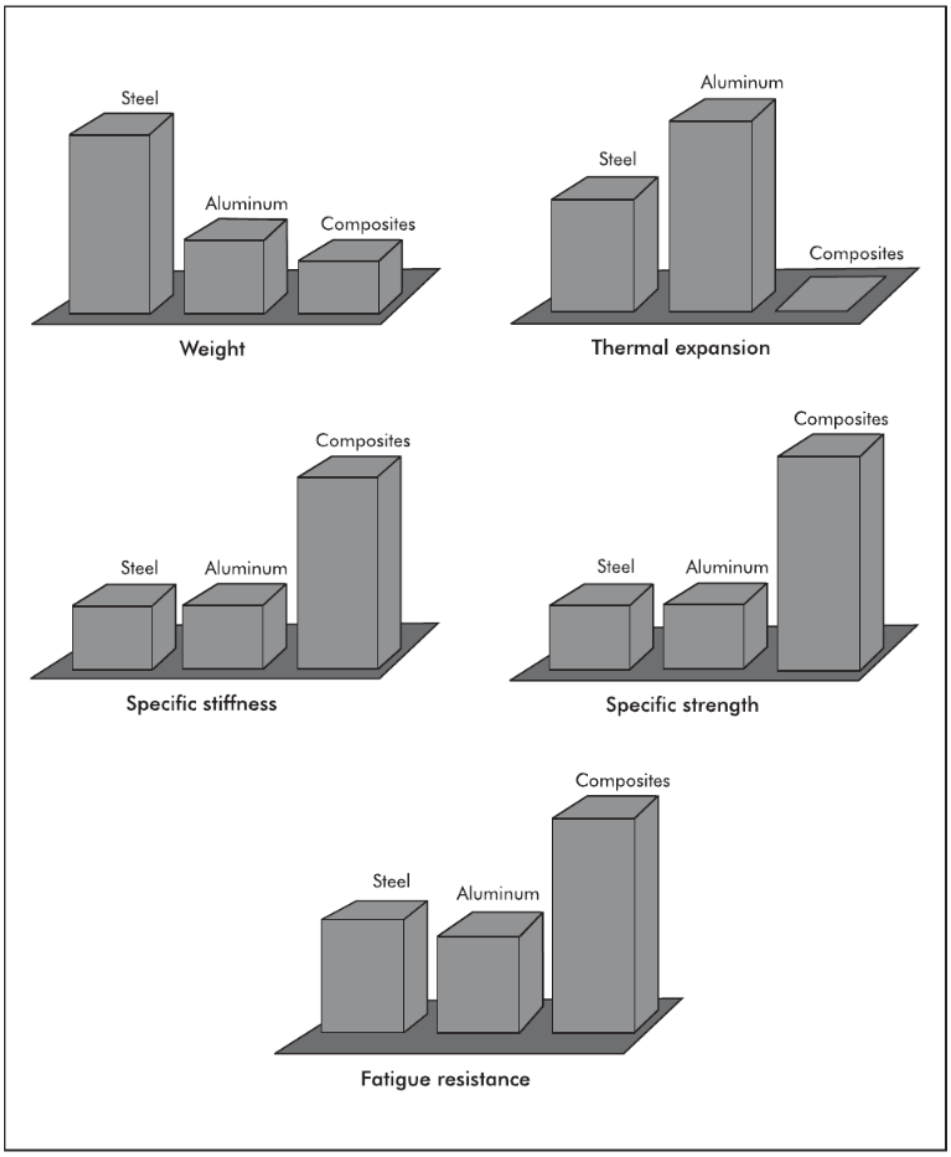

Figure 1.1 - Property comparison of metals and composites

1.1.1 Historical Background

The first man-made composite based upon polymers appeared in about 5000 BC, in the Middle East where pitch was used as a binder for reeds in boat-building. Pitch is still being used for this purpose in the UK, more specifically in Wales, by the descendants of the Celts who themselves had a connection with the Middle East, as it has been for perhaps 2000 or more years in the building of coracles for fishing. Incidentally, it is of interest to note that the same material, pitch, is presently being assessed as a precursor for one of the most important components of ultra-modern reinforced plastics, namely carbon fiber. Laminated wood dating to about 1500 BC has been found at Thebes and similar laminates based upon shellac resin have been known and used in India for at least 3000 years.

Later, in 1200 AD, the Mongols invented the first composite bow. They combined wood, bone and animal glue and wrap everything with birch bark. The result was an extremely accurate and powerful bow.

Many more historical examples could be find in the literature, such as mud wall reinforced with bamboo, glued laminated wood or laminated metals (Kaw 2005).

In early 1900s, with the invention and development of plastic, such as vinyl, polystyrene or polyester, the modern era of composite begins. The history of modern composites probably began in 1937 when salesmen from the Owens-Corning Fiberglas® Company began to sell fiberglass to interested parties around the United States and those customers found that the fiberglass could serve as a reinforcement.

The rapid development and use of composite materials beginning in the 1940s had three main driving forces.

- Military vehicles, such as airplanes, helicopters, and rockets, placed a premium on high-strength, light-weight materials. While the metallic components that had been used up to that point certainly did the job in terms of mechanical properties, the heavy weight of such components was prohibitive. The higher the weight of the plane or helicopter itself, the less cargo its engines could carry.
- Polymer industries were quickly growing and tried to expand the market of plastics to a variety of applications. The emergence of new, light-weight polymers from development laboratories offered a possible solution for a variety of uses, provided something could be done to increase the mechanical properties of plastics.

- The extremely high theoretical strength of certain materials, such as glass fibers, was being discovered. The question was how to use these potentially high-strength materials to solve the problems posed by the military's demands.

The fast pace of composites development accelerated even more during World War II. Some of the products made during the post-war era now represent the major markets for composite materials. In addition to aircraft, these include boats, automobiles, tub and shower assemblies, non-corrosive pipes, appliance parts, storage containers, and furniture. The push for aerospace dominance that began in the 1950s (during the Cold War) and picked up speed in the 1960s and 1970s gave a new impetus to further composite development. Hercules, Inc. acquired filament winding technology from W. M. Kellogg Company and began making small rocket motors. In 1961, a patent was issued for producing the first carbon (graphite) fiber, which then was used in many of the rocket motors and in aircraft. Other important fibers were also developed during this period, including boron fibers in 1965 and aramid fibers (DuPont's Kevlar®) in 1972. In 1978, the crowning jewel of this period was the development of the first fully filament wound aircraft fuselage, the Beech Starship. Recent material and process improvements and the development of higher performing fibers and resins have led to tremendous advances in aerospace, armor (structural and personal), sports equipment, medical devices, and many other high-performance applications.

The introduction composite materials in the civil infrastructure has been a very rapid process in comparison to other civil engineering materials when they were in their infancy. Composite materials have hitherto been utilized predominately in the aerospace and marine industries but for the last four decades there has been a growing awareness amongst civil/structural engineers of the importance of the unique mechanical and in-service properties of these materials together with their customized fabrication technologies. These extraordinary properties have enabled the design engineers to have greater confidence in the materials' potential and consequently to use them in the renewal of civil infrastructure ranging from the strengthening of reinforced concrete, steel, and cast iron, and the seismic retrofitting of bridges and columns to the use in replacement bridge decks and in the new bridge and building structures.

A chrono- logical variation of the relative importance of material development from 10,000 B.C. through the year 2020 is shown in Figure 1.2.

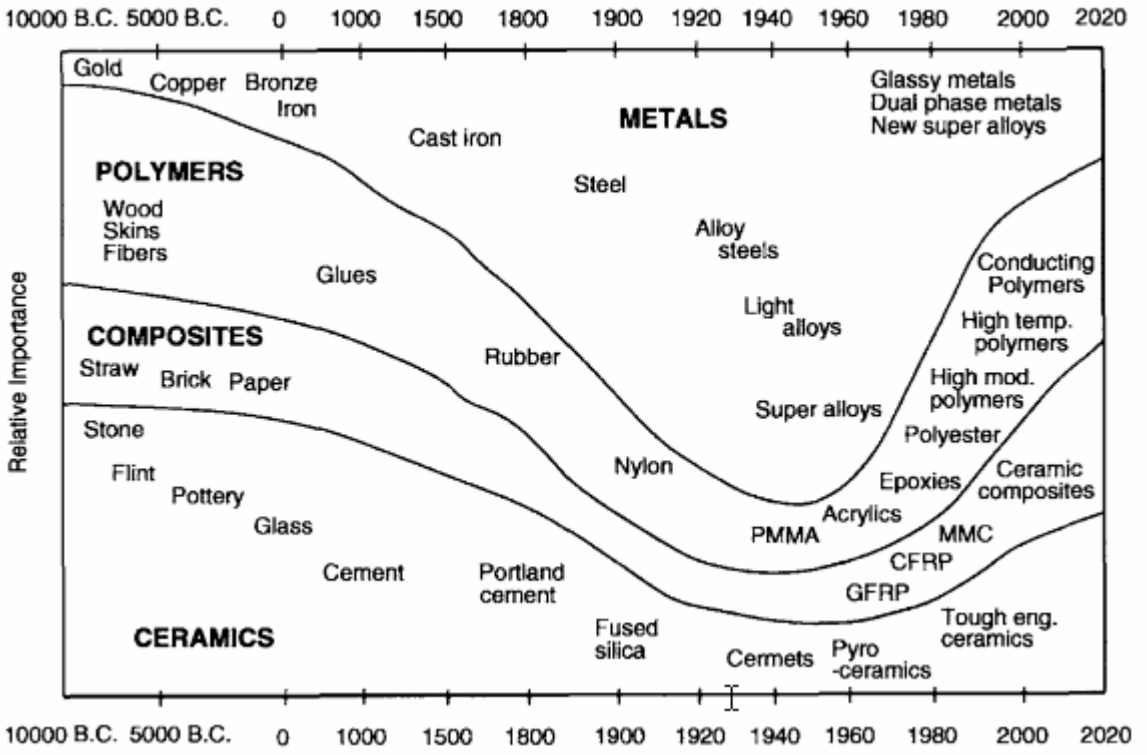

Figure 1.2 - Relative importance of material development through history

A chrono- logical variation of polymer composites development is shown in Table 1.2.

Date	Material
(c. 5000 BC)	Papyrus/pitch (boats)
(c. 1500 BC)	Wood veneer
1909	Phenolic composite
1928	Urea formaldehyde composite
1938	Melamine formaldehyde composite
1942	Glass reinforced polyester
1946	Epoxy resin composites
1951	Glass reinforced polystyrene
1956	Phenolic-asbestos ablative composite
1964	Carbon fibre reinforced plastics
1965	Boron fibre reinforced plastics
1969	Carbon/glass fibre hybrid composites
1972	Aramid fibre reinforced plastics
1975	Aramid/graphite fibre hybrids

Table 1.2 - Historical development of polymer composites

1.1.2 Characteristics

The constituents of a composite are generally arranged so that one or more discontinuous phases are embedded in a continuous phase. The discontinuous phase is termed the *reinforcement* and the continuous phase is the *matrix*. Both constituents are required, and each must accomplish specific tasks if the composite is to perform as intended.

The principal role of the *matrix* is to give shape to the structure. Therefore, matrix materials that can be easily shaped and then hold that shape are especially useful. The most common materials with this characteristic are polymers. Therefore, well over 90% of modern composites have polymeric materials (sometimes referred to as plastics or resins) as their matrix. As the continuous phase, the matrix surrounds and covers the reinforcements. Hence, the matrix is the component of the composite exposed directly to the environment. Another role of the matrix is, there-fore, to protect the reinforcements from the environment. The degree of protection desired is one of the key considerations in choosing the type of polymeric matrix for the composite. he matrix is the component of the composite that first encounters whatever forces might be imposed. Generally, the matrix is not as strong as the fibers and is not expected to withstand these imposed forces. However, the matrix must transfer the imposed loads onto the fibers. The effectiveness of load transfer is one of the most important keys to the proper performance of the composite.

The principal role of the *reinforcement* is to provide strength, stiffness, and other mechanical properties to the composite. Generally, the mechanical properties are highest in the direction of orientation of the fibers. For example, if all the fibers in a composite are oriented in the long direction of the part (like strands in a rope), the composite is strongest when pulled in the long direction. This characteristic of composites allows the part designer to specify certain percentages of the fibers to be in certain exact orientations for a particular application. If the forces on the part would come from all directions, then the designer would specify randomization or multi-directionality of the fibers.

The graph in Figure 1.3 illustrates the relationship between the stress and the strain of the reinforcement. Clearly, the reinforcement has a much greater mechanical strength than the matrix so that the bond between them generates a material, called composite, of intermediate mechanical properties.

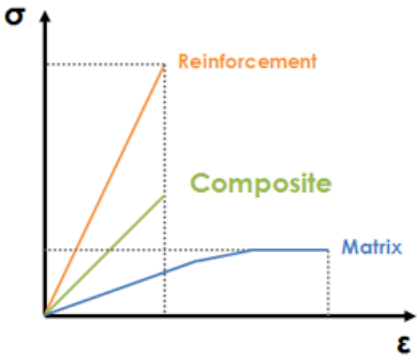

Figure 1.3 - Stress/Strain relationship for a composite material

The roles of matrix and reinforcement are summarized in Table 1.3.

Matrix	Reinforcements
• Gives shape to the composite part	• Give strength, stiffness, and other mechanical properties to the composite
• Protects the reinforcements from the environment	• Dominate other properties such as the coefficient of thermal expansion, conductivity, and thermal transport
• Transfers loads to the reinforcements	
• Contributes to properties that depend upon both the matrix and the reinforcements, such as toughness	

Table 1.3 - Roles of the matrix and reinforcement in a composite

The physical and mechanical properties of composites are dependent on the properties, geometry, and concentration of the constituents. There are many factors to be considered when designing with composite materials. The type of reinforcement and matrix, the geometric arrangement and volume fraction of each constituent, the anticipated mechanical loads, the operating environment for the composite, etc., must all be taken into account.

Upon application of a uniaxial tensile load, an isotropic material deforms in a manner similar to that indicated in Figure 1.4 (the dashed lines represent the undeformed specimen). Assuming a unit width and thickness for the specimen, the transverse in-plane and out-of-plane displacements are the same. Unlike conventional engineering materials, a composite material is generally nonhomogeneous and does not behave as an isotropic material. Most composites behave as either anisotropic or orthotropic materials.

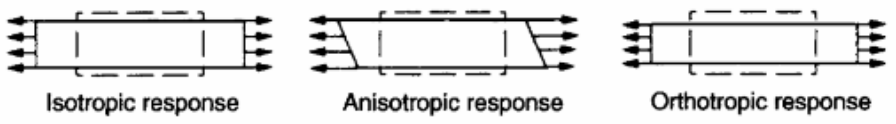

Figure 1.4 - Typical material responses for isotropic, anisotropic, and orthotropic materials subjected to axial tension

The material properties of an anisotropic material are different in all directions. The material properties of an orthotropic material are different in three mutually perpendicular planes, but there is generally no shear-extension coupling as with an anisotropic material.

1.1.3 Classifications

Composite materials can be categorized using the processing. Two broad classes of composites are fibrous and particulate. Each has unique properties and application potential, and can be subdivided into specific categories:

Fibrous. A fibrous composite consists of either continuous (long) or chopped (whiskers) fibers suspended in a matrix material. Typical fibers include glass, boron, aramid and carbon, which may be continuous or discontinuous. Continuous fibers have long aspect ratios, while discontinuous fibers have short aspect ratios. Continuous-fiber composites normally have a preferred orientation, while discontinuous fibers generally have a random orientation.

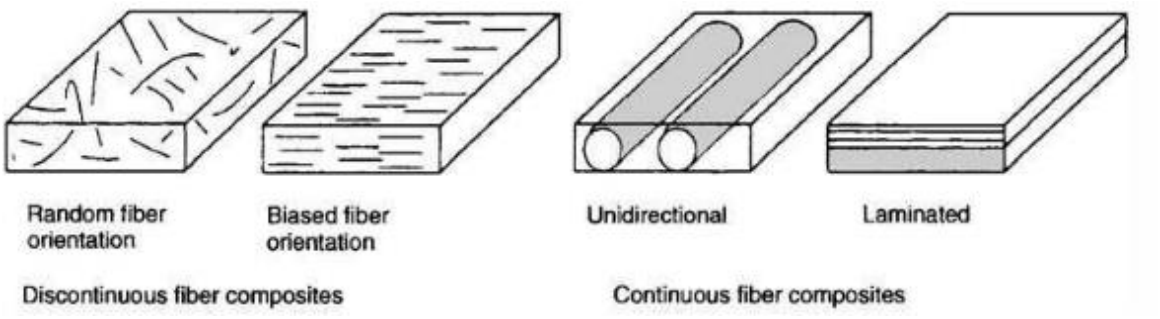

Figure 1.5 - Schematic representation of fibrous composites

Particulate. A particulate composite is characterized as being composed of particles suspended in a matrix. Particles can have virtually any shape, size or configuration. Examples of well-known particulate composites are concrete and particle board.

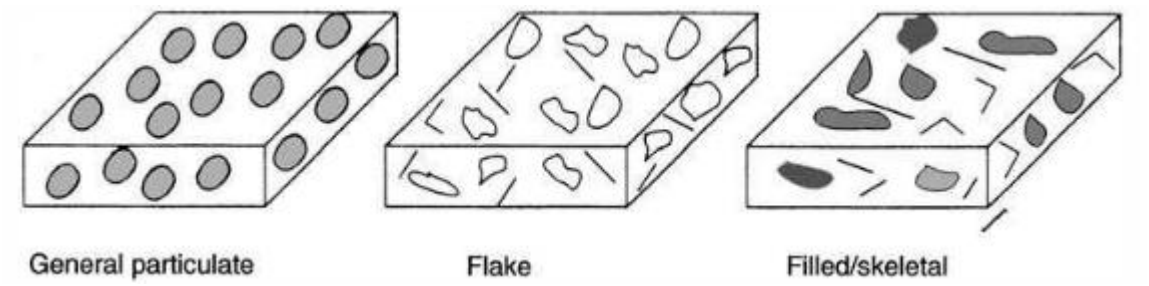

Figure 1.6 - Schematic representation of particulate composite

1.2 Fiber Reinforced Polymer (FRP)

A fiber-reinforced-polymer (FRP) is a specific type of composite material which consist of high-strength fibers surrounded in a resin matrix.

1.2.1 Overview

What was originally developed for military purposes to be light and strong, proved to be an ideal solution for durability-critical applications in civil engineering. Fiber Reinforced Polymers (FRP) generally have worst mechanical properties compared to steel, but have the major advantage of being unrusting, meaning that a FRP structure, at least a carbon fiber one, has the potential of lasting virtually forever (Nanni, 1999). FRPs have excellent characteristic, such as high strength, lightweight, resistance to corrosion, easy handling and installation. In addition, FRP does not need to be covered by a protection, as in the case of steel reinforcement, and can be exposed to many more environments. On the other hand, the presence of the polymer matrix limits its fire resistance. FRP materials are commonly used wherever high strength-to weight ratio and rigidity is required, such as aerospace, automotive and civil engineering. The fields in which this material can be applied are increasing due to its incredible properties. The most important application, for what concerns civil engineering, is the strengthening of concrete, masonry, steel, cast iron and timber structures. Increasing the load capacity of old structures which were designed for a lower service loads then they are expecting today, seismic retrofitting or repairing damaged structures are some very common example of application.

1.2.2 Components

In this sub-chapter a quick and general description of different types of the main components (fibers, resins) of a Fiber-Reinforced-Polymer (FRP) system is provided.

1.2.2.1 Fibers

The fibers are the element of the composite material that carries the load, due to their high strength and stiffness when pulled in tension. Different types of fibers are commercially available, ranging over different prices, mechanical and durability properties.

Glass Fibers (GFRP)

Glass fiber-reinforced-polymer (GFRP) is the least expensive compared to BFRP, CFRP and AFRP. It is the most widespread and it is also known commonly as “fiberglass.” It has lower strength and stiffness in comparison with the above mentioned FRPs (Kalpana, 2013). GFRP is mostly used for naval and industrial purposes. It shows durability issues in application exposed to hot/wet cycles and highly alkaline environments (Nanni, 1999), it has poor fatigue performances and high sensitivity to abrasion. Among the advantages, it provides good electrical isolation and thermal insulation (Nanni et al. 2014). It has tensile strength of 2000 to 4800 MPa and its E modulus is about 70 GPa, although different types of glass fibers are available (E-glass and S-glass) with values of the E modulus that can go up to 90GPa (CNR). GFRP is susceptible to fatigue and creep affect and is most effective for situations where the load is applied for a limited time since sustained loading causes creep in GFRP (Kalali 2012 and CNR 2013).

Basalt Fibers (BFRP)

Basalt fiber-reinforced-polymer (BFRP) is made from the igneous rock basalt. BFRP is non-toxic and can be considered a "green" material. It has an elastic structure. Basalts fibers are slightly stronger and stiffer than standard E-glass (Nanni et al. 2014) (Fiore et al. 2015). Its tensile strength is 1000 to 2600 MPa and its E modulus is between 100 to 160 GPa (Brik 1997). BFRP is very resistant to high temperature and keeps its mechanical integrity. It can keep 90% of its strength when exposed to temperature over 600 degrees and performs better than CFRP and GFRP in extreme high temperatures. In addition, BFRP produces relatively less toxic fumes when subjected to fire (Sim et al 2005).

Aramid Fibers (AFRP)

Aramid is an aromatic polyamide organic fiber (Nanni et al. 2014), it is not widely used in civil engineering, even though its application in FRCM is spreading. It has mechanical properties in between Glass and Carbon, with the addition of an excellent impact resistance – hence why it is commonly applied to manufacturing of bulletproof vests (Nanni, 1999) – along with a low density, that grants it to be the best mechanically performing fiber per unit weight (Berneschi, 2015). It is also a good thermal and electrical insulator, resistant to organic solvents, fuels and lubricant. Among the side effects a high UV sensitivity as well as poor durability performances in humid environment and when exposed to high temperatures. To give a clear idea, it is well known that bulletproof vests expire after in a couple of years.

Carbon Fibers (CFRP)

Carbon Fiber is produced from a variety of precursors, including polyacrylonitrile (PAN), rayon and pitch. Carbon fibers are the most commonly used material for FRP. CFRP has the best performance among AFRP and GFRP and has a relatively good resistance to creep and fatigue. Carbon fiber is generally the best choice either for its superior mechanical properties, good performances under fatigue and permanent loads (no creep phenomena) and high resistance to most environmental conditions, either acid and alkaline (Nanni, 1999). CFRP has an approximate E modulus of 240 to 760 GPa and tensile strength of 2400 to 5100 MPa. Carbon fibers are divided into two groups of high modulus and high strength (CNR 2013). In comparison with GFRP and AFRP, CFRP is stiffer, has better durability and is more expensive (FIB 2007, Kalpana 2013). CFRP has a brittle failure but still its overall performance is better than AFRP and GFRP (CNR 2013).

The better performances come for a high price: roughly a standard CFRP performs 3 times better than a GFRP counterparts, but also costs 10 times more (Nanni et al. 2014). Apart for the high price, the main negative aspect is a low coefficient of thermal expansion that becomes eventually negative in the composite material (Ashraf et al. 2012). This can cause compatibility issues in case the structure is subjected to sensitive thermal gradients. Also, the electrical conductivity can cause problem such as galvanic corrosion in steel-coupled solutions and the impact resistance is relatively low. Fabricators overcome the latter problem by using a barrier material or veil ply — often fiberglass/epoxy — during laminate layup.

Generally, CFRP materials are famous for their high stiffer and great strength. Figure 1.7 presents a stress-strain curve, with the data of the V-Wrap C200 H material plotted as the blue curve. Clearly, carbon fiber material present a brittle behavior with a very high ultimate strength, while by way of comparison, in the same figure is also plotted in violet the typical behavior of a ductile material: steel (type AISI 1020 HR).

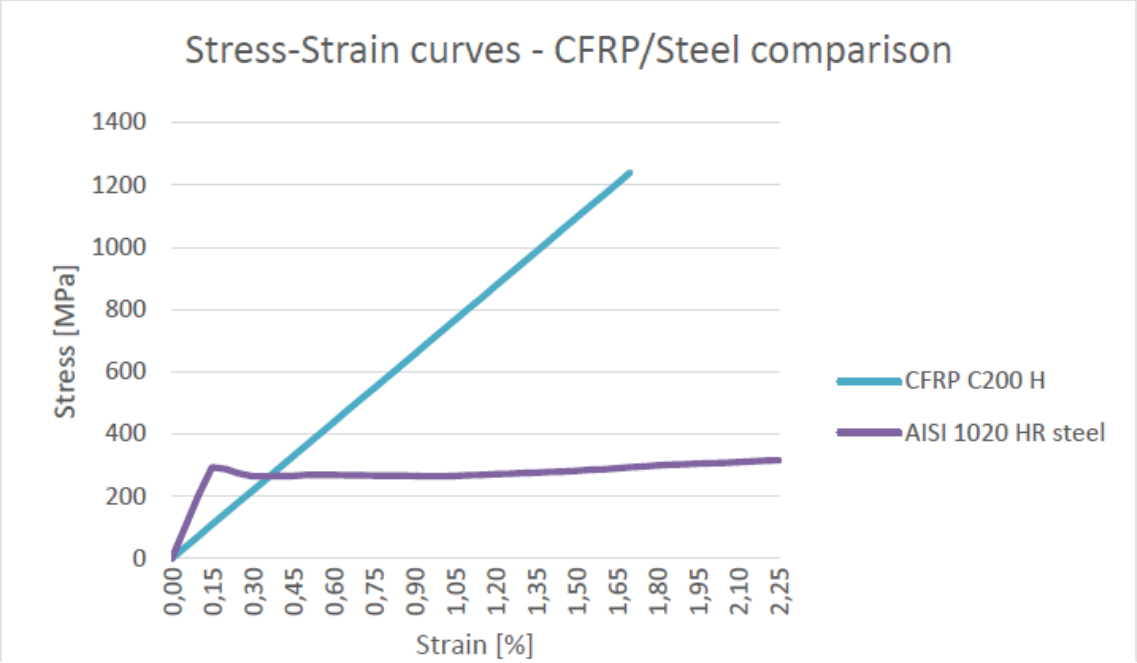

Figure 1.7 – Stress/Strain curves – CFRP/Steel comparison

Typical properties of the most common fibers (Nanni, 1999) are shown in table 1.4.

Type of Fiber	ρ [kg/m^3]	σ [Mpa]	E [Gpa]	ϵ_{ult} [÷]	μ -
E-glass	2450	3445	72.4	2.4	0.22
S-galss	2450	4547	85.5	3.3	0.22
AR-glass	2253	1793÷3447	69.6÷75.8	2.0÷3.0	N/A
High-modulus carbon	1951	2482÷3999	349.6÷650.2	0.5	0.2
Low-modulus carbon	1749	3496	239.9	1.1	0.2
Aramid (Kevlar 29)	1440	2758	62.1	4.4	0.35
Aramid (Kevlar 49)	1440	3620	18.0	2.2	0.35
Aramid (Kevlar 149)	1440	3447	124.1	1.4	0.35
Basalt	2799	4826	88.9	3.1	N/A

Table 1.4 - Typical properties of fibers (single filament)

1.2.2.2 Resins

Basing on their thermal behaviors, two different typologies of polymeric matrices can be defined: thermosetting and thermoplastic

Thermoplastic resins are typically solid at ambient temperature and turns to viscous liquid as the temperature increase, undergoing an endothermic reaction. The need to heat the resin before impregnation makes thermoplastic solutions difficult to apply in the FPR industry. Thermoplastic polymers are usually formed into shape and used to create a variety of products: PET for water bottles, Polypropylene for packaging containers, polycarbonate for safety goggles, PBT for toys, Vinyl for windows' frame and PVC for pipes (Berneschi, 2015).

Thermoset resins are most used for FRP composites. They are partially polymerized and in a viscous state but when they are mixed with the proper reagent and left to cure, they achieve a solid state (CNR 2013). In FRP, the fibers provide the tensile strength whereas the resin provides the compressive strength and ties the fibers together (Kalpana 2013). Resins are also used in conjunction with FRP material (e.g., sheets or bars) to bind the material to a surface, such as a masonry wall. Several different types of resins are available, each with their own advantages and disadvantages:

Epoxy. Epoxy is a viscous fluid resin with good adhesive properties. It also has a good resistance to moisture and hear which makes it a suitable choice for FRP composites. Epoxy resins are more expensive than polyester and vinyl ester resins (CNR 2013, FIB 2007).

Polyester. Polyester resins are the most widely used thermoset resins for FRP composites. They have lower viscosity than epoxy resins and have to be dissolved in solvent in order to be ready to use. They have lower mechanical and resistance capacities than epoxy resins but their price is lower (CNR 2013, FIB 2007).

Vinyl ester. For situations with harsh chemical environments and or high temperatures vinyl ester resins are used. They have a higher volumetric shrinkage than epoxy resons. Their mechanical properties are between those of epoxy resins and polyester resins (CNR 2013, FIB 2007).

To date, to the best knowledge of the authors, epoxy resins have been dominantly used in the structural repairs industry due to its good adhesion to substrate materials. Typical properties of resin matrices (Nanni 1999) are shown in table 1.5.

Type of Resin Matrix	ρ [kg/m³]	σ [Mpa]	E [Gpa]	μ -	CTE [10⁻⁶/°C]	Moisture content [÷]	Tg [°C]
Epoxy	1186÷1423	2067÷3445	35÷103	2.88÷5.4	0.35÷0.39	0.15÷0.60	95÷175
Polyester	1186÷1423	2756÷4134	48÷131	2.34÷3.42	0.38÷0.40	0.08÷0.15	70÷100
Vinylester	1127÷1364	2997÷3445	69÷76	2.7÷3.96	0.36÷0.39	0.14÷0.30	70÷165

Table 1.5 - Typical properties of resin matrices

Epoxy is the most used matrix material for FRP due to its good properties, such as high strength, low viscosity, low flow rate, low volatility during curing, low shrinkage rates and low cost.

The presence of the polymeric matrix is fundamental in order to redistribute the load among adjacent fibers:

- *Unimpregnated Fibers*. If a single fiber breaks, the load is equally redistributed among the remaining fibers in the bundle. This behavior is commonly referred to as Equal Load Sharing (Phoenix and Taylor 1973).
- *Impregnated Fibers*. If a single fiber breaks, the load distribution is restrained by the matrix: the overload is carried by the fibers nearest to the broken fiber, then the stress is redirected back to the broken fiber by plain shear interaction with the matrix at the interface (Harlow and Phoenix 1978). This behavior critically reduces the brittleness of the system, allowing broken fibers to still contribute to the overall strength and stiffness until large scale ruptures occur.

In other words, the presence of the matrix allows adjacent fibers to interact in shear. The main consequence reflects in the ability of a polymeric material to redistribute localized stress peaks among less loaded fibers, preventing localized failure in the system.

As a result, a dry fiber bundle, theoretically way stronger, usually experiences earlier failures with respect to an impregnated counterpart, because of the occurrence of localized stress concentration that the material is unable to distribute among the rest of the fibers.

A comparison of Fiber, Epoxy and FRP properties is shown in Figure 1.8, while an FRP composite sample is shown in Figure 1.9.

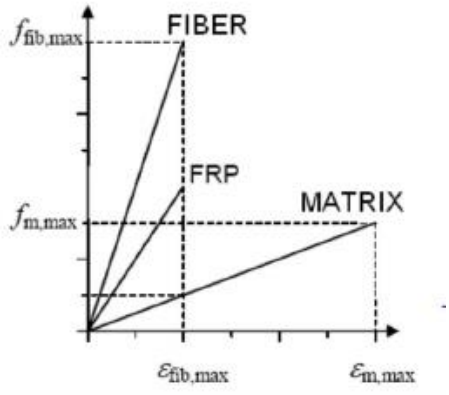

Figure 1.8 - Fiber/Epoxy/Composite's properties comparison (CNR, 2013)

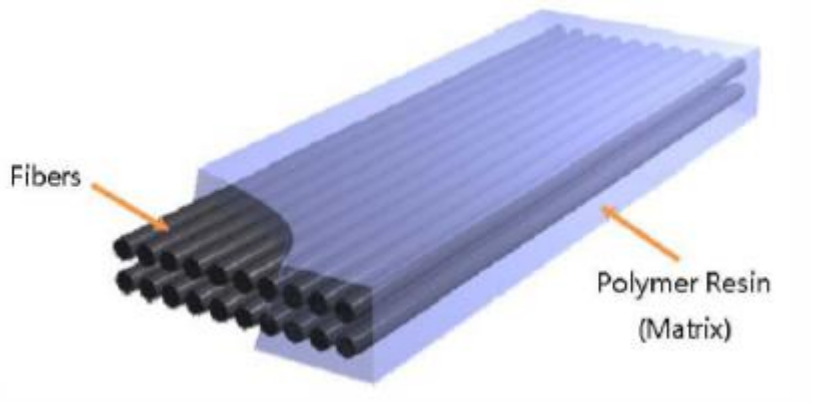

Figure 1.9 - FRP Composite sample

1.2.3 Applications

After a brief introduction about FRP materials and their main components, this section introduces how they are mostly applied in civil engineering.

Carbon fibers FRP are the standard and most applied solution in the repairing and retrofitting industry, thanks to their durability performance and their stiffness. The most important application, for what concerns civil engineering, is the strengthening of concrete, masonry, steel, cast iron and timber structures. Increasing the load capacity of old structures which were designed for a lower service loads then they are expecting today, seismic retrofitting or repairing damaged structures are some very common example of application. FRP shapes and manufacturing depends on the final application, in the civil field they are most commonly found as laminates for external application and rebar for internal

reinforcement. Two techniques are typically adopted to enhance the shear or flexure strength of structure:

- *Internal Reinforcement:* FRP rebar are currently used as reinforcing solution for newly built reinforced concrete structures (Nanni 1999, 2000). These structures have the potential to be almost everlasting – with service lives comparable to the great structures of the classical age – as none of the involved materials undergo severe time-related degradation processes. The internal application of FRP is not yet fully normed in the US and Europe, but the research has already showed the effectiveness of these solutions and a full implementation of the technology in standard buildings is getting closer and closer (Nanni 1999, 2000) (Nanni et al. 2014).
- *External Reinforcement:* internal applications are clearly inapplicable to structures already built and undergoing serious degradation, in this case the application of externally bond fibers is a well settled and reliable solution (Nanni 1999, 2000) although yet not fully exploited in terms of efficiency, mainly due to the debonding problem that will be fully discussed in the following section. FRP laminates are applied to the external surface of existing structures, like steel plate bonding, FRP laminate bonding involves adhering a thin, flexible fiber sheet to the concrete surface with a thermoset resin. This technique, known as manual lay-up, may be used to increase the shear and flexural capacity of beams and slabs and to increase confinement in columns. This solution does not add significant dead load to the structure, and may be installed in a relatively short period of time (Nanni, 2000). In this field, reliable design references are already available (CNR-DT 200 R1/2013) (ACI 440.2R-08) (ACI 440.7R-10) and the rehabilitation industry proves more confident in implementing these kind of solutions, made available as standardized systems (Nanni, 1999).

I will not go much in too deep in describing general information over composite materials which could be easily find in literature, I would rather focus the attention on the core of this research:" CFRP Anchors for external reinforcement", providing some general information about externally bonded fiber reinforced polymer and FRP anchorage system.

1.2.4 Externally Bonded Fiber Reinforced Polymer

Early post-strengthening techniques of reinforced concrete beams, which have been studied and used in field applications, were directed toward the use of epoxy bonded steel plates. Although the use of steel plates provided insight into the increase in flexural strength and flexural stiffness capabilities of externally applied reinforcement, steel plates had some disadvantages: difficulty in handling during installation; possibility of corrosion affecting the bond surface at the steel/adhesive interface; and the problem of forming clean butt joints with relatively short plates (Meier et al. (1991)). This prompted further investigation into the use of alternative materials (FRPs).

Externally bonded FRP is considered a really efficient alternative to the traditional technique written above, thanks to the many advantages described in the previous sections. FRP can be bonded to the structure in form of laminates. The sheets are essentially glued to the surface of the masonry, not unlike wallpaper. These laminates can be applied using three methods: wet lay-up, dry lay-up and plate bonding. Wet lay-up is where the FRP sheet is drenched in resin and then applied to the surface of the building, layer by layer. In the dry lay-up method, the resin is applied to the layer/masonry interface and the layers are not drenched in the resin. Plate bonding is when the layers are first glued together and then applied to the structure (Willis, 2009).

Typical applications of externally bonded FRP are: flexural strengthening of slabs and beams (strips or sheets), shear strengthening of beam (angles, sheets, fabrics), shear strengthening and confinement of column (sheets, fabrics, shells), wrapping of concrete tank (sheets, fabrics) and shear strengthening of beam-column joint (strips, sheets, fabrics). Among many other applications, concrete and masonry walls may be strengthened to better resist seismic and wind loads, concrete pipes may be lined with externally bonded FRP to resist higher internal pressures, and silos and tanks may be strengthened to resist higher pressures.

Figure 1.10 shows some typical applications of externally bonded CFRP.

Figure 1.10 - Typical applications of externally bonded CFRP

1.2.5 The Debonding Issue

The strengthening of RC members by externally bonded fiber reinforced polymer (FRP) laminates, using polymer adhesive as bonding agent, is a well-established technique and is increasingly used in practice. However, premature debonding of the laminate from the concrete substrate is a problem that does not allow effective utilization of the strength of the laminate and accordingly increases the cost of the retrofit. In the case of members retrofitted for increased flexural strength, debonding initiates either near the ends of the laminate or in the region of maximum moment within the span.

In general, the FRP/concrete interface can be separated into the elastic region (region 'A' in Figure l.11 (a)), where no damage has occurred and the debonded zone, with interfacial damage leading to separation of materials from the two sides. The debonded zone can be further divided into two parts: a process zone within which the shear stress is decreasing with interfacial sliding (region 'B' in Figure l.11 (a)), and a stress-free zone where the debonded surfaces have completely separated (region 'C' in Figure l.11 (a)). The debonding process can then be analyzed as the propagation of an interfacial crack, with the interfacial constitutive behavior described by a particular shear stress vs shear displacement (τ -δ) curve (Figure l.11 (b)). The shear displacement can be interpreted as the relative displacement between the FRP plate and the concrete. Before debonding occurs, this is resulted from the deformation of the adhesive. After debonding, it represents the relative sliding between the two surfaces of the debonded zone. Physically, the area represents the fracture energy (G_F) required for complete separation of the debonded surfaces to occur.

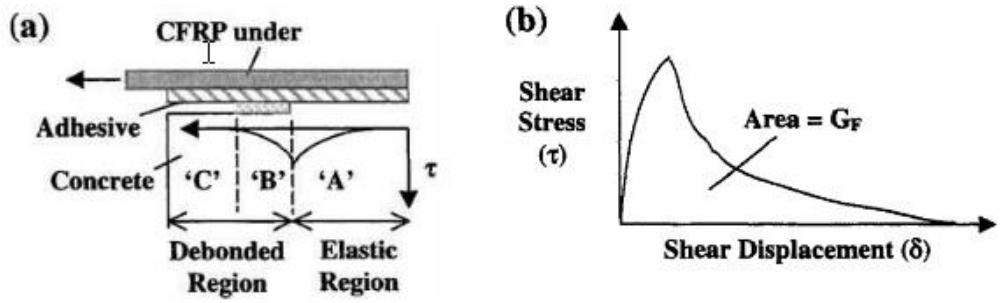

Figure 1.11 - (a) Various zones along the FRP/Concrete Interface. (b) A typical Shear Stress vs Displacement Curve.

Many theoretical formulations have been proposed to evaluate the bond strength in a concrete element with externally bonded reinforcement (FIB 2001, CNR 2004, ACI

committee 440 2008, Chen and Teng 2001, De Lorenzis et al. 3001, Smith and Teng 2002, Brosens and Van Gement 1999, Oejilers et al. 2007, Taljsten 1997, Bilotta et al. 2011).

The main part of these formulations is usually similar and the differences are in some numerical coefficients calibrates by experimental results and bond tests and in some safety factor (Nicolais and Borzaccheillo 2012).

Many solutions have been proposed to account for the problem of debonding, from surface preparation (Mostofinejad & Mahmoudabadi, 2010) to the most various kind of mechanical anchoring device (Kalfat et al. 2011). Up to now, the only normed solution force designers to limit the strains in the laminate to levels way lower than the ultimate one, thus guaranteeing a safe, though inefficient design.

In order to evaluate the effectiveness of alternative solutions, namely anchoring devices, it is fundamental to deeply understand the various debonding mechanisms and their mechanical modeling.

There is a considerable amount of experimental work reported in the literature on the bond strength of FRP-to-concrete joints. Based on the experimental results and observations made during the experiments on RC beams and slabs strengthened for flexure, the types of bond failures can be broadly classified into two main categories: *crack-induced interfacial debonding* and the *end-zone interfacial debonding*. In RC members subjected to bending, formation of flexural cracks is inevitable as the flexural capacity of the member is approached. Once such cracks are formed, the parts of FRP plate under the cracks are highly stressed. These stresses are transferred to the concrete, which causes a concentration of shear stresses in the interface eventually leading to bond failure of the FRP-to-concrete joints under the cracks. This interfacial separation progresses towards the less stressed regions as shown in Figure 1.12(a, b). On the other hand, high interfacial stresses also build up in the end zones of the FRP-to-concrete joints. Since the level of axial stress in the FRP plate is low near the ends, the stresses normal to the interface layer (peeling stresses) cause a premature bond failure by separation of the FRP plate from the concrete surface (Figure 1.12(c)). The separation of the concrete cover is also possible in the end zones, as shown in Figure 1.12(d), in cases when the concrete strength is low or when the cover concrete is on the verge of spalling (breaking into chips) as a result of corrosion in the steel rebars. In the literature, this type of failure is sometimes referred to as concrete cover rip-off failure, concrete cover delamination, and concrete cover separation. Therefore, some extra measures are necessary to anchor the externally bonded FRP plates in these end zones. For

FRP plates or sheets bonded to a concrete substrate, there is an effective bond length beyond which any increase in the bonded length cannot increase the total load the bonded FRP is able to carry. In this sense, the bond behavior of FRP-to-concrete is essentially different to the behavior of the steel rebar-to-concrete bond.

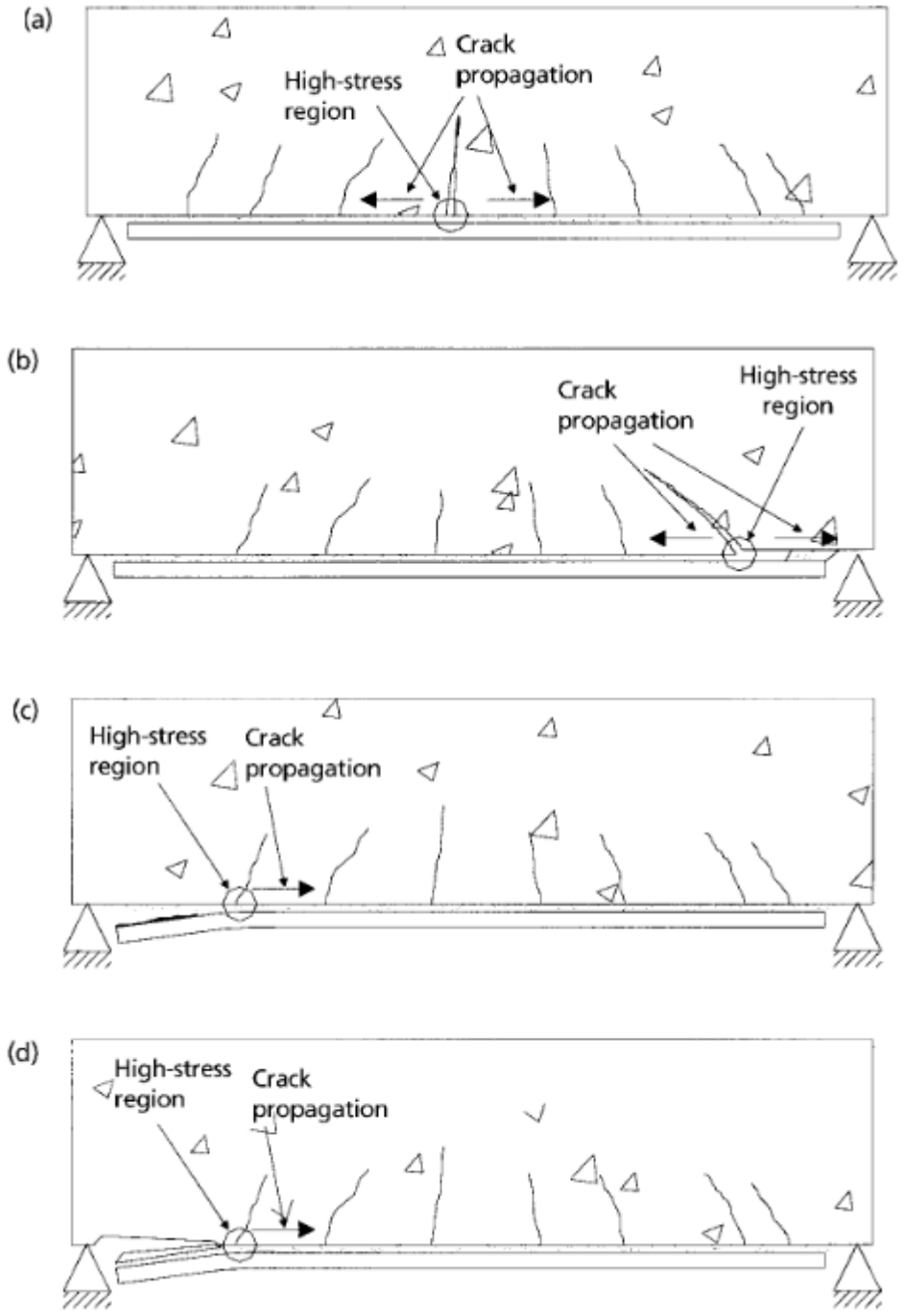

Figure 1.12 - Bond failure modes of FRP-to-concrete joints: (a) flexural crack-induced interfacial debonding; (b) shear crack-induced interfacial debonding; (c) end-zone interfacial debonding; (d) end-zone interfacial debonding accompanied by concrete cover separation.

A more detailed classification of debonding mechanisms can be done depending on where they occur along the beam/FRP sheet and depending on which is the failing element in the concrete-adhesive-FRP system (ACI, 2008) (CNR, 2013) (ASTM, 2013):

- Debonding inside the concrete (Cohesive Failure)
- Debonding between adhesive & concrete (Adhesive Failure)
- Debonding inside the adhesive (Cohesive Failure)
- Debonding between multiple laminate sheets, wet lay-up (Cohesive Failure)
- Debonding between multiple laminate sheets, pre-cured (Adhesive Failure)

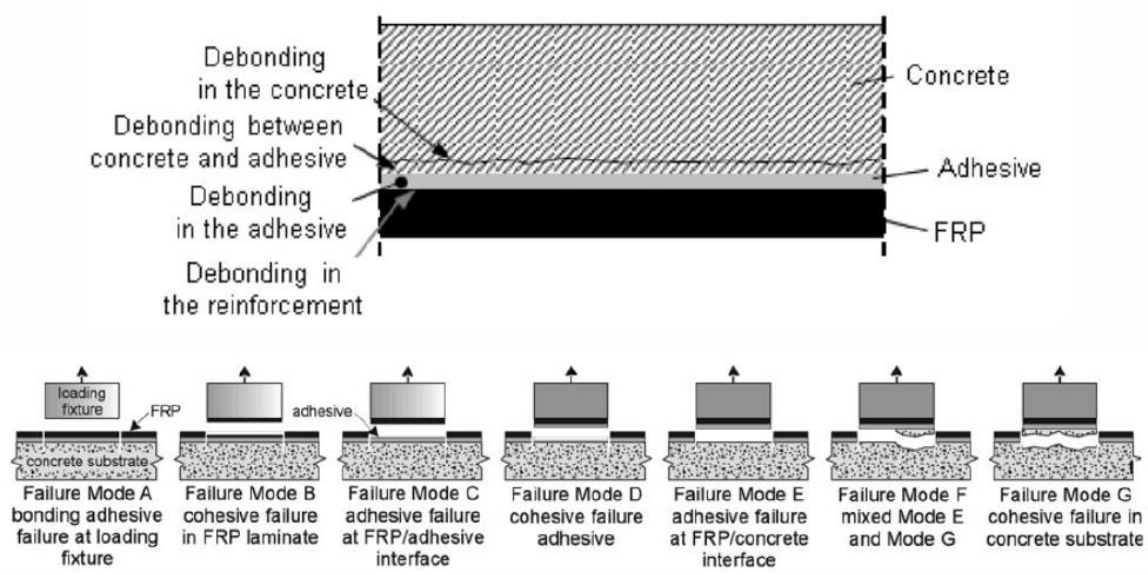

Figure 1.13 - Debonding modes between FRP and concrete

In bended members, the end portions of the FRP system are subjected to high interfacial shear and normal stresses for a length of approximately 100-200 mm (4-8 in) (CNR, 2013). Normal stresses namely arise because of the severe stiffness of the FRP sheet, that refuses to bend along with the concrete element. These stresses tend to reduce the tangential component, reducing the bond effectiveness and actively pulling the FRP laminate away from the concrete surface (CNR, 2013).

This debonding mechanism happens in zones of low stresses for the beam and usually is not critical in defining the ultimate strength of well-designed strengthening solutions, while

its understanding is fundamental in order to define the proper development length for the FRP laminate, further discussed later on.

In general, before designing for flexural and shear, the evaluation of the maximum force transferred from the concrete to the FRP, as well as the evaluation of shear and normal stresses at the concrete-FRP interface, is required. The CNR DT-200 gives several simplified expressions for the calculation of these quantities that are analyzed in Appendix F.

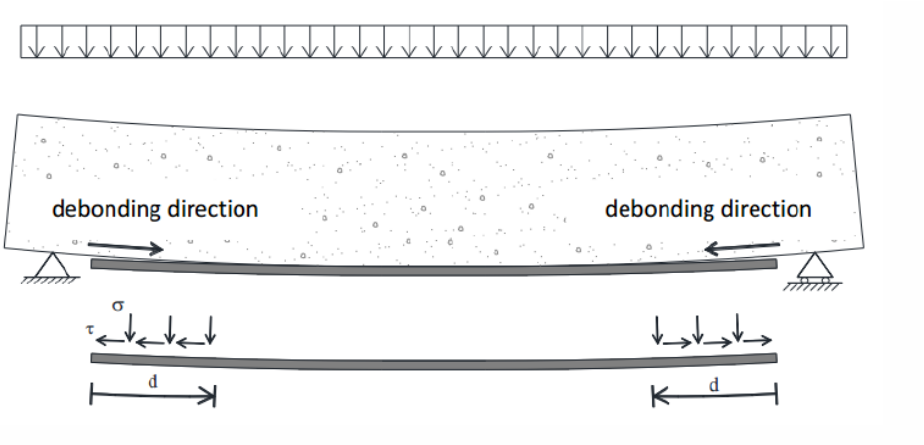

Figure 1.14 - Plate end debonding (CNR DT200, 2013)

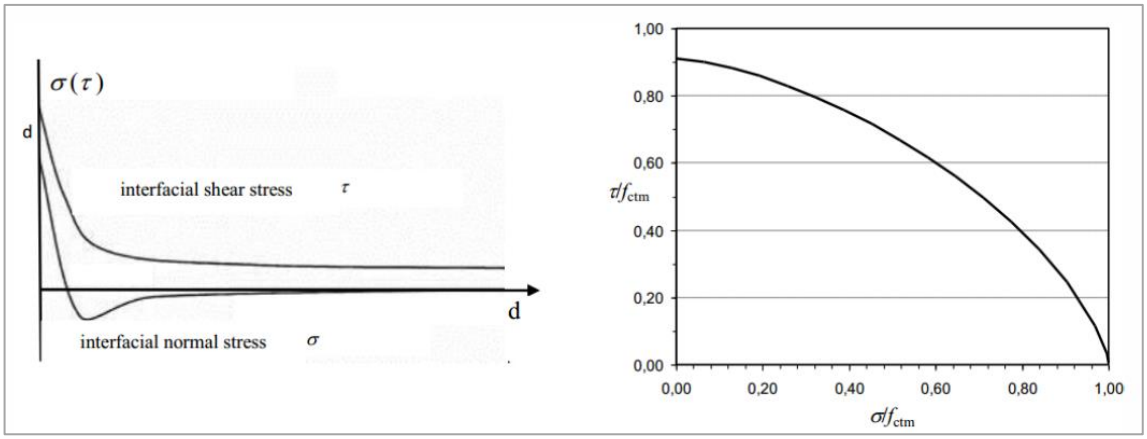

Figure 1.15 – Laminate end debonding & Stresses at sheet's ends (CNR, 2013)

1.3 FRP Anchorage System

The primary role of FRP anchorage systems is to prevent or delay the process of debonding, which occurs when externally bonded FRP detaches from the RC substrate because of the low tensile strength of concrete (Ceroni et al. 2008).

1.3.1 Overview

RC structures are strengthened by externally bonding FRP plates and sheets to its members using epoxy resin. For the externally bonded FRP to be effective in increasing the load-carrying capacity of the structure, effective stress transfer between the FRP composite and the concrete is essential. The bond mechanism is fundamental because is responsible to transfer the load from the concrete to the FRP material. The main challenge for this type of strengthening system is to design against the various debonding failure modes.

The debonding failure modes shown in the previous section, especially concrete cover separation, have been frequently documented. The current approach to preclude debonding failure is to limit the strain design in the FRP to levels much less than the strain rupture (ACI Committee 440 2008), which as a result, limits the efficiency of the strengthening system. It must also be noted that increasing the number of layers of FRP can reduce the ductility of the strengthened member. Proposed solution to counter debonding consists in mechanically anchoring the fiber sheet to the concrete substrate. The solution has proved to be feasible and to significantly improve the efficiency of the FRP system (Kalfat et al. 2011) and in some case to guarantee a ductile failure for the reinforced element (Grelle & Sneed, 2013). A wide variety of anchoring devices has been proposed in order to avoid the debonding problem: U-Wrapping, spikes, staples, …

1.3.2 Purpose

Anchorage systems for externally bonded FRP typically serve one or more of the following purposes: (I) to prevent or delay interfacial crack opening; (II) to increase the total available interfacial shear stress transfer; or (III) to provide a stress transfer mechanism where no bond length is available beyond the critical section.

Type I Anchorage. Anchorage systems with Type I characteristics can be used to prevent or delay crack opening at the onset of debonding or failure of the concrete substrate due to tensile normal forces associated with certain debonding failure modes such as “plate-end” interfacial debonding or concrete cover separation. Type I anchorage is most commonly used at the termination of FRP laminates, and sometimes throughout their entire length. An example application of Type I anchorage is shown in Figure 1.16, in which the FRP on a RC beam soffit used for flexural strengthening is anchored at the laminate end in order to prevent concrete cover separation and “plate-end” interfacial debonding.

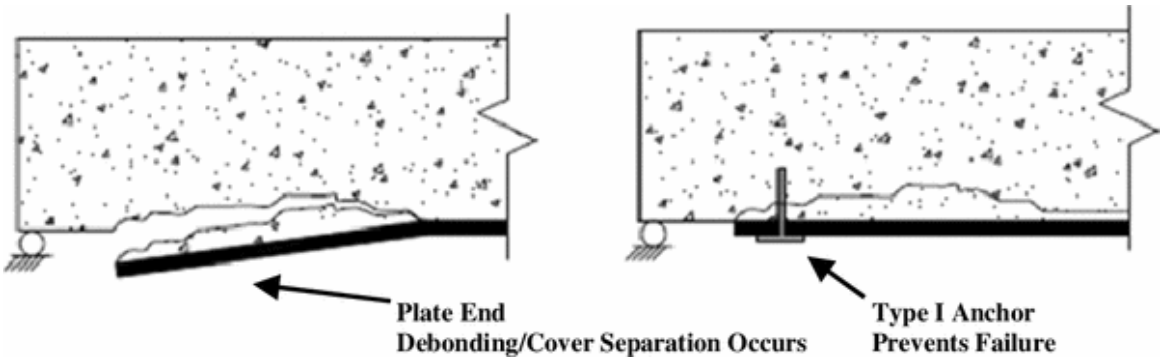

Figure 1.16 - Example of Type I device

Type II Anchorage. Anchorage systems with Type II characteristics can be used to improve the interfacial shear stress transfer. This is usually achieved by increasing the area over which the shear stress is transferred. Type II anchorage is often used when the transfer length is less than the effective bond length, usually due to the geometric conditions of the structural member, or simply to reduce the length of FRP used by increasing the interfacial stress transfer.

Type III Anchorage. Type III anchorage is used to provide an alternative stress transfer mechanism where no bond length is available beyond the critical section. This condition applies when the critical design section is located at a sheet or plate end, or near an abrupt change in fiber direction, such as at the location of an interface between two orthogonal structural members. Type III anchorages present a very special and difficult challenge because the FRP strengthening system can be considered to have no contribution to the strength without their inclusion. While some Type III anchorages may have Type I and Type II characteristics, it should be noted that anchorage forces in a Type III application are transferred beyond the bonded length. In Figure 1.17, the example of a U-Anchor is

used to illustrate the difference in behavior of the same anchorage system being used in Type II (Figure 1.17 (a)) and Type III (Figure 1.17 (b)) applications.

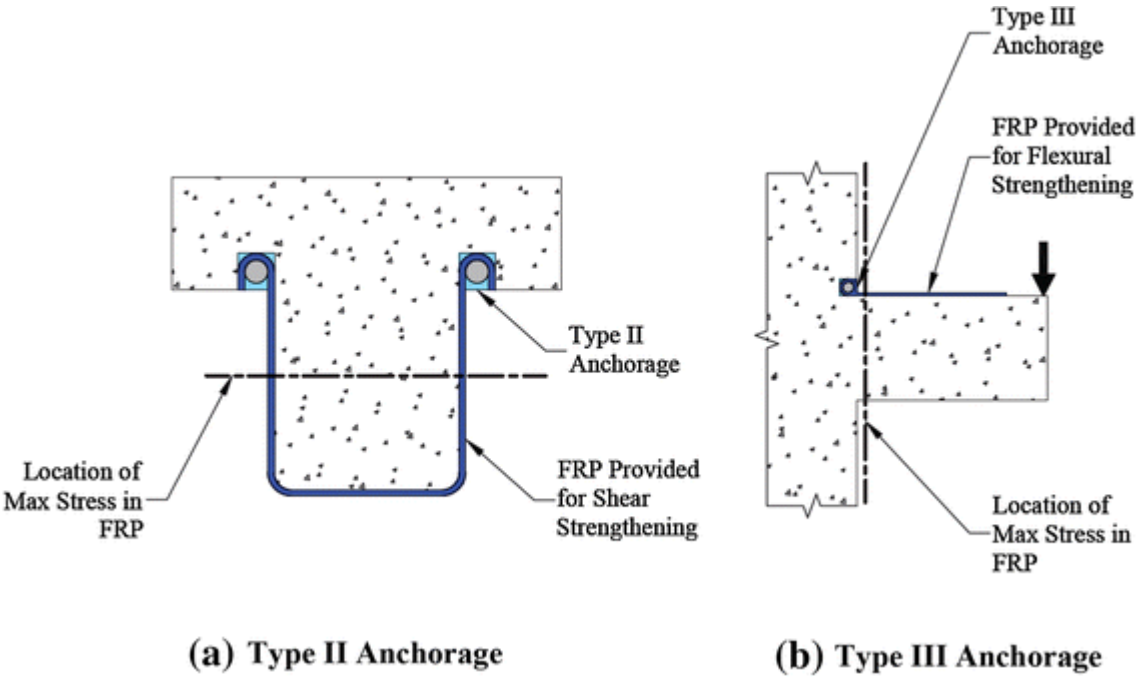

Figure 1.17 - Comparison of Type II and Type III (U-Anchor example)

Research on systems to mechanically anchor externally bonded FRP strengthening systems has included anchor spikes, transverse wrapping, U-Anchors, longitudinal chases, FRP strips, plate anchors, bolted angles, cylindrical hollow sections, ductile anchorage systems, and other miscellaneous systems. Each of these anchorage systems has unique geometrical constraints, installation limitations, and force (stress) transfer characteristics. Although published research focusing specifically on FRP anchorage system behavior has been limited, studies have shown promising results regarding the functionality of various systems.

In this section, the different anchorage systems presented in existing literature are just summarized in Table 1.6. If needed, the reader who is not familiar on this topic could find information on these representative studies involving FRP anchorage systems reading those studies.

System/device	Application	Study	Test type	FRP strengthening application
90° Anchor spike	Type I	Kim et al. (2011)	–	Confinement of RC columns
		Zhang and Smith (2012)	*SS*	Representative testing only
		Zhang et al. (2010)	*SS*	Representative testing only
		Niemitz et al. (2010)	*SS*	Representative testing only
		Kim and Smith (2010)	–	Analytical anchor model only
		Sami et al. (2010)	*BT, PO, DS*	Representative testing only
		Pham (2009)	*DS, BT*	Representative testing only
		Ozbakkaloglu and Saatcioglu (2009)	*PO*	Representative testing only
		Li and Grace Chua (2009)	–	Flexure of RC beam-column and beam-wall joints
		Orton (2007)	*BT*	Flexure of RC beams with height transition
		Eshwar et al. (2005)	*PO*	Flexure of RC beams with curved soffits
		Karantzikis et al. (2005)	–	Confinement of RC columns
		Piyong et al. (2003)	*PO*	Flexure of RC slab with prestressed flexural FRP
		Lam and Teng (2001)	–	Flexure of RC cantilever slabs
180° Anchor spike	Type II	Kim and Smith (2010)	–	Analytical anchor model only
	Type III	Sadone et al. (2010)	*SS*	Representative testing only
		Prota et al. (2005)	–	Flexure/shear and axial loads of RC columns
Transverse wrapping	Type I	Aiello and Ombres (2011)	–	Flexure of continuous RC beams
		Khan and Ayub (2010)	–	Flexure of rectangular RC beams
		Pan et al. (2010)	–	Flexure of rectangular RC beams
		Sadeghian et al. (2010)	–	Flexure of eccentrically loaded RC columns
		Zhuo et al. (2009)	–	Prestressed FRP strap
		Yalim et al. (2008)	–	Flexure of RC T-beams
		Orton (2007)	*BT*	Flexure of RC beams with height transition
		Al-Amery and Al-Mahaidi (2006)	–	Flexure of RC beams
		Pham and Al-Mahaidi (2006)	–	Prestressed FRP strap
		Kotynia (2005)	–	Flexure of RC beams
		Antonopoulos and Triantafillou (2003)	–	Flexure and shear of RC beam-column joints
		Sawada et al. (2003)	–	Flexure of RC beams
		Shahrooz et al. (2002)	–	Flexure of RC T-beams
		Spadea et al. (2001)	–	Flexure of RC beams (steel plates used as anchorage)
		Grace et al. (2000)	–	Flexure and shear of RC beams
	Types I/II	Sagawa et al. (2001)	–	Flexure of RC beams with inclined straps

System/device	Application	Study	Test type	FRP strengthening application
U-Anchor	Type II	Petty et al. 2011	–	Shear of PC girders
		Beigay et al. (2010)	–	In- and out-of-plane flexure in masonry shear wall
		Ceroni et al. (2008)	*DS*	Representative testing only
		Micelli et al. (2002)	–	Shear of RC T-beams
		Khalifa et al. (1999)	–	Shear of RC T-beams
	Type III	Beigay et al. (2010)	–	Flexure of masonry shear wall
		Teng et al. (2001)	–	Flexure of RC cantilever slab
Longitudinal chase	Type II	Kalfat and Al-Mahaidi (2010)	*DS*	Representative testing only
FRP strips	Types I/II	Petty et al. (2011)	–	Shear of PC girders
		Donchev and Nabi (2010)	–	Flexure of RC slabs
		Ortega (2009)	–	Shear of RC and PC girders
		Antonopoulos and Triantafillou (2003)	–	Flexure and shear of RC beam-column joints
		Lamothe et al. (1998)	–	Shear of RC T-beams
Steel/FRP plates	Types I/II	Jin and Leung (2011)	*SS*	Representative testing only
		Ortega (2009)	–	Shear of RC and PC girders
		Wu and Huang (2008)	–	Flexure of RC beams
		Ceroni et al. (2008)	*DS*	Representative testing only
FRP sandwich plate	Types I/II	Ortega (2009)	–	Shear of RC and PC girders
Bolted U-Anchor/angle	Types I/II	Nagy-György et al. (2005)	–	Flexure and axial loads of RC shear walls
After-joint plate	Types I/II	Ceroni et al. (2008)	*DS*	Representative testing only
Steel angle	Types I/II	Antonopoulos and Triantafillou (2003)	–	Flexure and shear of RC beam-column joints
Bolted angle	Types I/II	Tanarslan and Altin (2010)	–	Shear of RC T-beams
	Type III	Deifalla and Ghobarah (2010)	–	Shear and torsion of RC T-beams
		Hiotakis (2004)	–	Flexure of RC shear wall
		Hwang et al. (2004)	–	Flexure of RC shear wall
		Hall et al. (2002)	*DS*	Flexure of masonry shear wall
		Foo et al. (2001)	–	Flexure of RC shear wall
CHS anchor	Type III	Hiotakis (2004)	–	Flexure of RC shear wall
Plate & angle/pipe	Type III	Hall et al. (2002)	*DS*	Flexure of masonry shear wall
Plate & pipe	Type III	Grelle (2011)	–	Flexure of RC column

Table 1.6 - Summary of FRP anchorage applications and test types

So far, among the anchoring devices, the staple anchoring system revealed to be the most effective device. In particular, two types of staple anchoring devices were studied: flat staple anchor and rounded staple anchor. In a previous research (Cadenazzi, 2016) the behavior of those kind of staples acting on their dimensions was studied.

This research will focus on the most recent and innovative anchor system called “staple anchor”, characterizing it, comparing it with the others studied previously and analyzing the improvement they give applied with a newer technique on slabs.

CHAPTER 2

Experimental Campaigns

In the previous chapter, general concepts of composite material and externally bonded FRP were provided. Chapter 2 wants to give the reader an overview of the experimental campaigns the author carried out pointing out the main goals of this research.

2.1 Overview

In the field of the concrete structures a lot of studies exist on the use of FRP anchors systems. It has been demonstrated that this mechanical anchor typology increases the strength peak and the ductility of the reinforced elements. Therefore, in the field of CFRP Staple anchors, more studies should be conducted to improve this anchor system that seems to show high potentialities. This lack of researches leads to an absence of scientific basis to define the correct design modality and anchor application methodologies; in this context, the engineers employ the new joint technologies using only the proper experience or the FRP producer advices.

Also, confusion still exists towards understanding anchors mechanical behavior, identifying critical parameters involved and defining research priorities. In general, the need for a uniform approach toward assembling a big anchor-related data-base has been underlined by many (Grelle & Sneed, 2013) and some efforts are already undergoing (Kalfat et al. 2011) (Grelle & Sneed, 2013). Much more needs to be done though.

The experimental study proposed here has been designed to analyze the performance of mechanical anchors applied over CFRP straightened concrete blocks.

The general requirement, either from ACI (2008) and CNR (2013), is to fully characterize the applied anchoring solution, that should be heavily scrutinized through representative physical testing (ACI, 2008) otherwise no enhances in strength and ductility should be accounted for (CNR, 2013). It is worth noticing that requiring an experimental characterization of the implemented solution doesn’t provide a complete solution to the problem, not even from a temporary perspective: a standardized testing approach is not available yet, leading to the already discussed confusing situation.

2.2 Purpose

The purpose of this research is to provide accurate information to engineers, specifiers, and owners. This thesis wants to provide guidance for the selection, preparation, installation, and design of Carbon Fiber-Reinforced-Polymer (CFRP) anchors for external reinforcement of concrete structural elements.

Currently, no specific criteria or guidelines exist to help the designer to choose the best anchor configuration to improve the strength of the existing concrete structure by FRP sheets avoiding the debonding problem. In order to develop a quantitative approach to anchors' design, firstly is required a reliable characterization for the single anchor's strength and a reliable model to describe a multiple anchors joint's behavior.

The following thesis wants to investigate the behavior of the staple anchor system applied to the FRP sheet on a slab. The research is composed of two experimental campaigns:

- In order to study the fundamental behavior of the slab-FRP laminate-anchor system a ***first*** experimental campaign is carried out. A series of double shear tests on concrete blocks strengthened with FRP sheets connected to the concrete blocks settled via these carbon staple anchors were performed in order to characterize the single anchor's strength.

Figure 2.1 - Double Shear Test on a concrete block

In particular, two series of double shear tests over five specimens each were performed: five specimens were prepared with **Flat** staple anchors and other five with **Round** staple anchors.

Figure 2.2 - Flat Staple (left) and Round Staple (right) anchors

Figure 2.3 – Cutting and drilling process for anchors' installation

The purpose is to test the effectiveness of staple anchors characterizing them and providing engineers the necessary information to make design decisions when incorporating a staple anchor system to enhance the bond of externally bonded FRP laminates.

- Once the best anchor's system is found, a series of 3-point bending (flexural) tests on slabs with different FRP anchor configurations, in order to characterize the behavior and to identify the key parameters that affect the performance of the whole system (slab-FRP laminate-Anchor) were performed in the ***second*** experimental campaign.

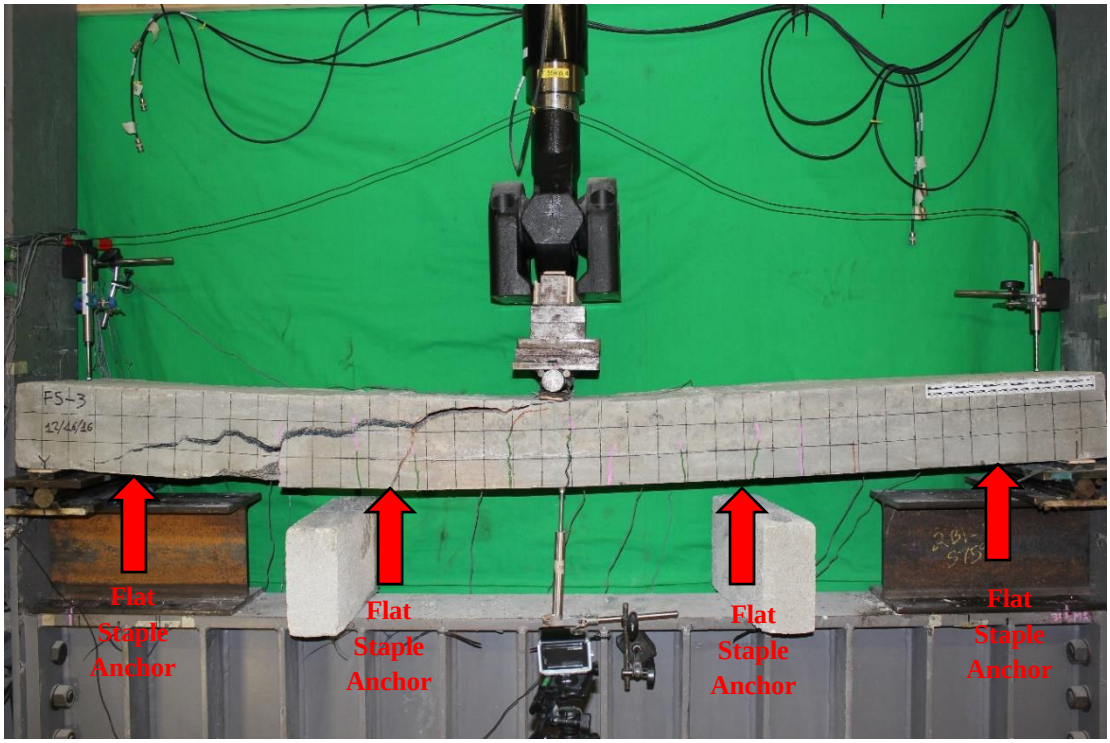

Figure 2.4 – 3-Point bending test on R/C slab

This second experimental campaign investigates the behavior of the **Flat** Staple anchors, which showed better performances than Round Staple anchors, applied on RC slabs.

This investigation is based on experimental work on RC slabs strengthened with FRP sheets connected to the concrete via these carbon Flat staple anchors improved with a "FRP patch" as a new installation process tested in the previous experimental program (Chapter 2).

The experimental campaign is composed by 3-point bending (flexural) tests through which it is investigated the increasing in terms of resistance of the anchors under tension load, in order to find the best configuration that is sufficient to enhance the bond of the FRP sheets.

In particular, a series of 3-point bending tests was performed: four specimens were prepared with **Flat** staple anchors installed in two different configurations. Two specimens were provided of two anchors at the ends (configuration 1), other two specimens were provided

of four anchors, two at the ends and other two along the slab's span, at one third of the length (configuration 2).

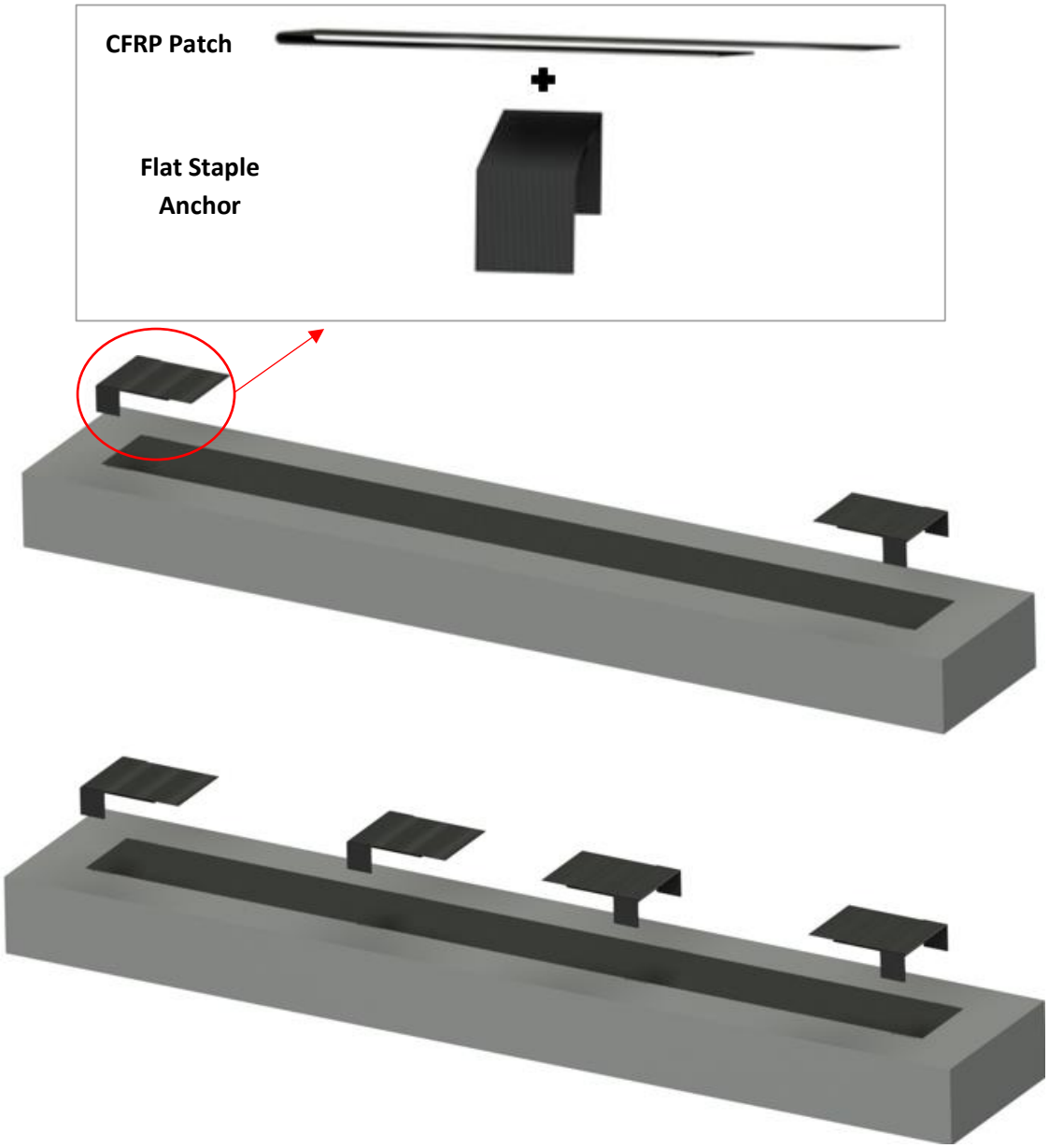

Figure 2.5 - Anchors on slab in configuration 1 (top) & configuration 2 (bottom)

This investigation entered more into deep on the study of staple anchors, analyzing their performance in a larger scale than what was studied before. This thesis wants to be a step forward toward the creation of new specific design guidelines aimed to help engineers providing the necessary information to make design decision on the use of staple anchor system in effective way to enhance the bond of externally bonded FRP laminates applied on slabs.

CHAPTER 3

Experimental Program 1: Staple Anchors on Blocks

Chapter 3 covers all the aspects related to the ***first*** experimental campaign that was carried out over staple anchors on blocks. The first section presents the purpose of this chapter, the following sections will provide detailed information over specimens 'preparation, test set-up and instrumentation used. Finally, the materials used will be characterized.

3.1 Purpose

This research investigates the improvement due to a new technique used to apply the most recent type of anchorage system, called "staple anchor" as a mean of anchoring externally bonded fiber-reinforced polymers (FRP) sheets into concrete. In a previous research (Cadenazzi, 2016) the behavior of different anchor types (flat and round staples) set up in different configurations and dimensions was studied.

This investigation is based on experimental work on concrete blocks strengthened with FRP sheets connected to the concrete blocks settled via these carbon staple anchors improved with a **"FRP patch"** as a *new installation process*.

The staples anchors are provided as prefabricated elements formed by strands of carbon fibers that are inserted into epoxy filled holes in the concrete, and an external part that is also impregnated and connected externally to the bonded FRP laminate. They appear in different shapes and sizes and they can be installed in different ways but they share the same aim: enhance the bond of externally bonded FRP laminates into concrete.

This *first* experimental campaign is composed by double shear tests through which it is investigated the resistance of the anchors under tension load, in order to find the best configuration that is sufficient to enhance the bond of the FRP sheets.

In particular, two series of double shear tests over five specimens each were performed: five specimens were prepared with **Flat** staple anchors and other five with **Round** staple anchors. Since the past method already used in the University of Miami laboratory to investigate the performance of another type of anchor, called "spikes' anchors", revealed some difficulties in the set-up procedure of the test and mostly inaccurate results, the tests are now performed with an innovative installation procedure improved by a new installation process, which gives successful and consistency results through a more reliable set-up of the test.

As a reminder, the purpose of this experimental program is to test the effectiveness of staple anchors characterizing them and providing engineers the necessary information to make design decisions when incorporating a staple anchor system to enhance the bond of externally bonded FRP laminates.

Finally, also a comparison between the performance of the old and the new anchors' type installation is provided in order to show the enhancement made by this new installation process using an FRP patch.

3.2 Specimens Fabrication

A detailed description of specimen preparation is provided in this section.

3.2.1 Concrete Blocks

The blocks size was decided, as well as in the previous researches (Cadenazzi, 2016), considering the diameter of the steel support that was about 14 inches, in order to have the FRP sheet in tension perfectly aligned during the test.

The blocks size was 10" x 10" x 14" (254 mm x 254 mm x 356 mm) as shown in Figure 3.1

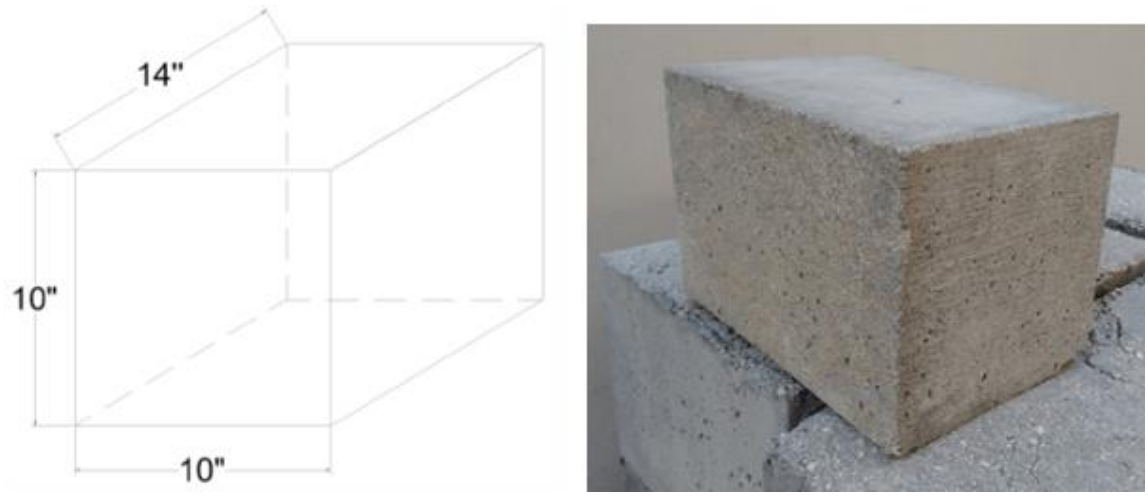

Figure 3.1 - Concrete block's geometry

3.2.2 Surface Preparation

A total of 10 specimens were prepared, 5 for the Flat Staple and other 5 for the Round Staple anchors. Both procedures are almost the same, the only difference consist in the hole needed for the Round Staple that is different from the cut needed for the Flat Staple.

A step-by-step procedure used for the specimen's preparation is hereinafter provided, starting from having the block already casted.

All the blocks used were sandblasted; in fact, it is widely accepted that surface roughness influences bond capacity, increasing the bond once the FRP is applied on the concrete. Also, the removal of the smoothness concrete paste helps to recreate an old concrete surface (usually the sandblast is required for old concretes to renew it).

Figure 3.2 shows the operation of sandblasting.

Figure 3.2 - Operation of Sandblasting

The surface on the external edge, in which the FRP sheet will be installed, was rounded with a grinder, in order to avoid the problem of spalling and a sudden load reduction on the FRP sheet during testing (Brena and McGuirk, 2013).

One of the two surfaces on the external edges was prepared as the "failure side" and the other one as the "un-failure side", as meaning that the blocks were strengthened on a side to prevent the failure, steering the failure precisely on the other side. This choice was made to avoid monitoring both sides, applying double number of strain gauges with a significant saving in terms of time and money on material used.

Each specimen that would have a **Flat** staple anchor was cut in the center of the upper surface using a special grinder, as shown in Figure 3.3.

Figure 3.3 - Cutting process for the failure side of the Flat Staple anchors

Each specimen that would have a **Round** staple anchor, instead, was drilled in the center of the upper surface using a Hilti hammer driller, as shown in Figure 3.4.

Figure 3.4 - Drilling process for the failure side of the Round Staple anchors

Obviously, after this procedure, the dust was blown up from the holes using an air compressor to clean perfectly the inside before anchors installation. Regarding the “un-failure side”, the procedure was exactly the same for both Flat and Round staple anchors. As shown in Figure 3.5, the bottom edge of that side was grinded to make it rounded and smooth because, as will be described in the next chapter, the CFRP sheet was wrapped underneath the block in order to strength the “un-failure side”.

Figure 3.5 – Blocks’ edge smoothing process

3.2.3 Anchors Preparation

As already mentioned, the anchors were provided as prefabricated elements. They needed to be cut using a particular blade as 6” (152.4 mm) long, 2” (50.8 mm) width and 1” (25.4 mm) depth for the Flat Staple and 7” (177.8 mm) long and 2” (50.8 mm) depth for the Round Staple anchors as shown in chapters 3.5.4 and 3.5.5.

Figure 3.6 - Anchors' cutting process

3.2.4 CFRP Preparation

Once specimens were prepared for FRP bonding, CFRP sheets and CFRP patches were prepared for installation.

One CFRP sheet per each specimen was cut as 6 inches wide and 112 inches long from V-Wrap C200 H material. Moreover, also one sheet per each specimen was cut as 6 inches wide and 14 inches long, as patch needed for the new installation process. So, a total of 10 long CFRP sheets and 10 FRP patches were cut; five of them were used for Flat Staple anchors and other five for Round Staple anchors.

Note: *The length of the FRP sheet (and the dimensions of the EPS foam blocks) was computed based on the dimensions of the hydraulic jack, of the load cell and of the plates used to perform the test*

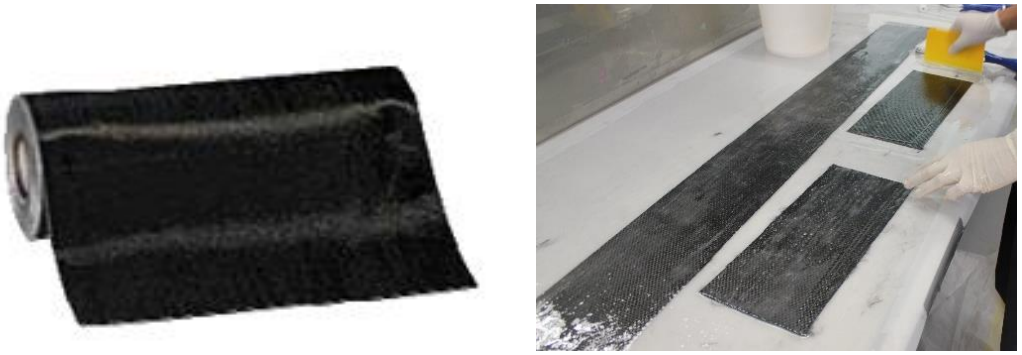

Figure 3.7 - V-Wrap C200H roll, 112" FRP sheet & 14" FRP patches

3.3 Installation Procedure

In order to allow a good bonding between the FRP sheet and the concrete surface, the latter had to be cleaned. An air compressor and a brush were used to remove all the particles of sand resulting from the sandblasting.

3.3.1 Epoxy Application

The epoxy resin (part A) and the curing agent (part B) were mixed together with the mixing ratio reported in the manufacturer's instructions of 100:33 by weight. The two parts were completely mixed together for 3 minutes until a smooth and uniform consistency was reached. Part of epoxy resin was mixed with fume silica in order to make the epoxy thicker. The fume silica was added as a mixing ratio by volume of 1:1 to the primer. Again, once a uniform consistency was obtained, the thickened epoxy (the primer mixed with the fume silica) was applied using a spatula, in order to fill all the concrete cavities and little holes as shown in Figure 3.8.

Figure 3.8 - Epoxy resin mixing & fume silica application on block surface

3.3.2 CFRP Sheet Application

Once the blocks were ready, the EPS (expanded polystyrene) foam shapes were assembled and covered by a Mylar sheet of 8" wide, 106" long in order to prevent the adhesion of the impregnated sheet on the EPS shape surface during the curing period. The EPS shape was also taped on the concrete block in order to prevent them from any movement as shown in Figure 3.9.

Figure 3.9 - EPS foam shapes assembling & Mylar installation

Then, all the CFRP sheet previously cut were disposed over a clean table and they were impregnated for their entire length using the pre-mixed part A & part B epoxy as shown in Figure 3.10.

Figure 3.10 - CFRP sheet impregnation process

After that, each lamina was carefully placed on the EPS foam shape and rolled all over the EPS shape surface and the concrete substrate at the ends, to avoid the formation of air bubbles along all the entire length. On the "failure side" the FRP sheet was extended until

the bottom of the block, while on the “un-failure side” the FRP sheet was extended underneath the block to prevent the failure of that side, as already explained previously.

Figure 3.11 - Impregnated FRP sheet application

Figure 3.12 – Block’s "Failure side" (left) & "Un-failure side" (right)

3.3.3 Anchors' Installation – Improved process

The anchors were installed on both sides of the specimens, on the "failure side" being the test side, on the "un-failure side" along with the FRP sheet underneath the block to prevent the failure strengthening that side. As explained in previous chapters, the main differences in preparation between the two series of specimens are the anchors used (Flat vs Round) and the cuts on the blocks (cuts vs holes).

So, hereinafter the anchors' installation procedure that is valid for both typologies of anchors will be described.

Once the impregnated CFRP sheet was positioned, the pre-mixed epoxy (Fortress 4020 Fast Epoxy Hi-Mod Gel) was poured into the stripe holes with a specific epoxy gun actioned by compressed air, designed for this work. With the same technique, an epoxy layer was poured also on the legs and on the under part of the anchor, on the surface into direct contact with the FRP lamina.

Figure 3.13 - Epoxy pouring process

Figure 3.14 - Epoxy soaked process on anchors

In this research a **new installation process** was developed in order to improve the strength of the external reinforcement provided by the CFRP sheet and the anchor.

The new installation process consists of applying an overlapped impregnated CFRP patch (6” wide and 14” long) folded as 6” below and 8” wrapped above the anchor inserted and squeezed into the holes soaked of epoxy as shown in Figure 3.15.

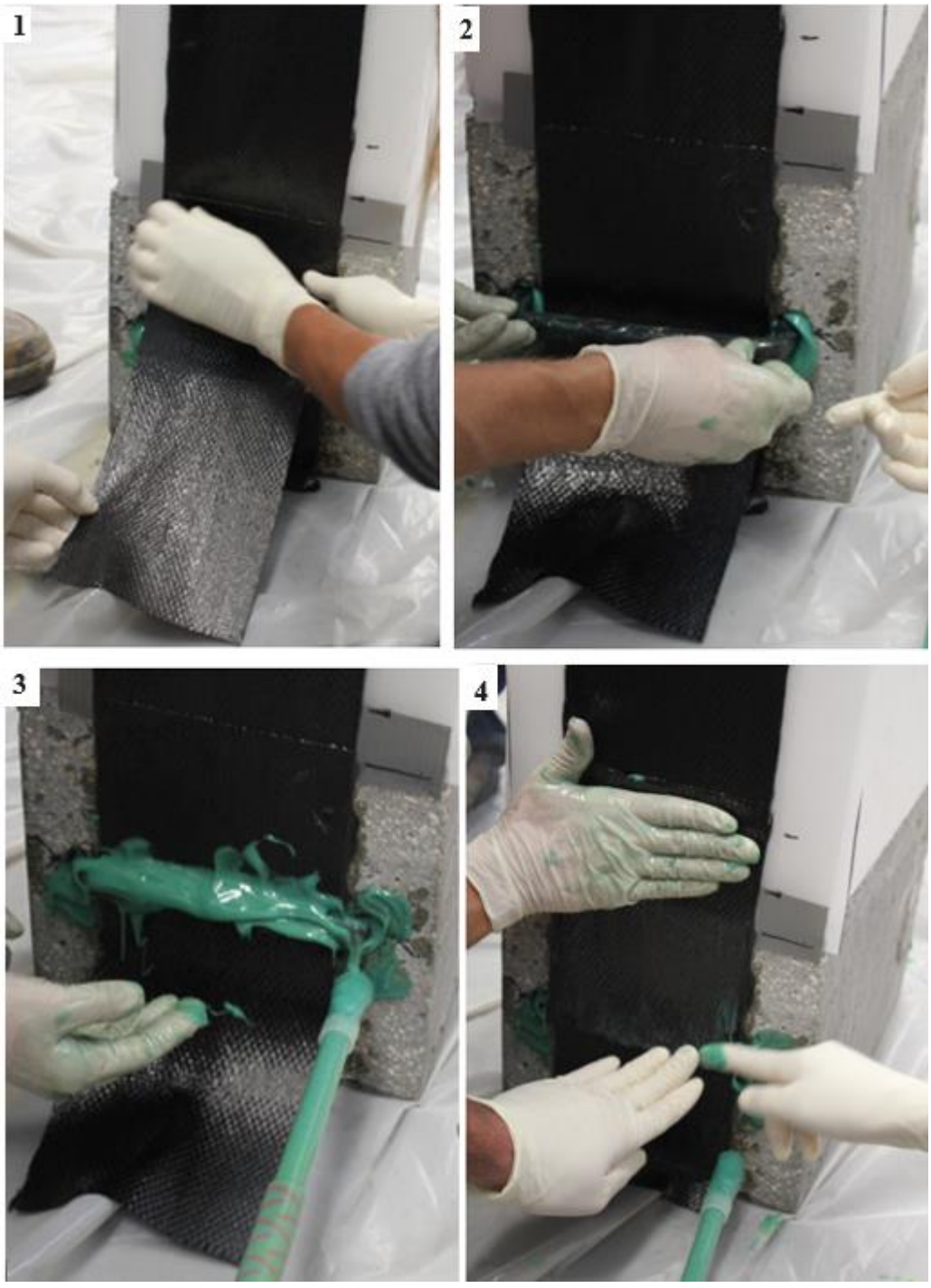

Figure 3.15 - CFRP Patch installation process

Anchor patches allow better force transfer from the CFRP sheet to the anchor, improving the resistance of the system on the side in which they are installed. This patch is oriented with fibers in the same direction of the fibers of the flexural sheet. Moreover, the choice of using an CFRP patch was made analyzing previous tests conducted, which shown partial delamination as failure mode; a patch was used also on spikes anchor's tests in order to catch more fibers to be able to redistribute stresses. So, it seemed reasonable borrowing it and applying a patch also for the staple anchor's tests.

Figure 3.16 - Round Staple (left) & Flat Staple (right) anchor final product

Figure 3.17 shows a 3D view of the whole structure composed by the concrete block + Carbon FRP laminate + Flat Staple anchor + Carbon FRP patch.

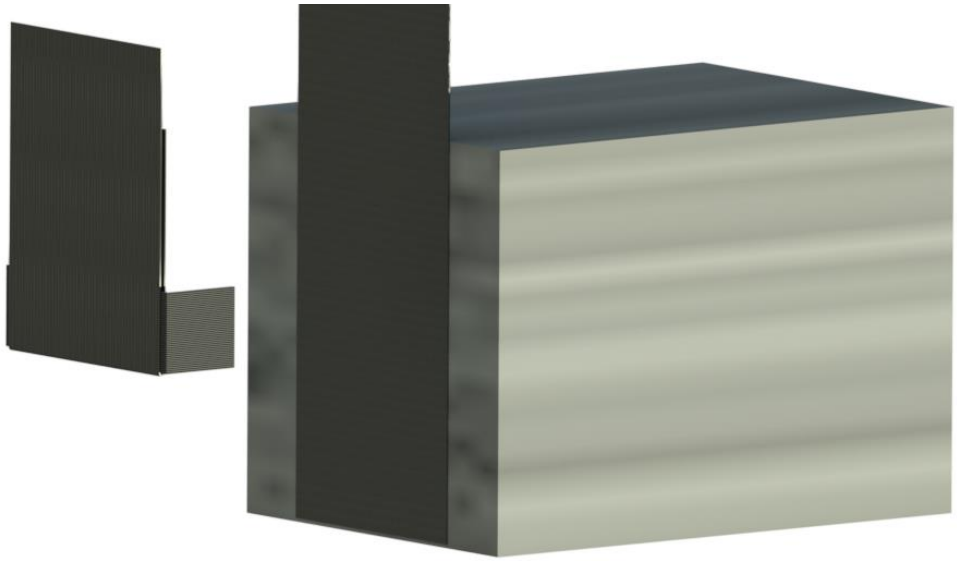

Figure 3.17 - 3D view of Concrete block + CFRP Sheet + Flat Staple Anchor + CFRP Patch

Figure 3.18 shows a 3D view of the Carbon FRP patch and Flat Staple anchor.

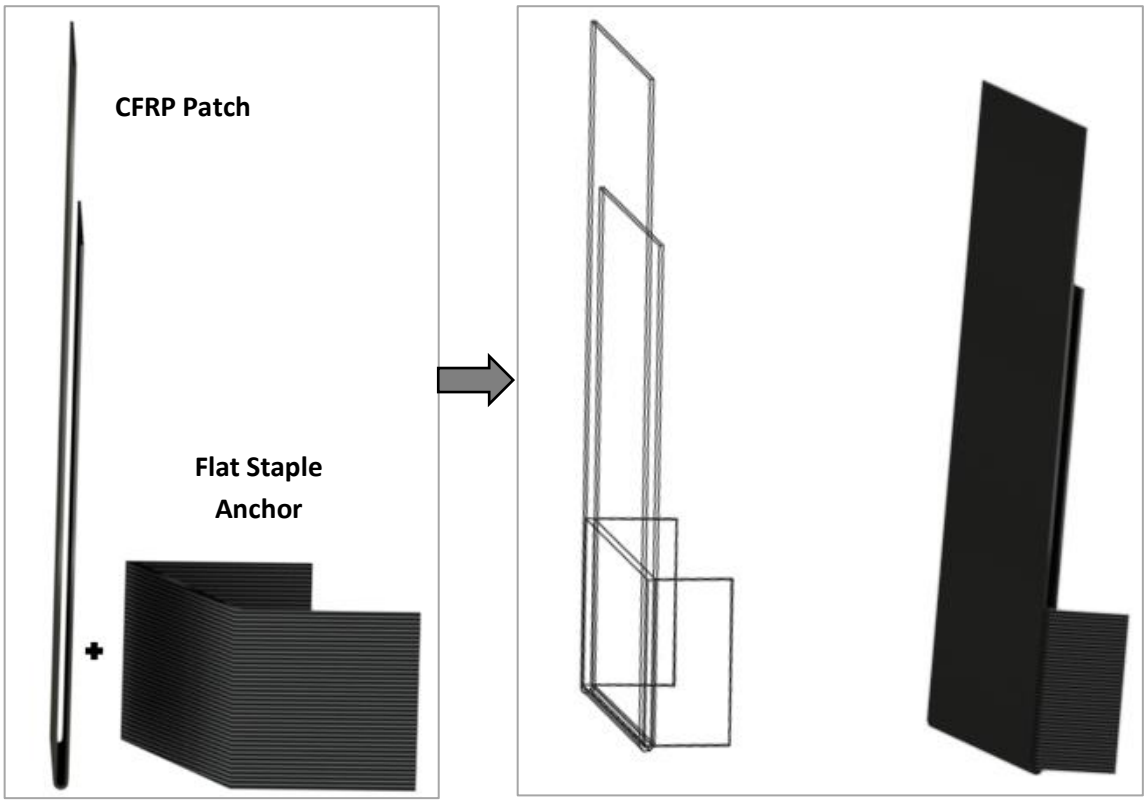

Figure 3.18 - 3D view of CFRP Patch and Flat Staple anchor

3.4 Test set-up

Due to symmetry and for better control of induced normal stresses, the double shear test is generally preferred over the single shear test. The specimens were arranged into two groups depending on the anchors used. The first group, consists of five specimens in which the FRP sheets were attached to the concrete substrate and anchored by Flat Staple anchors; the second group, consists of other five specimens in which the FRP sheets were attached to the concrete substrate and anchored by Round Staple anchors.

3.4.1 Instrumentation

The instrumentation used to perform the double shear test as shown in Figure 2.37 was:

- *Big rounded steel plate*, used to keep straight the CFRP sheet following the rounded shape.
- *Hydraulic jack*, used to apply load manually.
- *Load Cell*, used to measure the load.
- *Strain Gauges*, used to measure the strains.
- *Square steel plates*, used to create a "pyramid" shape in order to uniformly distribute the load.
- *DAQ (Data Acquisition)*, the system used to acquire data from the Load Cell and Strain Gauges.

Figure 3.19 - Instrumentation used to perform the Double Shear Test

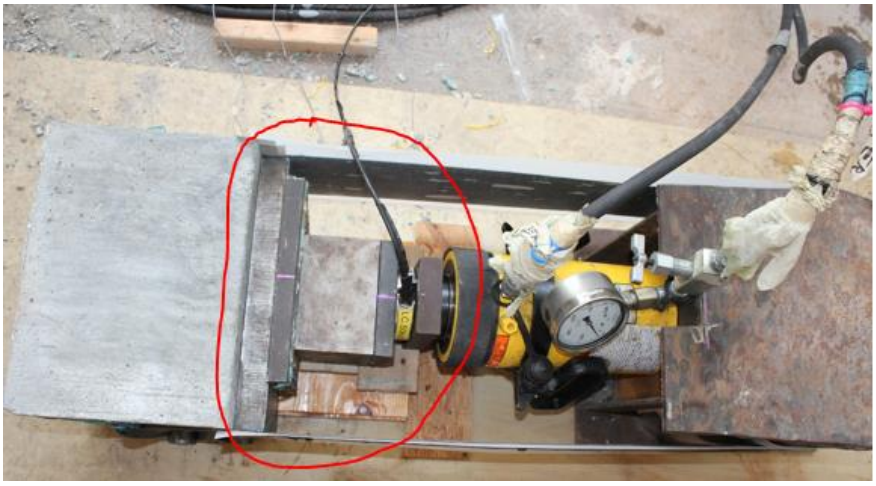

Figure 3.20 - Steel plates set with a "pyramid" shape

In the double shear test performed, the debonding force over the instrumented side of the block was evaluated as half of the applied peak load P. The following Figure 3.21 illustrates the approximated distribution of the loads in this test and the final set up of the test.

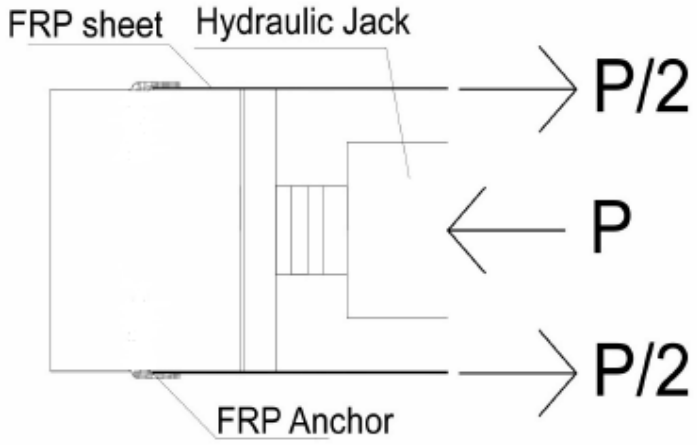

Figure 3.21 - Sketch of the approximated symmetric distribution of load

3.4.2 Strain gauges

The strain gauges were used to read the strain distribution in the CFRP sheet and patch giving interesting parameters of what is happening in terms of internal forces in front and behind the patch as explained in the next chapter.

The gauge is attached to the specimens thanks to a suitable adhesive and as the CFRP sheet is deformed, tension or compression, cause its electrical resistance to change. This resistance change is then related to the strain by the quantity known as the gauge factor.

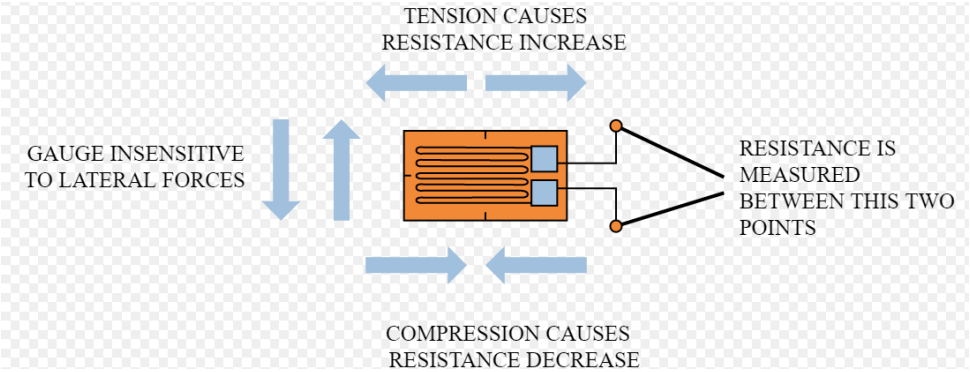

Figure 3.22 - Strain Gauge

Figure 3.23 - Box of a 6mm Strain Gauge

All those information (electrical resistance, gauge factor and gauge length) were carefully updated and calibrated before starting each specimen test in the data acquisition system, which records the strains.

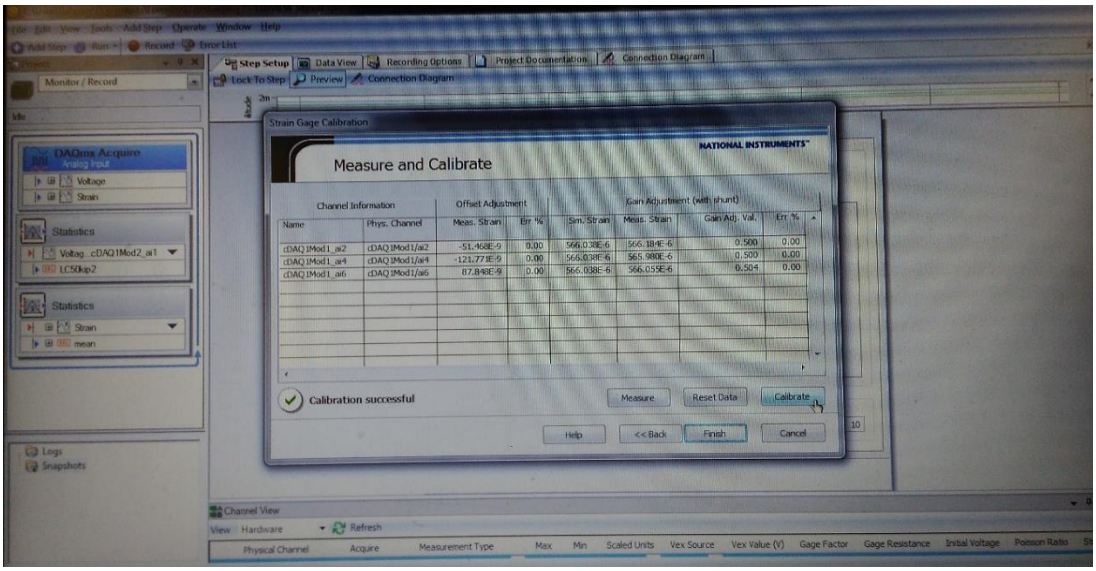

Figure 3.24 - Strain Gauge Calibration on DAQ

Electrical strain gauges of 6 mm length were used to instrument the specimens. They were placed on the surface of the CFRP sheets, in the same position for all the specimens both for Flat and Round staple anchors, as shown in Figure 3.25. The position of the strain gauges was decided depending on what we were looking for. They were place along the centerline of the FRP sheet. Identified with SG-A, SG-B and SG-C, they were positioned respectively: SG-A on the CFRP laminate, far from the anchor, precisely 5 inches far from the end of the CFRP patch, in order to evaluate the longitudinal strains of the laminate without the influence either of the patch or the anchor. SG-B were positioned just in front of the CFRP patch and SG-C were positioned on the patch in order to evaluate the strengthen given by the patch. No Strain Gauges were positioned along the width of the CFRP laminate considering the scrupulous attention paid on setting up all the testing specimens very straight in order to apply the load evenly over the FRP laminate width. Further discussion over strains are provided in the following chapter.

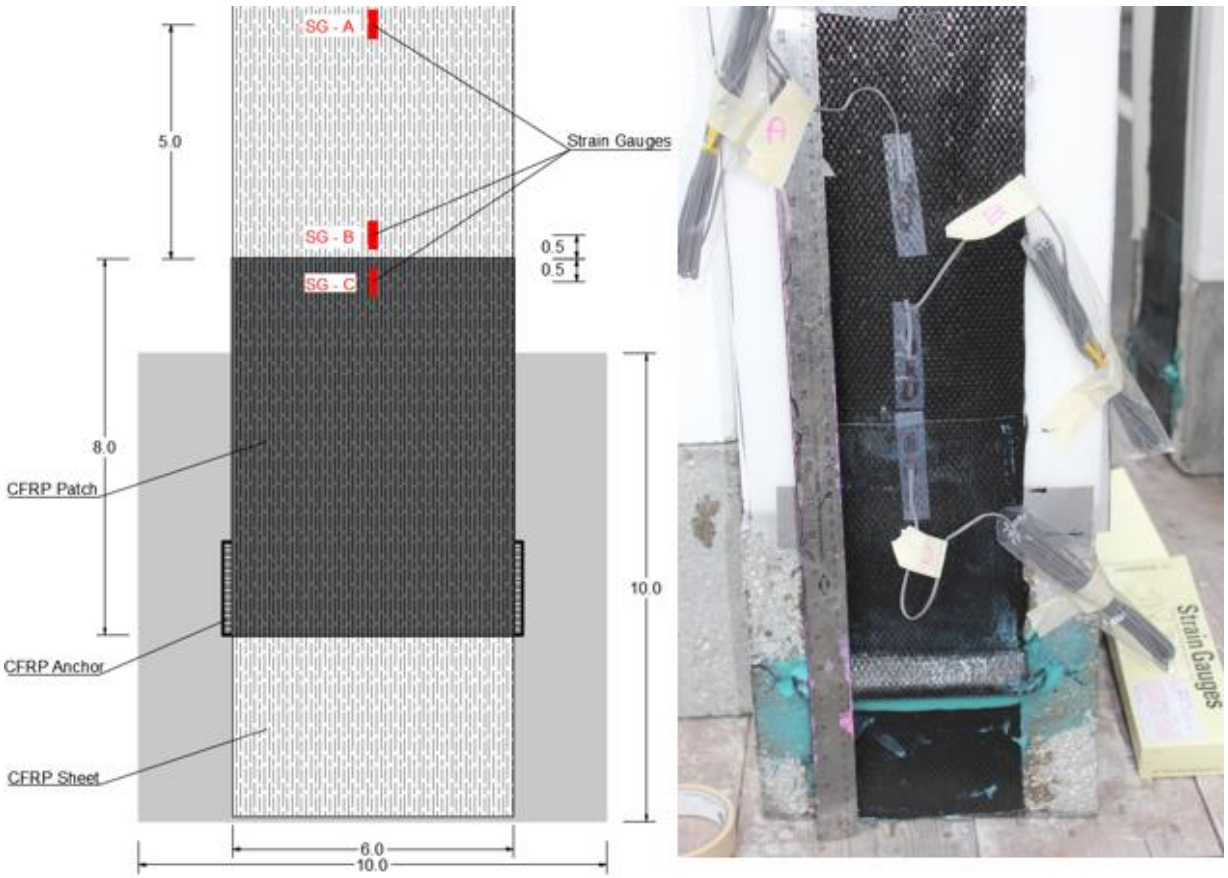

Figure 3.25 - Strain gauges' position on a specimen

3.4.3 Testing

Firstly, each specimen was careful positioned on a flat surface and proper leveled in order to have the CFRP sheet very straight and the load to be evenly applied.

Figure 3.26 - Specimen leveling

Secondly, the instrumentation (Strain Gauges and Load Cell) were connected to the DAQ. Then the double shear test was performed with the following test set-up procedure:

Figure 3.27 - Strain Gauges and Load Cell connection

After that, they were both calibrated as the following:

- Strain gauges' info: 6mm length, 120 ± 0.5 Ω resistance, 2.11% gauge factor.
- Load cell info: up to 50 kips (= 222 KN) of applied load.

Each specimen was pre-loaded to a load of 1-3 KN to allow the hydraulic jack to be engaged. The DAQ started recording the data from the very begging of the applied load; both the load and the displacement data were acquired and recorded every 0.1 seconds during the loading.

Figure 3.28 - Double Shear Test Set-up

The load was increased manually (by load control) at a rate of 0.3-0.4 KN/s. The load was then applied until the failure of the system occurred.

Figure 3.29 - Specimen failure at the end of the test

3.5 Material Properties

3.5.1 Concrete

According to ASTM C39 (2014), the characterization of the concrete used in this research was performed by a compression test on standardized concrete cylinders in order to find their compressive strength (f'c). A total of nine cylinders, obtained casting the concrete into plastic molds in accordance with ASTM C31 (2014), were tested. The test consists on applying a compressive axial load to molded cylinders (plane surfaces were provided on the ends of the cylinders by following the "Standard Practice for Capping" (ASTM C617, 2015)) at a rate which is within a prescribed range until failure occurs.

As a long-term observation, 3 different tests were run. After 14 days (half curing period) the first 3 specimens were tested. Then, other 3 specimens were tested after 21 days and finally after 28 days, period through which the concrete should have reached an almost stationary plafond, the 28-days-average will hence be the value used for design and matching purposes. Figure 3.30 illustrates the casting of the cylinders.

Figure 3.30 – Casting of the cylinders

Figure 3.31 shows the test set-up for the compression test performed with SATEC while Figure 3.32 illustrates the cylinder before and after the compression test, respectively.

Figure 3.31 - SATEC (Compression Test Machine)

All the specimens show a failure mode 3. As described in ASTM C39, failure mode 3 represent the rupture type in which columnar vertical cracking through both the ends and no well-formed cones are presented (see Figure 3.32).

Figure 3.32 - Specimen before (left) and after (right) the compression test

Table 3. summarizes the results obtained from each test: here, the diameter is presented in inches calculated at the mid span, top and bottom of the cylinder. Then, an average between

those values has been calculated. The area is the average cross-sectional area, based on the diameter's average. The peak load represents the maximum axial load reached by the machine during the test and f'c is the compressive strength. The compressive strength of the specimen (f'c) is calculated by dividing the maximum load reached during the test by the cross-sectional area of the specimen. Finally, based on the results in terms of compressive strength, the standard deviation (Sn) and the coefficient of variation (C.O.V.) are calculated.

In addition, during the casting of the concrete the Abrams Cone Slump Test was performed, following the guidelines provided from the ASTM C143-12. The ASTM C143-12 attests that for this test the slumps range should be from 2 to 8 inches to have a good workability of the fresh concrete. As shown in Figure 3.33, the obtained slump of the provided concrete was about 6 inches, which is clearly in this accepted range.

Figure 3.33 - Abrams Cone Slump Test

Cylindrical concrete specimen test results														
	Specimen ID	Date cast	Date tested	Diameter [inches]			Area [inches^2]	Diameter	Diameter [mm]	Area [mm^2]	Peak load [lbs]	Peak load [KN]	f'c [Mpa}	Failure mode
				Midspan	Top	Bottom		Average						
14 days after	_001	04.15.2016	04.29.2016	4.014	4.009	4.004	12.65449	4.009	101.8286	8143.842	104510	464.8836	57.08407	Type 3
	_002	04.15.2016	04.29.2016	4.046	4.032	4.019	12.85706	4.032333	102.4213	8238.916	103320	459.5903	55.78285	Type 3
	_003	04.15.2016	04.29.2016	4.051	4.052	4.033	12.88885	4.045333	102.7515	8292.125	109250	485.9682	58.60599	Type 3
	Average										*105693.33*	***470.15***	***57.16***	
	St deviation										*2561.44*	*11.39*	*1.15*	
	*Coefficient of variation (C.V) ((%)**										*2.42*	*2.42*	*2.02*	

Cylindrical concrete specimen test results														
	Specimen ID	Date cast	Date tested	Diameter [inches]			Area [inches^2]	Diameter	Diameter [mm]	Area [mm^2]	Peak load [lbs]	Peak load [KN]	f'c [Mpa}	Failure mode
				Midspan	Top	Bottom		Average						
21 days after	_001	04.15.2016	05.06.2016	4.013	4.038	4.009	12.64818	4.02	102.108	8188.594	114960	511.3676	62.44876	Type 3
	_002	04.15.2016	05.06.2017	4.012	4.056	4.044	12.64188	4.037333	102.5483	8259.361	114240	508.1648	61.52593	Type 3
	_003	04.15.2016	05.06.2018	4.032	4.057	4.045	12.76823	4.044667	102.7345	8289.392	98340	437.4381	52.77083	Type 3
	Average										*109180.00*	***485.66***	***58.92***	
	St deviation										*7670.67*	*34.12*	*4.36*	
	*Coefficient of variation (C.V) ((%)**										*7.03*	*7.03*	*7.40*	

Cylindrical concrete specimen test results														
	Specimen ID	Date cast	Date tested	Diameter [inches]			Area [inches^2]	Diameter	Diameter [mm]	Area [mm^2]	Peak load [lbs]	Peak load [KN]	f'c [Mpa}	Failure mode
				Midspan	Top	Bottom		Average						
28 days after	_001	04.15.2016	05.06.2016	3.998	4.058	4.029	12.5538	4.028333	102.3197	8222.578	116830	519.6857	63.20228	Type 3
	_002	04.15.2016	05.06.2017	4.011	4.054	4.027	12.63558	4.030667	102.3789	8232.107	116520	518.3068	62.96162	Type 3
	_003	04.15.2016	05.06.2018	4.011	4.051	4.008	12.63558	4.023333	102.1927	8202.179	98380	437.616	53.35363	Type 1
	Average										*110576.67*	***491.87***	***59.84***	
	St deviation										*8625.27*	*38.37*	*4.59*	
	*Coefficient of variation (C.V) ((%)**										*7.80*	*7.80*	*7.67*	

Table 3.1 - Compressive strength test results

The graphic in Figure 3.34 shows the trend and progress of the concrete curing after 14, 21 and 28 days.

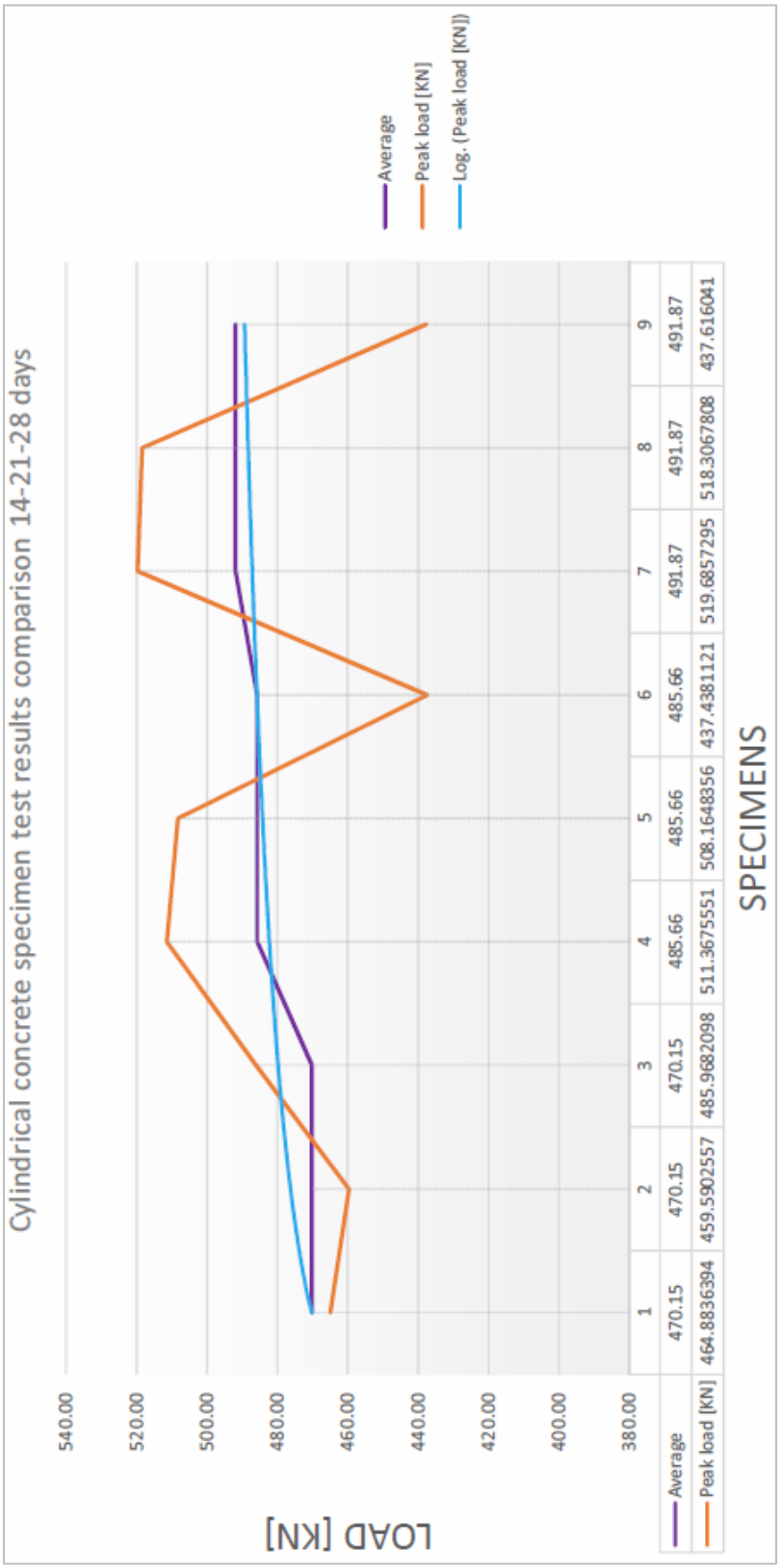

Figure 3.34 – Cylindrical concrete specimen test results comparison 14-21-28 days

Finally, the concrete tensile strength (f_t), elastic modulus (E_c) and shear modulus (G) were calculated from the following formulas:

$$f_t = k \cdot (f'_c)^n = 0.27 \cdot (59.84)^{\frac{2}{3}} = 4.13\ MPa \qquad \textit{(Neville, 2000)}$$

$$E_c = 4700 \cdot (f'_c)^{\frac{1}{2}} = 4700 \cdot (59.84)^{\frac{1}{2}} = 36357.47\ Mpa \qquad \textit{(ACI 318-14 Concrete, 2014)}$$

$$E_c = 2200 \cdot \left(\frac{(f'_c+8)}{10}\right)^{0.3} = 2200 \cdot \left(\frac{(59.84+8)}{10}\right)^{0.3} = 39072.25\ MPa \qquad \textit{(D.M., 2008)}$$

$$E_c = \frac{E}{2\cdot(1+\nu)} = \frac{39072.25}{2\cdot(1+0.2)} = 16280.1\ MPa$$

3.5.2 Carbon Fiber Reinforced Polymer Sheet

The CFRP material used to bond FRP materials to the test specimens, according to the specifications from the manufacturer (Structural Technologies), was V-Wrap C200 H. V-Wrap C200H is a unidirectional carbon fiber fabric with fiber oriented in the 0° direction. V-Wrap C200H system is field laminated using environmentally friendly, two-part 100% solids and high strength structural adhesives to form a carbon fiber reinforced polymer (CFRP) system used to reinforce structural elements.

Typical Data for V-Wrap C200H

Storage Conditions:	Store dry at 40°F – 90°F (4°C – 32°C)
Color:	Black
Primary Fiber Direction:	0° (unidirectional)
Weight:	17.7 oz/yd² (600 g/m²)
Shelf life:	10 years

Fiber Properties (Dry)

Tensile Strength:	700,000 psi (4,830 MPa)
Tensile Modulus:	33 x 10^6 psi (227,500 MPa)
Elongation:	2.1 %

Cured Laminate Properties	Average Values	Design Values*
Tensile Strength:	180,000 psi (1,240 MPa)	150,000 psi (1,034 MPa)
Modulus of Elasticity:	10.7 x 10^6 psi (73,770 MPa)	10.7 x 10^6 psi (73,770 MPa)
Elongation at Break:	1.7%	1.4%
Thickness:	0.04 in. (1.02 mm)	0.04 in. (1.02 mm)
Strength per Unit Width:	7,200 lbs/in. (1.26 kN/mm)	6,000 lbs/in. (1.05 kN/mm)

Figure 3.35 - Typical V-Wrap C200H properties

Higher values of ultimate strength and modulus of elasticity could be reach in case of wet fibers. The properties reached with the wet fibers refer to the case in which the fibers of the C200 H CFRP material are impregnated with the epoxy resin (V-Wrap 770 epoxy resin).

Wet fibers:

The CFRP impregnated sheet characterization was performed in the Structures and Material Laboratories at the University of Miami in compliance with ASTM D3039 (2008). Test details and a full material characterization can be found in the Certified Test Report Number R-5.10_STe_ESR-3606.5 (Revision 5, March 2015).

Specimen	A_{exp}		A_{nom}		P^{max}		F^{tu}_{exp}		F^{tu}_{nom}		E^{chord}		ε_u	Mode of
ID	mm^2	in^2	mm^2	in^2	kN	lbs	MPa	ksi	MPa	ksi	GPa	Msi	%	failure*
STe_C277_TNS_CC_00_001	22.528	0.035	26.503	0.041	37.64	8458	1670.1	242.22	1419.6	205.89	79.12	11.48	1.79	XGM
STe_C277_TNS_CC_00_002	23.806	0.037	26.452	0.041	34.35	7720	1442.5	209.21	1298.2	188.29	72.71	10.55	1.78	XGM
STe_C277_TNS_CC_00_003	22.747	0.035	26.761	0.041	34.37	7724	1510.4	219.07	1283.9	186.21	74.64	10.83	1.72	XGM
STe_C277_TNS_CC_00_004	23.805	0.037	25.058	0.039	35.17	7903	1476.8	214.19	1402.9	203.48	79.94	11.60	1.75	SGM
STe_C277_TNS_CC_00_005	22.155	0.034	26.064	0.040	32.22	7241	1453.8	210.86	1235.8	179.23	72.09	10.46	1.71	XGM
STe_C277_TNS_CC_00_006	27.097	0.042	25.806	0.040	35.05	7877	1293.1	187.55	1357.8	196.93	74.36	10.79	1.83	SGM
STe_C277_TNS_CC_00_007	23.388	0.036	25.987	0.040	33.50	7529	1431.9	207.69	1288.7	186.92	81.19	11.78	1.59	XGM
STe_C277_TNS_CC_00_008	24.295	0.038	25.574	0.040	33.53	7534	1379.4	200.06	1310.4	190.06	72.02	10.45	1.82	SGM
STe_C277_TNS_CC_00_009	21.077	0.033	25.548	0.040	33.16	7452	1572.7	228.10	1297.5	188.18	71.81	10.42	1.81	XGM
STe_C277_TNS_CC_00_010	21.017	0.033	26.271	0.041	35.59	7997	1692.6	245.49	1354.1	196.39	69.68	10.11	1.94	SGM
STe_C277_TNS_CC_00_011	21.892	0.034	25.755	0.040	37.07	8331	1692.8	245.52	1438.9	208.69	76.91	11.16	1.87	SGM
STe_C277_TNS_CC_00_012	24.614	0.038	25.910	0.040	37.45	8415	1520.7	220.57	1444.7	209.54	75.12	10.90	1.92	SGM
STe_C277_TNS_CC_00_013	23.919	0.037	25.858	0.040	35.67	8015	1490.6	216.19	1378.8	199.98	79.74	11.57	1.73	XGM
STe_C277_TNS_CC_00_014	22.694	0.035	25.935	0.040	34.27	7700	1509.3	218.91	1320.6	191.54	72.09	10.46	1.83	XGM
STe_C277_TNS_CC_00_015	23.752	0.037	25.677	0.040	31.48	7074	1324.8	192.15	1225.5	177.74	72.57	10.53	1.69	XGM
STe_C277_TNS_CC_00_016	24.516	0.038	25.806	0.040	36.72	8251	1497.1	217.13	1422.2	206.28	72.36	10.50	1.96	XGM
STe_C277_TNS_CC_00_017	22.016	0.034	25.161	0.039	33.95	7630	1541.6	223.59	1348.9	195.64	73.54	10.67	1.83	SGM
STe_C277_TNS_CC_00_018	23.756	0.037	25.006	0.039	34.18	7682	1438.4	208.63	1366.5	198.19	75.05	10.89	1.82	SGM
STe_C277_TNS_CC_00_019	23.295	0.036	25.884	0.040	32.67	7341	1401.8	203.31	1261.6	182.98	73.81	10.71	1.71	XGM
STe_C277_TNS_CC_00_020	24.614	0.038	25.910	0.040	34.49	7750	1400.6	203.13	1330.5	192.98	73.05	10.60	1.82	XGM
AVERAGE	23.349	0.036	25.846	0.040	34.63	7781	1487.0	215.68	1339.4	194.26	74.59	10.82	1.80	
ST.DEV.	1.414	0.002	0.453	0.001	1.70	382	86.3	12.51	65.4	9.49	3.19	0.46	0.09	
C.O.V. (%)	6.1	6.1	1.8	1.8	4.9	4.9	5.8	5.8	4.9	4.9	4.3	4.3	5.1	

Figure 3.36 - Experimental V-Wrap C200H properties

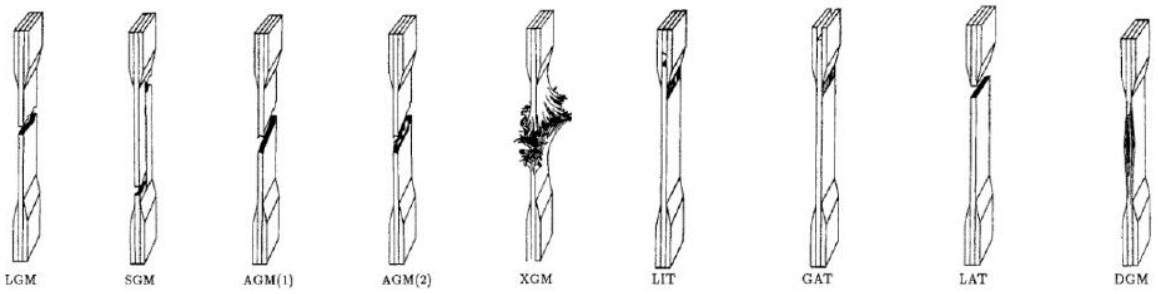

Figure 3.37 - Failure modes from ASTM D3039 (2008)

It is important to underline that the material is one directional and, in both cases of dry and wet configuration, it has very small tensile capacity in the transverse fiber direction. Also, the wet fibers avoid intensifications or different stresses distribution along the CFRP sheet.

Figure 3.38 shows the difference in terms of stress-strain between the dry and wet fibers configuration.

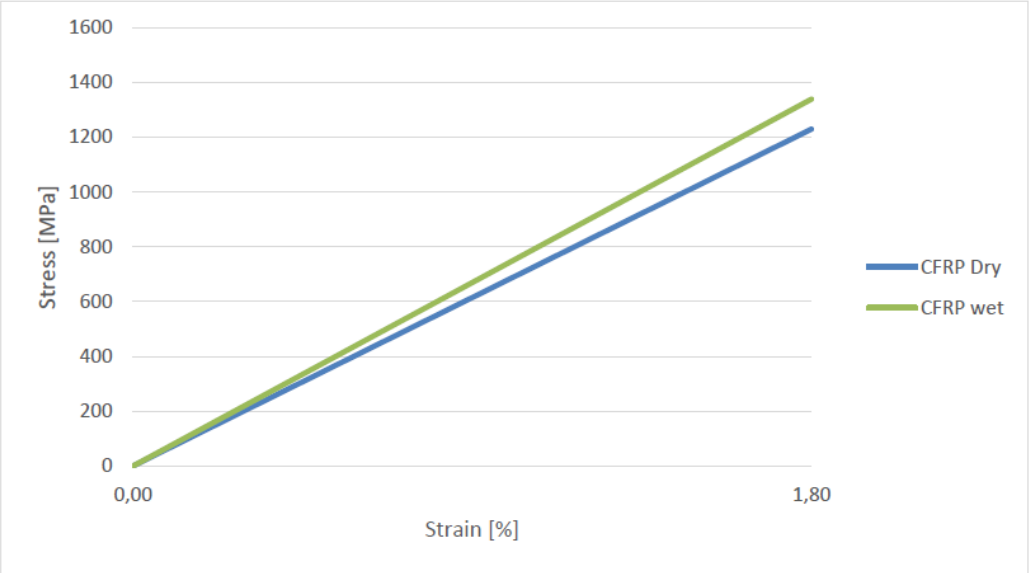

Figure 3.38 - Stress/Strain curves - CFRP Dry/Wet

3.5.3 Epoxy

The resin used to bond CFRP sheets to specimens, according to specifications from the manufacturer (Structural Technologies), was V-Wrap 770 Epoxy Adhesive (a liquid epoxy), while the one used to apply the anchors over the CFRP sheet into the concrete holes according to specifications from the manufacturer (Fortress Stabilization Systems) was the Fortress 4020 Hardened Hi Modulus Epoxy Gel (a denser epoxy).

V-Wrap 770 is a two-part, 100% solids, epoxy for high strength composite bonding applications. V-Wrap 770 matrix material is combined with V-Wrap carbon and glass fabrics to provide a wet-layup composite for strengthening of structural members. It is formulated to provide high elongation to optimize properties of the V-Wrap composite systems. It provides a long working time for application, with no offensive odorV-Wrap 770 is an environmentally friendly product with no Volatile Organic Compounds (VOC) or solvents. V-Wrap 770 is a multi-use epoxy that performs as a primer, tack coat/putty, and saturating resin for the V-Wrap carbon and glass fiber systems. Fumed silica may be added to thicken the resin. The maximum ratio by volume is 1.5 of fumed silica to 1 part of resin.

Epoxies are different from polyester resins, since they are cured by an 'hardener' rather than a catalyst. The hardener, often an amine, is added in order to cure the epoxy. Both the materials take place in the chemical reaction. The chemistry of this reaction means that there are usually two epoxy sites binding to each amine site. This forms a complex three-dimensional molecular structure.

In order to have a complete reaction it is important to pay attention on the mixing ratio; if amine and epoxy are not mixed together in the correct ratio, unreacted epoxy or hardener will remain inside the matrix. This affects the final properties of the material after the curing period. That is why every company that produces epoxy resins provides the precise mixing ratio (by weight or by volume). V-Wrap 770 Epoxy used is shown in Figure 3.39.

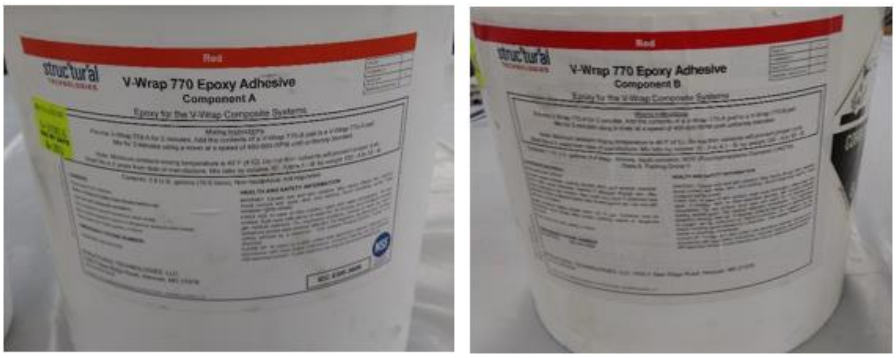

Figure 3.39 - V-Wrap 770 Epoxy

Mix ratio: Premix Part A for 2 minutes. Add the full contents of Part B pail to the full contents of Part A pail, or use equal fractions of each pail. Blend Part A and Part B with a mechanical mixer for 3 minutes until uniformly blended.

Figure 3.40 shows a summary of the typical properties of the epoxy used in this research.

Physical Properties[1]:	
Tensile Strength (ASTM D638):	8,800psi (60.7 MPa)
Tensile Modulus (ASTM D638):	400,000 psi (2,760 MPa)
Elongation at Break (ASTM D638):	4.4%
Flexural Strength (ASTM D790):	13,780 psi (95 MPa)
Flexural Modulus (ASTM D790):	380,000 psi (2,620 MPa)
Compressive Strength (ASTM D695):	12,450 psi (85.8 MPa)
Compressive Modulus (ASTM D695):	387,000 psi (2,670 MPa)
Tg (ASTM D4065):	180°F (82°C)
Density:	
Mixed Product	9.17 lbs/gal (1.11 kg/L)
Part A	9.7 lbs/gal (1.16 kg/L)
Part B	7.9 lbs/gal (0.95 kg/L)
VOC Content (ASTM D2369):	0% VOC

(1) Curing schedule: 72 hours post cure at 140°F (60°C)

Figure 3.40 – Typical V-Wrap 770 Epoxy Physical Properties

The Fortress 4020 epoxy is a specially designed true gel. It borrows marine technology bonding capabilities for carbon fiber, which is one of the hardest substrates to bond to. It combines a viscosity of paste and the wetting capacity of a low viscosity resin. It will cure in the presence of water, even under water. It is manufactured in a process that provides for minimal air entrapment. The gel and cure times are affected by ambient temperature and epoxy mass, or glue line thickness. Curing data is based on 72°F (22°C) ambient temperature. Warmer temperatures and a larger mass will increase cure speed, reducing cure time. Cure time is reduced by approximately one half with every 18°F (10°C) increase in temperature. A smaller mass or cooler temperature will reduce the cure speed, increasing cure time. Always dispense adhesive at or above 70°F to assure the proper mix ratio. Fortress 4020 Epoxy used is shown in Figure 3.41.

Figure 3.41 - Fortress 4020 Fast Epoxy Hi-Mod Gel & the specific epoxy gun working with compressed air

Figure 3.42 shows a summary of the typical properties of the hardened used in this research.

HANDLING CHARACTERISTICS	
MIX RATIO(Resin: Hardener by weight)	2.12:1 Do not use ratio by weight in Product Data Sheet
MIX RATIO(Resin: Hardener by volume)	2.0:1
MIX DENSITY(lb/gal)	9.3
POT LIFE OF 70ml@ 72°F ASTM C-881	10 mm
WORKING TIME (1/2" bead)	20 mm
CLAMPS OFF CURE TIME (1/16" bond line)@ 75°F	2 hr
MINIMUM CURE TEMPERATURE	45°F*

*The product will cure at temperatures as low as 45°F; however,keep cartridges at 70°F or above when dispensing.

CURED CHARACTERISTICS	
TENSILE STRENGTH (psi)ASTM D-638	7,100
TENSILE ELONGATION (%)ASTM D-638	4.0 min.
TENSILE MODULUS (x 103 psi)ASTM D-638	3.80
FLEXURAL STRENGTH (psi)ASTM D-790	12,500
FLEXURAL MODULUS(x 105 psi)ASTM D-790	3.75
HARDNESS (Shore D)	
1 DAY ASTM D-2240	78
2 WEEKS ASTM D-2240	85
COMPRESSION YIELD(psi)2 WEEKS ASTM D-695	10,720
ONSET OF TgBY DSC	125°F
HEAT DEFLECTION TEMPERATURE ASTM D-648	140°F

Typical values,not to be construed as specifications.

Figure 3.42 - Typical Fortress 4020 Epoxy Properties

Among the various anchor system presented in chapter 1.3, a more detailed description of the ones used for this research (Flat & Round Staple Anchor) is provided.

3.5.4 Flat Staple Anchor

The flat staple anchors are called so thanks to their shape that literally recall the shape of a staple. They are provided as prefabricated elements formed by strands of carbon fibers that are inserted into epoxy filled holes in the concrete, and an external part that is also impregnated and connected externally to the bonded FRP laminate. They appear in different shapes and sizes and they can be installed in different ways but they share the same aim: enhance the bond of externally bonded FRP laminates into concrete. Also, the flat staple anchors are very competitive thanks to their low material cost of fabrication.

The Table 3.2 describes the carbon fibers' characteristics, which the flat staple (but also the round staple) anchors are made of.

TYPICAL PROPERTIES	SI	US
Tensile Strength	1,850 MPa	268 ksi
Tensile Modulus	130 GPa	18.9 msi
Compressive Strength	1,320 MPa	191 ksi
Compressive Modulus	125 GPa	18.1 msi
Interlaminer Shear Strength	70 MPa	10 ksi
Glass Translation Temperature (Tg,G")	120°C	248°F

Table 3.2 - Carbon Fiber's characteristics of a Flat Staple

Figure 3.43 shows a sample and a 3D view of a flat staple anchor with the indication of the fibers direction.

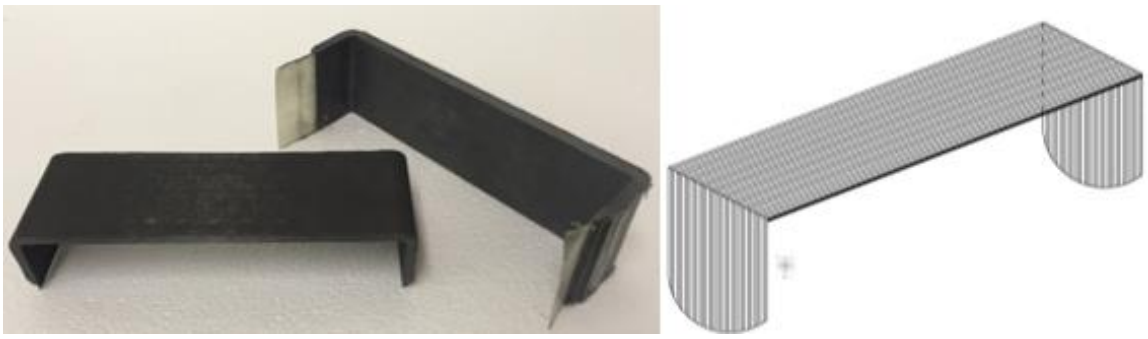

Figure 3.43 – Sample & 3D view of a Flat Staple Anchor

The geometry used, as shown in Figure 3.44, was: 6” (152 mm) long, 2” (50.8 mm) width and 1” (25.4 mm) depth.

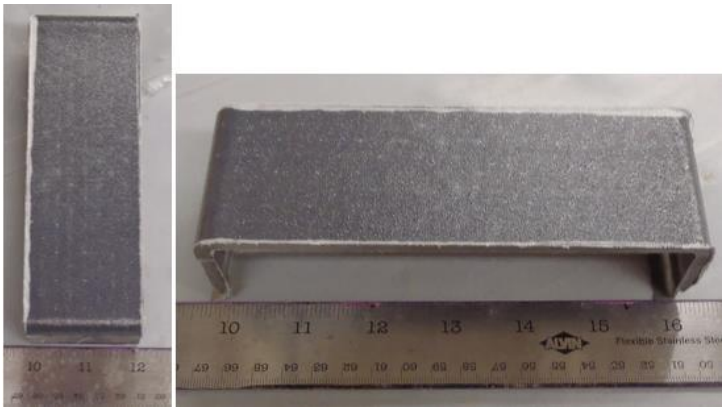

Figure 3.44 - Flat Staple Anchor's Dimension

3.5.5 Round Staple Anchor

The round staple anchors are called so thanks to their rounded shape. Again, the unidirectional fibers of the anchor are aligned in a longitudinal way to the flexural FRP sheet, covered by an epoxy layer that keeps the fibers together.

An improved shape of the Round Staple anchors was used for this research: the under part of the anchor is not anymore rounded but it is flat, increasing the contact area with the FRP laminate; the upper part of the anchor is no more rounded but elliptical in order to prevent the formation of air bubbles in between the folded part of the flexural FRP sheet over the anchor and the anchor itself. Also, this shape allows the squeezed epoxy in excess to come out laterally, by the legs sides of the anchor. Finally, many fibers were concentrated on the bend radius, improving the resistance in this location, where the stresses are more concentrated. The following sketch in Figure 3.45 represents the shape of a round staple anchor.

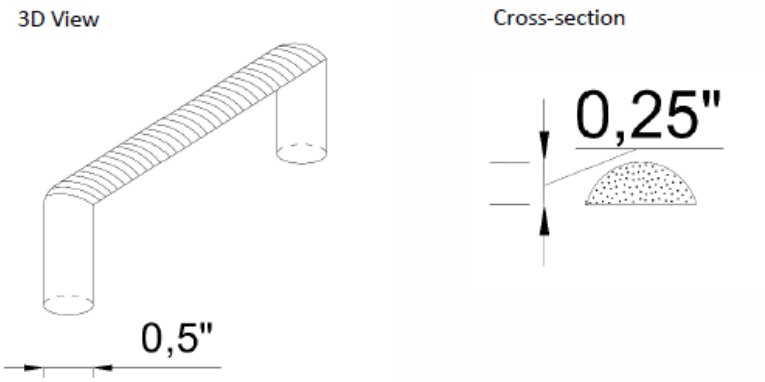

Figure 3.45 - 3D view and cross section of the Round Staple anchor

The geometry used, as shown in Figure 3.46, was: 7” (177.8 mm) long and 2” (50.8 mm) depth.

Figure 3.46 - Round Staple Anchor's Dimension

The picture in Figure 3.47 shows a comparison between the Flat and the Round Staple anchors.

Figure 3.47 - Flat vs Round Staple anchor

3.6 Quality Control

A proper surface preparation is required in order to guarantee a good concrete-sheet adherence to fully develop the system's strength. Beside the mechanical behavior of the system, the durability issues coming along an improper installation are the most critical aspect, making inspection an essential step in real-case applications.

Among the standard inspection method, knocking on the sheet's surface with a hammer, in order to spot eventual voids, is the most commonly employed on the field. Clearly is a non-systematic solution, with the advantages of being inexpensive and easily performable.

A slightly more expensive and onerous solution is proposed, coming with the advantage of guaranteeing a systematic inspection of the installation and allowing an easy detection and documentation of the eventual voids. Thermal analysis instruments are used to measure a variety of physical and chemical changes, including fusion, transition, crystallization, expansion, contraction, decomposition, and combustion, while the sample is heated or cooled. Typical analysis methods include DSC, TGA, and TMA, which are effective for evaluating the thermal properties of thermoplastic resins, thermosetting resins, and composite materials.

An inspection was performed using the thermal camera after the fiber sheet was uniformly heated with a heat-gun. The voids appear sensibly warmer than the surrounding properly-bonded zones. Here it is possible to notice how the thermal camera revealed a uniform surface meaning of a good surface preparation performed. As expected, voids are mostly concentered along the edges of the anchors as shown in Figure 3.48. The same solution was used in thesis developed last year (Cadenazzi & Rossini, 2016).

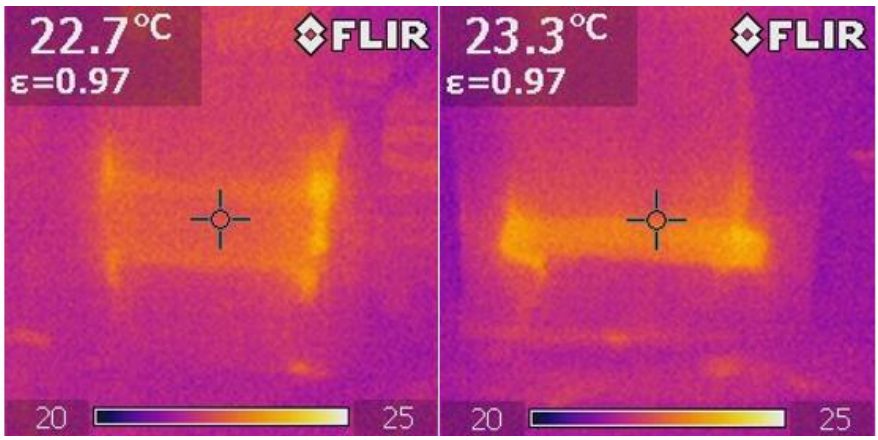

Figure 3.48 - Thermal Camera Inspection on Flat Staple (left) and Round Staple (right) anchor specimens

This research is based on the investigation about the improvement of the Staple anchors. The decision of using Flat and Round staple anchors to improve instead of the most used, so far, spikes anchors was based on the following reasons:

- The 2-inches anchor outclasses the spikes 60 degrees' fan opening in terms of peak load, strain interpretation and type of rupture. Moreover, the results are very close between the 2-inches flat staple anchors and the 90 degrees' fan opening of spikes anchors, but the big disadvantage of the spike anchors is that of not distribute the stresses evenly all along the FRP width (Cadenazzi, 2016).
- Regarding the round staples, the double round staple configuration is the preferred one (Cadenazzi, 2016). In fact, with an ideal rupture type and a uniform strain distribution it reaches high value of peak loads (in between the 2-inches and the 3-inches flat staple anchors). However, the shape of the round staples, lately, was improved since the last research on it, so, as will be shown in the following paragraphs, a single configuration with the same new installation method used for the Flat Staple anchors is used successfully in this research.

A comparison of the old anchors peak loads is provided in order to summarize the results obtained in previous researches (Cadenazzi, 2016).

Anchor's type	Anchor's Configuration	Peak Load [KN]
Spike anchors	60 degrees fan opening	57,8
	90 degrees fan opening	66,38
Flat staple anchors	1 in. width – 1 in. depth	57,35
	2 in. width - 1 in. depth	62,21
	3 in. width - 1 in. depth	66,42
Round staple anchors	Single conf. - 1 in. depth	52,62
	Double conf. - 1 in. depth	65,61

Table 3.3 - Anchors' Peak Load Comparison

CHAPTER 4

Experimental Program 1:
Test Results

The previous chapter covers all the aspects of the experimental campaign that was carried out, from the materials used to the FRP installation and test set-up.

The specimens were tested to examine the performance of a new installation method for two types of anchors, the flat staple and the round staple anchors, in order to understand the improvements in terms of distribution of strains, stresses and peak loads.

This chapter is divided into four main sections according to the main studies developed in this research. The first section presents a full analysis of the results obtained from the *flat staple* anchorage system. The second section is dedicated to the results deduced from testing the *round staple* anchorage system. Also, in these two sections a comparison with the results obtained in previous research (Cadenazzi, 2016) is provided to better understand the improvement of the new installation method. A detailed description of the failure modes observed during the experimental campaign is given in the third section. The last section wants to be a results recap and recommendation for future studies.

4.1 Test 1 – Flat Staples

The following Table 4.1 summarizes the results in terms of peak loads, increases of the load (in percentage) with respect to the benchmark, rupture side and type, measured strains in the CFRP sheet, failure modes and pressure at the peak load. The Peak Load P represents the maximum load applied by the hydraulic jack during the tests.

In order to allow the reader better understanding the numbers hereinafter shown, some old results are provided as comparison with the new ones. The first 2 blocks of the table are referred respectively to “benchmarks”, as meaning of blocks tested without any anchor, and “Flat Staples (old)” as meaning of the old test performed in previous research (Cadenazzi, 2016). While the last part of the table, “Flat Staples (**new**)” is referred to the results obtained in this dissertation.

It is very important to remind that, for all the tests run for this research, the side without strain gauges was strengthened as shown in the previous Figure 3.12 in order to make each specimen fail on the other side provided with the instrumentation of the strain gauges. For this reason, in Table 4.1, there is also a column “rupture side” which explain if the rupture occurred on the expected left side (the instrumented one) or on the reinforced side (on the right side, the one not instrumented).

Table 4.1 - Flat Staple Anchors' Summary

Double Shear Test (WET FRP) - FLAT STAPLES (2" Width - 1" Depth)

	Date	Specimen ID	Anchor's dimensions	Peak Load [pounds]	Peak Load [Kips]	P [KN]	P/2 [KN]	Increase in Peak Load [%]	Rupture Side	Rupture Type	Strains in % at peak load SG1 [%]	SG2 [%]	SG3 [%]	SG4 [%]	SG5 [%]
BENCHMARKS	06.01.2016	T2_BM_001	No anchor	13041.25	13.04	58.01	29.01	-19.68%	Left (instrum.side)	A	0.340	0.276	0.302	0.530	0.021
	06.07.2016	T2_BM_002	No anchor	17083.74	17.03	75.77	37.88	4.91%	Right (not instrum. side)	A	x	0.402	0.482	0.441	0.005
	06.27.2016	T2_BM_003	No anchor	18634.67	18.63	82.89	41.45	14.77%	Right(not instrum. side)	A	x	x	x	x	x
			Average	16236.55	16.24	72.22	36.11				0.340	0.339	0.392	0.485	0.013
			Standard deviation	2352.05	2.35	8.88	4.44	0.00%			0.000	0.063	0.090	0.044	0.008
			C.V. [%]	14.49	2.35	12.29	12.29				0.000	0.186	22.863	9.164	59.988
FLAT STAPLES (OLD)	06.14.2016	T2_FS_2W_001	2"W - 1"D	24528.42	24.63	109.55	54.78	51.69%	Left (instrum. side)	B	0.293	0.878	0.654	0.584	0.082
	06.27.2016	T2_FS_2W_002	2"W - 1"D	30117.59	30.12	133.97	66.98	85.49%	Left (instrum. side)	C/F	0.245	0.379	0.677	0.559	x
	06.28.2016	T2_FS_2W_003	2"W - 1"D	29169.54	29.17	129.75	64.88	79.65%	Left (instrum. side)	C/F	x	x	x	x	x
			Average	27971.85	27.97	124.42	62.21				0.269	0.629	0.665	0.571	0.082
			Standard deviation	2395.63	2.40	10.66	5.33	72.28%							
			C.V. [%]	8.56	2.40	8.56	8.56								

	Date	Specimen ID	Anchor's dimensions	Peak Load [pounds]	Peak Load [Kips]	P [KN]	P/2 [KN]	Increase in Peak Load [%]	Rupture Side	Rupture Type	Strains in % at peak load SG-A [%]	SG-B [%]	SG-C [%]	Pressure at peak load [psi]
FLAT STAPLES (NEW)	10.13.2016	NEW_FS_2W_001	2"W - 1"D	34479.52	34.48	153.37	76.69	112.36%	Left (instrum. side)	F	0.651	0.478	0.308	3900
	10.14.2016	NEW_FS_2W_002	2"W - 1"D	43131.06	43.13	191.86	95.93	165.64%	Left (instrum. side)	D/E	0.709	0.466	0.375	4000
	10.14.2016	NEW_FS_2W_003	2"W - 1"D	45927.0313	45.93	204.29	102.15	182.86%	Left (instrum. side)	F	1.025	0.304	0.180	4300
	10.14.2016	NEW_FS_2W_004	2"W - 1"D	41411.55	41.41	184.21	92.10	155.05%	Left (instrum. side)	F	0.771	0.655	0.126	4000
	~~10.14.2016~~	~~NEW_FS_2W_005~~	~~2"W - 1"D~~	~~22963.156~~	~~22.96~~	~~102.15~~	~~51.07~~	~~41.43%~~	~~Left (instrum. side)~~	~~D/E~~	~~1.179~~	~~0.765~~	~~0.259~~	~~4000~~
			Average	41237.29	41.24	183.43	91.72				0.789	0.476	0.246	
			Standard deviation	4221.31	4.22	18.78	9.39	153.98%						
			C.V. [%]	10.24	4.22	10.24	10.24							

OLD CONFIGURATION

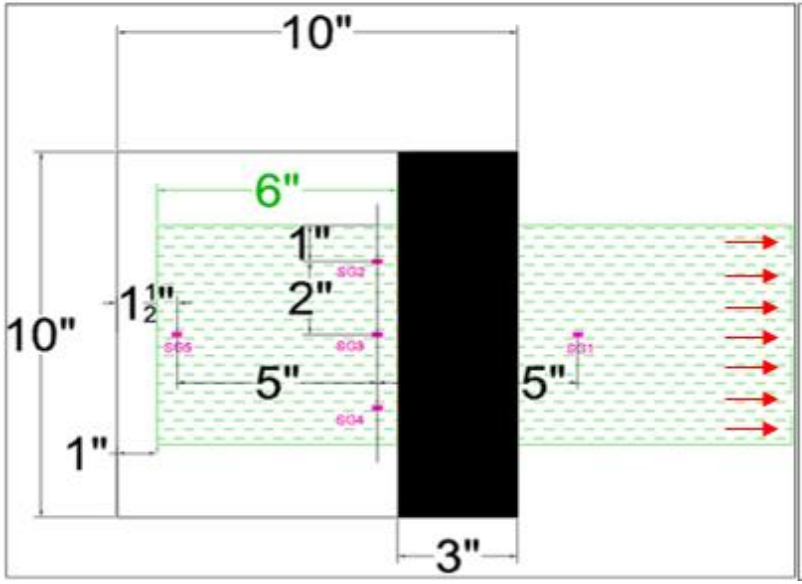

NEW CONFIGURATION

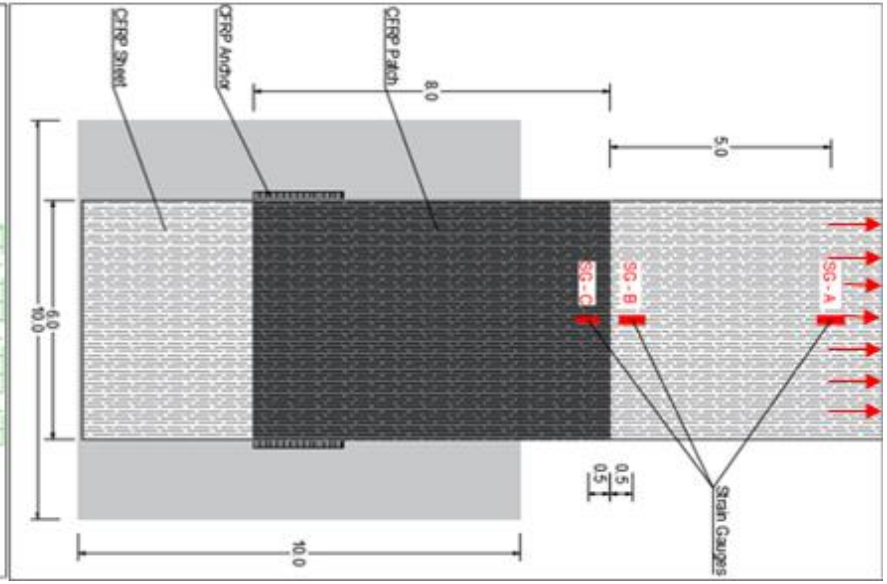

It is worth noting that the specimen "NEW_FS_2W_005" was discarded due to an improper installation; in fact, the premature failure, at a very low peak load if compared with the other specimens, was due to a no perfect positioning of the CFRP sheet, causing that the load was not be evenly applied. So, the load was not applied straight, concentrated to a side of the anchor, inducing the rupture of the anchor on its leg.

While characterizing the anchor resistance in terms of load, we must refer to the load identified as P/2 because this represents the load applied to one side. Figure 4.1 represents the average in terms of peak loads reached by the specimens.

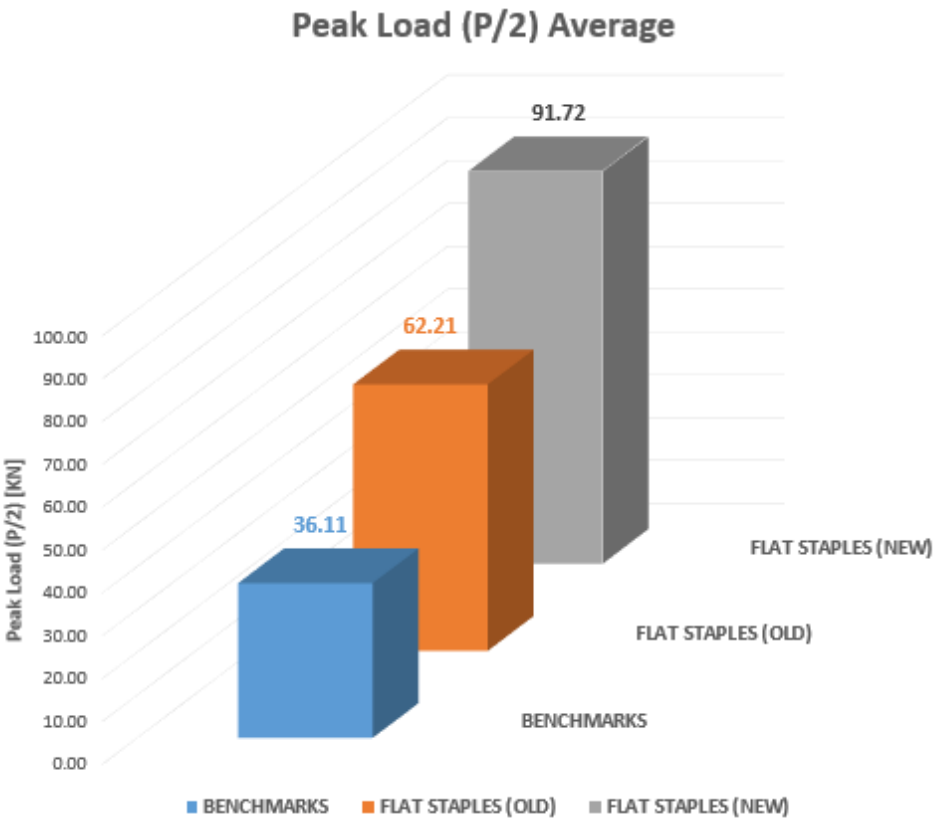

Figure 4.1 - Peak load's average (P/2) – Flat Staple Anchors

As the reader can easily understand, the Flat Staple anchors installed with the new method are much more effective comparing with the old method; in fact, the peak load increased from 62.21 KN to 91.72 KN. Figure 4.2 shows the increase in percentage reached by the average of the types of anchor system installed.

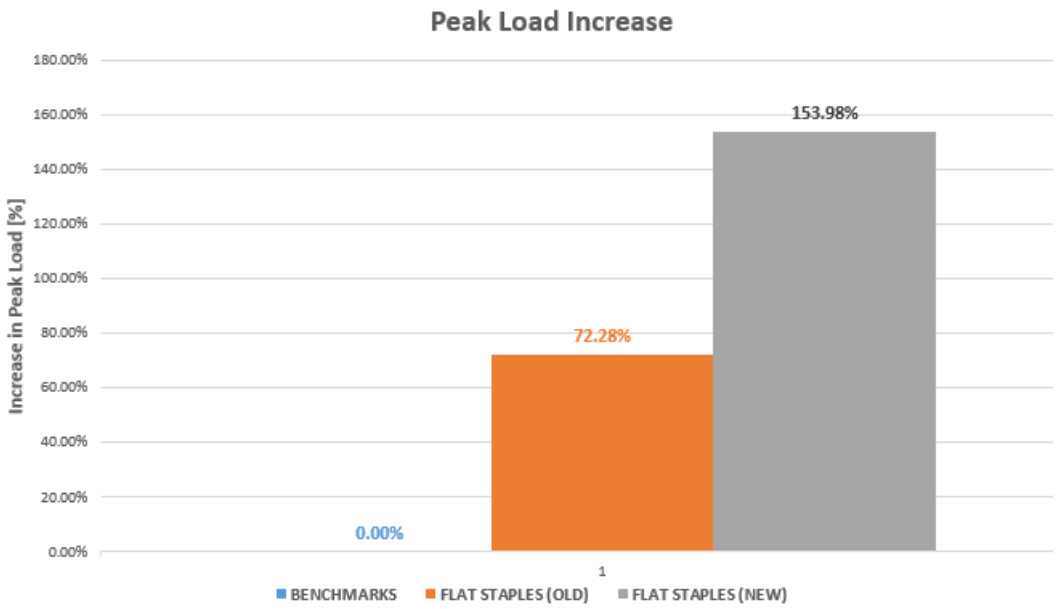

Figure 4.2 - Peak Load Increase - Flat Staple Anchors

Regarding the strains, the data obtained from the Strain Gauges were analyzed. The gauges layout on the FRP sheet has been already described in chapter 2 (Figure 3.25) and the results in terms of strain are listed in the table above (Table 4.).

It is important noting that, the configuration of strain gauges in this research was different from the one in the previous research. This decision was taken based on the following considerations: in this current investigation, no strain gauge was positioned at the bottom of the block (SG5) because, as shown in the previous research, the strains there are almost zero; no strain gauges were positioned along the width of the laminate (SG2, SG4) because there were no significantly differences between the strains recorded on the sides (SG2, SG4) and the strain recorded at the centerline (SG3), so, only centerline strain gauges were positioned.

As, predictable, the bigger strain is the one recorded by the strain gauge A (SG-A), being positioned far from the anchor, in the debonded laminate. Keeping in mind that the ultimate strain of the FRP sheet is 1.8%, depending from the specimen tested, the strains recorded by SG-A varies between 0.65% and 1%. SG-B, placed in the midline in front of the CFRP patch, shows lower values of strains ranging from 0.3% to 0.6%. Finally, SG-C, positioned over the CFRP patch, shows the lowest strain, as expected, ranging from 0.1% to 0.3%. Again, as expected, even if SG-C and SG-B are very close each other, one is positioned on top of the patch (more material means less stretch) and the other one directly on the laminate sheet, that is why their strains are not exactly the same.

The following graphics illustrate the response recorded by the strain gauges for each specimen.

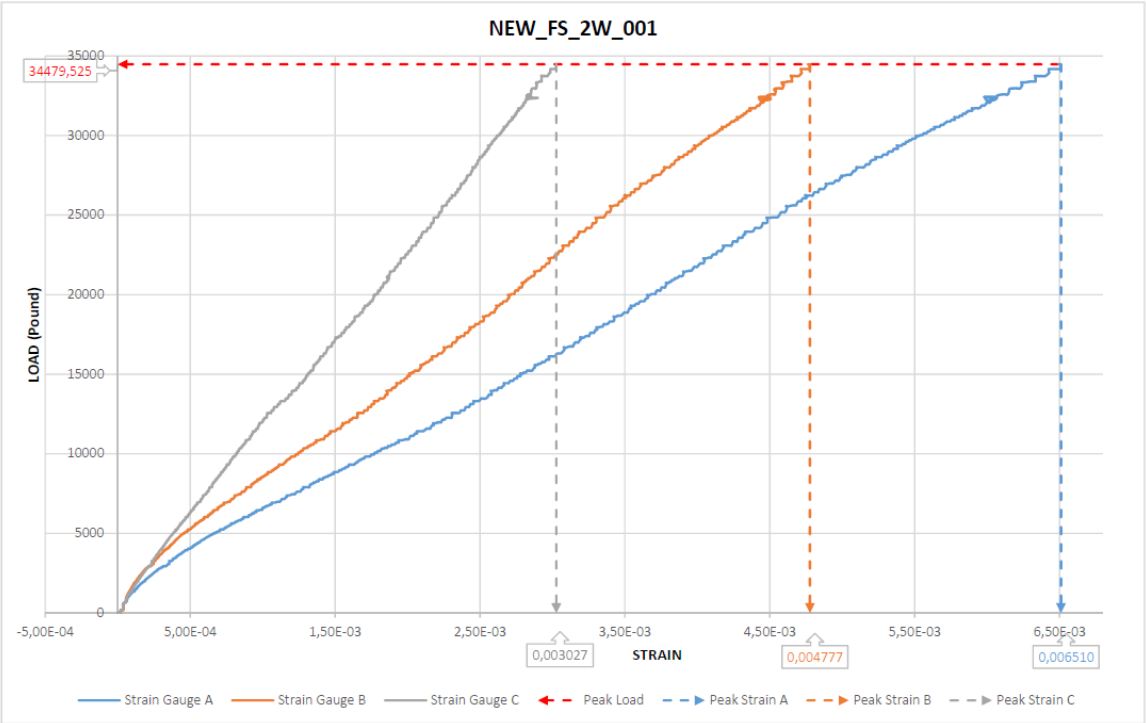

Figure 4.3 - Load vs Strain curve for the "NEW_FS_2W_001" specimen

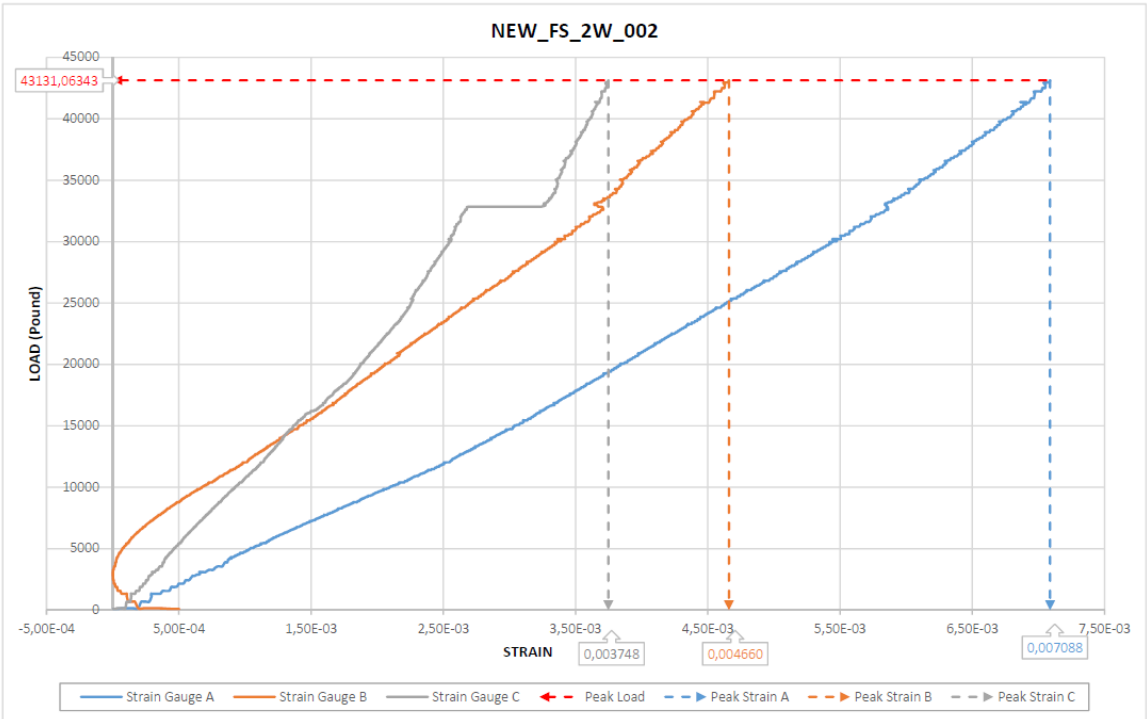

Figure 4.4 - Load vs Strain curve for the "NEW_FS_2W_002" specimen

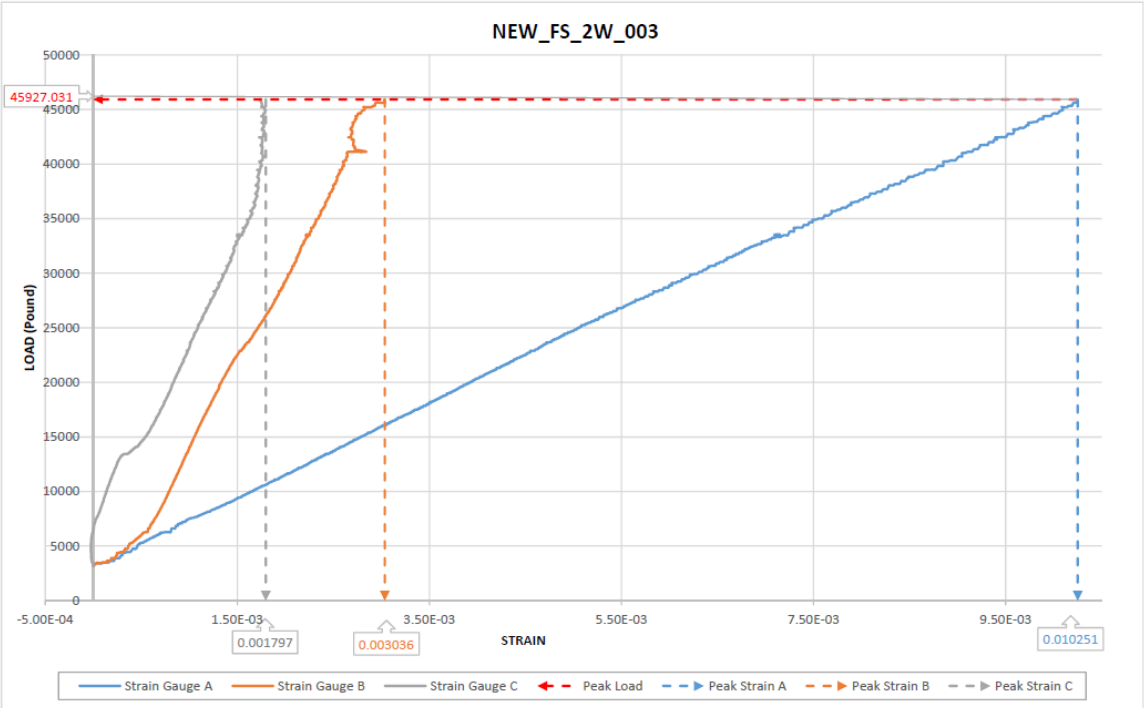

Figure 4.5 - Load vs Strain curve for the "NEW_FS_2W_003" specimen

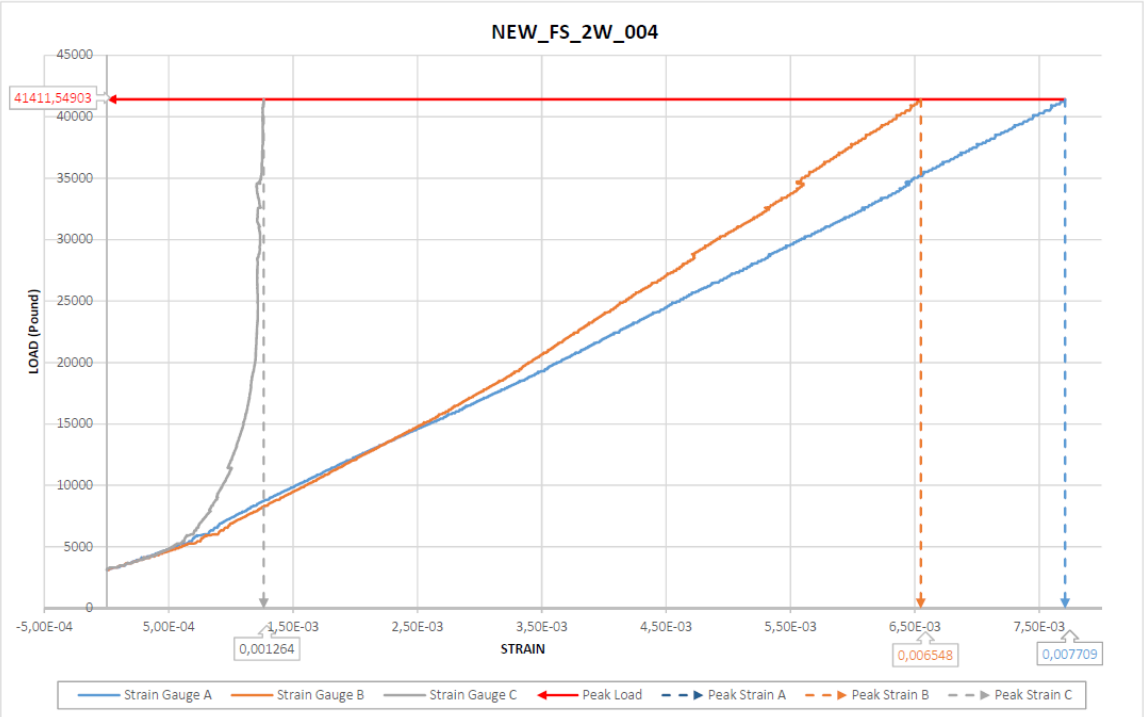

Figure 4.6 - Load vs Strain curve for the "NEW_FS_2W_004" specimen

The following graphic illustrates the response recorded by the strain gauge A for all the specimens.

The linear trend of SG-A is, actually, the behavior we did expect and the corresponding peak load is the key factor for design purposes

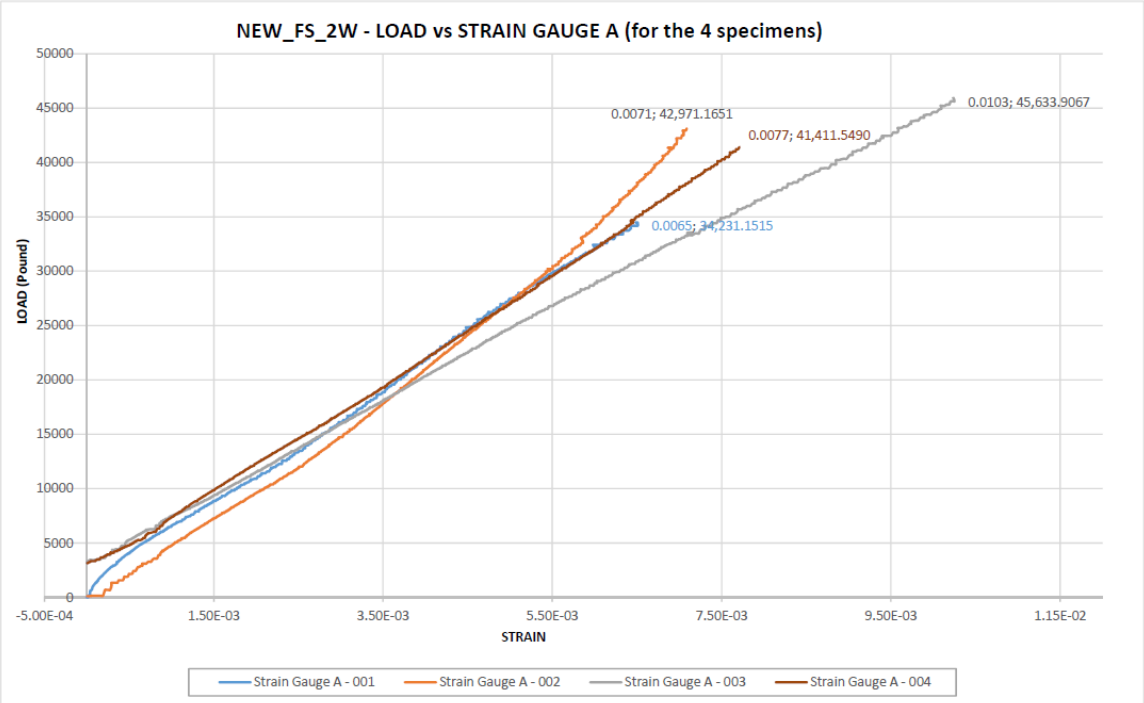

Figure 4.7 - Load vs Strain gauge A curve for the 4 specimens

The following graphic shows the average strains acquired by each strain gauge for all the specimens.

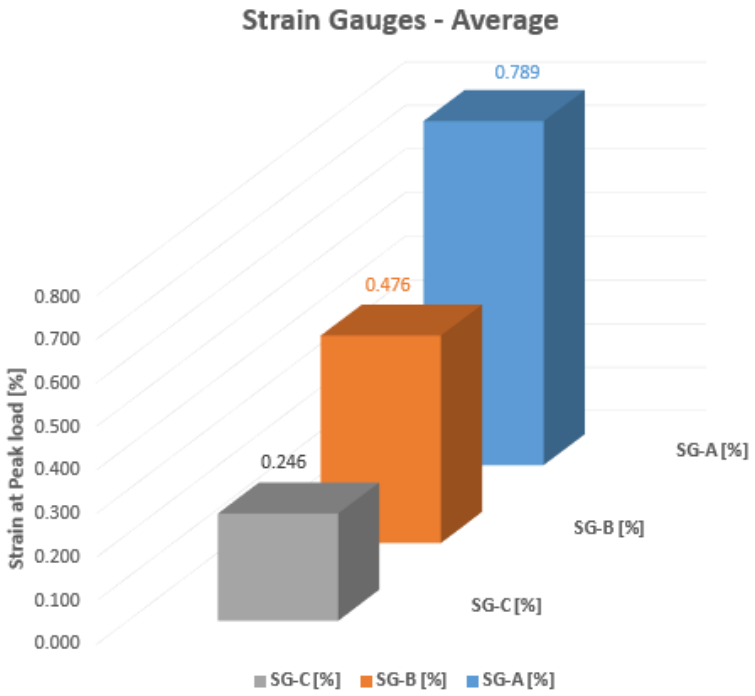

Figure 4.8 - Strain Gauges at Peak Load – Average – Flat Staple anchors

4.2 Test 2 – Round Staples

Again, the following table (Table 3.2) summarizes the results in terms of peak loads, increases of the load (in percentage) with respect to the benchmark, rupture side and type, measured strains in the CFRP sheet, failure modes and pressure at the peak load. The Peak Load P represents the maximum load applied by the hydraulic jack during the tests.

In order to allow the reader better understanding the numbers hereinafter shown, some old results are provided as comparison with the new ones. The first 3 blocks of the table are referred respectively to "benchmarks", as meaning of blocks tested without any anchor, "Round Staples (old)" and "Double Round Staples" as meaning of the old test performed in previous research (Cadenazzi, 2016). While the last part of the table, "Round Staples (**new**)" is referred to the results obtained in this research.

It is very important to remind that, for all the tests run for this research, the side without strain gauges was strengthened as shown in the previous Figure 3.12 in order to make each specimen fail on the other side provided with the instrumentation of the strain gauges. For this reason, in Table 4.2, there is also a column "rupture side" which explain if the rupture occurred on the expected left side (the instrumented one) or on the reinforced side (on the right side, the one not instrumented).

The location of the strain gauges was exactly the same of the Flat Staple specimens as shown in Figure 3.25.

While characterizing the anchor resistance in terms of load, we must refer to the load identified as $P/2$ because this represents the load applied to one side.

Figure 4.9 represents the average in terms of peak loads reached by the specimens.

Double Shear Test (WET FRP) - ROUND STAPLES (2" Depth)																
	Date	Specimen ID	Anchor's dimensions	Peak Load [pounds]	Peak Load [Kips]	P [KN]	P/2 [KN]	Increase in Peak Load [%]	Rupture Side	Rupture Type	Strains in % at peak load				
											SG1 [%]	SG2 [%]	SG3 [%]	SG4 [%]	SG5 [%]
BENCHMARKS	06.01.2016	T2_BM_001	No anchor	13041.25	13.04	58.01	29.01	-19.68%	Left (instrum.side)	A	0.340	0.276	0.302	0.530	0.021
	06.07.2016	T2_BM_002	No anchor	17033.74	17.03	75.77	37.88	4.91%	Right (not instrum. side)	A	x	0.402	0.482	0.441	0.005
	06.27.2016	T2_BM_003	No anchor	18634.67	18.63	82.89	41.45	14.77%	Right(not instrum. side)	A	x	x	x	x	x
			Average	16236.55	16.24	72.22	36.11				0.340	0.339	0.392	0.485	0.013
			Standard deviation	2352.05	2.35	8.88	4.44	0.00%			0.000	0.063	0.090	0.044	0.008
			C.V. [%]	14.49	2.35	12.29	12.29				0.000	0.186	22.863	9.164	59.988
ROUND STAPLES (OLD)	06.14.2016	RS_1D_001	1"D	20833.89	20.83	92.67	46.34	28.31%	Right (not instrum. side)	E	0.218	0.140	0.295	0.120	x
	06.15.2016	RS_1D_002	1"D	26618.29	26.62	118.40	59.20	63.94%	Left (instrum. side)	E	0.242	0.089	x	0.081	x
	06.15.2016	RS_1D_003	1"D	23519.51	23.52	104.62	52.31	44.86%	Right (not instrum. side)	D	0.333	0.085	0.219	0.397	x
			Average	23657.23	23.66	105.23	52.62				0.264	0.105	0.257	0.199	x
			Standard deviation	2363.48	2.36	10.51	5.26	45.70%							
			C.V. [%]	9.99	2.36	9.99	9.99								
DOUBLE ROUND STAPLES (OLD)	06.29.2016	DRS_1D_001	1"D	29282.32	29.28	130.25	65.13	80.35%	Left (instrum. side)	C	0.519	x	0.178	0.085	x
	06.29.2016	DRS_1D_002	1"D	30967.95	30.97	137.75	68.88	90.73%	Left (instrum. side)	C/F	0.376	x	0.258	0.065	x
	06.29.2016	DRS_1D_003	1"D	28254.09	28.25	125.68	62.84	74.02%	Left (instrum. side)	E	x	x	x	x	x
			Average	29501.45	29.50	131.23	65.61				0.448	x	0.218	0.075	x
			Standard deviation	1118.71	1.12	4.98	2.49	81.70%							
			C.V. [%]	3.79	1.12	3.79	3.79								
	Date	Specimen ID	Anchor's dimensions	Peak Load [pounds]	Peak Load [Kips]	P [KN]	P/2 [KN]	Increase in Peak Load [%]	Rupture Side	Rupture Type	Strains in % at peak load			Pressure at peak load [psi]	
											SG-A [%]	SG-B [%]	SG-C [%]		
ROUND STAPLES (NEW)	12.02.2016	NEW_RS_2D_001	2"D	37016.03	37.02	164.66	82.33	127.98%	Left (instrum. side)	F	0.750	0.579	0.234	3800	
	12.02.2016	NEW_RS_2D_002	2"D	37404.99	37.40	166.39	83.19	130.38%	Left (instrum. side)	E	0.726	0.588	0.145	3800	
	12.02.2016	NEW_RS_2D_003	2"D	31733.97	31.73	141.16	70.58	95.45%	Left (instrum. side)	F	0.766	0.546	0.097	3600	
	12.02.2016	NEW_RS_2D_004	2"D	35262.28	35.26	156.85	78.43	117.18%	Left (instrum. side)	F	0.654	0.611	0.392	3800	
	12.02.2016	NEW_RS_2D_005	2"D	40281.13	40.28	179.18	89.59	148.09%	Left (instrum. side)	E	0.583	0.573	0.158	4000	
			Average	36339.68	36.34	161.65	80.82				0.696	0.579	0.205		
			Standard deviation	2810.72	2.81	12.50	6.25	123.81%			0.012	0.004	0.045		
			C.V. [%]	7.73	2.81	7.73	7.73				1.745	0.715	21.782		

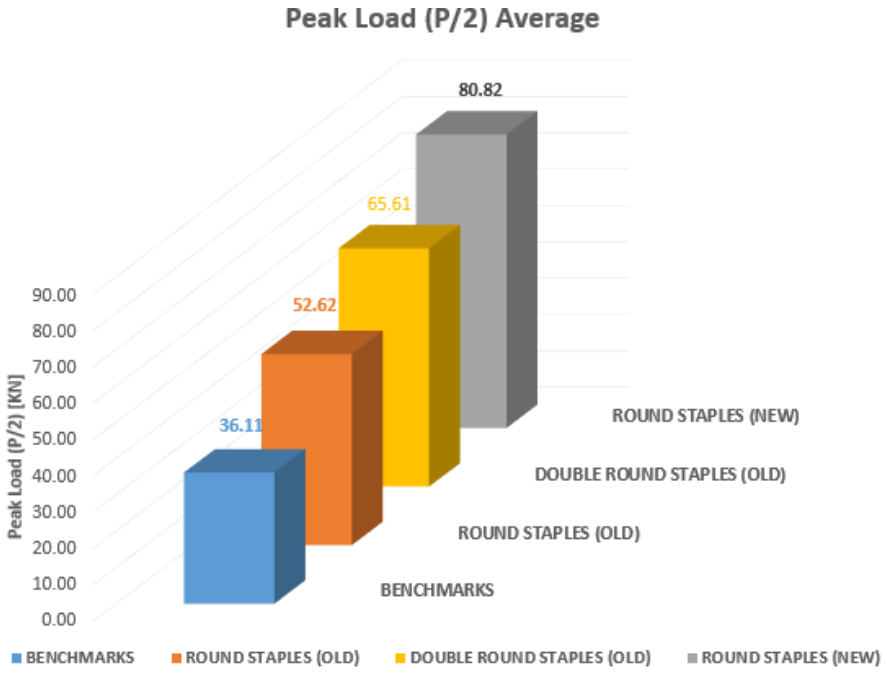

Figure 4.9 - Peak load's average (P/2) – Round Staple Anchors

As the reader, can easily understand, the Round Staple anchors installed with the new method even if they are not better than the *new* flat staple anchorage system, they are much more effective comparing with the old method. The effectiveness of this new method allows to reach better results even if compared with the Double Round Staple configuration used in previous research (Cadenazzi, 2016), outclassing them; in fact, the peak load increased from 65.61 KN to 80.82 KN.

Figure 4.10 shows the increase in peak load in percentage reached by the average of the types of anchor system installed.

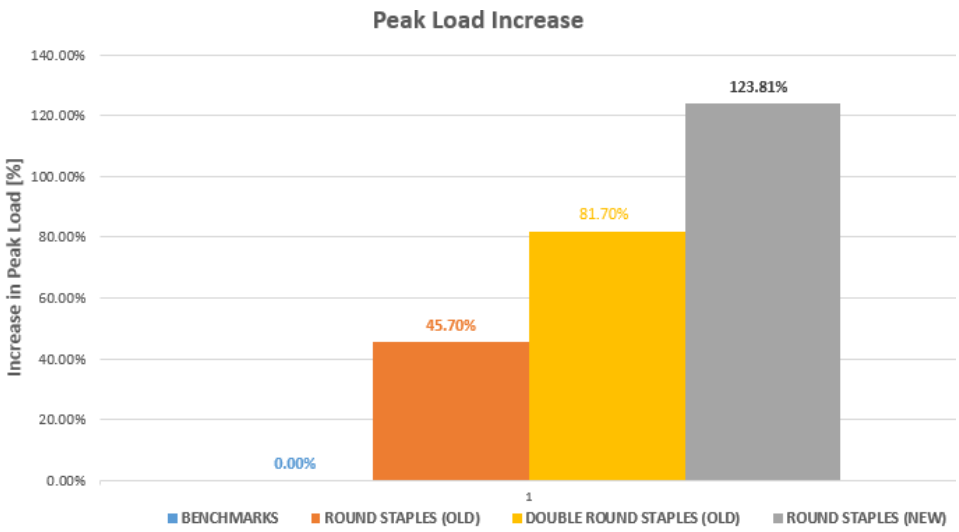

Figure 4.10 - Peak Load Increase - Round Staple Anchors

Again, regarding the strains, the data obtained from the Strain Gauges were analyzed. The gauges layout on the FRP sheet has been already described in chapter 2 (Figure 3.25) and the results in terms of strain are listed in the table above (Table 4.).

The following graphics illustrate the response recorded by the strain gauges for each specimen.

As, predictable, the bigger strain is the one recorded by the strain gauge A (SG-A), being positioned far from the anchor. Keeping in mind that the ultimate strain of the FRP sheet is 1.8%, depending from the specimen tested, the strains recorded by SG-A varies between 0.58% and 0.76%.

SG-B, placed in the midline in front of the CFRP patch, shows lower values of strains ranging from 0.54% to 0.61%.

Finally, SG-C, positioned over the CFRP patch, shows the lowest strain, as expected, ranging from 0.1% to 0.3%.

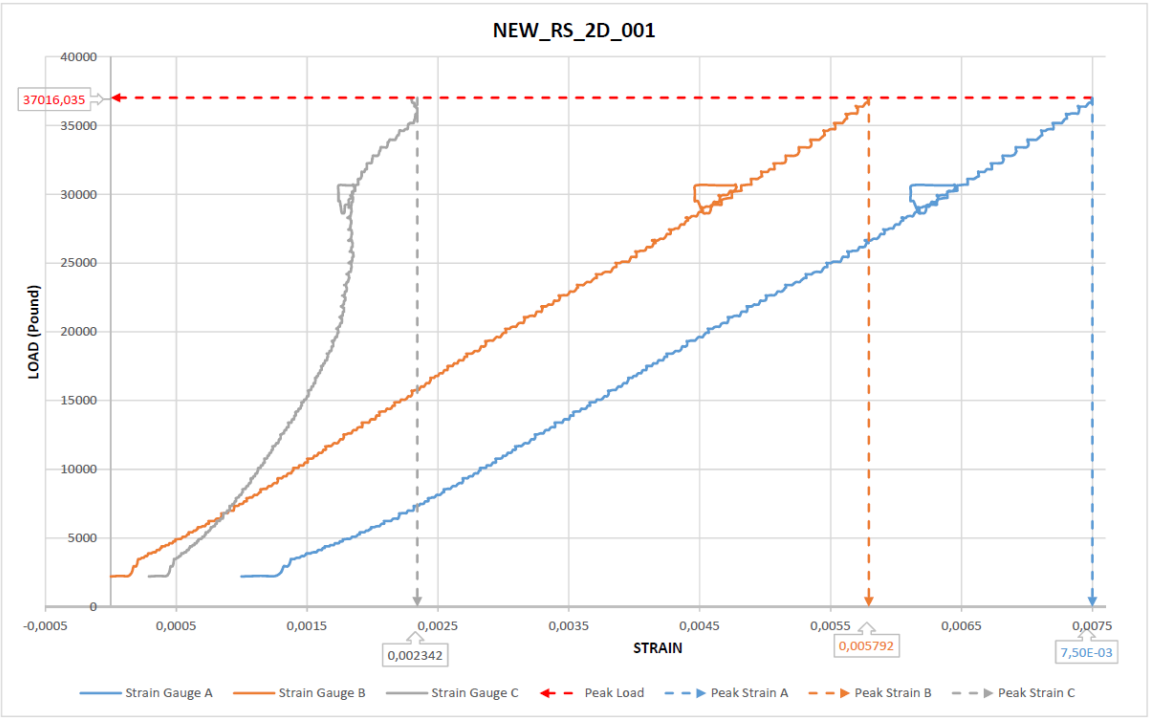

Figure 4.11 - Load vs Strain curve for the "NEW_RS_2D_001" specimen

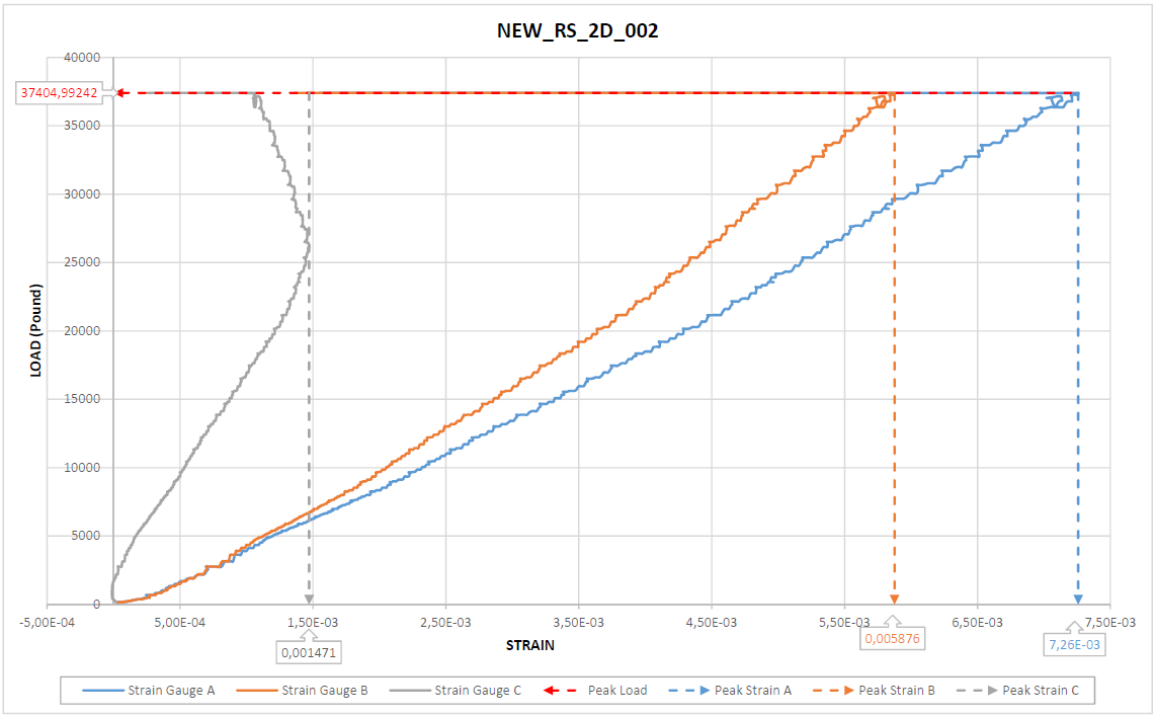

Figure 4.12 - Load vs Strain curve for the "NEW_RS_2D_002" specimen

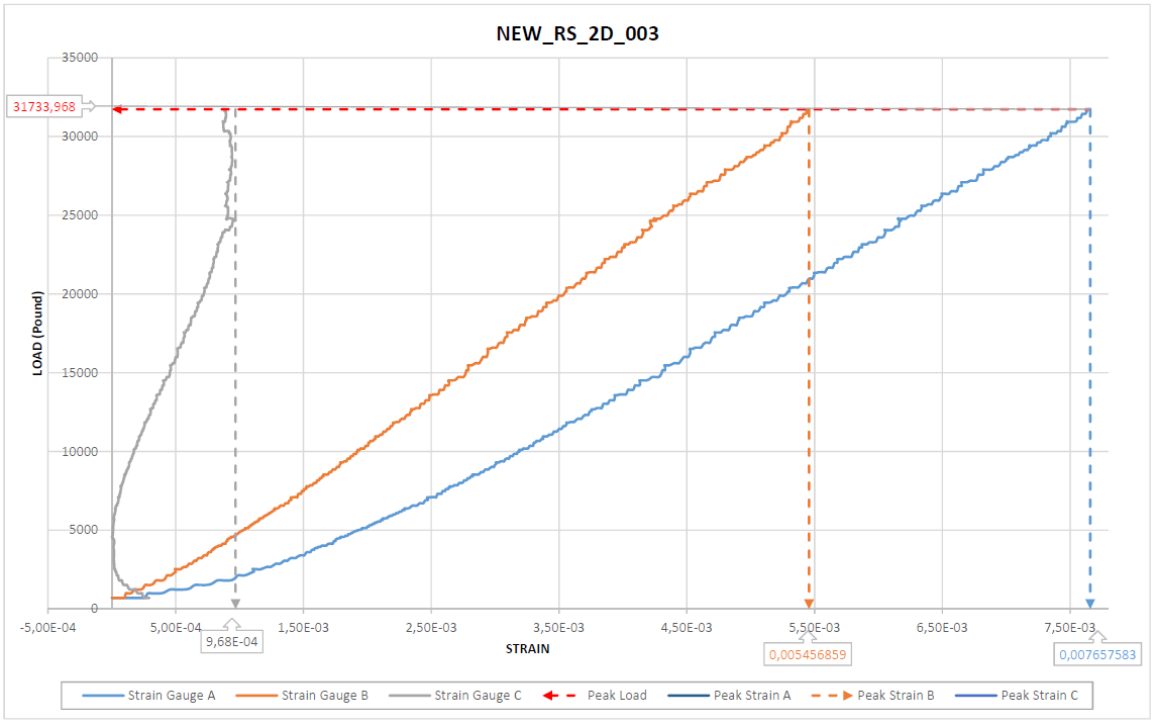

Figure 4.13 - Load vs Strain curve for the "NEW_RS_2D_003" specimen

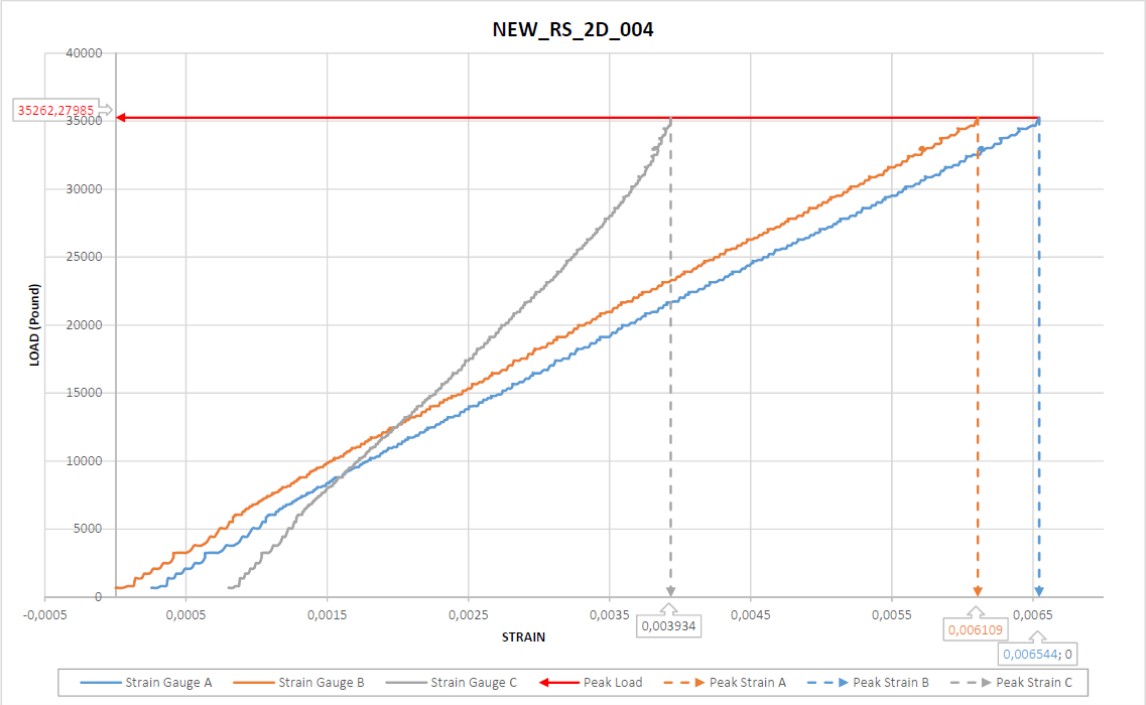

Figure 4.14 - Load vs Strain curve for the "NEW_RS_2D_004" specimen

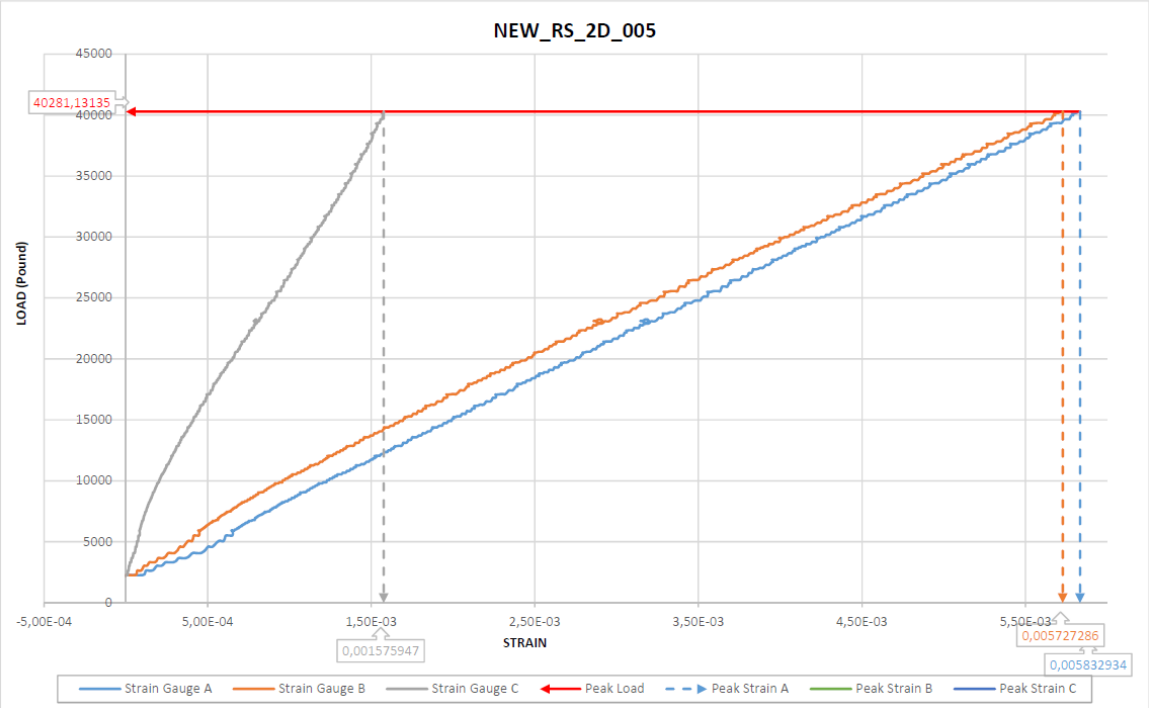

Figure 4.15 - Load vs Strain curve for the "NEW_RS_2D_005" specimen

The following graphic illustrates the response recorded by the strain gauge A for all the specimens.

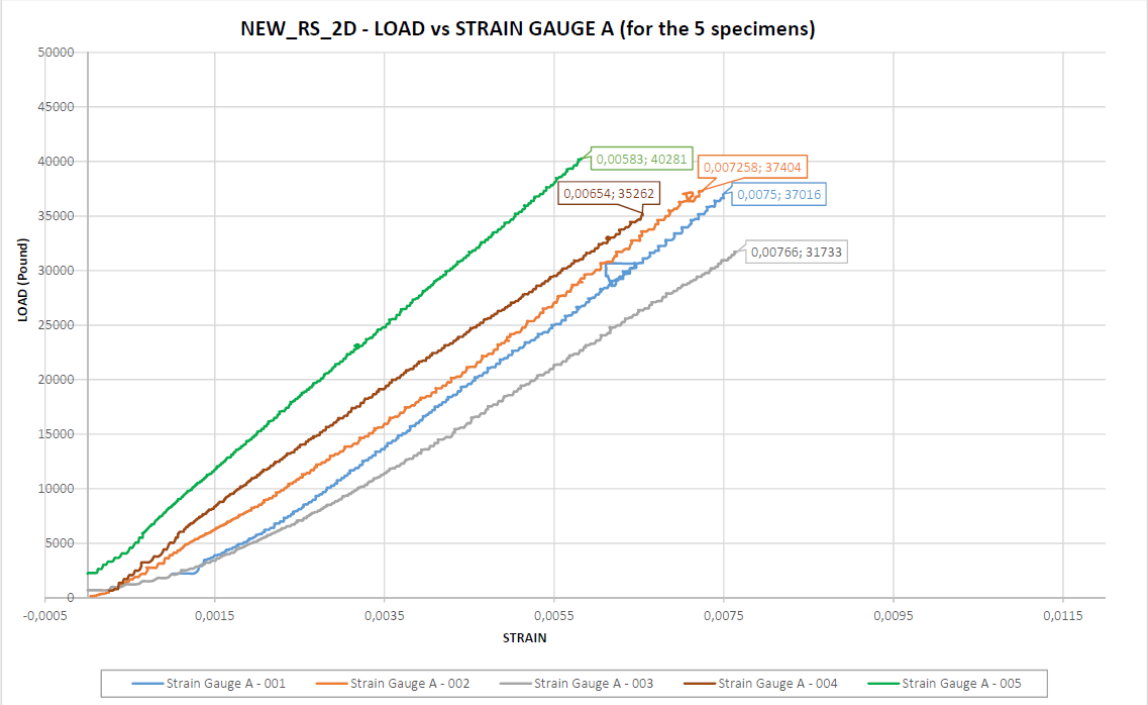

Figure 4.16 - Load vs Strain gauge A curve for the 5 specimens

The following graphic shows the average strains acquired by each strain gauge for all the specimens.

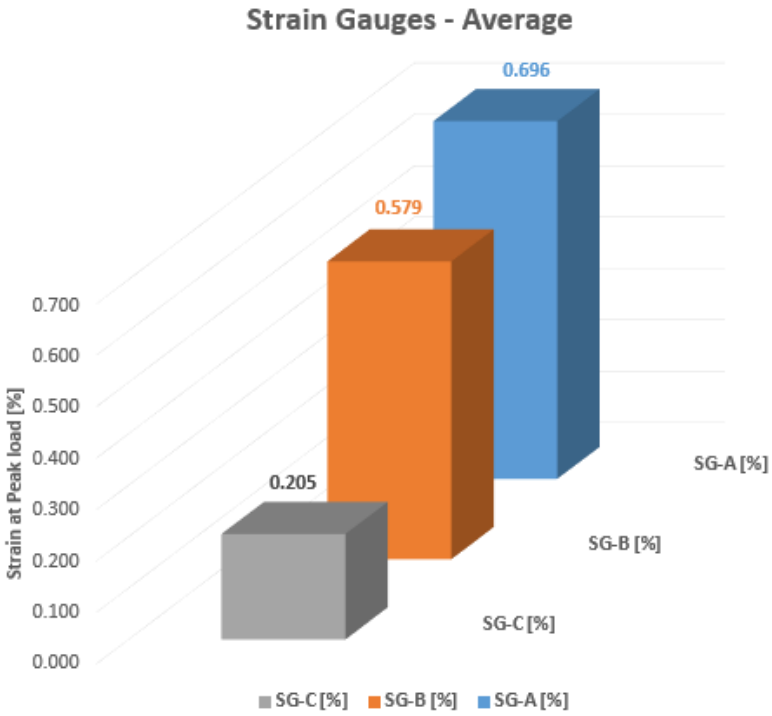

Figure 4.17 - Strain Gauges at Peak Load – Average – Round Staple anchors

4.3 Failure Modes

For sake of completeness a list of the most common failure modes could happen in this kind of tests is provided, but only the failure modes observed in this current research are fully analyzed describing each type of rupture, analyzing case by case the reason, giving an interpretation and a potential understanding of what each failure means.

The main failure modes are summarized as letters consistently with previous research (Cadenazzi, 2016); in such a way, a standardized scheme could be adopted to recognize and classify the failure modes in a univocal way:

A) Rupture as delamination of the CFRP sheet
B) Slippage of the CFRP sheet beneath the anchor, without their ruptures
C) Slippage of the CFRP sheet beneath the anchor, with the rupture of the CFRP sheet
D) Rupture of the anchor with the delamination of the CFRP
E) Rupture of the concrete substrate and rupture of the anchor
F) Rupture of the concrete substrate without the rupture of the anchor
G) Rupture of the CFRP sheet outside the bond area

As mentioned in Table 4. and Table 4.2 the rupture types observed in this research were D, E and F. Hereinafter, a full description of these failure modes is presented.

Failure Mode D) Rupture of the anchor with the delamination of the CFRP

The failure of the anchor indicates that anchor does not have sufficient capacity to develop the full strength of the CFRP sheet and is generally an undesirable failure mode. From previous studies, it has been stated that anchor failures depend on several factors as the size of the anchor, the force transfer mechanism between the sheet and anchor (bend radius and CFRP patches), and finally the adherence to installation procedures.

This type of failure (partially mixed with the failure mode E) was observed only for one flat staple anchor specimen (NEW_FS_2W_002). As shown in Figure 4.18 the failure mode D presents the rupture of the anchor on its right leg and the delamination of the CFRP sheet.

Figure 4.18 - Failure Mode D

Failure Mode E) Rupture of the concrete substrate and rupture of the anchor

The failure of the concrete indicates that concrete has reached the maximum load capacity, consequently it does not have sufficient capacity to develop the full strength of the anchorage system. Moreover, the concrete rupture provokes the rupture of the anchor.

The failure mode E, as shown in Figure 4.19, was observed in two Round staple specimens and partially in one Flat staple specimen.

Figure 4.19 - Failure Mode E - Concrete's Rupture (left) & Anchor's Rupture (right)

Failure Mode F) Rupture of the concrete substrate without the rupture of the anchor

In this case, the failure was due entirely to the rupture of the concrete substrate since the maximum shear capacity of the non-reinforced concrete was reached, the anchor was still performing well, without getting broken, as a meaning of a very strong anchor, assuming that it could have been achieved a higher load. Basically, the rupture of the concrete causes the anchor does not be engaged anymore pulling itself out of the block.

The failure mode F, as shown in the following Figures, was the most observed, on three Flat staple and three Round staple specimens.

Figure 4.20 - Failure Mode F - Flat Staple anchor

Figure 4.21 - Failure Mode F - Round Staple anchor

4.4 Results Discussion

In this section, a brief comparison between the performance of the new anchor system used as the purpose of this research and old anchor systems used in previous researches in terms of peak load and strains distribution is provided in order to highlight the improvement reached in this most recent research the author carried out.

Table 3.3 and Figure 4.22 present a comparison in terms of peak load between different anchorage systems studied at the University of Miami so far.

	Anchor's Type	Anchor's Configuration	Peak Load [KN]
Berneschi, 2015	Spike Anchors	60 degrees fan opening	57.80
		90 degrees fan opening	66.38
Cadenazzi, 2016	Flat Staple anchors (old)	1 in. width - 1 in. depth	57.35
		2 in. width - 1 in. depth	62.21
		3 in. width - 1 in. depth	66.42
	Round Staple anchors (old)	Single conf. - 1 in. depth	52.62
		Double conf. - 1 in. depth	65.61
Girotti, 2017	**Flat Staple anchors (new)**	**2 in. width - 1 in. depth + patch**	**91.72**
	Round Staple anchors (new)	**Single conf. - 2 in. depth + patch**	**80.82**

Table 4.3 – Anchors' peak loads summary

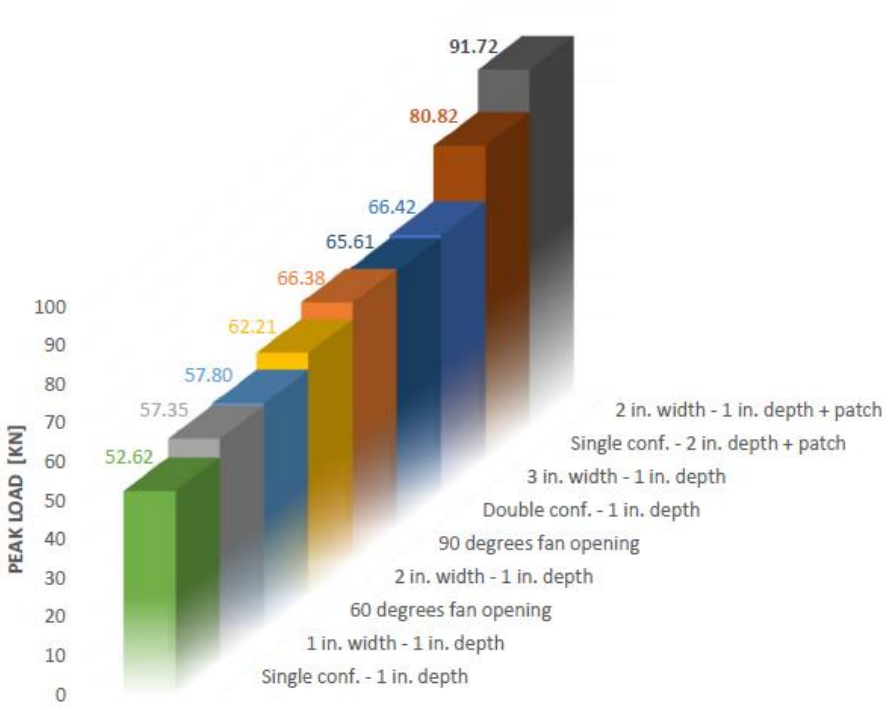

Figure 4.22 - Peak Loads Comparison

The reader can easily understand, from the following Figure 4.23, how much the new improved installation method, used both for Flat and Round staple anchors, increases the performance in terms of peak load in comparison with blocks tested without any anchor.

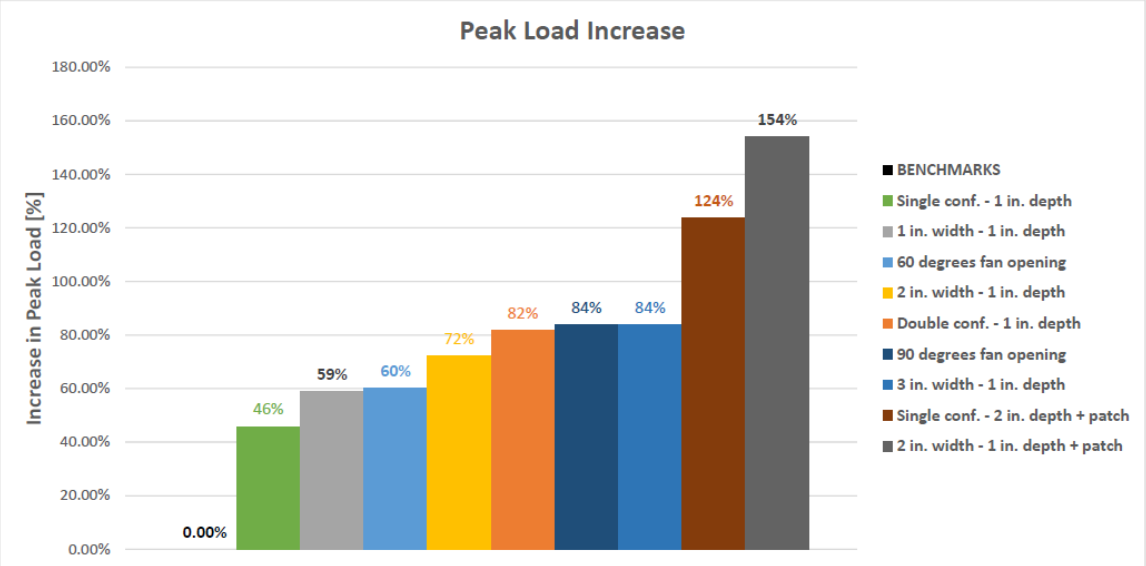

Figure 4.23- Peak Loads Increase Comparison respect to benchmark

Again, comparing the peak load of the new anchorage system studied in this research with the best anchorage system studied in previous researches, the increase in peak load, as shown in Figure 4.24, is still very good.

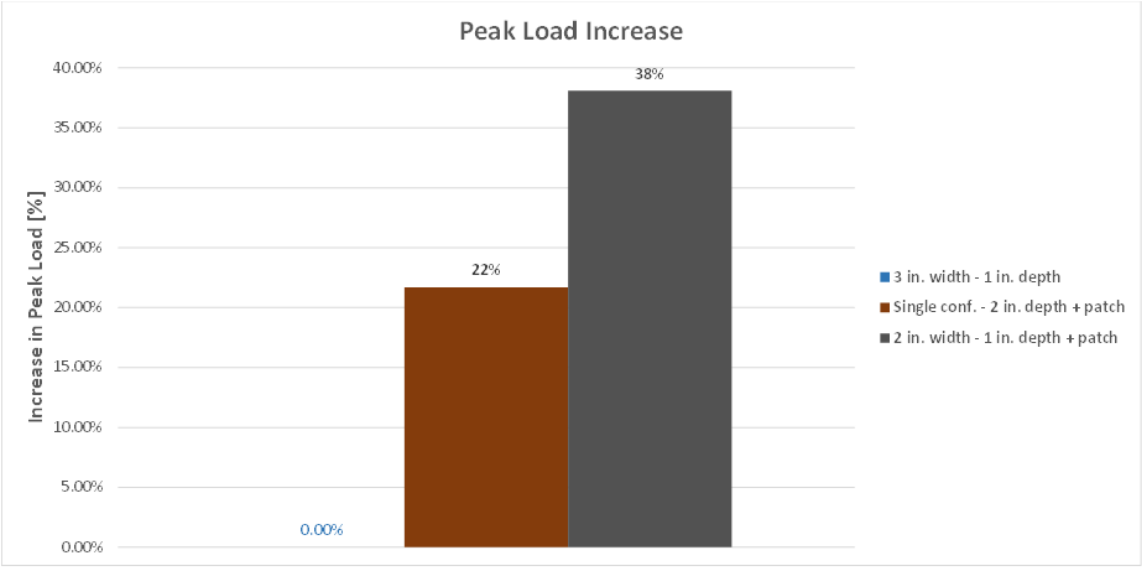

Figure 4.24 - Peak Loads Increase Comparison respect to the best old anchorage system

Regarding the strains, as widely studied, the staple anchors distribute better the stresses. In fact, for the spike anchors, the strains were concentrated in front of the anchor (and that covered area was not along the entire FRP sheet width). Staple anchors, instead, distribute better the strains over the entire area of the FRP, since they literally cover all the entire FRP laminate width of 6 inches, used for this study.

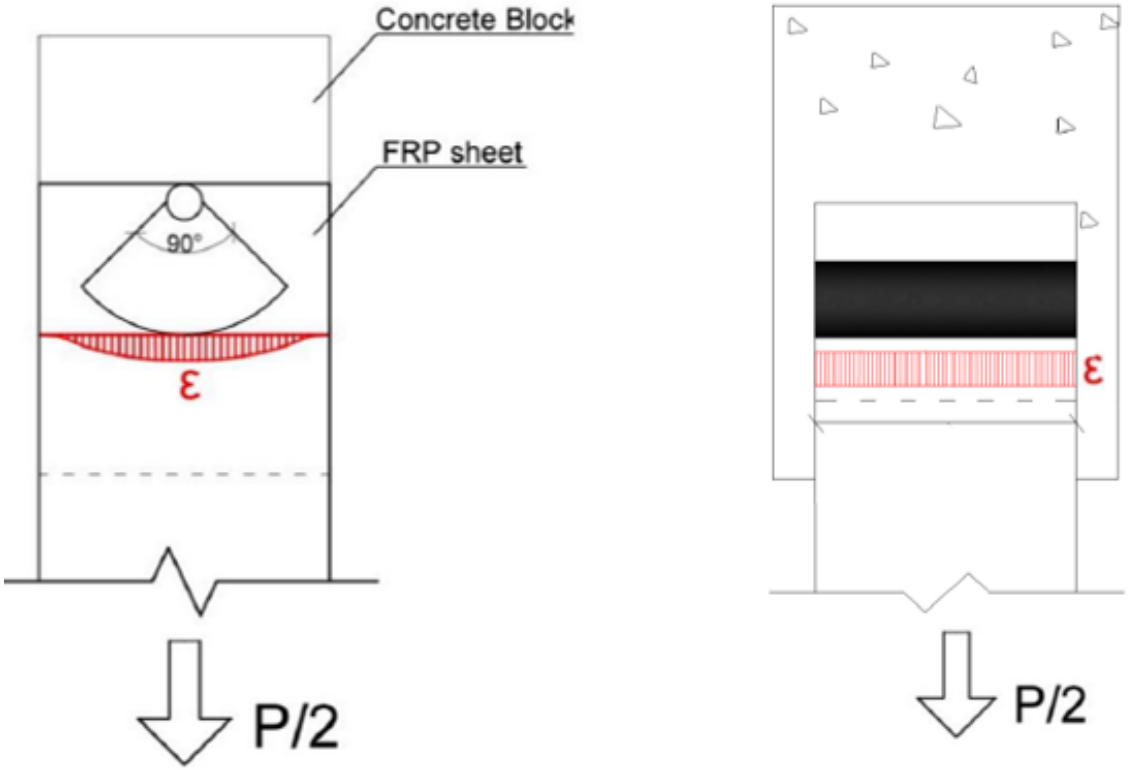

Figure 4.25 - Strain distribution on Spike (Berneschi, 2015) and on Staple anchors (Cadenazzi, 2016)

Strains are also more evenly well distributed in the specimens tested during this research considering the CFRP patch applied, that not only contributes to a better force transferring from the CFRP sheet to the anchor, but, being this patch oriented with fibers in the same direction of the fibers of the flexural sheet allows the development of higher stresses and strains (higher values of stresses and strains are obviously preferred).

The following Figure 4.26 show the average strains recorded by the Strain Gauges SGA located in front of the anchors for the Flat and Round staple specimens. We can observe bigger average strains on Flat staples. In this way, again, we can clearly identify the Flat Staple anchor as the one that is strong enough to develop the full capacity of the CFRP sheet.

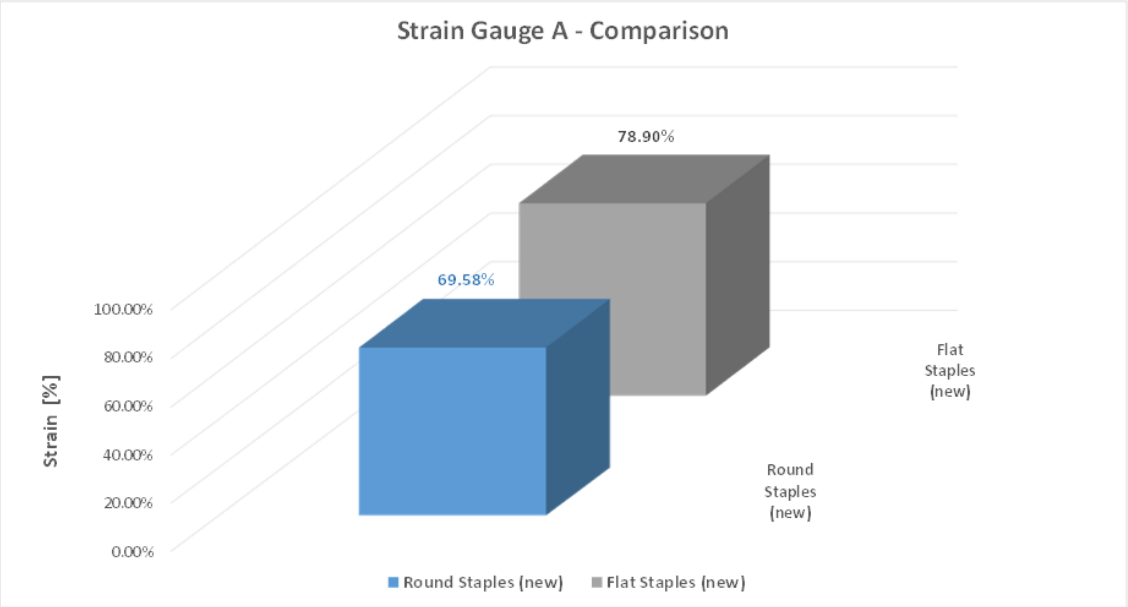

Figure 4.26 - Average of the strain distribution in front of the new Flat & Round staple anchors

It is important noting that, because of different anchor types and installation methods, the only strain gauges that are meaningful of comparison are the one on the CFRP laminate far from the anchor (SGA & SG-1).

Figure 4.27 shows a comparison of strains at laminate between all the staple anchors tested both in this research as well as old researches, pointing out the increment reached by the newest anchorage system developed as purpose of this investigation.

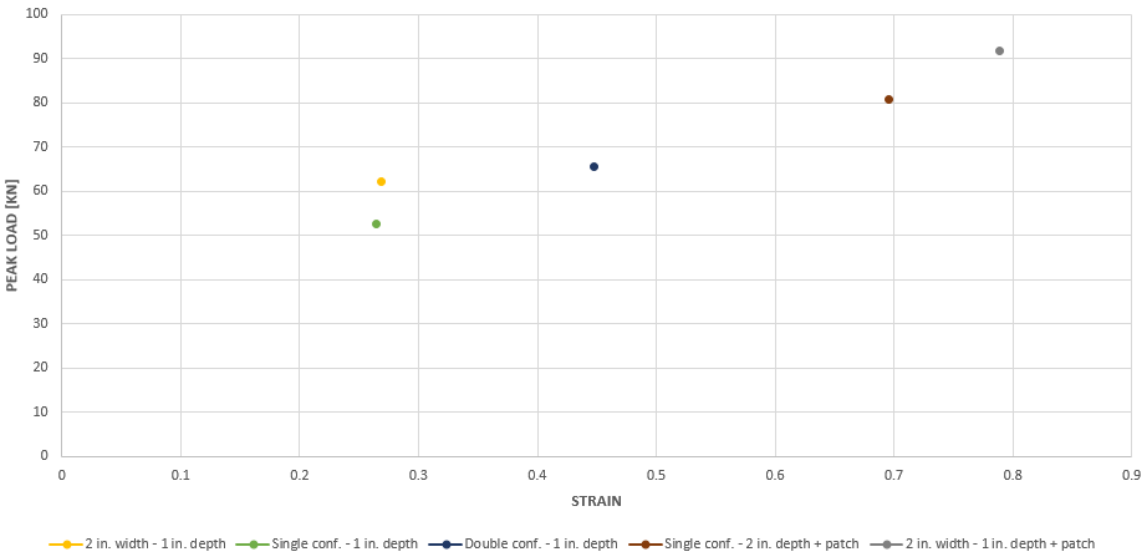

Figure 4.27 - Strain at laminate (SGA & SG-1) comparison

In conclusion, based on the results obtained in this research, we can say that:

- *Regarding the **Flat** Staple anchorage system:* the new installation method using the CFRP patch gives a really big improvement both in terms of peak load and strains compared with old anchorage systems. Unfortunately, as shown analyzing the failure modes, the rupture of the concrete substrate *without* the rupture of the anchor was the most common failure type, as meaning that the maximum shear capacity of the non-reinforced concrete was reached, consequently it does not have sufficient capacity to develop the full strength of the anchorage system. So, with the crashing of the concrete we reached the compressing capacity of the concrete. Unlike the concrete, the anchor was still performing well, without getting broken, as a meaning of a very strong anchor, assuming that it could have been achieved a higher load. A suggestion for further studies is to create bigger blocks and test again the flat staple anchors, carefully positioning them far away from the edges in order to engage more concrete.

- *Regarding the **Round** Staple anchorage system:* again, the new installation method using the CFRP patch gives also a big improvement both in terms of peak load and strains compared with old anchorage systems. But, unlike the new Flat staple anchorage system, here, the rupture of the concrete substrate and the rupture of the anchor was the most common failure type (even if in two specimens the round staple anchor did not break). Even if the Round staple anchors used in this research were improved by the manufacturer, since last tests, they still present some weakness on their edges (common point where they got broken). Despite it all, the author, believes that further improvements strengthening the edges, could allow Round staple anchors to achieve better results, reaching the Flat staples ones, with the advantage of a simpler and less "invasive" installation. In fact, making a drill (Figure 3.4) instead of a cut (Figure 3.3) could be very advantageous in some situations such as the installation of an anchor on the edge between two walls.

Although if the tests run on the staple anchors with the new installation process were only ten (of which one was discarded as explained in chapter 4.1), based on the dispersion of the results observed (a low coefficient of variation (C.V)), the type of rupture, the strains interpretation, and the peak load significantly high, we can prove the consistency of the results.

CHAPTER 5

Experimental Program 2: Staple Anchors on Slabs

In the previous chapters, the ***first*** experimental campaign that was carried out over staple anchors was presented, analyzing the results, and appreciating the improvement made by the new installation method through the CFRP patch.

Chapter 5 covers all the aspects related to the ***second*** experimental campaign that was carried out, over slabs. The first section presents the purpose of this chapter, the following sections will provide detailed information over specimens 'preparation, test set-up and instrumentation used. Finally, the materials used will be characterized.

5.1 Purpose

This research investigates the behavior of the ***Flat*** Staple anchors, the most recent type of anchorage system, studied in the previous chapter, applied on RC slabs following the new installation method presented in chapter 3.3.3 (Anchors' Installation – Improved process). In a previous research (Rossini, 2016) the behavior of a different anchor, spike anchors, set up in different configurations was studied.

This investigation is based on experimental work on RC slabs strengthened with FRP sheets connected to the concrete via these carbon Flat staple anchors improved with a "FRP patch" as a new installation process tested in the previous experimental program (Chapter 3).

The staples anchors are provided as prefabricated elements formed by strands of carbon fibers that are inserted into epoxy filled holes in the concrete, and an external part that is also impregnated and connected externally to the bonded FRP laminate. They appear in different shapes and sizes and they can be installed in different ways but they share the same aim: enhance the bond of externally bonded FRP laminates into concrete.

This experimental campaign is composed by 3-point bending (flexural) tests through which it is investigated the improvement in terms of resistance of the anchors under tension load, in order to find the best configuration that is sufficient to enhance the bond of the FRP sheets. In particular, a series of 3-point bending tests were performed: four specimens were prepared with **Flat** staple anchors installed with the innovative installation procedure already discussed, which gives successful and consistency results through a more reliable set-up of the test.

The purpose is to test the effectiveness of flat staple anchors, providing to engineers, in this way, the necessary information to make design decisions when incorporating a staple anchor system to enhance the bond of externally bonded FRP laminates.

5.2 Specimens Fabrication

The experimental effort is focused on four bending tests on slabs, all CFRP-externally-reinforced and characterized by different anchors configurations. A detailed description of specimen preparation is provided in this section.

5.2.1 RC Slabs

It is important to underline how a particularly strong concrete (10 kip, C60/65) was prescribed, in order to avoid shear failures; while the choice of a stronger steel (S70, B450) was mainly dictated by material availability and doesn't really make a difference with respect to standard S60 generally used in the US.

Only two #3 (Ø10) rebars were used as internal reinforcement, in order to be sure, the element is under-reinforced. The small amount of rebars is chosen in order to maximize the strength increment provided by the external reinforcement, allowing easier results interpretation. In fact, external reinforcement on over-reinforced elements is, if not ineffective, surely largely inefficient, considering that the internal reinforcement's strength is already non-entirely exploited at failure. The minimal bond length provided to the rebars passing the external supports is justified by the assumption that no severe cracks will develop away from the mid span, thanks to the particularly high concrete strength, hence no slipping-induced collapses should happen. Rebars' bonding is also promoted by the particularly little diameter chosen. The results will show that slipping did not happen at all, even at very high deflections, after load drop.

The element's geometry was decided, as well as in the previous research (Rossini, 2016), considering the limits imposed by the available testing frame: the total length of the concrete element is fixed at 78 inches (1.98 m) while the supports are located in order to provide a 73.5 inches (1.87 m) free span. The will to maximize the free span comes from the consideration that a non-slender element tends to deviate from the behavior predicted

by the standard beam theory. The effect is surely negligible on real-scale applications, but can be significant on the small span tested, mainly considering the presence of anchors along the span itself.

Regarding the section, the width is fixed at 14 inches (356 mm) for the sake of consistency with anchors' shear characterization (Berneschi 2015, Cadenazzi 2016, Girotti 2017), while 6 inches (152 mm) height was chosen in order to have a reasonable dimensional ratio and enough room for making cuts where to apply the flat staples anchors.

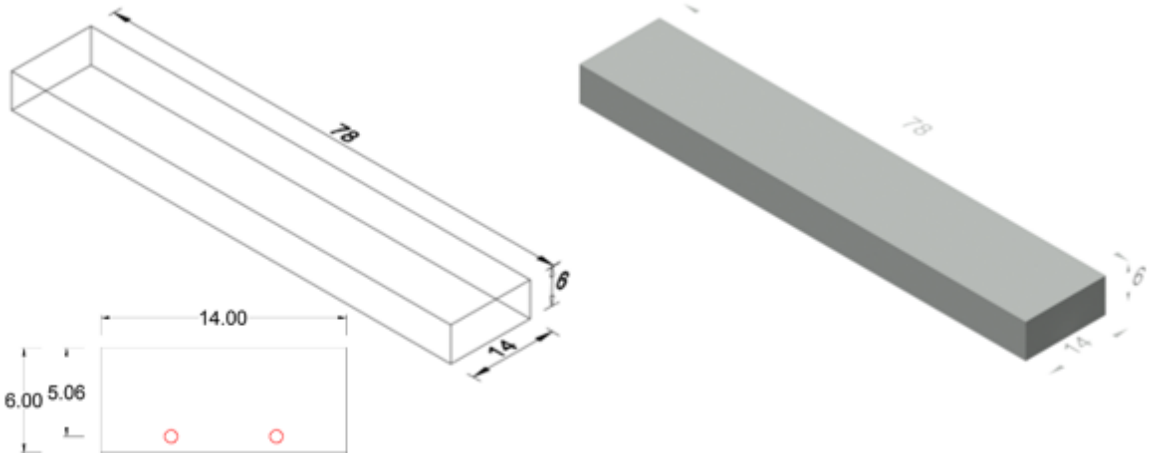

Figure 5.1 - RC slab's geometry

Again, a total of four specimens were prepared, all CFRP-externally-reinforced and characterized by different Flat Staple anchors configurations: two specimens were provided of two anchors at the ends (configuration 1), other two specimens were provided of four anchors, two at the ends and other two along the slab's span, at one third of the length (configuration 2), as shown in the following Figure 5.2 & 5.3.

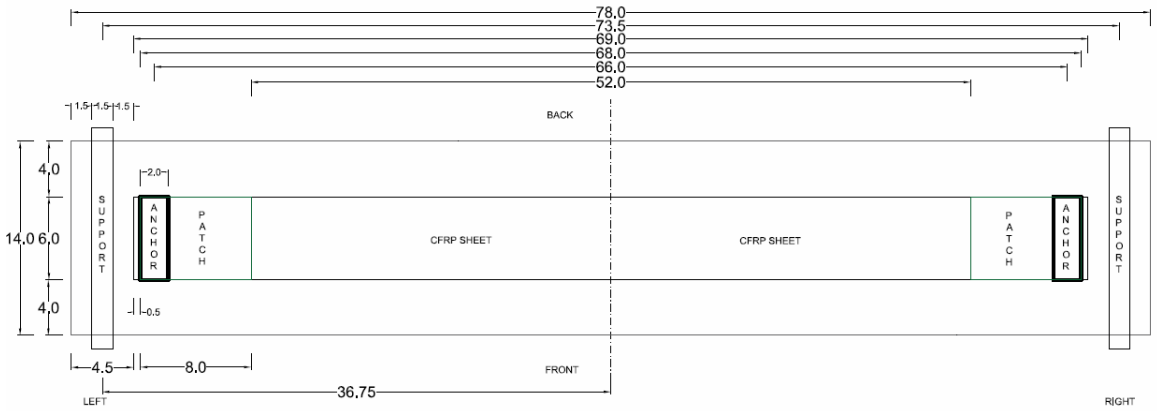

Figure 5.2 - Slabs 001 & 002 reinforcement configuration 1

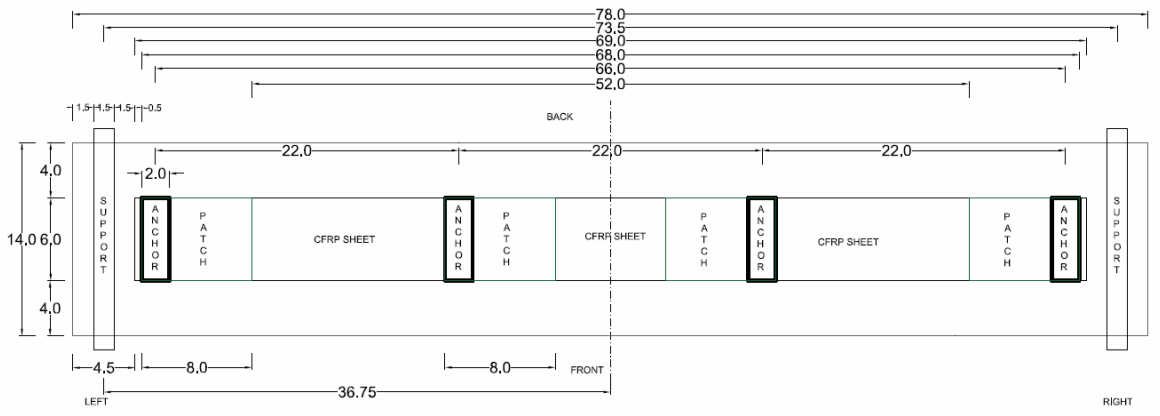

Figure 5.3 - Slabs 003 & 004 reinforcement configuration 2

The first step of the specimen's fabrication process consists in the mold and steel set-up. A steel strain gauge was applied on each rebar. In order for the gauge to properly stick to the steel, the rebar itself war sandpapered using a dremel, the strain gage was stick to the smoothed surface with superglue and covered with an insulating fluid solution. Everything was then electric-taped. Once the rebars were placed into the molds, it is critical to wire the gauges' lines outside the mold and properly secure the loose wires and protect them from concrete pouring.

Figure 5.4 - Rebar Instrumentation

Once all the rebars were all instrumented, they were linked two by two thorough proper spacers and placed in the already prepared wooden molds. A Voltmeter was used in order to verify all the applied strain gages were still working after installation, before sending the molds for concrete pouring. Before rebar positioning, a demolding agent was also sprayed on the wood surface, in order to favor concrete-mold separation after curing.

Casting was performed in a concrete factory: all the molds were brought to the facility and the finite product was brought back to the lab after 7 days for final curing. Right after

casting, the specimens were covered with plastic sheets in order to avoid any loss of moisture.

Figure 5.5 - Mold set-up

Demolding was manually performed in the laboratory, right after specimen were brought back from the factory. They were stored in open air waiting for sandblasting.

Figure 5.6 - Casting and Demolding

5.2.2 Surface Preparation

A step-by-step procedure used for the specimen's preparation is herein provided, starting from having the slabs already casted.

All the slabs used were sandblasted by an expert; in fact, it is widely accepted that surface roughness influences bond capacity, increasing the bond once the FRP is applied on the concrete. Also, the removal of the smoothness concrete paste helps to recreate an old concrete surface (usually the sandblast is required for old concretes to renew it).

Figure 5.7 shows the operation of sandblasting.

Figure 5.7 - Operation of Sandblasting

Furthermore, the surface where the CFRP sheet was applied was grinded, to improve the adherence between the concrete and the laminate.

Figure 5.8 - Surface grinding operation

The first two specimens were cut only at the ends using a special grinder, as shown in Figure 5.9 while the second two specimens were cut at the ends and at one third from each side, as shown in Figure 5.10

Figure 5.9 - Cutting Process specimens 001 & 002

Figure 5.10 - Cutting Process

Obviously, after this procedure, the dust was blown up from the holes using an air compressor to clean perfectly the inside before anchors installation.

5.2.3 Anchors Preparation

As already mentioned, the anchors were provided as prefabricated elements. The preparation process was exactly the same already explained in chapter 3.2.3, they needed to be cut using a particular blade as 6” (152.4 mm) long, 2” (50.8 mm) width and 1” (25.4 mm) depth.

Figure 5.11 - Anchors' cutting process

5.2.4 CFRP Preparation

Once specimens were prepared for FRP bonding, CFRP sheets and CFRP patches were prepared for installation. One CFRP sheet per each specimen was cut as 6” (152.4 mm) wide and 69” (1.75 m) long from V-Wrap C200 H material. Moreover, also a CFRP sheet per each anchor, was cut as 6” (152.4 mm) wide and 14” (355.6 mm) inches long, as patches needed for the new installation process. So, a total of four long CFRP sheets and twelve CFRP patches were cut, ready for the installation procedure.

Figure 5.12 - V-Wrap C200H roll, 69” FRP sheet & 14” FRP patches

5.3 Installation Procedure

In order to allow a good bonding between the FRP sheet and the concrete surface, the latter had to be cleaned. An air compressor and a brush were used to remove all the particle of sand resulting from the sandblasting.

5.3.1 Epoxy Application

The epoxy resin (part A) and the curing agent (part B) were mixed together with the mixing ratio reported in the manufacturer's instructions of 100:33 by weight. The two parts were completely mixed together for 3 minutes until a smooth and uniform consistency was reached. Part of epoxy resin was mixed with fume silica in order to make the epoxy thicker. The fume silica was added as a mixing ratio by volume of 1:1 to the primer. Again, once a uniform consistency was obtained, the thickened epoxy (the primer mixed with the fume silica) was applied using a spatula, in order to fill all the concrete cavities and little holes as shown in Figure 5.13.

Figure 5.13 - Epoxy resin mixing & fume silica application on slab surface

5.3.2 CFRP Sheet Application

Once the slabs were ready, all the CFRP sheet previously cut were disposed over a clean table and they were impregnated for their entire length using the pre-mixed part A & part B epoxy as shown in Figure 5.14.

Figure 5.14 - CFRP Sheet impregnation process

After that, the pre-mixed epoxy (Fortress 4020 Fast Epoxy Hi-Mod Gel) was poured into the stripe holes with a specific epoxy gun actioned by compressed air, designed for this work, then, each lamina was carefully placed on the slab's surface and rolled all over to avoid the formation of air bubbles along all the entire length.

Figure 5.15 - Epoxy pouring process & impregnated FRP sheet application

5.3.3 Anchors' Installation – Improved process

The same new installation process already discussed in chapter 3.3.3 was used to improve the strength of the external reinforcement provided by the CFRP sheet and the anchor.

An epoxy layer was poured on the legs and on the under part of the anchor, on the surface into direct contact with the FRP lamina.

The new installation process consists of applying an overlapped impregnated CFRP patch (6" (152.4 mm) wide and 14" (355.6 mm) long) folded as 6" (152.4 mm) below and 8" (203.2 mm) wrapped above the anchor inserted and squeezed into the holes soaked of epoxy as shown in Figure 5.16.

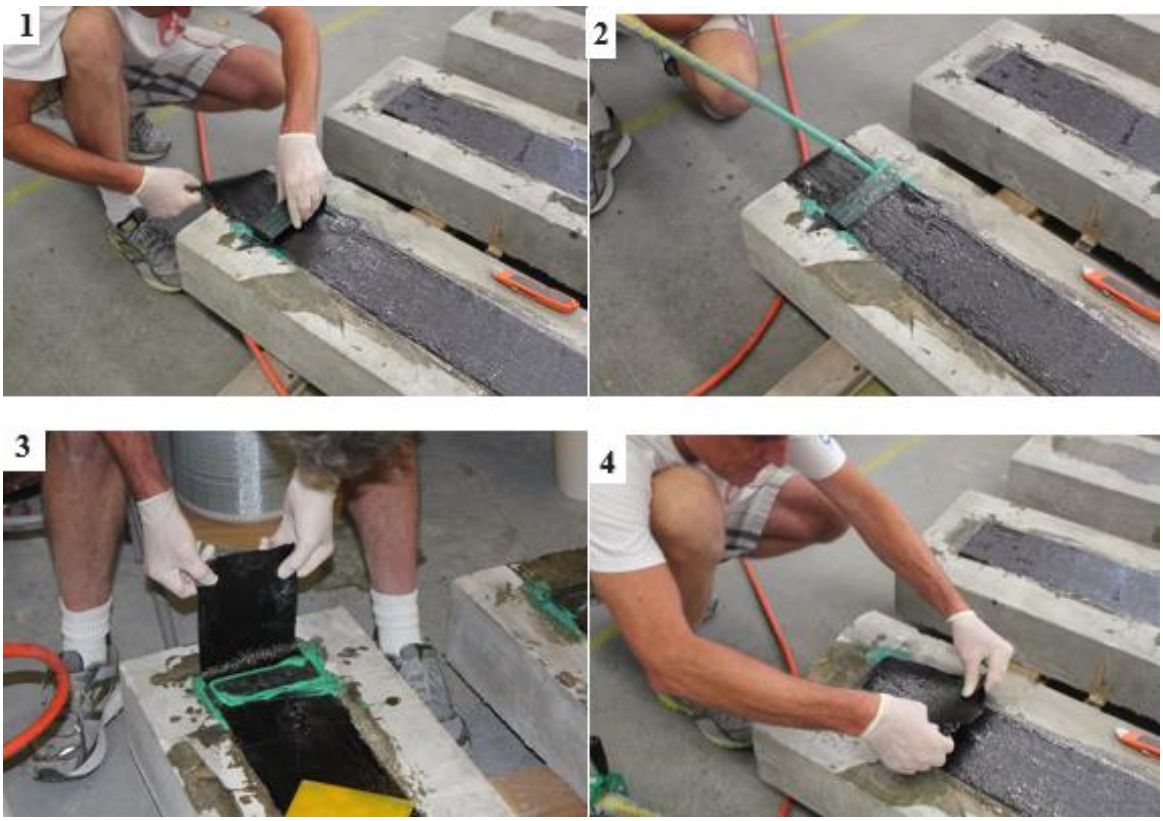

Figure 5.16 - CFRP Patch installation process

As we already said in the first experimental program, anchor patches allow better force transfer from the CFRP sheet to the anchor, improving the resistance of the system on the side in which they are installed. This patches are oriented with fibers in the same direction of the fibers of the flexural sheet. The choice of using a CFRP patch was made analyzing previous tests conducted, which shown partial delamination as failure mode; a patch was used also on spikes anchor's tests in order to catch more fibers to be able to redistribute

stresses. Moreover, the first experimental program the author carried out, shown the effectiveness of using CFRP patches as new installation method, reason for which it seemed reasonable borrowing it and applying a patch also for the staple anchor's tests on slabs.

Figures 5.17 and 5.18 show the final product obtained from the fabrication process.

Figure 5.17 - Final product of a Flat staple anchor on slab

Figure 5.18 - Final product of slabs

Figure 5.19 shows a 3D view of the whole structure composed by concrete slab + Carbon FRP laminate + Flat Staple anchor + Carbon FRP patch for the two different configurations.

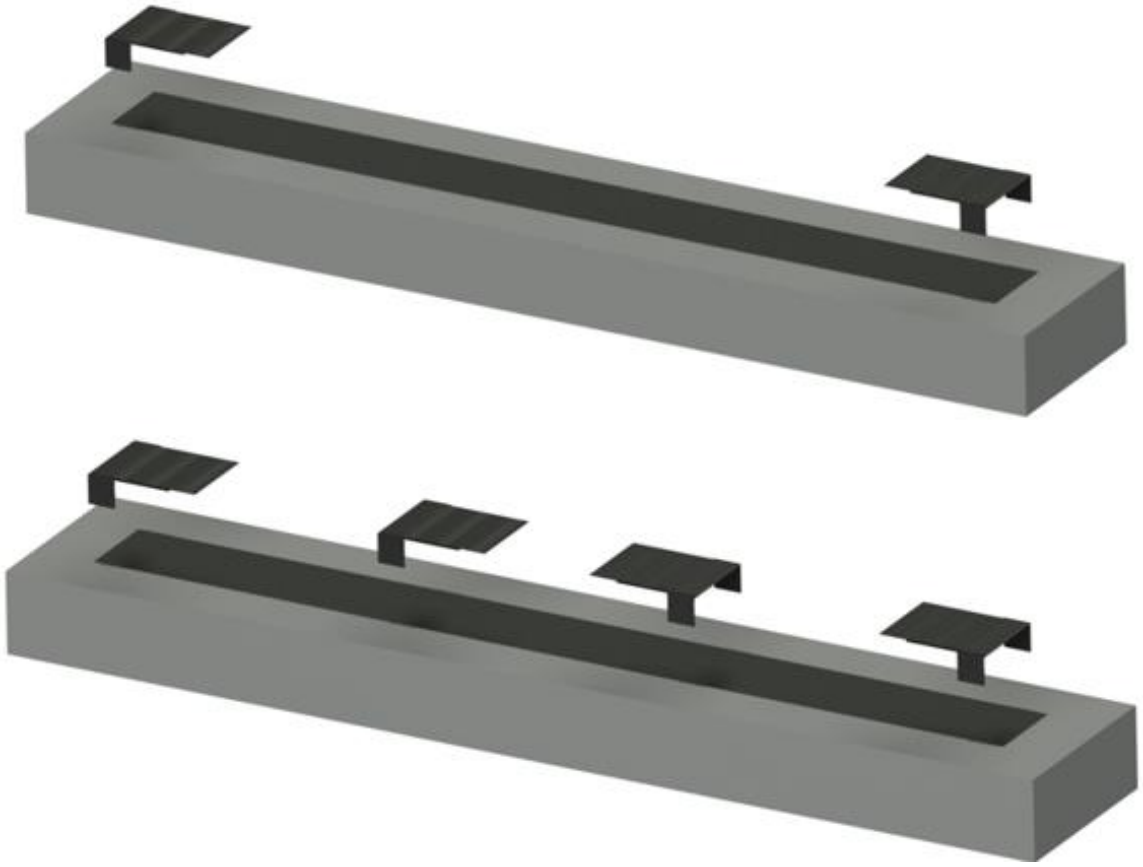

Figure 5.19 - 3D view of Concrete slab + CFRP Sheet + Flat Staple Anchor + CFRP Patch

Figure 5.20 illustrates a detail of the flat staple anchorage system on a slab.

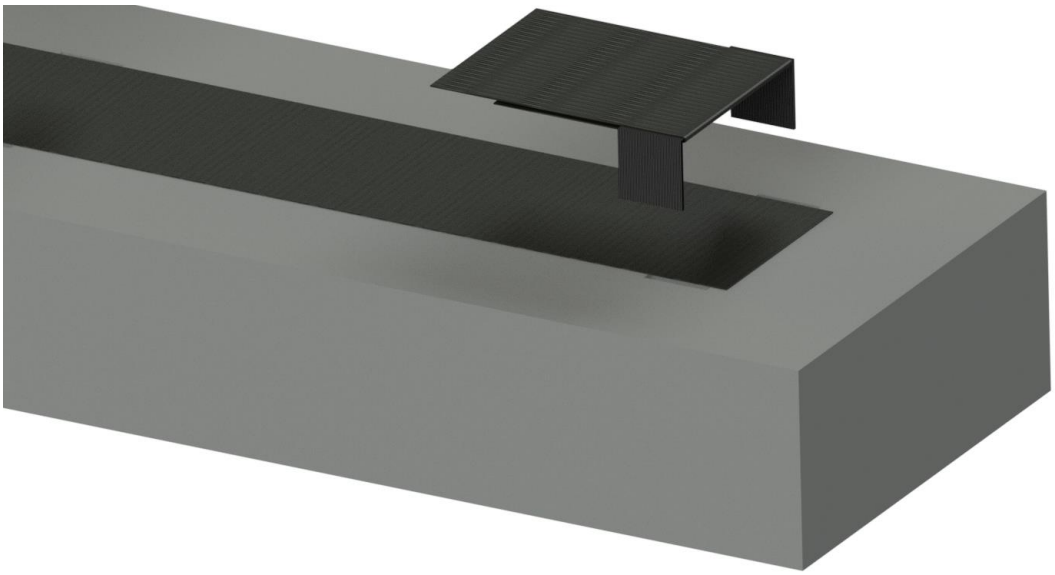

Figure 5.20 - Detail of the flat staple anchorage system on a slab

5.4 Test set-up

The experimental effort was focused on four bending tests on slabs, all CFRP-externally-reinforced, characterized by different anchors configurations (Figure 5.2).

The load is applied according to a three-point bending configuration, through a 55-kip MTS hydraulic actuator mounted on a testing frame. While a 4-point bending configuration is surely preferable, guaranteeing a pure bending behavior in the central portion of the span, the limited span of the tested elements, constrained by the geometry of the frame itself, forced to opt for the three-point solution. Applying concentrated load close to the supports in a 4-point shape would cause the element to move from a bending-prevalent behavior to a shear-controlled one. Preventing the effectiveness of the standard beam theory and making the tests not representative of a flexural reinforcement application.

5.4.1 Instrumentation

The 3-point bending tests were performed through a 55-Kip MTS hydraulic actuator mounted on a testing frame as shown in Figure 5.21.

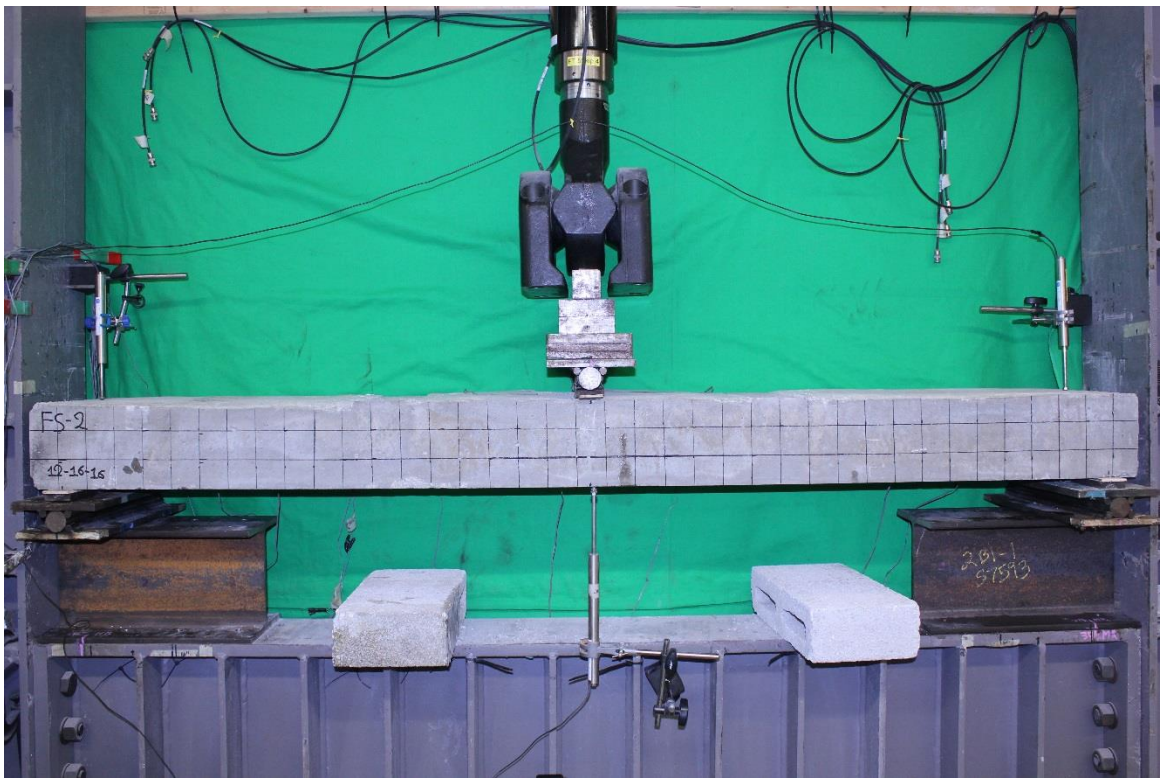

Figure 5.21 - 55-Kip MTS testing frame

The other instrumentation used was:

- *Steel plate*, used as supports.
- *Hydraulic jack*, used to apply load.
- *Load Cell*, used to measure the load.
- *Strain Gauges*, used to measure the strains.
- *LVDTs*, used to measure the displacements.
- *DAQ (Data Acquisition)*, the system used to acquire data from the Load Cell and Strain Gauges.

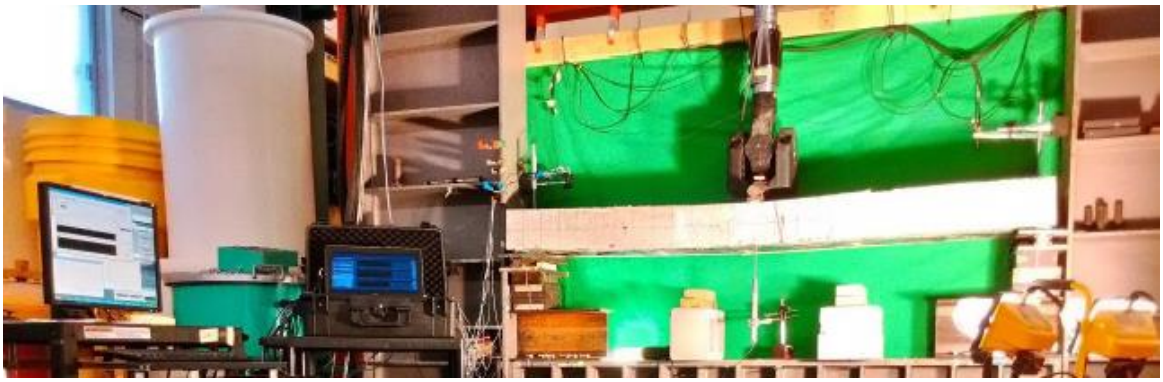

Figure 5.22 - Instrumentation used for the experimental program

The slabs were simply supported; the physical restraint was provided by two cylindrical hinges. Providing a roller at one end would have been preferable in order to avoid the confinement effect coming from the normal stresses, raising because of constrained sliding. The lack of available devices prevented this solution, however, on such a limited span, the prevented sliding and the related confinement effect is believed to be negligible.

Three LVDTs were applied to deflection measurement: a 10” (250 mm) one in mid-span and two 4” (100 mm) ones on the supports. The actuator also provides a mid-span deflection measurement backup itself. The consistency of the two measures has always been checked.

5.4.2 Strain Gauges

The strain gauges were used to read the strain distribution in the CFRP sheet and patch giving interesting parameters of what is happening in terms of internal forces in front and behind the patch as explained in the next chapter. Proper care should be taken in aligning the gauges along the fiber direction and in properly sticking them to the substrate. Also, concrete strain gauges were applied on the top of slabs as well as on internal steel re-bars.

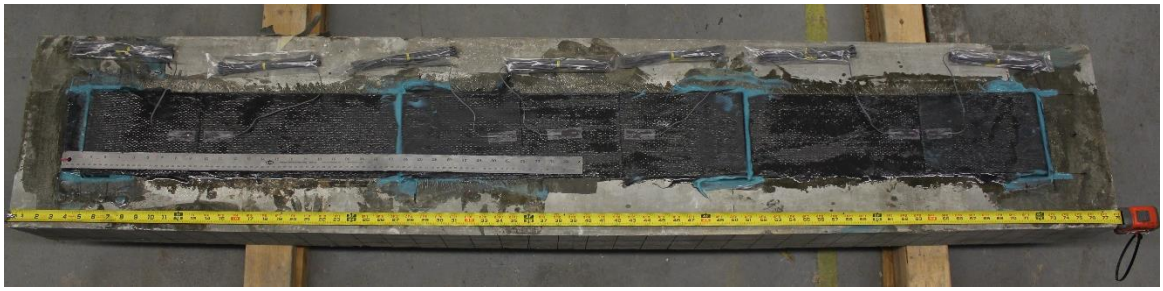

Figure 5.23 - Strain gauges on FRP

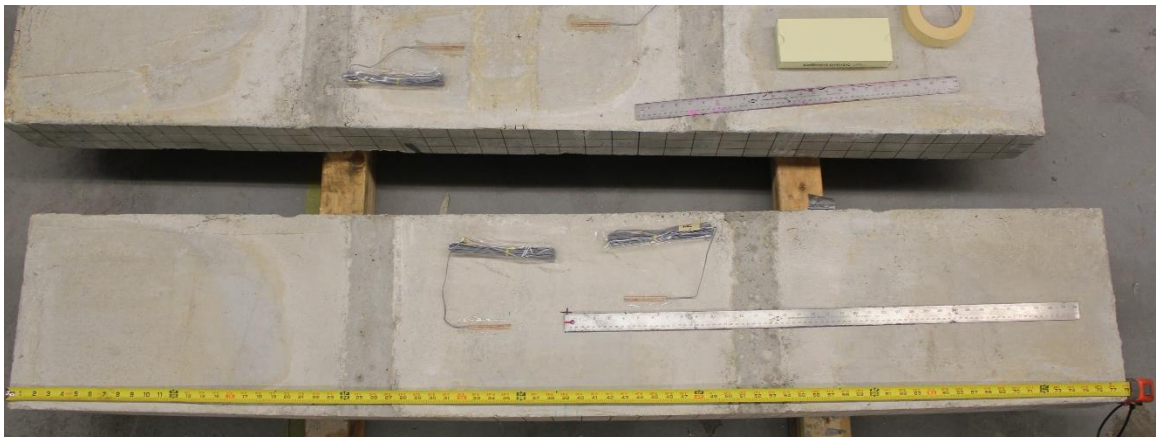

Figure 5.24 - Strain gauges on concrete

The gauge is attached to the specimens thanks to a suitable adhesive and as the CFRP sheet, concrete and steel rebar is deformed, tension or compression, cause its electrical resistance to change. This resistance change is then related to the strain by the quantity known as the gauge factor. All the information (electrical resistance, gauge factor and gauge length) were carefully updated and calibrated before starting each specimen test in the data acquisition system, which records the strains.

Electrical strain gauges of 6 mm length were used on FRP and steel, while 60mm length were used on concrete surface.

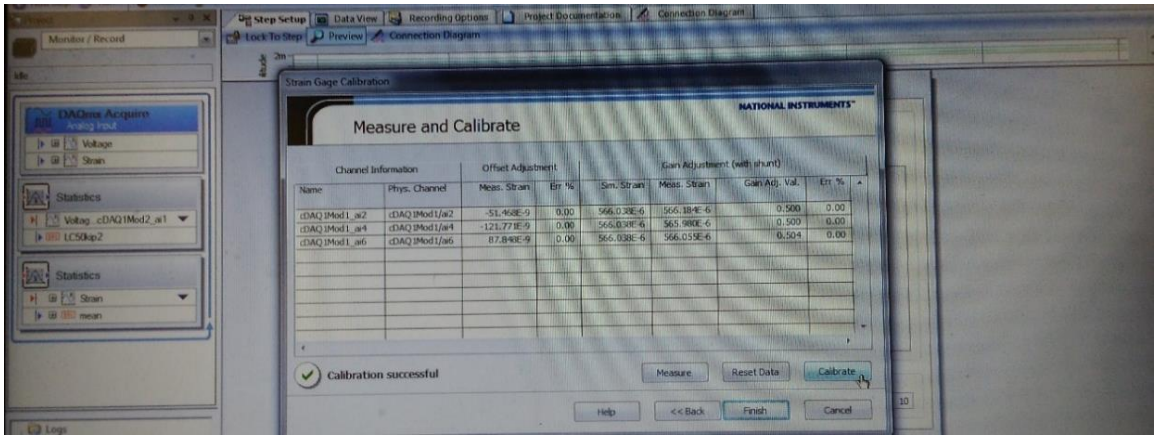

Figure 5.25 - Strain Gauge Calibration on DAQ

Strain gauges were placed, depending on the specimen, as shown in the following sketches. The position of the strain gauges FRP gages, directly applied on the impregnated sheet, was decided depending on what we were looking for. Considering the huge number of gauges, a careful labeling was required as well. Identified with FL, FR and FM, as meaning of "fiber left, right and middle", they were placed along the centerline in order to read the strain shape over the length of the FRP sheet; depending on the anchors' configuration strain gauges were positioned both on top of the CFRP patch as well on the laminate. Also, a strain gauge (FM) was positioned at mid-span, where highest strains are expected.

No Strain Gauges were positioned along the width of the CFRP laminate considering the scrupulous attention paid on setting up all the testing specimens very straight in order to apply the load evenly over the FRP laminate width.

Considering that the slabs were going to be flipped and positioned on the testing frame using a Forklift, the strain gages' wires were properly wired in order to avoid interferences during moving and positioning.

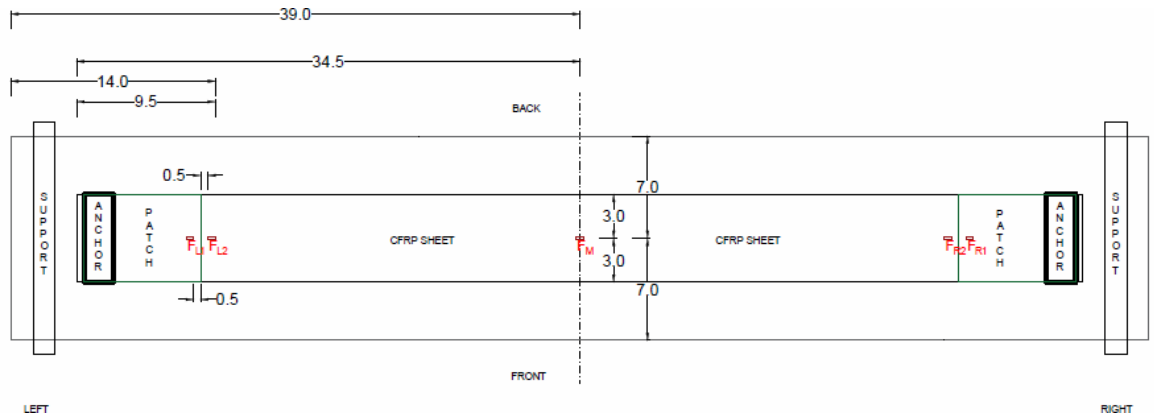

Figure 5.26 – FRP strain gauges' position on slabs 001 & 002 (bottom surface)

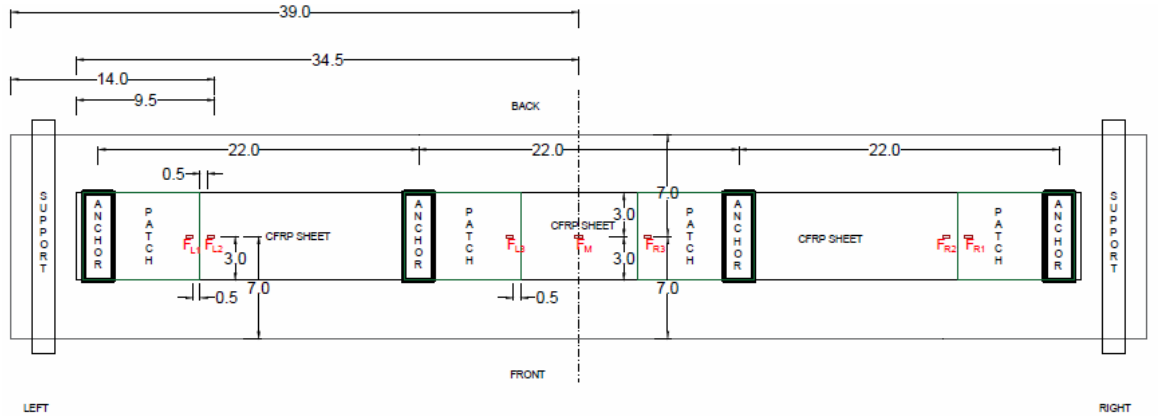

Figure 5.27 – FRP strain gauges' position on slabs 003 & 004 (bottom surface)

Concrete gauges, called “concrete left (CL) and concrete right (CR)” were applied on the top surface of slabs, as close as possible, considering the surface roughness, to the mid-span, where highest compression strains are expected. They are directly applied to the concrete surface, after a little sand-papering, over a thin epoxy layer, used to level and to make concrete surface flat.

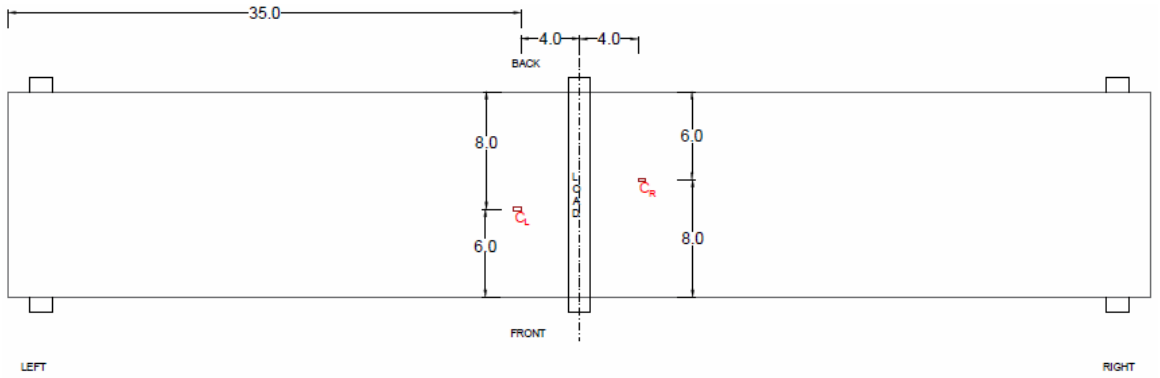

Figure 5.28 - Concrete strain gauges' position on all slabs (top surface)

Steel gauges, named “steel front (SF)” and “steel back (SB)”, were directly applied on rebars, after preparing the surface, and isolated in order to preserve them during casting operations as explained previously in chapter 5.2.

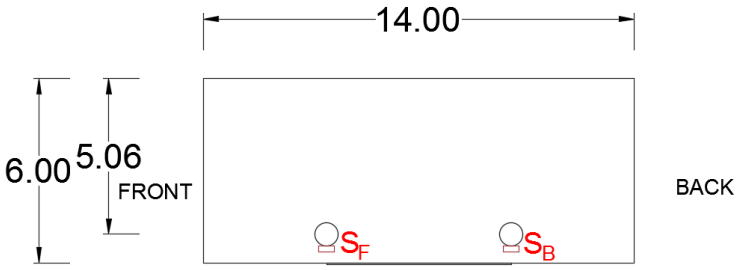

Figure 5.29 - Steel strain gauges' position on all slabs

5.4.3 Testing

Firstly, each specimen was careful positioned on the frame thanks to a forklift and properly aligned in order to have all the system straight. The steel supports were adjusted, before the positioning of the slab, to have a free span of 73.5 inches, as shown in the next chapter.

Figure 5.30 - Specimen set-up on the frame

Secondly, the instrumentation (Strain Gauges, LVDTs and Load Cell) were connected to the DAQ.

Figure 5.31 - Strain Gauges LVDTs and Load Cell connection

After that, they were calibrated as the following:

- FRP/Steel Strain gauges' info: 6mm length, 120 ± 0.5 Ω resistance, 2.11%-gauge factor.
- Concrete Strain gauges' info: 60mm length, 120.5 ± 0.5 Ω resistance, 2.13%-gauge factor.
- Load cell info: up to 55 kips (= 244 KN) of applied load.

Then, the 3-point bending test was performed with the following test set-up procedure: each specimen was pre-loaded to a load of 30-50 lbf. to allow the hydraulic jack to be engaged. The DAQ started recording the data from the very begging of the applied load; both the load and the displacement data were acquired and recorded every 0.01 seconds during the loading.

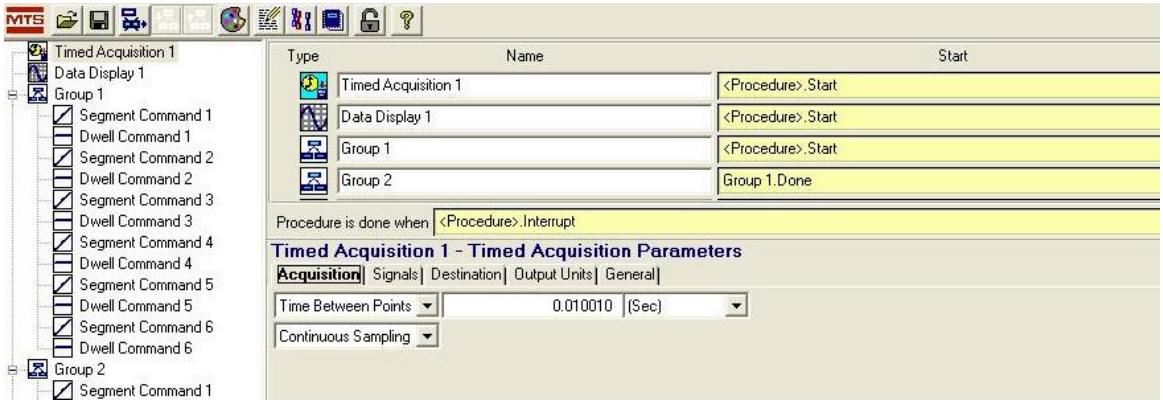

Figure 5.32 - MPT procedure - Time Acquisition

The load was increased by an automated procedure hereinafter explained. The load was applied in displacement control, with a load application rate varying from 0.0003 to 0.0024 in/s depending on the load goal for the particular cycle. The variation in the load application rate is believed to have no effect on the system's behavior, being anyway small enough to guarantee a quasi-static application. Even larger values are used after load drops, while trying to reach steel's failure, actually never reached because of the testing machine's limit on applicable deflection (about 5 in, 125 mm).

The displacement controlled cycles were programmed by an automated procedure created using "MPT Procedure Editor" of the MTS software. The procedure consists in different phases: loading at a certain rate, dwelling for 120 seconds, unloading. This because, reached a certain load, the slab need to dissipate the load energy, in fact some cracks came out during the dwell phase.

Load cycles were performed trying to catch each phase of the system failure (cracking, yielding, intermediate debonding, anchor failure, final collapse) and the related stiffness.

The following Figure 5.33 shows the first loading step; the load was increased as a ramp with a rate of 0.0003 in/sec in order to reach a controlled displacement of 0.15 inches.

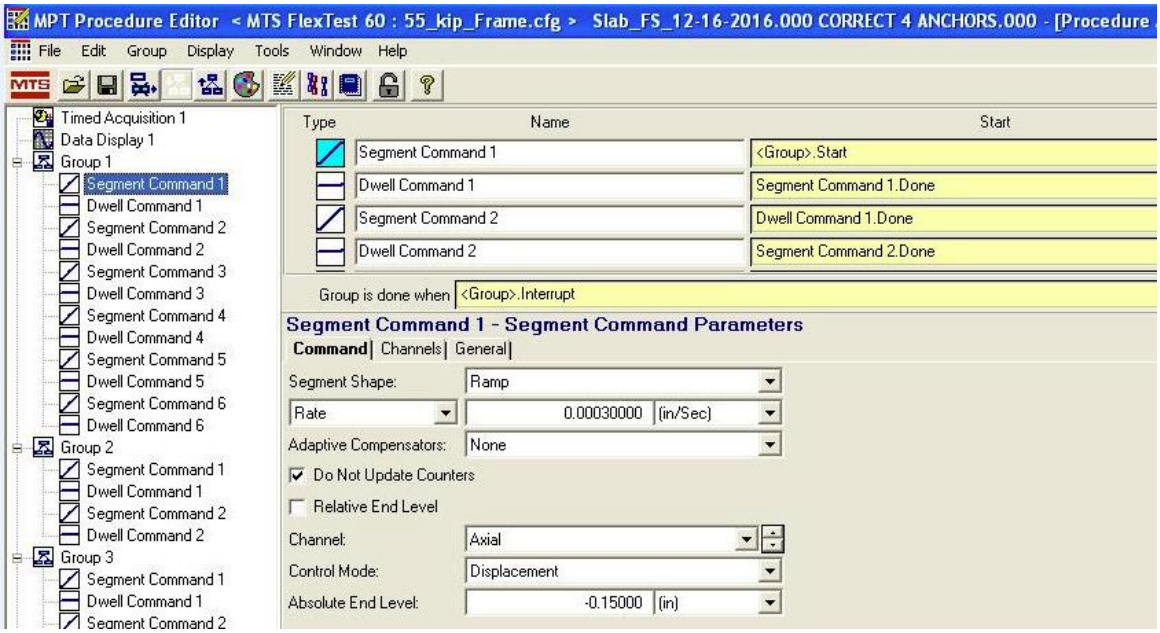

Figure 5.33 - MPT procedure - Loading step

The following Figure 5.34 illustrates the dwelling step; once the pre-set displacement of 0.15 inches was reached, the system was left dwelling for 120 seconds.

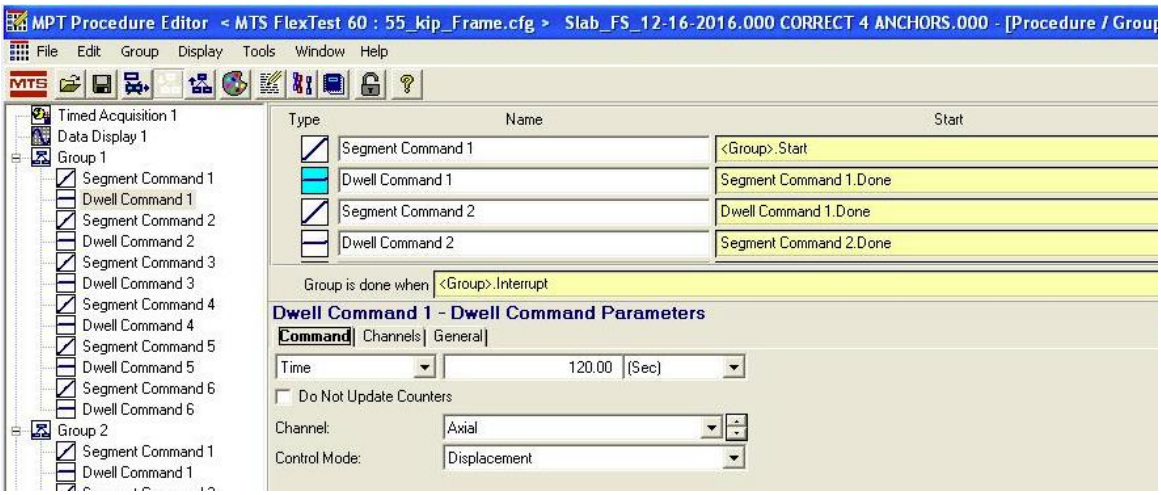

Figure 5.34 - MPT procedure - Dwelling step

After the dwelling phase, the specimen was unloaded; Figure 5.35 shows the unloading step; the displacement, with a rate of 0.00120 in/sec, was brought, basically, to 0 in, completely unloading the slab.

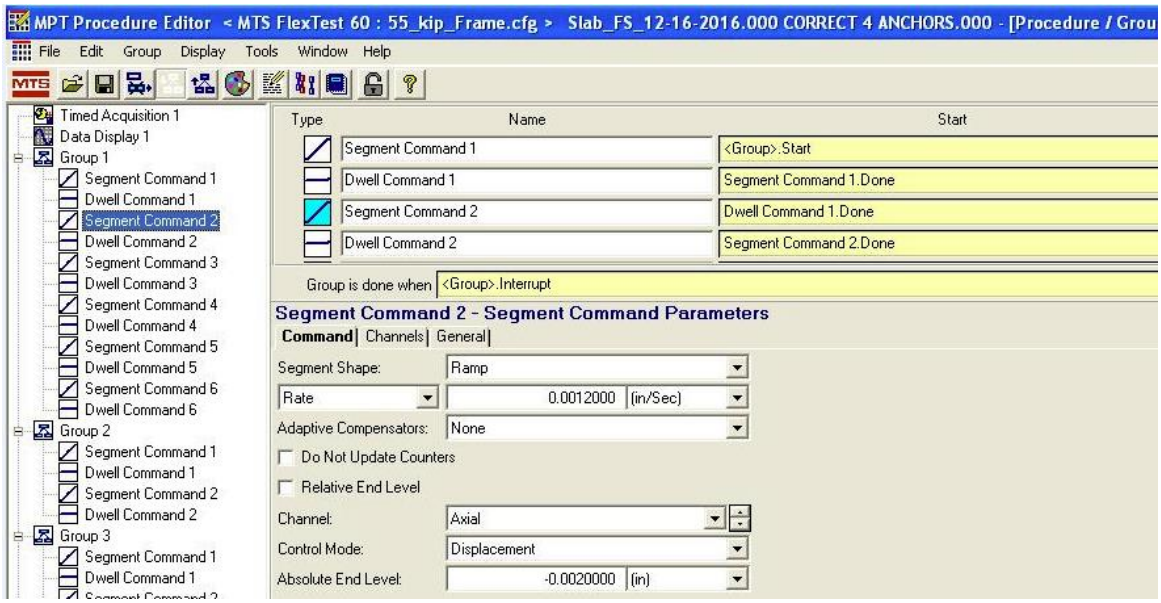

Figure 5.35 - MPT procedure - Unloading step

This loading, dwelling, unloading procedure was repeated cyclically catching each phase of the system failure according the following Table 5., which shows all the displacements set as absolute end levels for each step, where each critical phase is expected.

The load cycles, here reported for the sake of completeness, are defined according to the calculations and considerations reported in Appendix F.

		US	SI
		δ [in]	δ [mm]
Group 1	Cracking	0.15	3.81
		0.20	5.08
		0.25	6.35
Group 2	Yielding	0.50	12.70
Group 3	Intermediate Debonding	0.75	19.05
Group 4	Anchor's Failure	1.25	31.75
	Sheet Rupture	1.75	44.45
Group 5	Concrete Collapse	4.00	101.60
	Steel Rupture		

Table 5.1 - Load Cycles (displacement control)

Figure 5.36 illustrates a sample of the load cycles, just explained, of the configuration 2 of the specimen 003 obtained from the MTS.

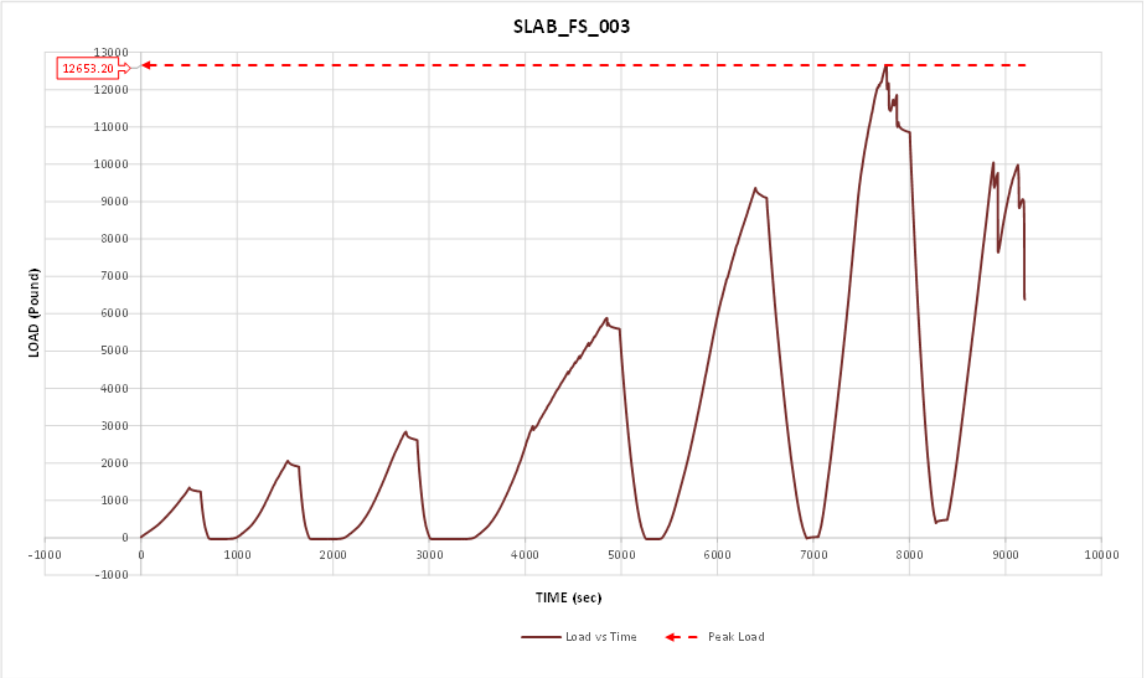

Figure 5.36 - Load Cycles' sample from MTS

Finally, as last step, the load was applied with a rate of a 0.0024 in/sec until the failure of the system occurred. Each test lasted between 2.5 and 3.5 hours.

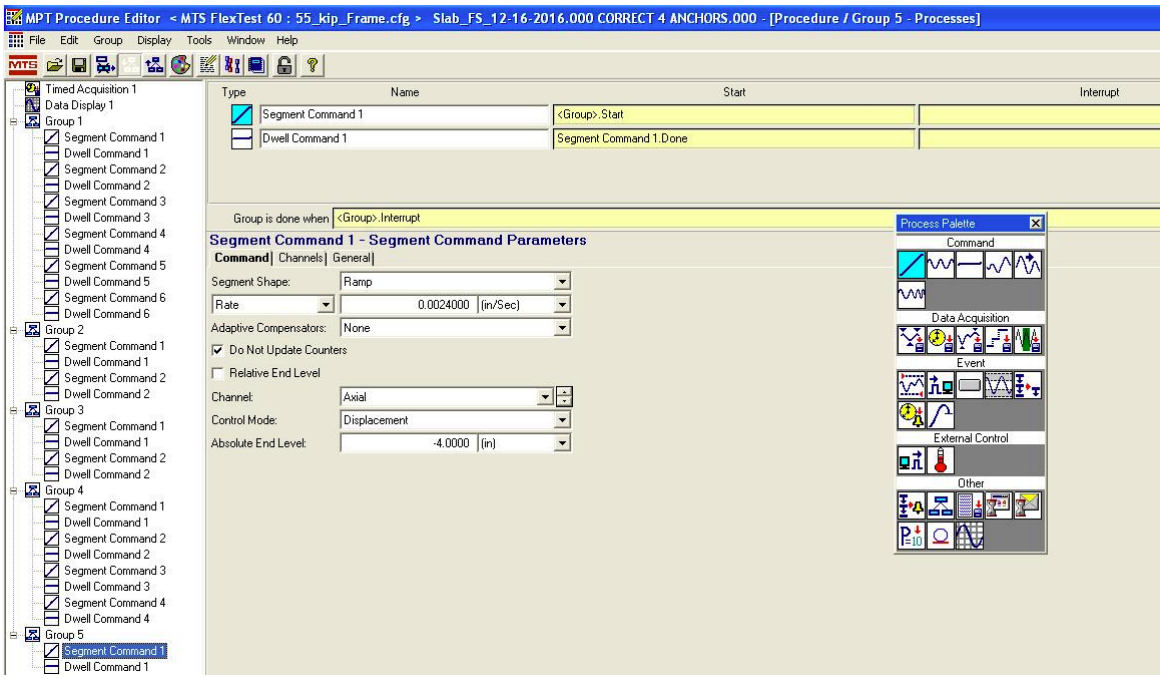

Figure 5.37 - MPT procedure - Loading until failure

Figure 5.38 shows the failure of a specimen at the end of the test.

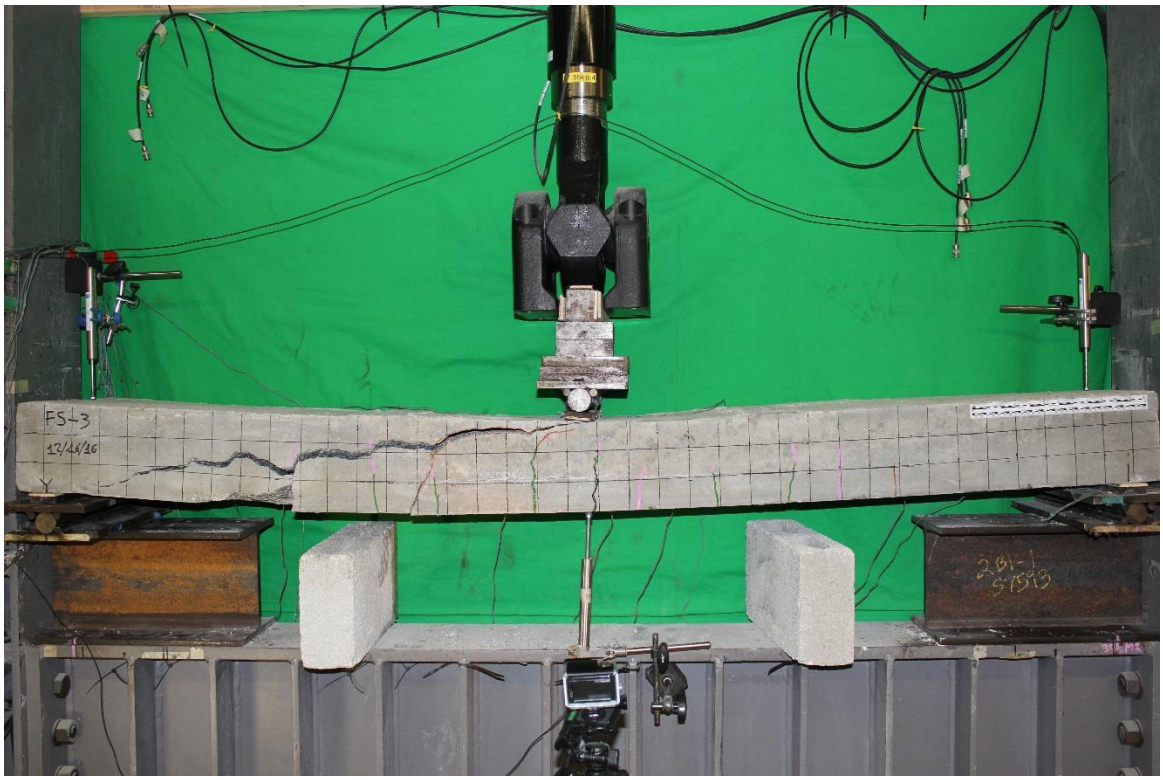

Figure 5.38 - Specimen failure at the end of the test

5.5 Material Properties

All the materials involved in the present research are here fully characterized.

5.5.1 Concrete

According with ASTM C39 (2014), the characterization of the concrete used in this research was performed by a compression test on standardized concrete cylinders in order to find their compressive strength (f'c). A total of ten cylinders, obtained casting the concrete into plastic molds in accordance with ASTM C31 (2014), were tested. The test consists on applying a compressive axial load to molded cylinders (plane surfaces were provided on the ends of the cylinders by following the "Standard Practice for Capping" (ASTM C617, 2015)) at a rate which is within a prescribed range until failure occurs.

The cylinders were subdivided in groups of 5 and tested at 28 and 60 days in compliance with ASTM C39 (2014). The compressive strength is assumed to remain constant after 28 days, the 28-days-average will hence be the value used for design and matching purposes. Figure 5.39 illustrates the test of the concrete cylinders, while Figure 5.40 shows the failure mode of the specimens.

Figure 5.39 - Compressive tests on concrete cylinders

Figure 5.40 - Specimen after the compression test

Table 5.2 - Compressive strength test results

Cylindrical concrete specimen test results															
	Specimen ID	Date cast	Date tested	Diameter [inches]			Area [inches^2]	Diameter Average	Diameter [mm]	Area [mm^2]	Peak load [lbs]	Peak load [KN]	f'c [Mpa]	f'c [psi]	Failure mode
				Midspan	Top	Bottom									
28 days after	_001	06.24.2016	07.29.2016	4.007	4.008	4.013	12.625	4.009	101.837	8145.196	105950	471.289	57.861	8392.026	Type 2
	_002	06.24.2016	07.29.2016	4.027	4.032	4.026	12.745	4.028	102.320	8222.578	116790	519.508	63.181	9163.578	Type 2
	_003	06.24.2016	07.29.2016	4.087	4.067	4.032	12.959	4.062	103.175	8360.593	114690	510.167	61.020	8850.258	Type 2
	_004	06.24.2016	07.29.2016	4.019	4.017	4.022	12.688	4.019	102.091	8185.878	105560	469.554	57.362	8319.583	Type 3
	_005	06.24.2016	07.29.2016	4.030	4.035	4.030	12.766	4.032	102.404	8236.192	107410	477.783	58.010	8413.674	Type 3
	Average										*110080.00*	*489.66*	*59.49*	*8627.82*	
	St deviation										*4709.40*	*20.95*	*2.25*	*326.49*	
	*Coefficient of variation (C.V) ((%)**										*4.28*	*4.28*	*3.78*	*3.78*	

Cylindrical concrete specimen test results															
	Specimen ID	Date cast	Date tested	Diameter [inches]			Area [inches^2]	Diameter Average	Diameter [mm]	Area [mm^2]	Peak load [lbs]	Peak load [KN]	f'c [Mpa]	f'c [psi]	Failure mode
				Midspan	Top	Bottom									
60 days after	_001	06.24.2016	08.19.2016	3.950	4.024	4.018	12.550	3.997	101.532	8096.512	103720	461.370	56.984	8264.793	Type 3
	_002	06.24.2016	08.19.2016	4.044	4.044	4.047	12.851	4.045	102.743	8290.759	111670	496.733	59.914	8689.798	Type 3
	_003	06.24.2016	08.19.2016	3.996	4.002	4.001	12.564	4.000	101.592	8105.967	111670	496.733	61.280	8887.899	Type 3
	_004	06.24.2016	08.19.2016	4.016	4.032	4.015	12.699	4.021	102.133	8192.668	110250	490.416	59.860	8682.018	Type 3
	_005	06.24.2016	08.19.2016	4.001	4.005	4.009	12.598	4.005	101.727	8127.599	106650	474.403	58.369	8465.761	Type 3
	Average										*108792.00*	*483.93*	*59.28*	*8598.05*	
	St deviation										*3130.65*	*13.93*	*1.47*	*213.56*	
	*Coefficient of variation (C.V) ((%)**										*2.88*	*2.88*	*2.48*	*2.48*	

** C.V. acceptable under 5% for tests on concrete*

Finally, results obtained from a full concrete characterization according both to ACI 318-14 (2014) and UNI EN 1992-1-1 (2008) are provided. The European norm allows a more detailed concrete characterization, the EC2 design data will hence be preferred in the following, as well as the EC2 notation. The ACI characterization will be referred for comparison purposes and will be used in ACI debonding formulas for the sake of consistency. Standard weight (150 lb./ft3, 2400 kg/m3) is assumed for the concrete.

Table 4.2 shows the results obtained from the characterization of the concrete.

	US			SI		
	EC2	ACI	[]	EC2	ACI	[]
ρc	150	145	[lb/ft3]	2400	2323	[Kg/m3]
f_{ck}	7.47	-	[Ksi]	51.49	-	[MPa]
f_{cm}	8.63	8.63	[Ksi]	59.49	59.49	[MPa]
f_{ctm}	0.60	0.70	[Ksi]	4.11	4.78	[MPa]
E_{cm}	5,448	5,448	[Ksi]	37,562	37,562	[MPa]
ν	0.2	-	[Ksi]	0.20	-	[MPa]
G	2,270	-	[Ksi]	15,651	-	[MPa]
ε_{crack}	0.11	0.13	[‰]	0.11	0.13	[‰]
ε_{c2}	2.10	-	[‰]	2.10	-	[‰]
ε_{c2u}	3.37	3	[‰]	3.37	3	[‰]
λ	0.80	0.85	[/]	0.80	0.85	[/]
η	0.99	0.85	[/]	0.99	0.85	[/]

Table 5.3 - Concrete design properties

A more detailed explanation of the constitutive laws and equations used to characterize all the material used in this research in order to obtain the design properties shown in this section is provided in Appendix F.

5.5.2 Steel

Five rebar specimens were tested in tension (Figure 5.), in compliance with ASTM A370. The yield strength was measured as the load corresponding to a 0.2% permanent deformation, referring to the experimentally measured stiffness to draw the offset line. All

the specimens showed a consistent elasto-plastic behavior and yielding starting at around 67 kips, as shown in Table 5.4.

Specimen	E [ksi]	Yield [ksi]
VP 6	27330	65.62
VP 7	28076	69.5
VP 8	28229	67.49
VP 9	28802	66.65
VP 10	29170	67.13
average	28321.4	67.28
st dev	632.9	1.28
cov	2.23%	1.90%

Table 5.4 - Steel measured properties

An elastic-perfectly plastic constitutive law is assumed for steel, in compliance either with EC2 (2008) and ACI 318 (2014). The experimental average values will be assumed as design values, both for elastic modulus and tensile strength, as shown in Table 5.5.

	US		SI	
f_y	67.28	[Ksi]	463.87	[MPa]
ε_y	0.24	[%]	0.24	[%]
$\varepsilon_{su,d}$	8.00	[%]	8.00	[%]
E_s	28,321	[Ksi]	195,270	[MPa]
n_s	5.20	[/]	5.20	[/]
ID	#3	[/]	Ø10	[/]
Ø	0.375	[in]	9.50	[mm]

Table 5.5 - Steel design properties

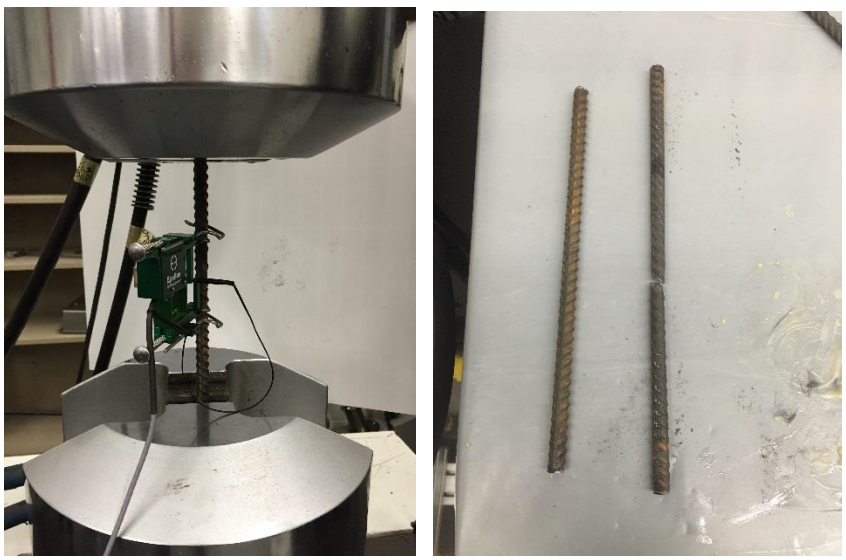

Figure 5.41 - Steel Tensile Characterization

5.5.3 CFRP Sheet, Epoxy and CFRP Anchor

Carbon Fiber Reinforced Polymer laminate, epoxy and CFRP Flat Staple anchors used for this second experimental program are exactly the same used for the first experimental program, already fully described in chapter 3.

Also for the FRP sheet the average measured properties are assumed as design ones. The material was always kept in laboratory condition and only few weeks passed between application and testing, also the applied FRP sheet was not engaged until testing, hence no exposure, aging or creep coefficient needs to be applied; also, considering the very good environmental performance of carbon material and low tendency to creep deformation.

Table 5.6 shows the results obtained from the characterization of the FRP.

FRP Sheet Design Properties

		US		SI	
Epoxy	f_{au}	10.50	[Ksi]	72.40	[MPa]
	E_a	461.00	[Ksi]	3,178.50	[MPa]
	ε_{au}	5.00	[%]	5.00	[%]
Dry Fiber	$f_{fu,dry}$	700.00	[Ksi]	4,826.36	[MPa]
	$E_{f,dry}$	40,000.00	[Ksi]	275,792.00	[MPa]
	$\varepsilon f_{u,dry}$	1.70	[%]	1.70	[%]
Impregnated Fiber	f_{fu}	194.26	[Ksi]	1,339.38	[MPa]
	E_f	10,820.00	[Ksi]	74,601.74	[MPa]
	n_f	1.99	[/]	1.99	[/]
	ε_{fu}	1.80	[%]	1.80	[%]
	t_f	0.04	[in]	1.02	[mm]
Bond	f_{bd}	0.79	[Ksi]	5.45	[MPa]
	l_{bd}	3.74	[in]	95.00	[mm]
	$\varepsilon_{fdd,1}$	0.42	[%]	0.42	[/]
	$\varepsilon_{fdd,2}$	0.70	[%]	0.70	[%]

Table 5.6 - FRP design properties

5.6 Final Matrix

The fundamental information and geometry data for each tested slab are summed up. Please refer to the Appendix for a complete configuration, geometry, and strain gauges' detail. The nomenclature, if ambiguous, is clarified on the list of symbols (at page XIX).

As already said, the experimental effort is focused on two slabs with config.1 anchor and other two with config. 2 anchor. The columns C-C and C-FRP are respectively referred to

an unreinforced specimen and to a control sample (only externally FRP bonded slab, with no anchors). Even if the author did not perform tests on C-C and C-FRP samples, results of those slabs were taken from previous research (Rossini, 2016) and normalized to be used also in this investigation in order to give the reader a complete overview of the test results discussed in the next chapter.

As a reminder, a 69 in (1.75 m) long, 6 in (152 mm) wide, 0.04 in (1 mm) deep, CFRP sheet is applied to the bottom of all the externally reinforced samples. The chosen width is consistent with the anchor's characterization, while 2.25 in (57.15 mm) from the physical supports, central lines are provided, in order to avoid interferences, hence the sheet length.

	CHARACTERIZATION [US]		C-C	C-FRP	Config.1	Config.2
GEOMETRY	L (tot)	[in]	78	78	78	78
	L (free)	[in]	73.5	73.5	73.5	73.5
	a	[in]	-	2.25	2.25	2.25
	a'	[in]	-	1.5	1.5	1.5
	l (frp)	[in]	-	69	69	69
	l (anchor)	[in]	-	66	66	66
	bc	[in]	14	14	14	14
	hc	[in]	6	6	6	6
	Ac	[in2]	84	84	84	84
	Jc	[in4]	252	252	252	252
REBAR	#	[/]	3	3	3	3
	n°	[/]	2	2	2	2
	Φ	[in]	0.375	0.375	0.375	0.375
	as	[in2]	0.110	0.110	0.110	0.110
	As	[in2]	0.221	0.221	0.221	0.221
	s	[in]	12.125	12.125	12.125	12.125
	c	[in]	0.75	0.75	0.75	0.75
	ds	[in]	5.06	5.06	5.06	5.06
FRP SHEET	n° plies	[/]	-	1	1	1
	bf	[in]	-	6	6	6
	tf	[in]	-	0.04	0.04	0.04
	Af	[in2]	-	0.24	0.24	0.24
	df	[in]	-	6.02	6.02	6.02

	CHARACTERIZATION [SI]		C-C	C-FRP	Config.1	Config.2
GEOMETRY	L (tot)	[mm]	1,981.20	1,981.20	1,981.20	1,981.20
	L (free)	[mm]	1866.90	1866.90	1866.90	1866.90
	a	[mm]	-	57.15	57.15	57.15
	a'	[mm]	-	38.10	38.10	38.10
	l (frp)	[mm]	-	1752.60	1752.60	1752.60
	l (anchor)	[mm]	-	1676.40	1676.40	1676.40
	bc	[mm]	355.60	355.60	355.60	355.60
	hc	[mm]	152.40	152.40	152.40	152.40
	Ac	[mm2]	54193.44	54193.44	54193.44	54193.44
	Jc	[mm4]	1.05E+08	1.05E+08	1.05E+08	1.05E+08
REBAR	#	[/]	3	3	3	3
	n°	[/]	2	2	2	2
	Φ	[mm]	9.53	9.53	9.53	9.53
	as	[mm2]	71.26	71.26	71.26	71.26
	As	[mm2]	142.51	142.51	142.51	142.51
	s	[mm]	307.98	307.98	307.98	307.98
	c	[mm]	19.05	19.05	19.05	19.05
	ds	[mm]	128.59	128.59	128.59	128.59
FRP SHEET	n° plies	[/]	-	1	1	1
	bf	[mm]	-	152.40	152.40	152.40
	tf	[mm]	-	1.02	1.02	1.02
	Af	[mm2]	-	154.84	154.84	154.84
	df	[mm]	-	152.91	152.91	152.91

Table 5.7 - Experimental Matrix

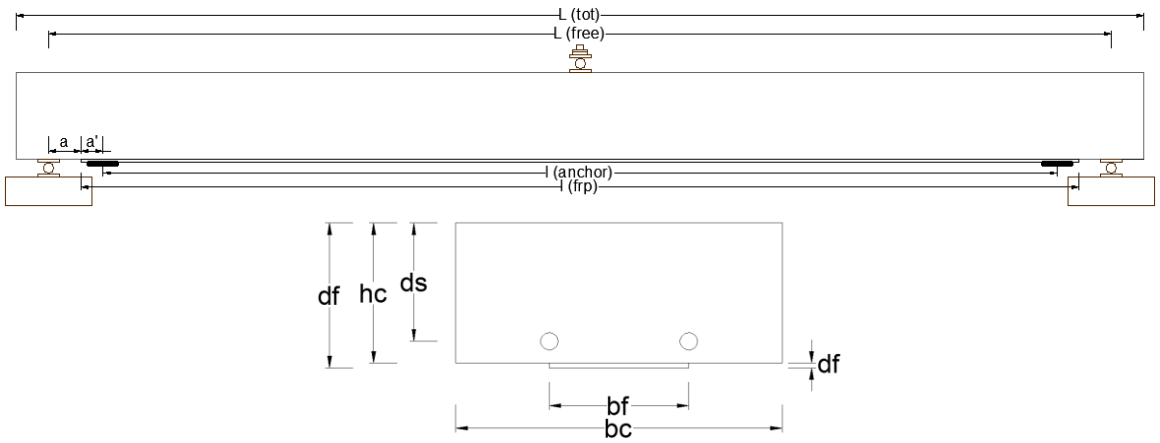

Figure 5.42 - Configuration's Geometry

CHAPTER 6

Experimental Program 2:
Test Results

The previous chapter covers all the aspects of the experimental campaign that was carried out, from the materials used to the FRP installation and testing set-up.

The specimens were tested in order to examine the performance of a new installation method for the flat staple anchors, to understand, eventually, the improvements in terms of distribution of strains, stresses and peak loads.

This chapter is divided into five main sections per the main studies developed in this research. To give the reader a better understanding of the tests results, a brief recap of the unreinforced sample (C-C) and the control sample (C-FRP) results coming from the previous research (Rossini, 2016) is, in the first two sections, provided. The third section presents a full analysis of the results obtained from the flat staple anchorage system installed at ends (configuration 1). The fourth section is dedicated to the results deduced from the testing of the flat staple anchorage system installed at ends and at a third of the slab's length (configuration 2). Also, in these two sections a description of the failure modes observed during the experimental campaign is given. The last section wants to be a results recap and recommendation for future studies. Also, in this section a comparison with the results obtained in previous research (Rossini, 2016) is provided to better understand, eventually, the improvement of the new installation method.

It is worth noting that, for the flat staple anchorage system installed at ends (configuration 1), we are interested on the safety, focusing on the ultimate capacity of the laminate. The aim is to avoid premature delamination (no bonding) of the CFRP sheet; in other word, the aim is to increase the capacity allowing the slab carrying more load when catastrophic events happen. In fact, the end anchor joints were designed in order to be engaged after intermediate debonding, providing the critical shear transfer mechanism required to further enhance the system strength at Ultimate Limit State, postponing collapse.

Regarding the flat staple anchorage system installed at a third of the slab's length (configuration 2), our main interest is to improve/increase the performance in terms of strains and load, engaging more of the FRP capacity and, so, allowing the system to sustain higher peak load developing more strains.

6.1 Unreinforced Sample (C-C) Recap

The unreinforced sample showed a Standard R/C response in bending, the tri-linear behavior is clearly visible in the load-deflection diagram. Ultimate theoretical strength was reached right after yielding, then the experimental value still rises slowly because of steel hardening, neglected in theoretical calculations (Rossini, 2016).

C-C [US]					
	Load	Deflection	Concrete	Steel	x
	[kip]	[in]	[%]	[%]	[in]
Elastic	1.57	0.09	-0.003%	0.03%	1.36
Cracked	3.30	0.33	-0.011%	0.22%	1.00
Yielding Start	4.41	0.48	-0.007%	0.31%	0.87
Zero	4.33	0.49	0.000%	0.31%	0.75
Failure	4.49	0.56	0.045%	0.39%	0.05

Table 6.1 - Unreinforced Sample (C-C) test results

Experimental Matching [US]									
	Load [kip]			Deflection [in]			x [in]		
	Exp.	Th.	Δ	Exp.	Th.	Δ	Exp.	Th.	Δ
Elastic	1.57	-	-	0.09	-	-	1.36	3.04	-55.20%
Cracked	3.30	-	-	0.33	-	-	1.00	0.98	2.22%
Yielding Start	4.41	4.01	9.86%	0.48	0.33	48.45%	0.87	0.64	35.54%
Failure	4.49	4.14	8.32%	0.56	0.42	34.45%	0.05	0.15	-66.12%

Table 6.2 - Unreinforced Sample (C-C) experimental matching

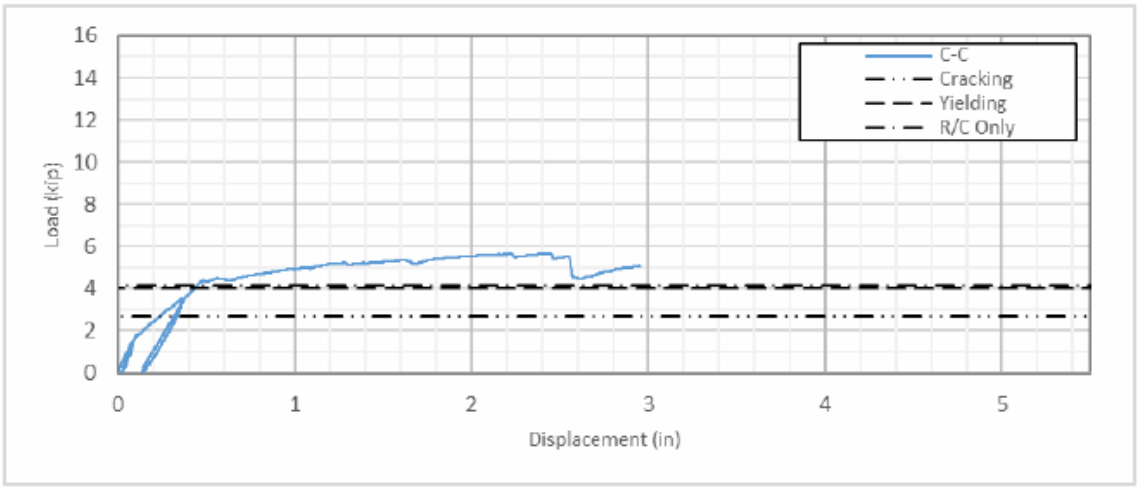

Figure 6.1 - Unreinforced Sample (C-C) load vs deflection diagram

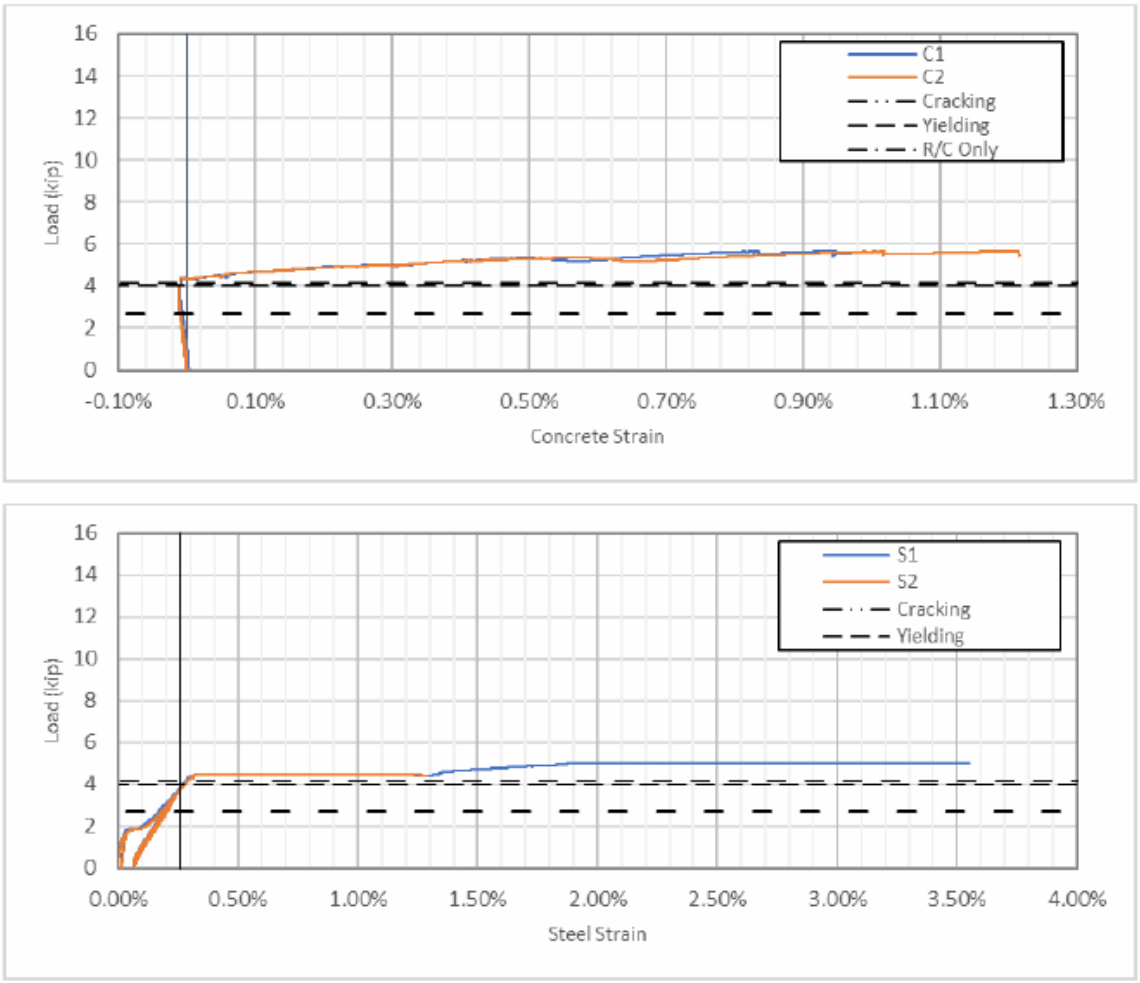

Figure 6.2 - Unreinforced Sample (C-C) load vs concrete/steel strain diagram

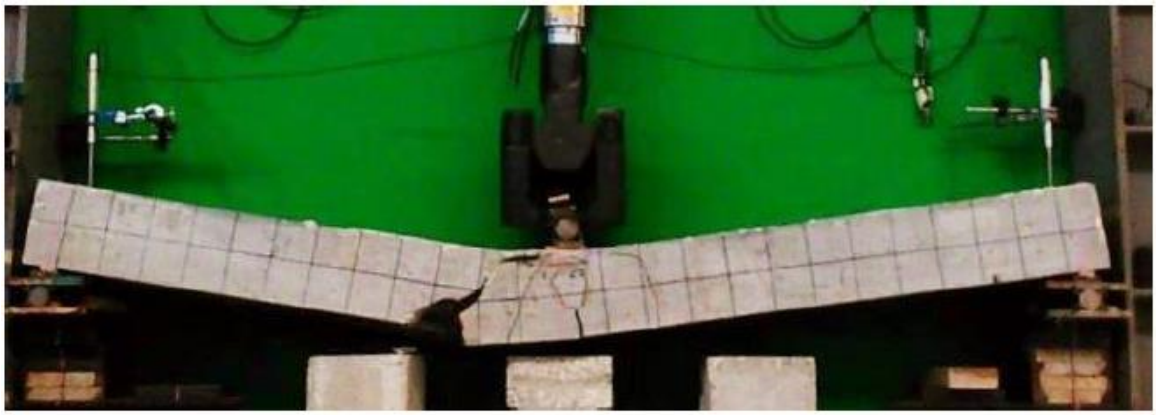

Figure 6.3 - C-C Specimen failure at the end of the test

6.2 Control (C-FRP) Sample Recap

The control sample (C-FRP) shows a bi-linear behavior up to intermediate debonding, when the slab's strength suddenly drops to standard R/C value. The strength than slowly linearly increases, because of rebars' hardening.

The measured strain value at FRP level is an average over three gages located at midspan: a concave strain distribution was spotted, with a peak on the side where debonding started. A very good average-strain matching can be noticed at failure. Notice also the very good matching on the deflection side.

Even more remarkable is how both theoretical load and strain show the same percentage error: this means the sectional theory perfectly applies to externally reinforced elements, while the small error is related to debonding prediction (Rossini, 2016).

C-FRP [US]						
	Load	Deflection	Concrete	Steel	FRP	x
	[kip]	[in]	[%]	[%]	[%]	[in]
Elastic	1.50	0.06	-0.011%	0.006%	0.010%	3.80
Cracked	3.89	0.24	-0.047%	0.11%	0.22%	2.00
Loose S2	4.91	0.33	-0.055%	0.15%	0.25%	1.94
Yielded	6.75	0.55	-0.088%	-	0.40%	1.69
Debonding	9.33	0.82	-0.112%	-	0.66%	1.51

Table 6.3 - Control Sample (C-FRP) test results

C-FRP Experimental Matching [US]												
	Load [kip]			Deflection [in]			ε_f [%]			x [in]		
	Exp.	Th.	Δ	Exp.	Th.	Δ	Exp.	Th.	Δ	Exp.	Th.	Δ
Elastic	1.50	-	-	0.06	-	-	0.01%	-	-	3.80	3.04	24.95%
Cracked	3.89	-	-	0.24	-	-	0.22%	-	-	2.00	0.98	103.85%
Loose S2	4.91	-	-	0.33	-	-	0.25%	-	-	1.94	0.98	97.74%
Yielding	6.75	6.55	3.12%	0.55	0.51	7.36%	0.40%	0.32%	26.37%	1.69	0.78	116.72%
Debonding	9.33	9.68	-3.58%	0.82	0.75	8.88%	0.66%	0.70%	-5.18%	1.51	0.66	130.74%

Table 6.4 - Control Sample (C-FRP) experimental matching

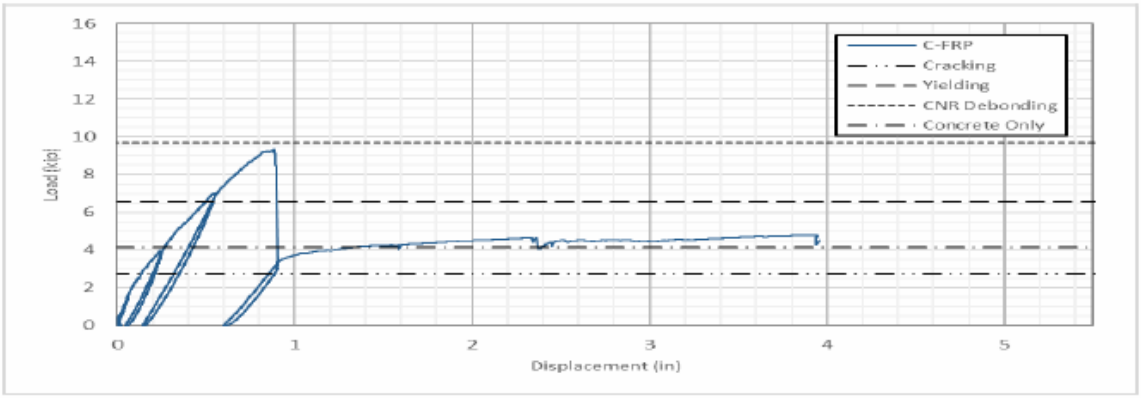

Figure 6.4 - Control Sample (C-CFRP) load vs deflection diagram

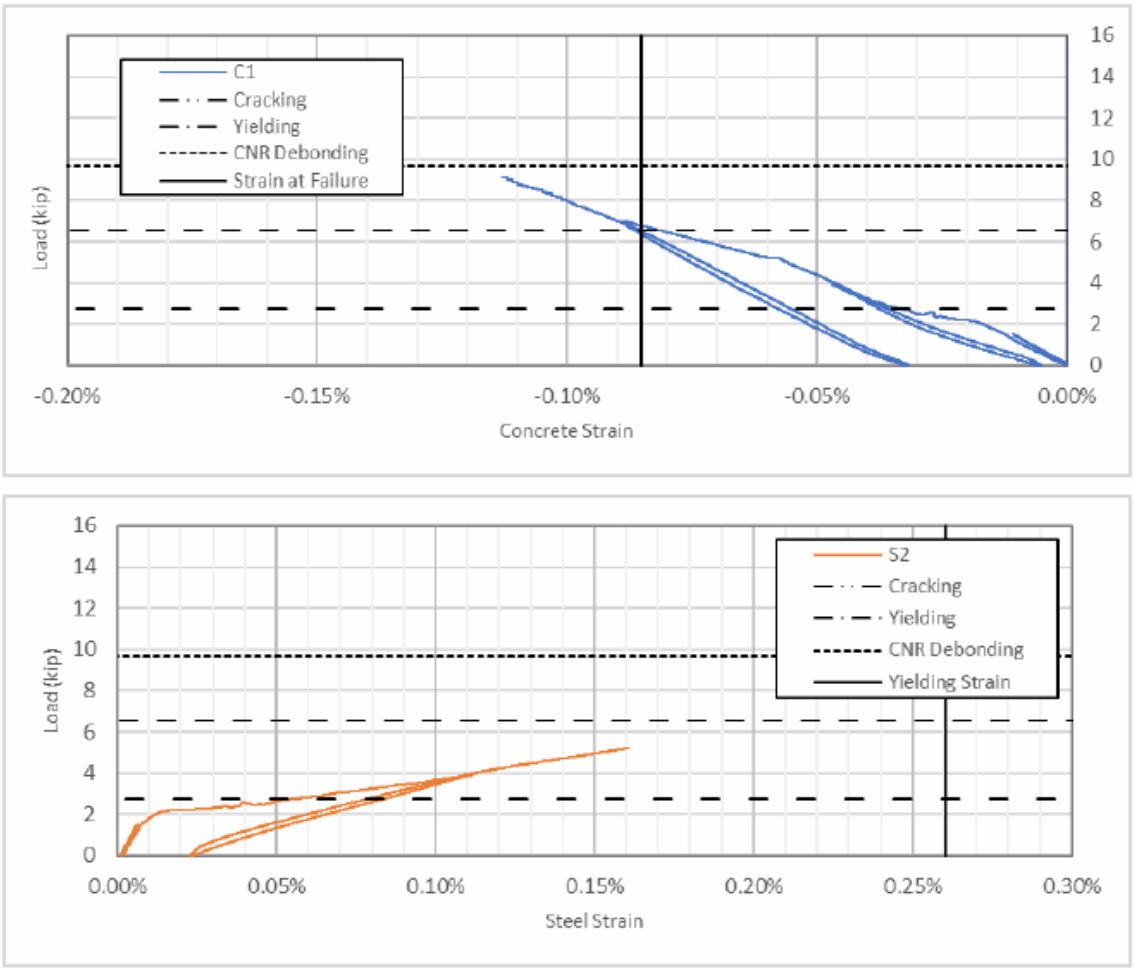

Figure 6.5 - Unreinforced Sample (C-C) load vs concrete/steel strain diagram

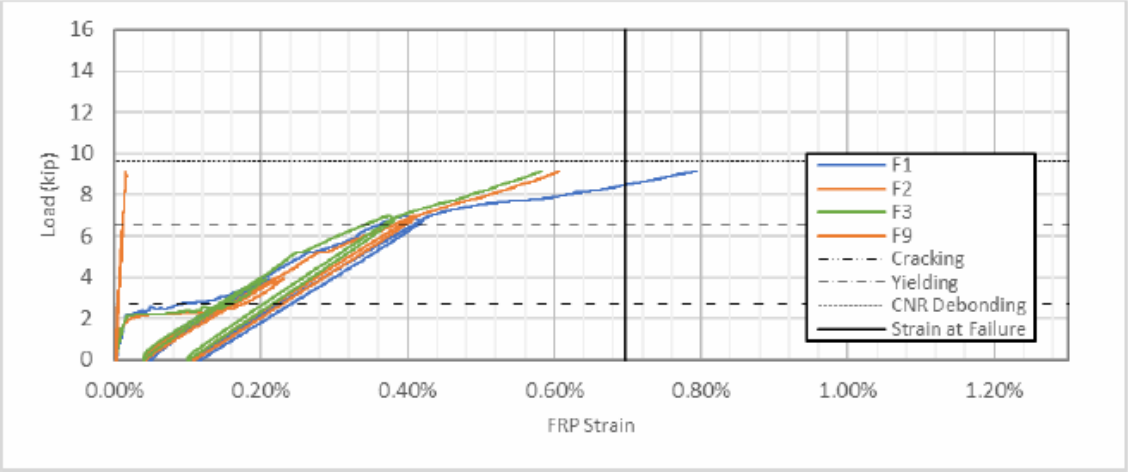

Figure 6.6 - Unreinforced Sample (C-C) load vs FRP strain diagram

Looking to the strains evolution in the FRP, the external reinforcement engagement as cracking starts can be clearly spotted, in good agreement with what theoretically computed. Also, a larger engagement ratio can be spotted as yielding starts.

Notice the very low level of strain in location F9, at the very end of the sheet, in line with what computed checking on end debonding. Also, notice the sudden strain increment in the concrete, as cracks appear. Regarding steel strain diagram, please notice the steel gage went lost before yielding.

It is important noticing that strain gauges' configuration was different to the one used in this research, as shown in Figure 6.7.

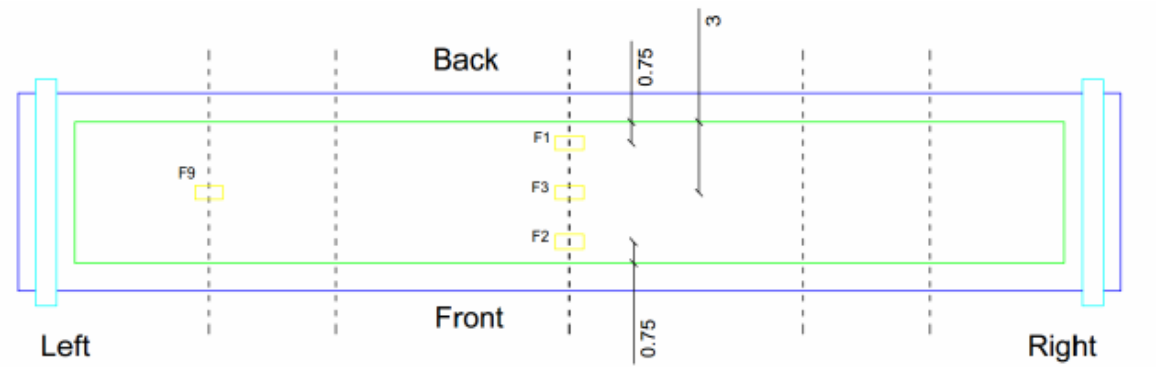

Figure 6.7 - Strain gauges' previous research configuration

Figure 6.8 shows the failure of the C-FRP specimen at the end of the test.

Figure 6.8 - C-FRP Specimen failure at the end of the test

6.3 Configuration 1 – Ends Flat Staples Anchors

As in the control sample, a bi-linear behavior up to debonding can be clearly spotted; as debonding happened, the end anchors were suddenly engaged, providing the critical mechanism for sheet-concrete load transfer. As debonding proceeded behind the end anchor, the system experienced a series of load drops and increments; after this transition phase, the strength started growing again, with a sensibly reduced stiffness, as bonding was no longer provided.

It should be noticed how the anchors' presence has no influence on the value of intermediate debonding load, suggesting end anchors do not provide any intermediate bonding improvement at serviceability, while provide a relevant strength and ductility increment at ultimate limit state.

Because of, from the first experimental program, it was spotted that strains over the sheet's width were even distributed and considering that an appropriate installation was performed, only mid-span strain gauges were positioned, as shown in Figure 5.26. Strain gauges were applied also on concrete top surface and on steel rebars.

The slab 002 showed the same behavior described above, as well as the same good matching on the strain and load side. Usually in these kind of test, due to the cost and time demanding to prepare specimens, no double test is performed as in this research. In fact, the willing to perform the same test for each configuration on two specimens was to get a validation of the results.

In the following, test results are provided, focusing on the two main phases of debonding and ultimate load reached by the slabs. For sake of completeness, all the results obtained from the 3-point bending tests are provided in Appendix E.

Table 6.5 and Table 6.6 shows the results obtained from the 3-point bending test performed on slab 001 and 002.

FLAT STAPLE 2" - Configuration 1 (ends) - TEST RESULTS - Slab 001

	US					SI				
	Load [Kip]	Deflection δ [in]	FRP Strain[%]	Concrete Strain[%]	x [in]	Load [KN]	Deflection δ [mm]	FRP Strain[%]	Concrete Strain[%]	x [mm]
Debonding	9.846	1.532	0.448	0.070	0.707	43.797	38.907	0.448	0.070	17.963
Ultimate	10.986	3.069	0.613	0.062	0.681	48.868	77.948	0.613	0.062	17.289

Table 6.5 - Slab 001 test results

FLAT STAPLE 2" - Configuration 1 (ends) - TEST RESULTS - Slab 002

	US					SI				
	Load [Kip]	Deflection δ [in]	FRP Strain[%]	Concrete Strain[%]	x [in]	Load [KN]	Deflection δ [mm]	FRP Strain[%]	Concrete Strain[%]	x [mm]
Debonding	9.210	1.257	0.548	0.077	0.828	40.967	31.927	0.548	0.077	21.034
Ultimate	10.730	2.631	0.685	0.085	0.717	47.729	66.831	0.685	0.085	18.217

Table 6.6 - Slab 002 test results

Table 6.7 and Table 6.8 illustrates the matching between the experimental results obtained from the 3-point bending test on slab 001 & 002 and the theoretical results coming from the preliminary design explained in Appendix F.

The anchor's ultimate load is quite close and even above the theoretical one confirming that specimens' preparation, anchors' installation and test procedure were well performed, giving consistency on the test's results.

FLAT STAPLE 2" - Configuration 1 (ends) - EXPERIMENTAL MATCHING [US] - Slab 001

	Load [kip]			Displacement [in]			FRP Strain[%]			x [in]		
	Exp.	Th.	Δ [%]	Exp.	Th.	Δ [%]	Exp.	Th.	Δ [%]	Exp.	Th.	Δ [%]
Debonding	9.846	9.018	9.18%	1.532	1.020	50.24%	0.448	0.658	-31.97%	0.707	0.710	-0.38%
Ultimate	10.986	9.561	14.91%	3.069	1.171	162.11%	0.613	0.724	-15.25%	0.681	0.700	-2.82%

FLAT STAPLE 2" - Configuration 1 (ends) - EXPERIMENTAL MATCHING [SI] - Slab 001

	Load [KN]			Displacement [mm]			FRP Strain[%]			x [mm]		
	Exp.	Th.	Δ [%]	Exp.	Th.	Δ [%]	Exp.	Th.	Δ [%]	Exp.	Th.	Δ [%]
Debonding	43.797	40.116	9.18%	38.907	25.897	50.24%	0.448	0.658	-31.97%	17.963	18.032	-0.38%
Ultimate	48.868	42.528	14.91%	77.948	29.739	162.11%	0.613	0.724	-15.25%	17.289	17.790	-2.82%

Table 6.7 - Slab 001 experimental matching (Exp.= experimental; Th.= theoretical)

FLAT STAPLE 2" - Configuration 1 (ends) - EXPERIMENTAL MATCHING [US] - Slab 002

	Load [kip]			Displacement [in]			FRP Strain[%]			x [in]		
	Exp.	Th.	Δ [%]	Exp.	Th.	Δ [%]	Exp.	Th.	Δ [%]	Exp.	Th.	Δ [%]
Debonding	9.210	9.018	2.12%	1.257	1.020	23.28%	0.548	0.658	-16.69%	0.828	0.710	16.65%
Ultimate	10.730	9.561	12.23%	2.631	1.171	124.73%	0.685	0.724	-5.38%	0.717	0.700	2.40%

FLAT STAPLE 2" - Configuration 1 (ends) - EXPERIMENTAL MATCHING [SI] - Slab 002

	Load [KN]			Displacement [mm]			FRP Strain[%]			x [mm]		
	Exp.	Th.	Δ [%]	Exp.	Th.	Δ [%]	Exp.	Th.	Δ [%]	Exp.	Th.	Δ [%]
Debonding	40.967	40.116	2.12%	31.927	25.897	23.28%	0.548	0.658	-16.69%	21.034	18.032	16.65%
Ultimate	47.729	42.528	12.23%	66.831	29.739	124.73%	0.685	0.724	-5.38%	18.217	17.790	2.40%

Table 6.8 - Slab 002 experimental matching (Exp.= experimental; Th.= theoretical)

Figure 6.9 illustrates the load cycles over the time.

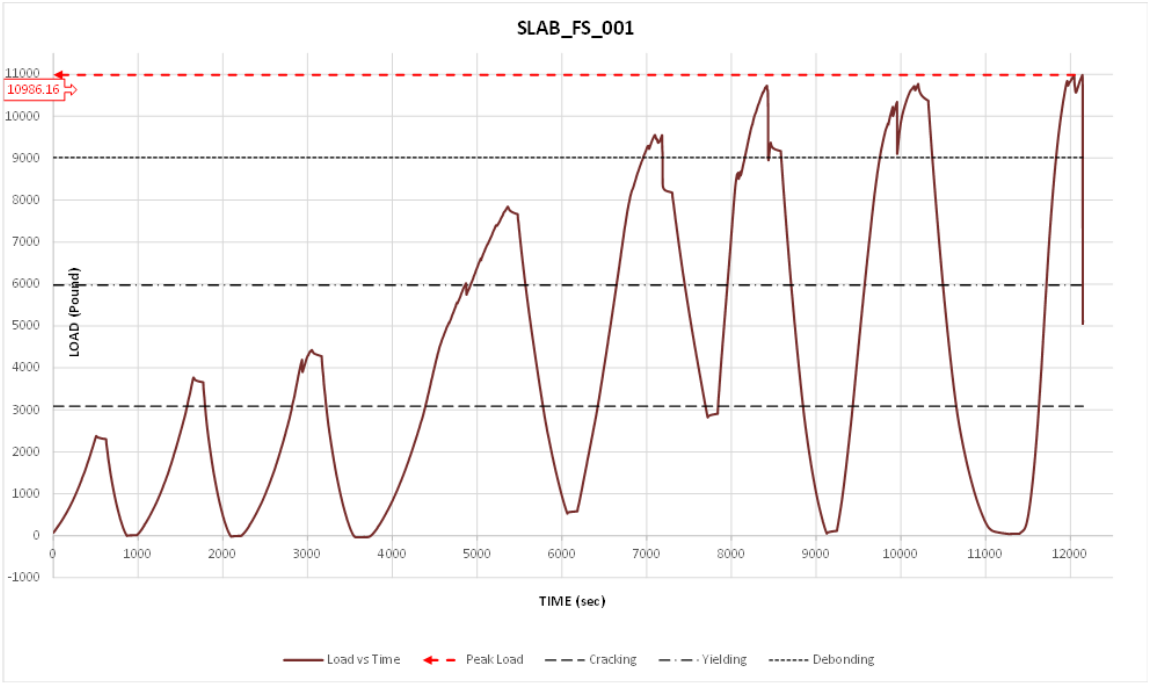

Figure 6.9 – Slab 001 load vs time diagram

Figure 6.10 shows the load vs deflection; as explained in the previous chapter it is possible to clearly see the cyclic load until the failure, marked by the peak load line, as meaning of the highest load reached by the slab.

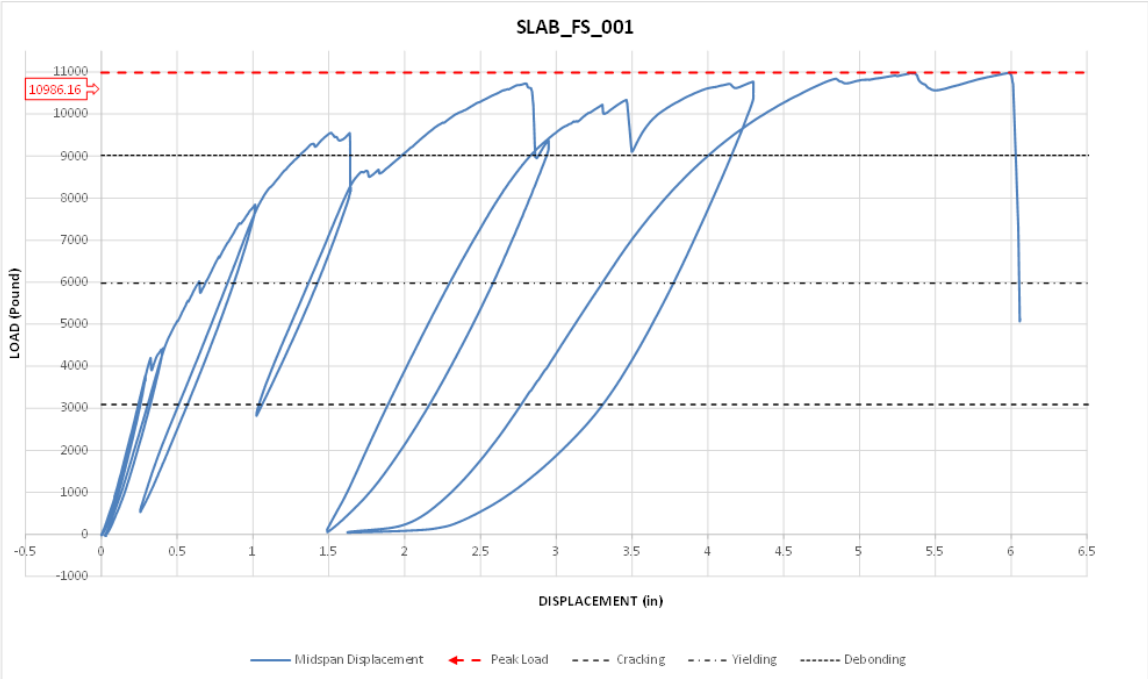

Figure 6.10 – Slab 001 load vs deflection diagram

Moreover, looking at the envelope it is possible to calculate the energy, corresponding to the area under the curve.

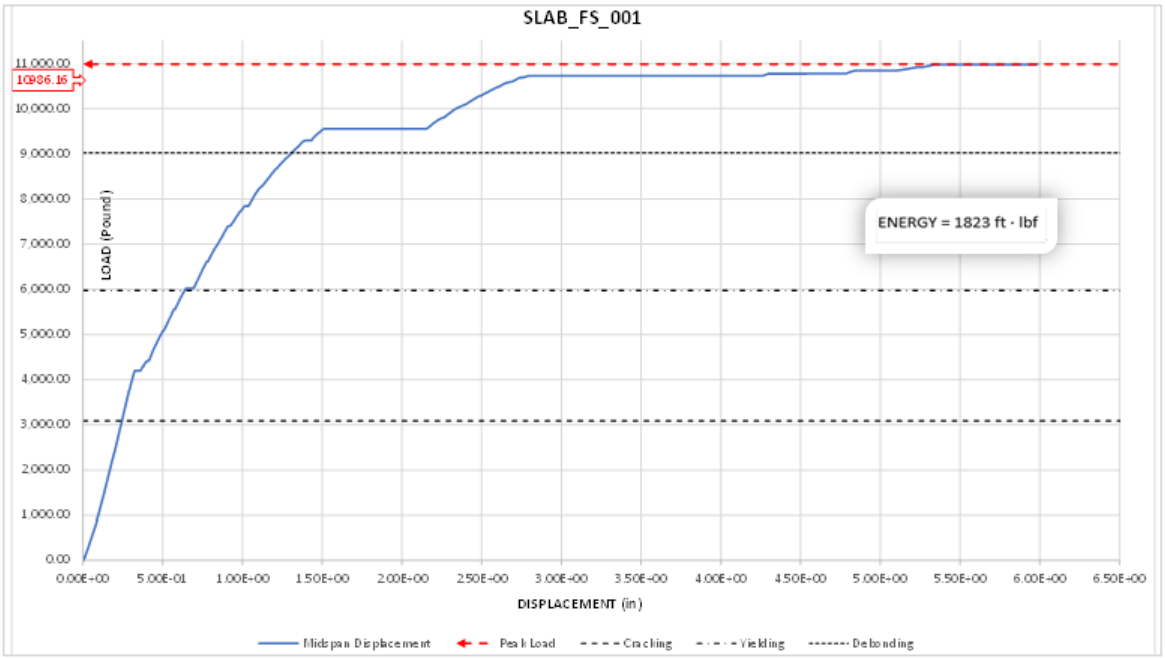

Figure 6.11 - Slab 001 load vs deflection envelope diagram

From the following Figure 6.12 it is possible noting that during the three first cycles the displacement came back to zero as meaning of the elastic behavior of the slab; after that, the slab experienced a permanent deformation, as meaning of a plastic behavior reached from the fourth loading cycle forward.

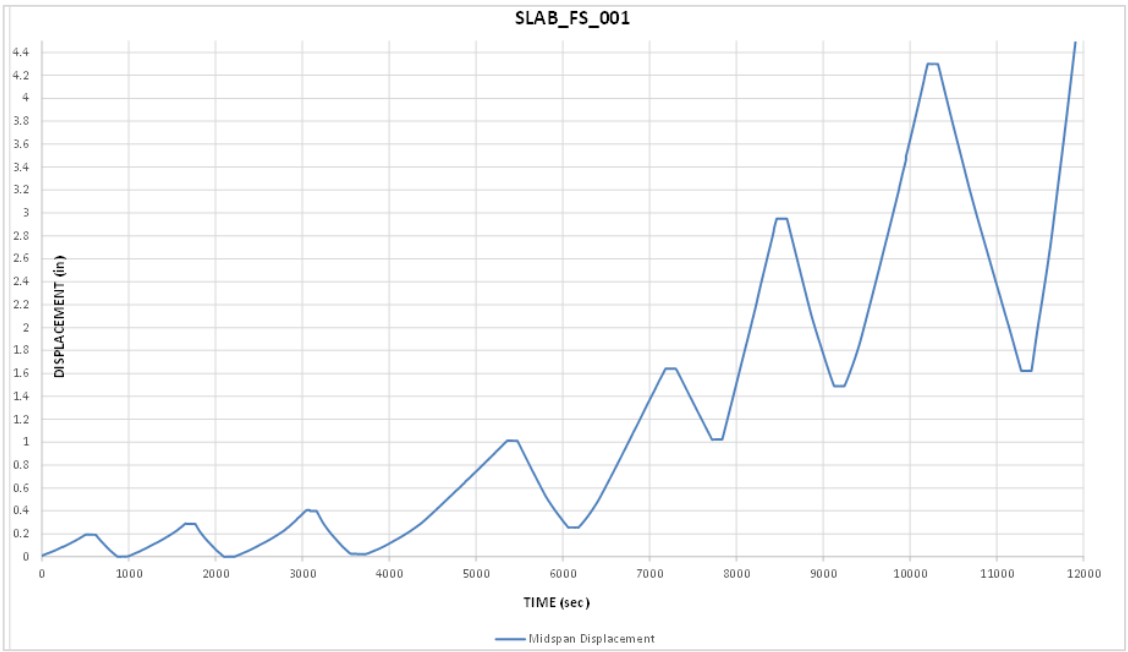

Figure 6.12 – Slab 001 displacement vs time diagram

The following figures show the evolution of concrete strains increasing the load over the time.

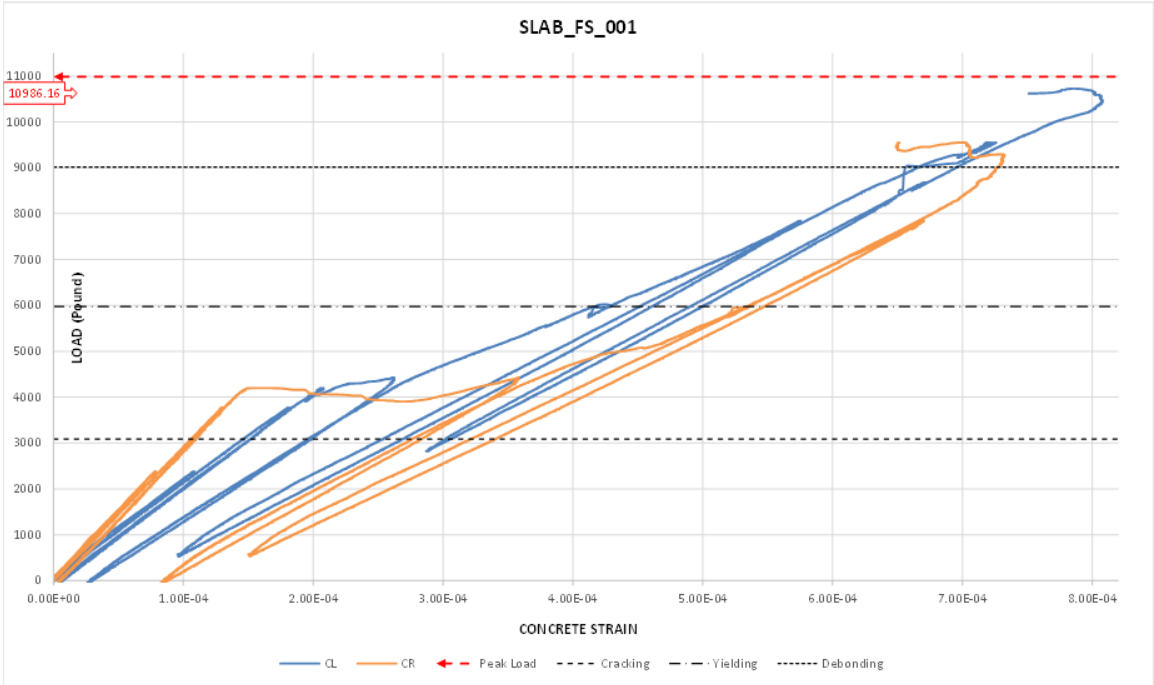

Figure 6.13 – Slab 001 load vs concrete strain diagram

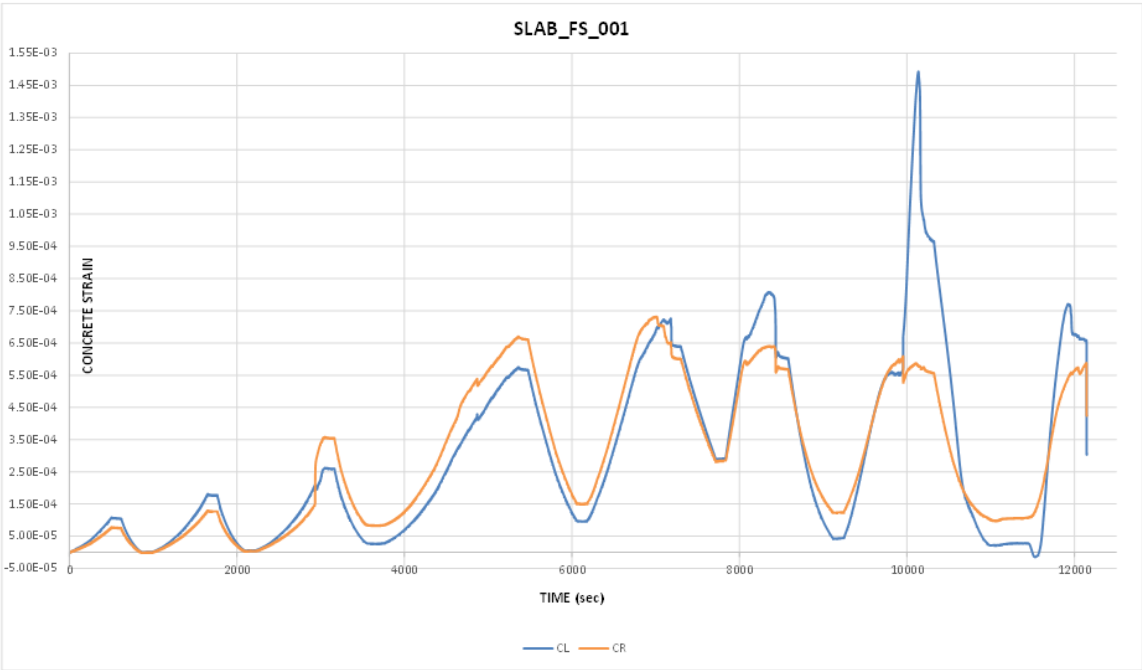

Figure 6.14 - Slab 001 concrete strain vs time diagram

The following figures show the evolution of steel strains increasing the load over the time. Steel strain gauges were lost before the peak load was reached, probably due to the slipping of steel rebars.

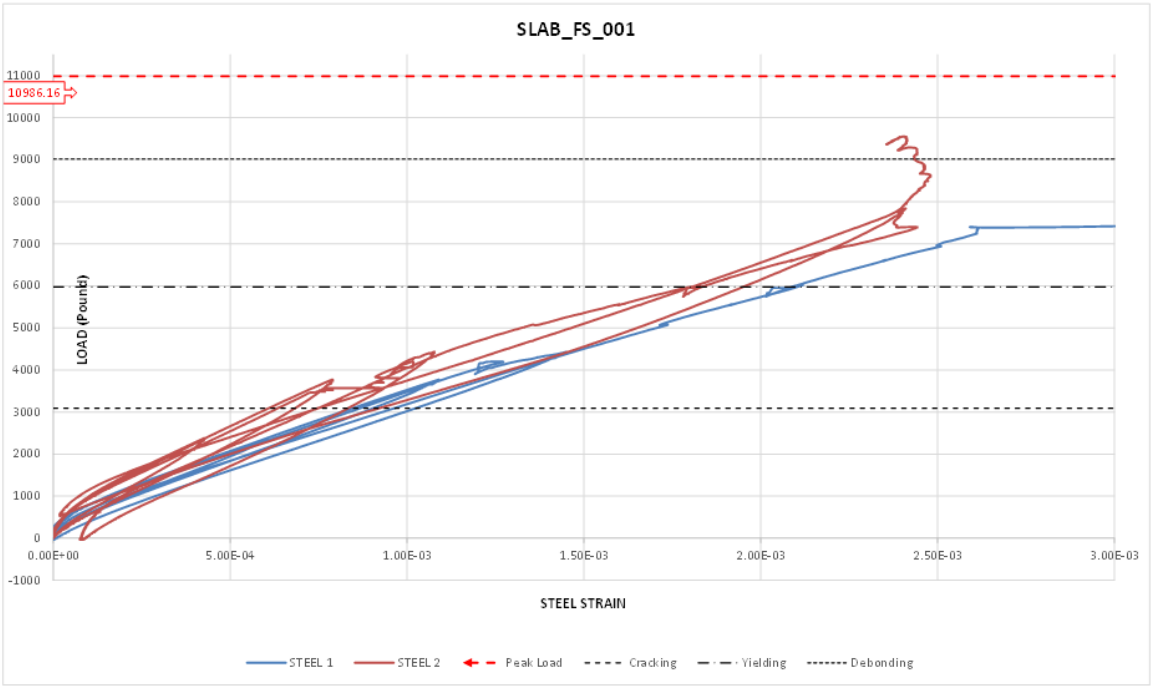

Figure 6.15 – Slab 001 load vs steel strain diagram

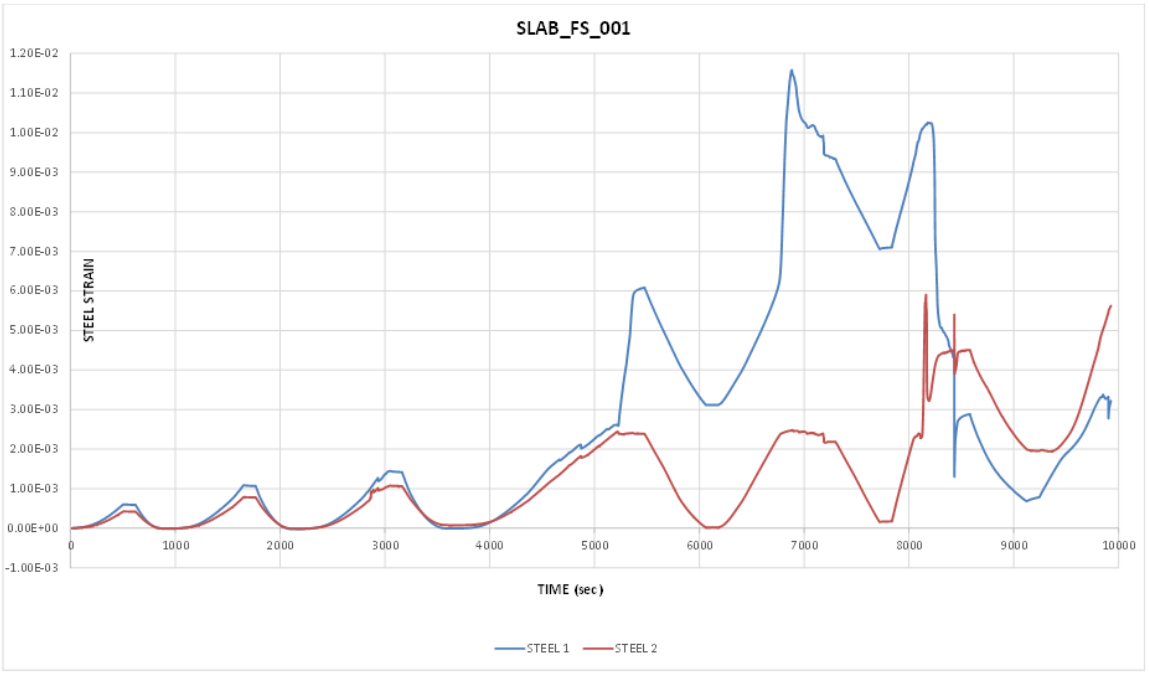

Figure 6.16 – Slab 001 steel strain vs time diagram

Looking at the FRP strain evolution over the time, it can be noticed how strains at the FRP sheet's end suddenly jump to the mid-span level as debonding happened.

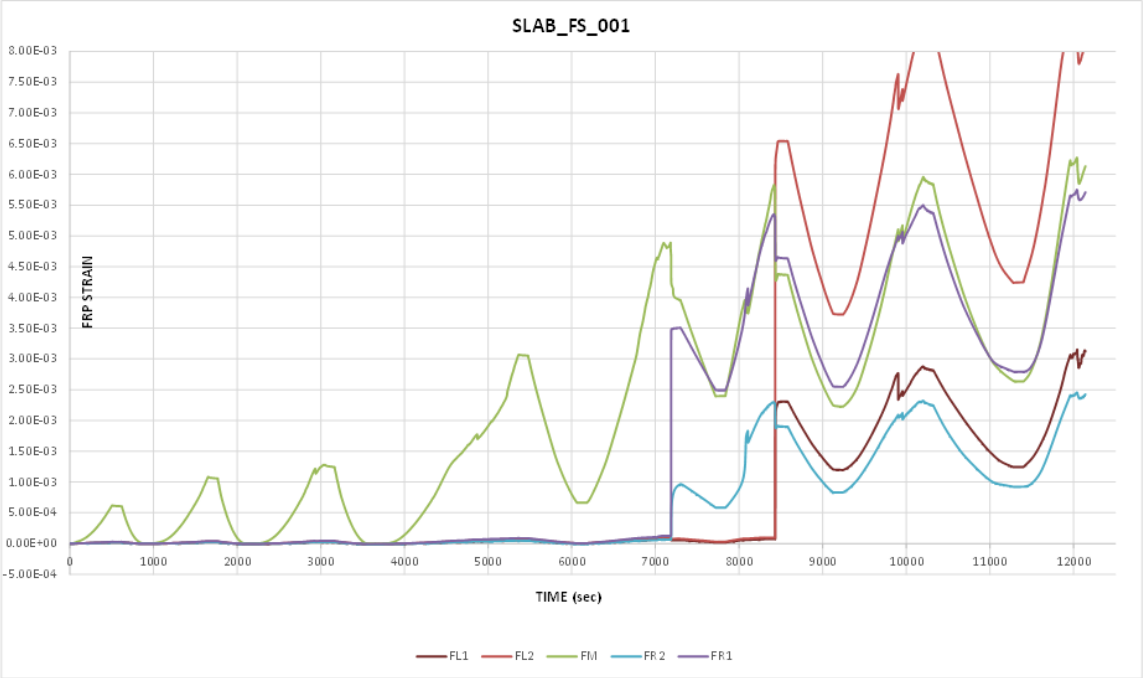

Figure 6.17 – Slab 001 FRP strain vs time diagram

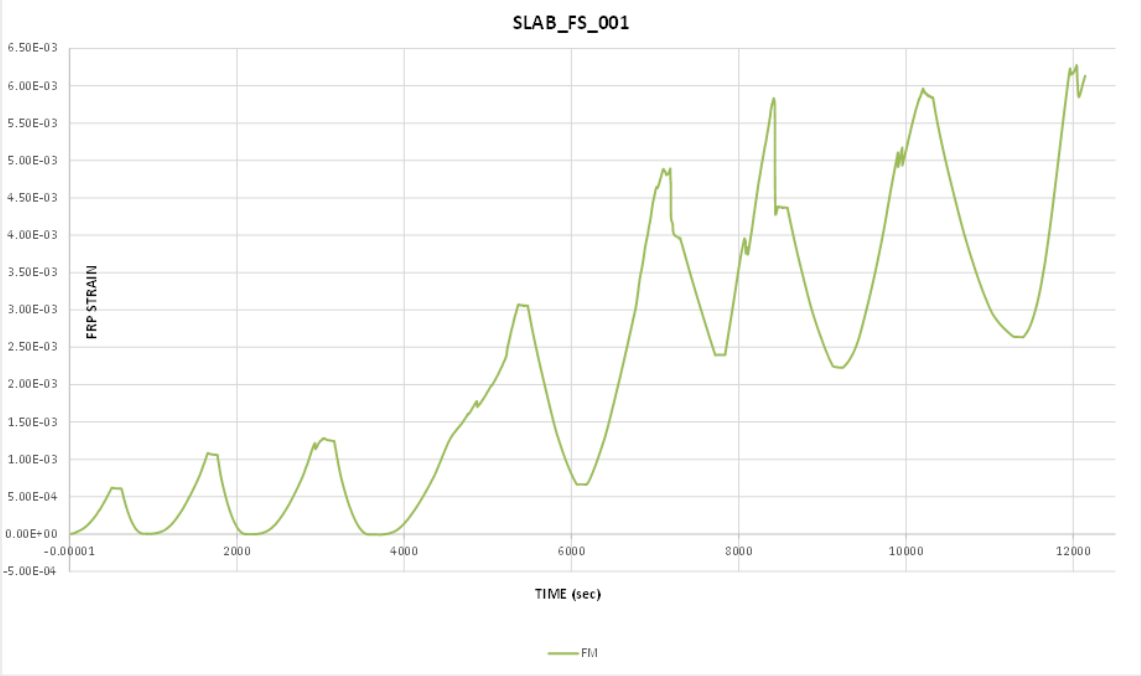

Figure 6.18 – Slab 001 FM FRP strain vs time diagram

In the following Figure 6.19 it can be noticed that, because debonding started on the right side of the slabs, FR1 and FR2 strain gauges, suddenly jumped to higher level, and were lost before the ultimate load was reached.

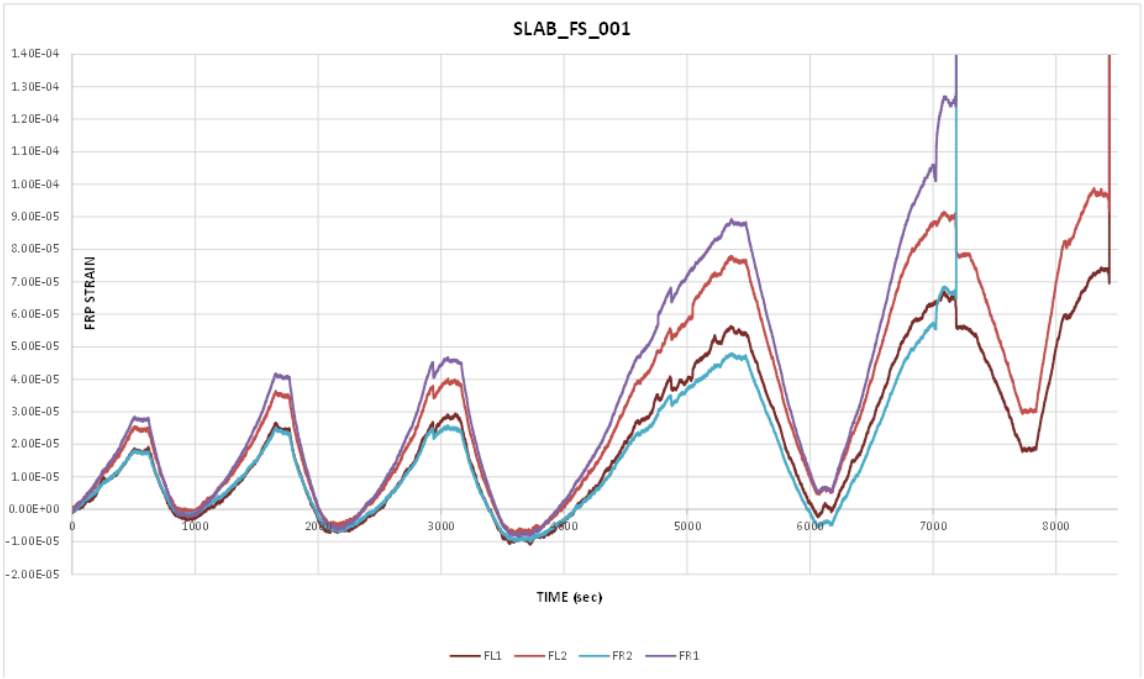

Figure 6.19 – Slab 001 FL & FR FRP strain vs time diagram

The following figures illustrate the the FRP strains evolution at increasing load.

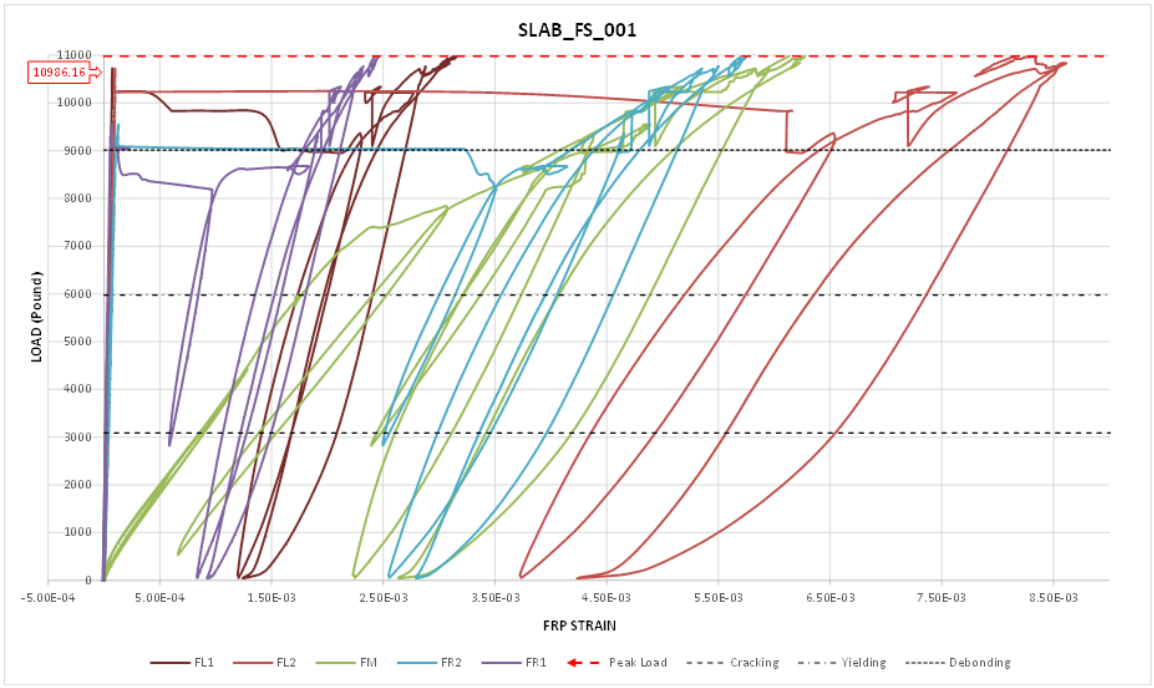

Figure 6.20 – Slab 001 load vs FRP strain diagram

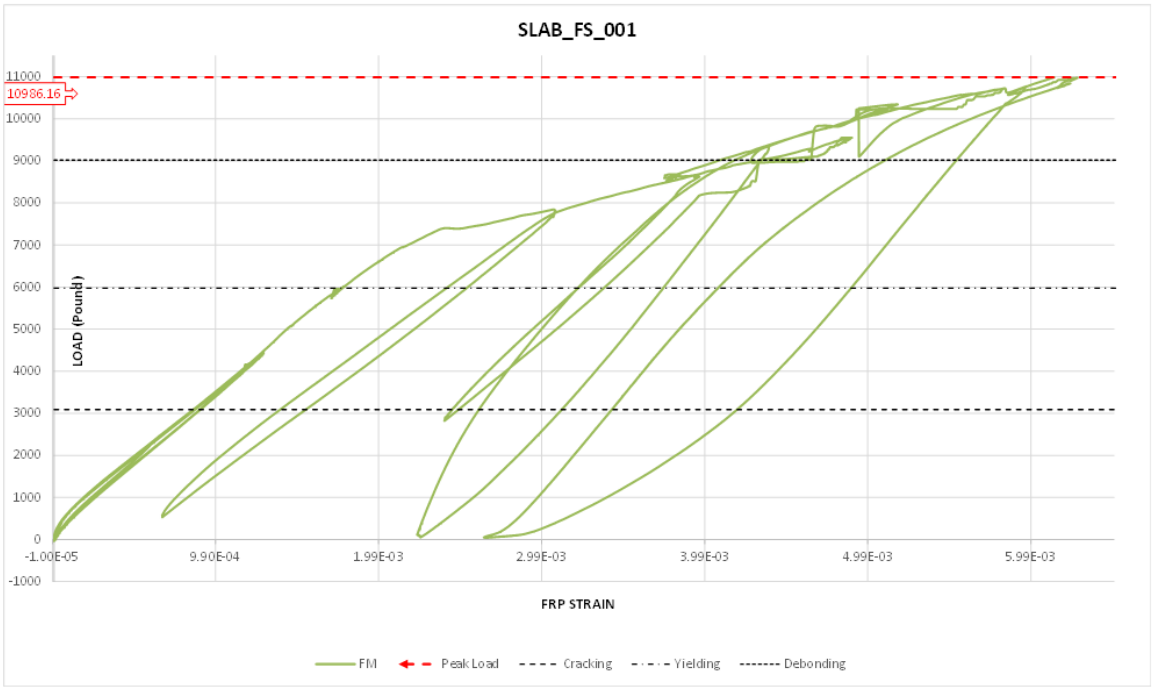

Figure 6.21 – Slab 001 load vs FM FRP strain diagram

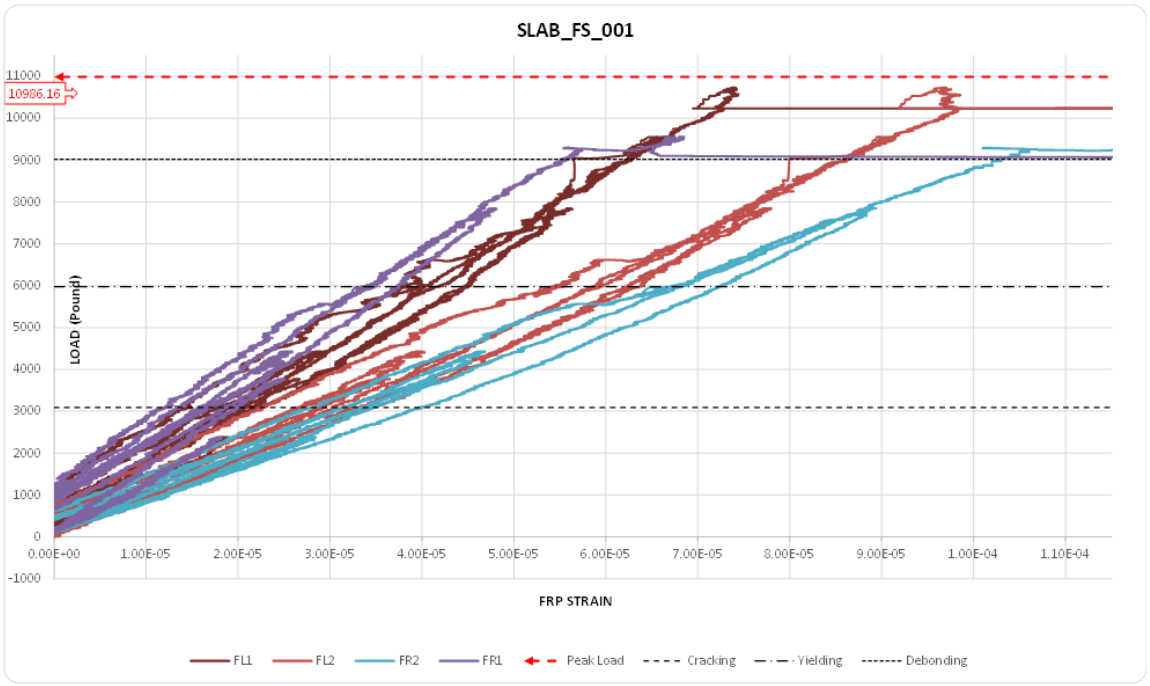

Figure 6.22 – Slab 001 load vs FL & FR FRP strain diagram

The anchors' failure was due to a pull-out mechanism, happened on the right side of the symmetrically anchored slab. As debonding happened, the end anchors were suddenly engaged, providing the critical mechanism for sheet-concrete load transfer. It is peculiar to notice that both anchors did not break, the same that happened on the first experimental program on blocks.

All the cracks were marked during the test, with different colors to identify the different phases (cracking, yielding, debonding, until collapse).

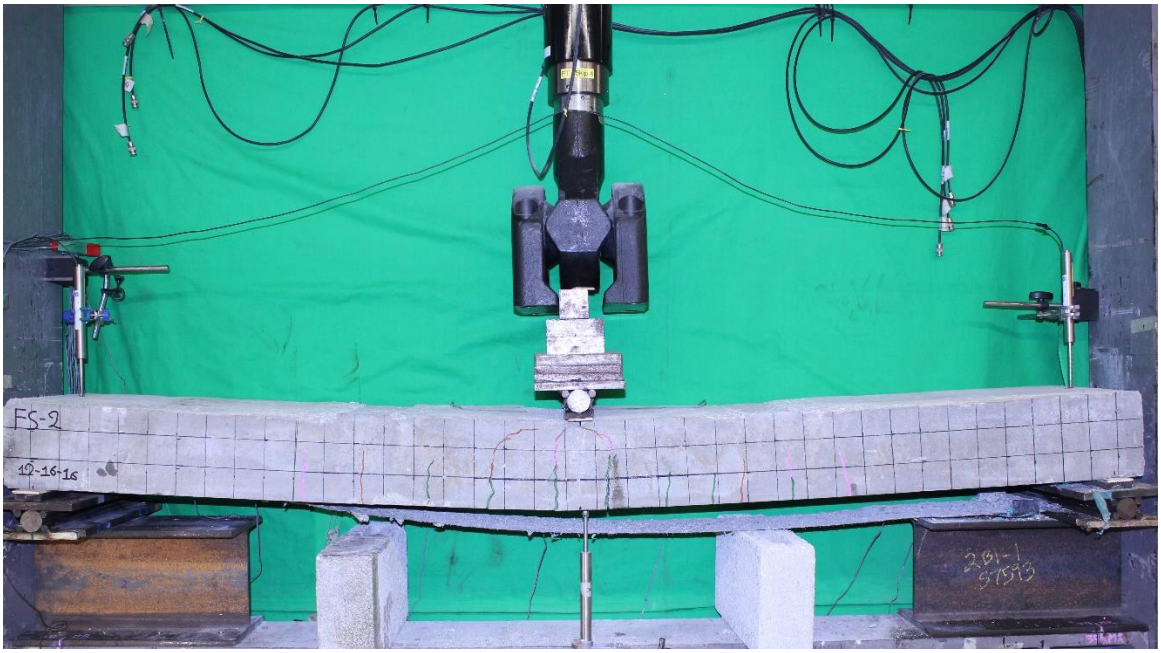

Figure 6.23 - Slab 002 failure and debonding at the end of the test

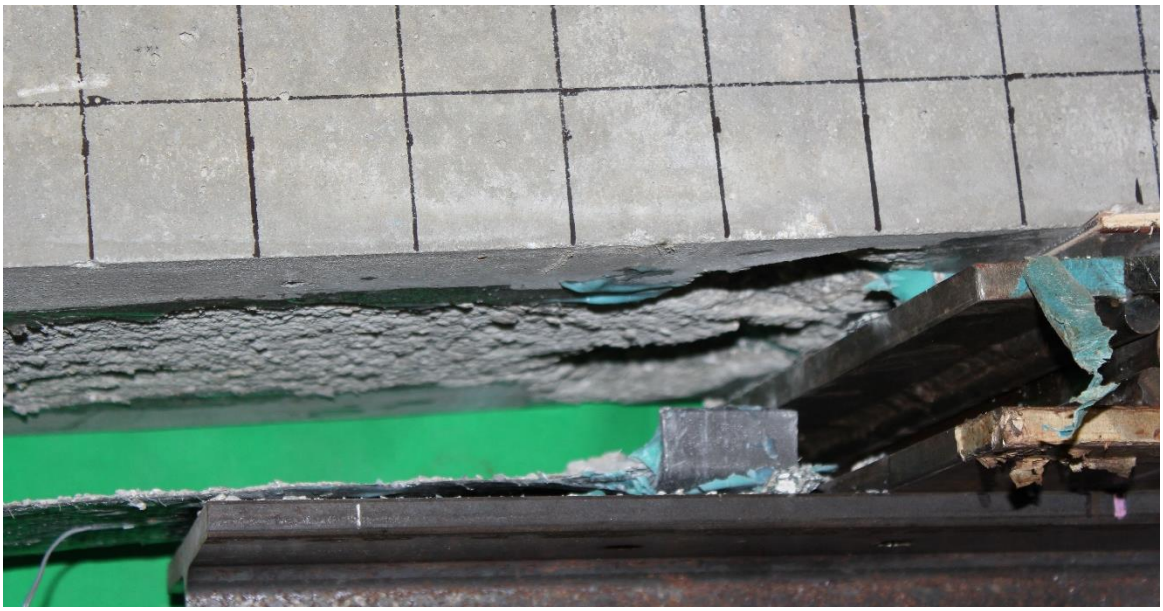

Figure 6.24 - Slab 001 debonding and anchor's failure at the end of the test

6.4 Configuration 2 – 4 Flat Staples Anchors (L/3)

The specimen 003 showed a decoupled anchors' behavior, as meaning that each anchor performed independently. Again, specimen 004 showed the same behavior of slab 003, as well as the same good matching on the strain and load side.

The 4 anchors specimens show higher load than ends' anchors specimens, as expected.

Since the slabs had not shear reinforcement, the failure mode was due to the concrete shear failure at a lower level than the expected one. It seems very well plausible that, if the concrete-failure would have not happened, the slab would have just continued up to anchors' failure at a higher ultimate load. It is worth noting that the theoretical shear capacity was much higher than the ultimate capacity reached by the experimental tests on slabs 003 &004, and it seems plausible that the anchor positioned at L/3 induced the premature shear failure of the concrete. More studies and analysis should be done to better understand the mechanical behavior of this failure mode.

In the following, test results are provided, focusing on the two main phases of debonding and ultimate load reached by the slabs. For sake of completeness, all the results obtained from the 3-point bending tests are provided in Appendix E.

Table 6.9 and Table 6.10 and shows the results obtained from the 3-point bending test performed on slab 001 and 002.

FLAT STAPLE 2" - Configuration 2 (L/3) - TEST RESULTS - Slab 003

	US					SI				
	Load [Kip]	Deflection δ [in]	FRP Strain[%]	Concrete Strain[%]	x [in]	Load [KN]	Deflection δ[mm]	FRP Strain[%]	Concrete Strain[%]	x [mm]
Debonding	9.226	1.384	0.611	0.068	0.750	41.040	35.162	0.611	0.068	19.050
Ultimate	12.653	2.269	0.950	0.095	0.667	56.284	57.622	0.950	0.095	16.936

Table 6.9 - Slab 003 test results

FLAT STAPLE 2" - Configuration 2 (L/3) - TEST RESULTS - Slab 004

	US					SI				
	Load [Kip]	Deflection δ [in]	FRP Strain[%]	Concrete Strain[%]	x [in]	Load [KN]	Deflection δ[mm]	FRP Strain[%]	Concrete Strain[%]	x [mm]
Debonding	9.138	1.065	0.561	0.067	0.739	40.648	27.053	0.561	0.067	18.766
Ultimate	13.205	2.031	0.949	0.093	0.657	58.738	51.589	0.949	0.093	16.678

Table 6.10 - Slab 004 test results

Table 6.11 and Table 6.12 illustrates the matching between the experimental results obtained from the 3-point bending test on slab 003 & 004 and the theoretical results coming from the preliminary design explained in Appendix F.

The average results of the anchor's ultimate capacity were below the theoretical one, because of the concrete failure. Even though the theoretical performance was above, assuming the full involvement of the FRP, we understand that sabs had no shear reinforcement and the L/3 anchor caused the premature shear failure of concrete.

FLAT STAPLE 2" - Configuration 2 (L/3) - EXPERIMENTAL MATCHING [US] - Slab 003

	Load [kip]			Displacement [in]			FRP Strain[%]			x [in]		
	Exp.	Th.	Δ [%]	Exp.	Th.	Δ [%]	Exp.	Th.	Δ [%]	Exp.	Th.	Δ [%]
Debonding	9.226	9.018	2.30%	1.384	1.020	35.78%	0.611	0.658	-7.10%	0.750	0.710	5.65%
Ultimate	12.653	15.452	-18.12%	2.269	1.258	80.38%	0.950	1.447	-34.38%	0.667	0.700	-4.80%

FLAT STAPLE 2" - Configuration 2 (L/3) - EXPERIMENTAL MATCHING [SI] - Slab 003

	Load [KN]			Displacement [mm]			FRP Strain[%]			x [mm]		
	Exp.	Th.	Δ [%]	Exp.	Th.	Δ [%]	Exp.	Th.	Δ [%]	Exp.	Th.	Δ [%]
Debonding	41.040	40.116	2.30%	35.162	25.897	35.78%	0.611	0.658	-7.10%	19.050	18.032	5.65%
Ultimate	56.284	68.736	-18.12%	57.622	31.945	80.38%	0.950	1.447	-34.38%	16.936	17.790	-4.80%

Table 6.11 - Slab 003 experimental matching (Exp.= experimental; Th.= theoretical)

FLAT STAPLE 2" - Configuration 2 (L/3) - EXPERIMENTAL MATCHING [US] - Slab 004

	Load [kip]			Displacement [in]			FRP Strain[%]			x [in]		
	Exp.	Th.	Δ [%]	Exp.	Th.	Δ [%]	Exp.	Th.	Δ [%]	Exp.	Th.	Δ [%]
Debonding	9.138	9.018	1.33%	1.065	1.020	4.46%	0.561	0.658	-14.76%	0.739	0.710	4.07%
Ultimate	13.205	15.452	-14.55%	2.031	1.258	61.49%	0.949	1.447	-34.41%	0.657	0.700	-6.25%

FLAT STAPLE 2" - Configuration 2 (L/3) - EXPERIMENTAL MATCHING [SI] - Slab 004

	Load [KN]			Displacement [mm]			FRP Strain[%]			x [mm]		
	Exp.	Th.	Δ [%]	Exp.	Th.	Δ [%]	Exp.	Th.	Δ [%]	Exp.	Th.	Δ [%]
Debonding	40.648	40.116	1.33%	27.053	25.897	4.46%	0.561	0.658	-14.76%	18.766	18.032	4.07%
Ultimate	58.738	68.736	-14.55%		31.945	-100.00%	0.949	1.447	-34.41%	16.678	17.790	-6.25%

Table 6.12 - Slab 004 experimental matching (Exp.= experimental; Th.= theoretical)

Figure 6.25 illustrates the load cycles over the time.

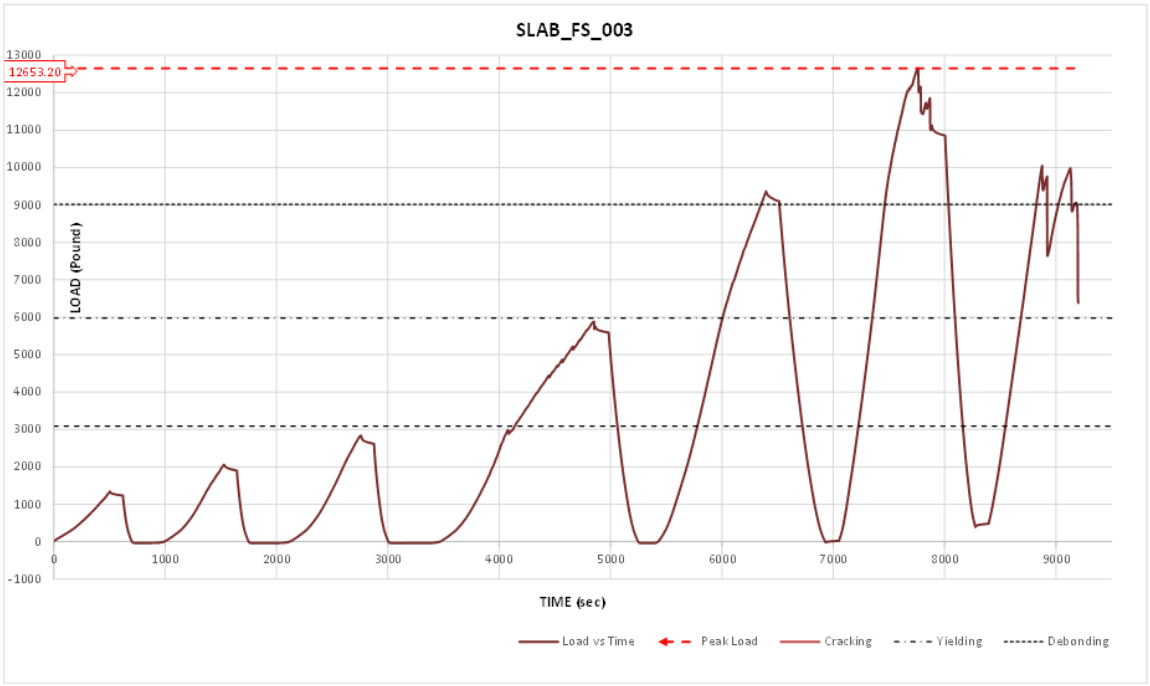

Figure 6.25 - Slab 003 load vs time diagram

Figure 6.26 shows the cyclic load until the failure in the load vs deflection diagram.

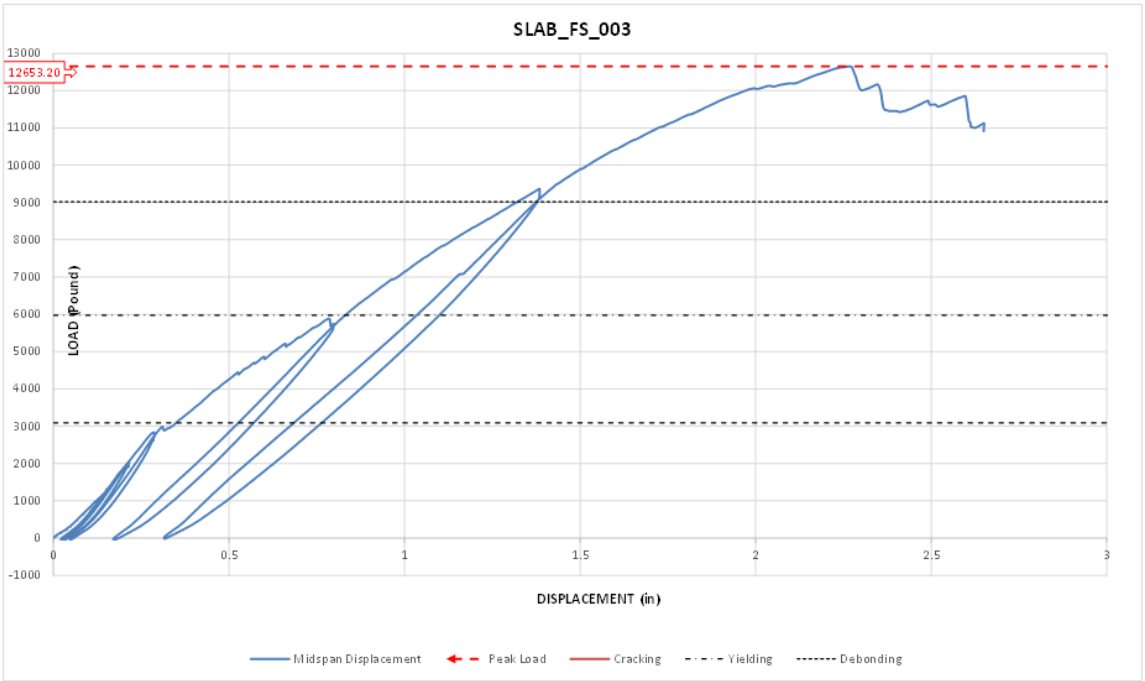

Figure 6.26 - Slab 003 load vs deflection diagram

Looking at the envelope it is possible to calculate the energy, corresponding to the area under the curve.

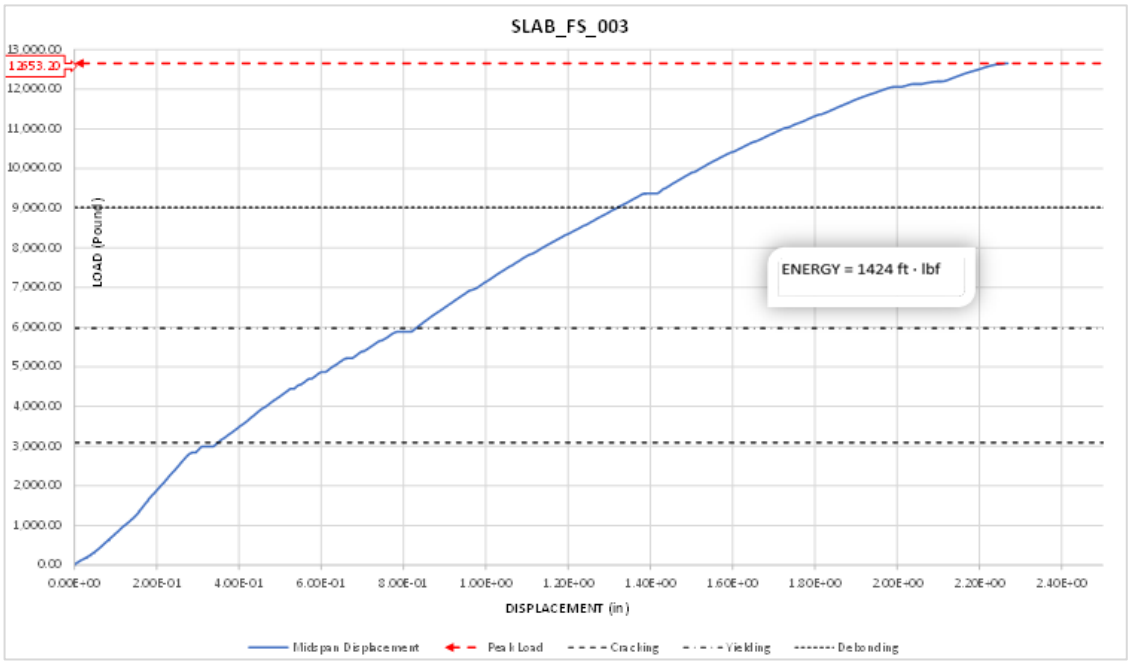

Figure 6.27 - Slab 003 load vs deflection envelope diagram

It is worth noting that 4-anchors slabs (specimens 003 & 004) were stiffer than 2-anchors slabs (specimens 001 & 002), that is the reason why they had smaller displacement during the cycles load.

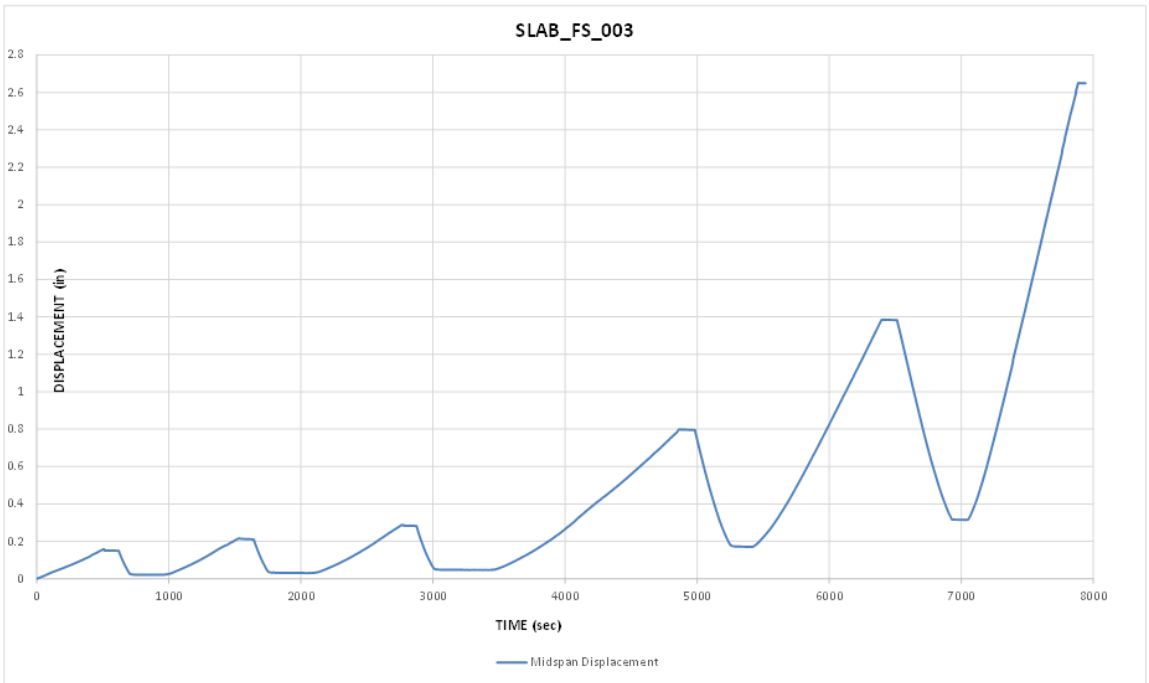

Figure 6.28 - Slab 003 displacement vs time diagram

The following figures show the evolution of concrete strain increasing the load over the time.

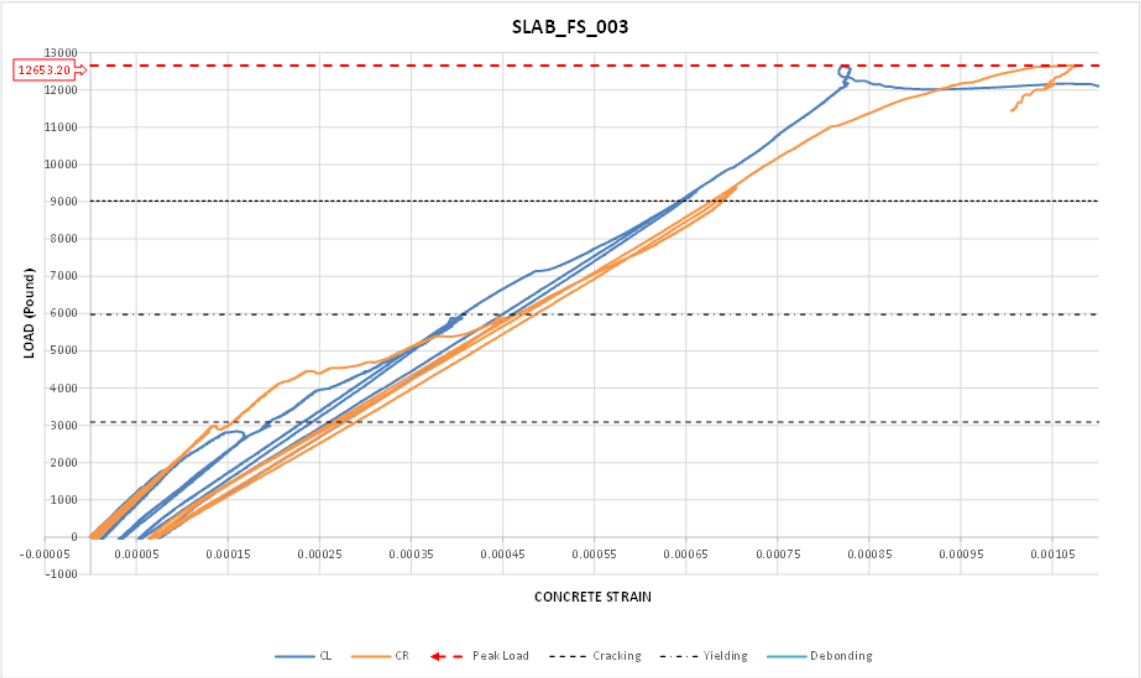

Figure 6.29 - Slab 003 load vs concrete strain diagram

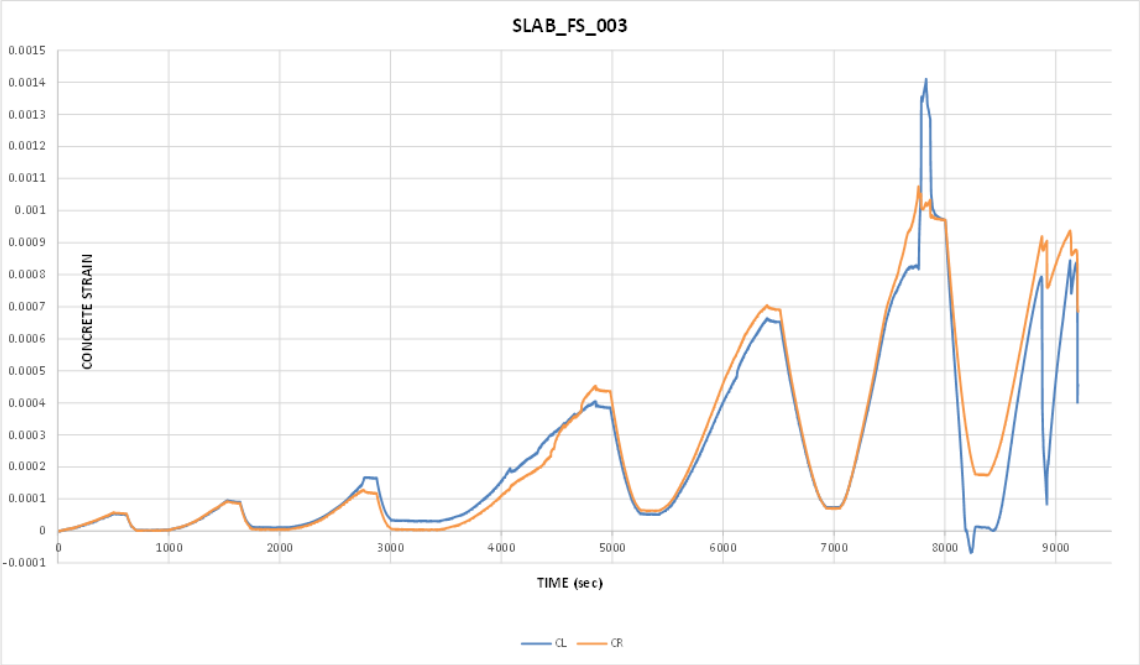

Figure 6.30 - Slab 003 concrete strain vs time diagram

The following figures show the evolution of steel strain increasing the load over the time. Steel strain gauges were lost before the peak load was reached, probably due to the slipping of steel rebars.

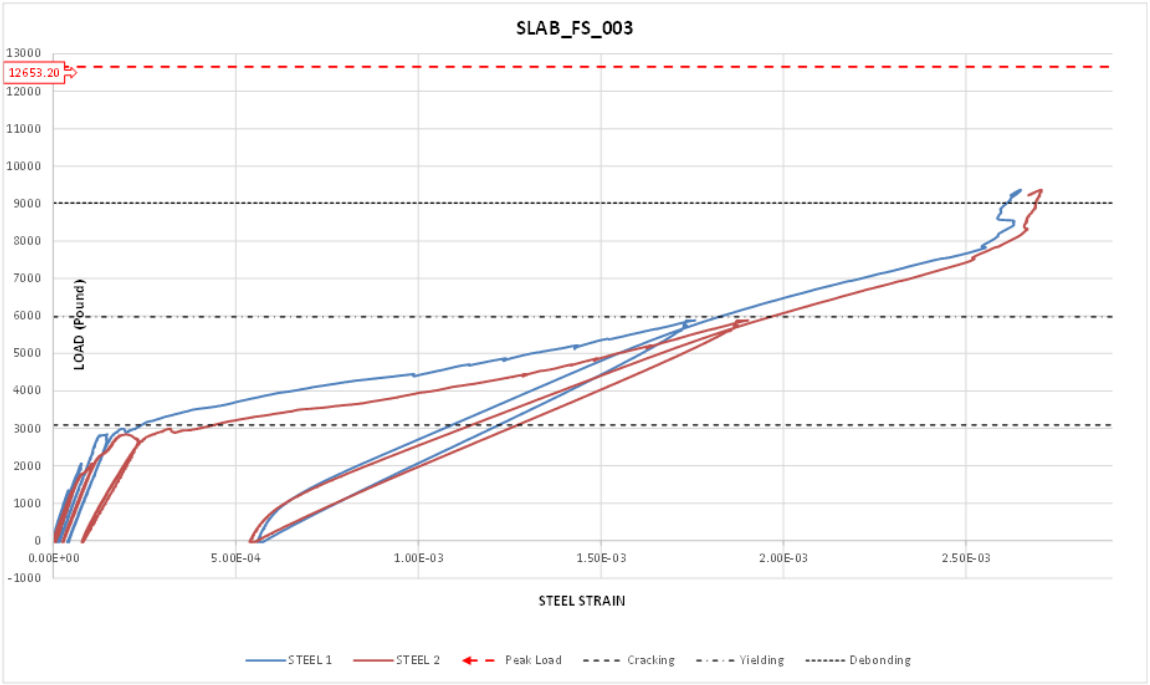

Figure 6.31 - Slab 003 load vs steel strain diagram

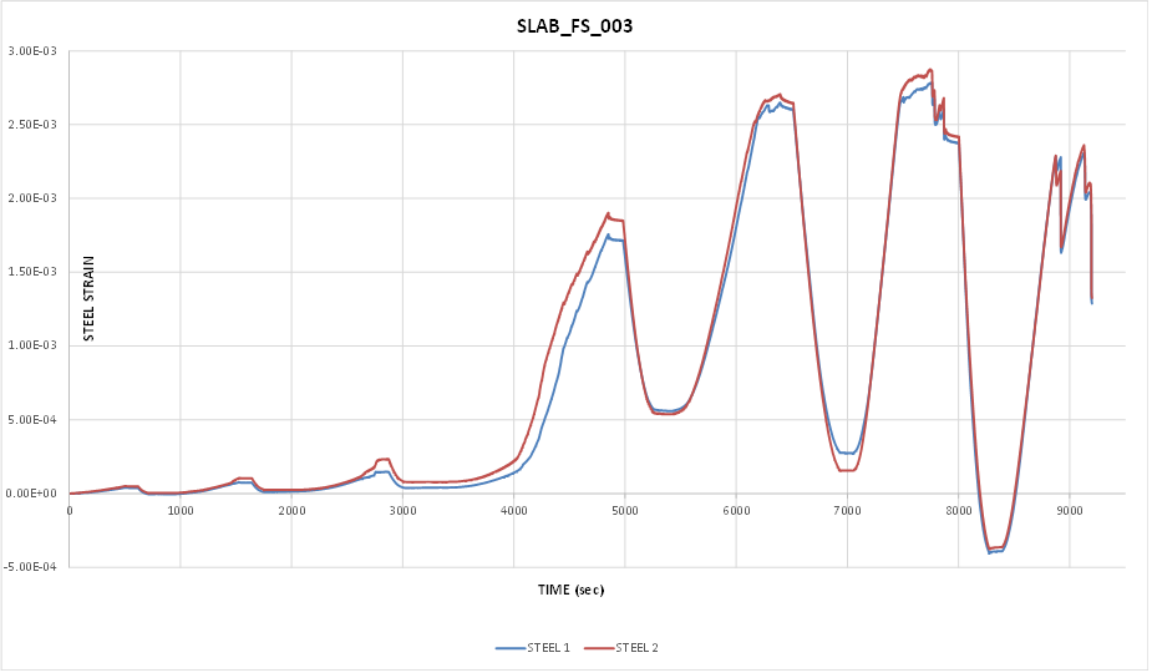

Figure 6.32 - Slab 003 steel strain vs time diagram

Looking at the FRP strain evolution over the time, it can be noticed how strains at the FRP sheet's end suddenly increased, even if less than in end-anchors specimens due to higher stiffness, as debonding happened.

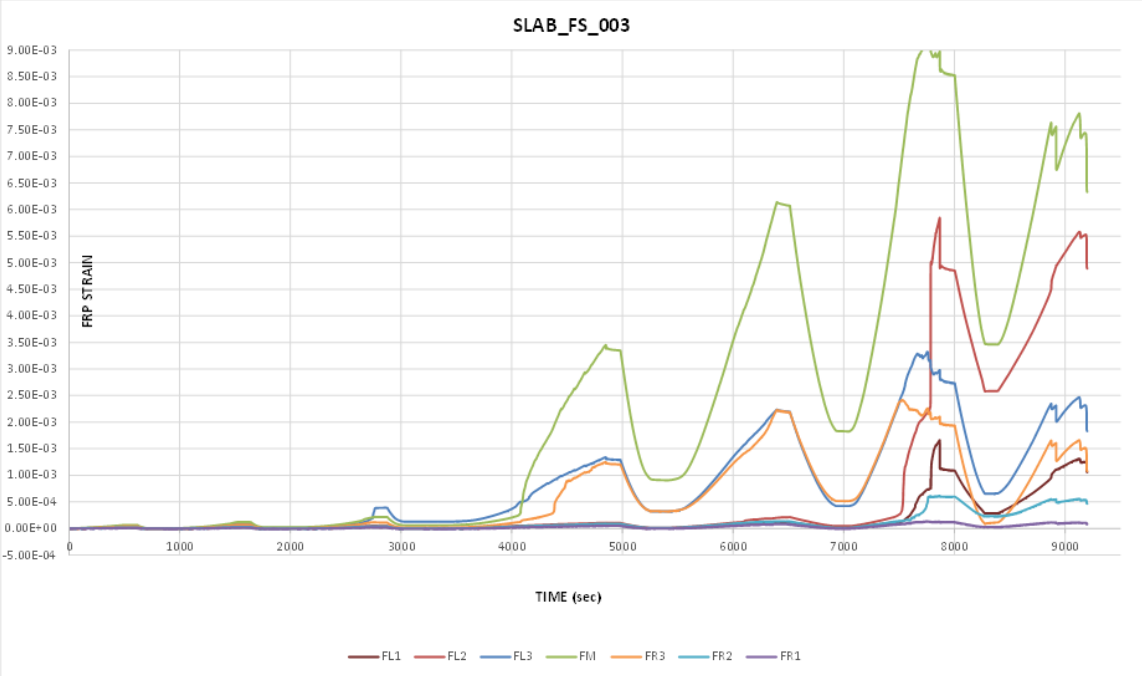

Figure 6.33 - Slab 003 FRP strain vs time diagram

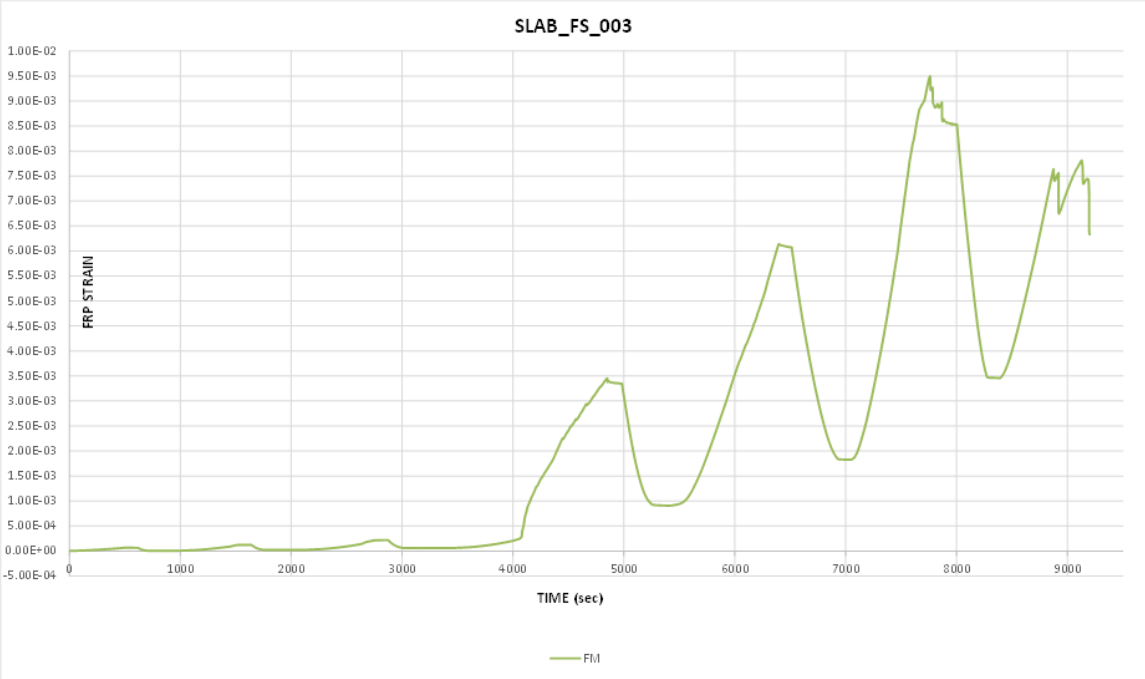

Figure 6.34 - Slab 003 FM FRP strain vs time diagram

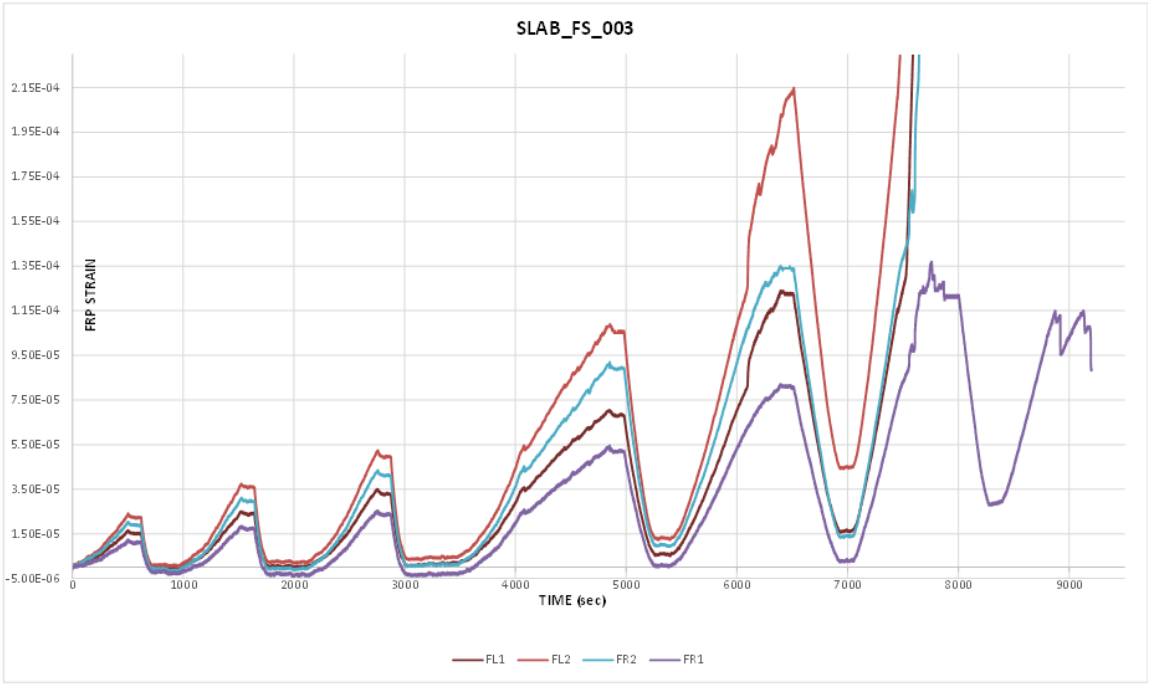

Figure 6.35 - Slab 003 FL & FR FRP strain vs time diagram

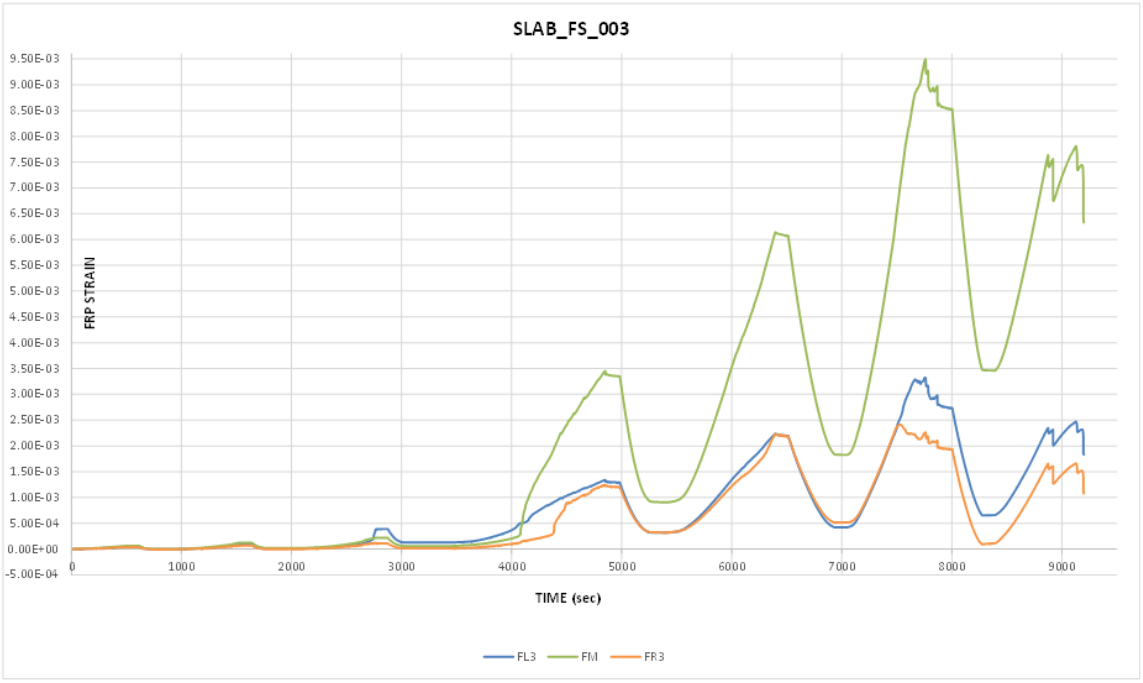

Figure 6.36 - Slab 003 FL3, FM & FR3 FRP strain vs time diagram

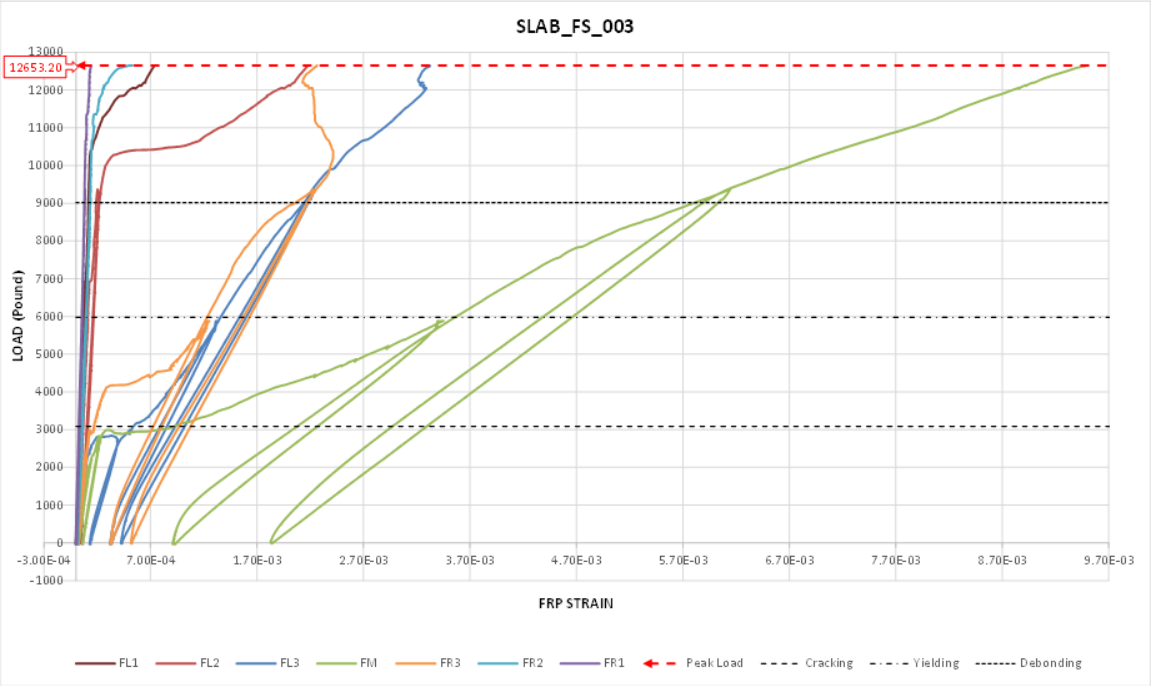

Figure 6.37 - Slab 003 load vs FRP strain diagram

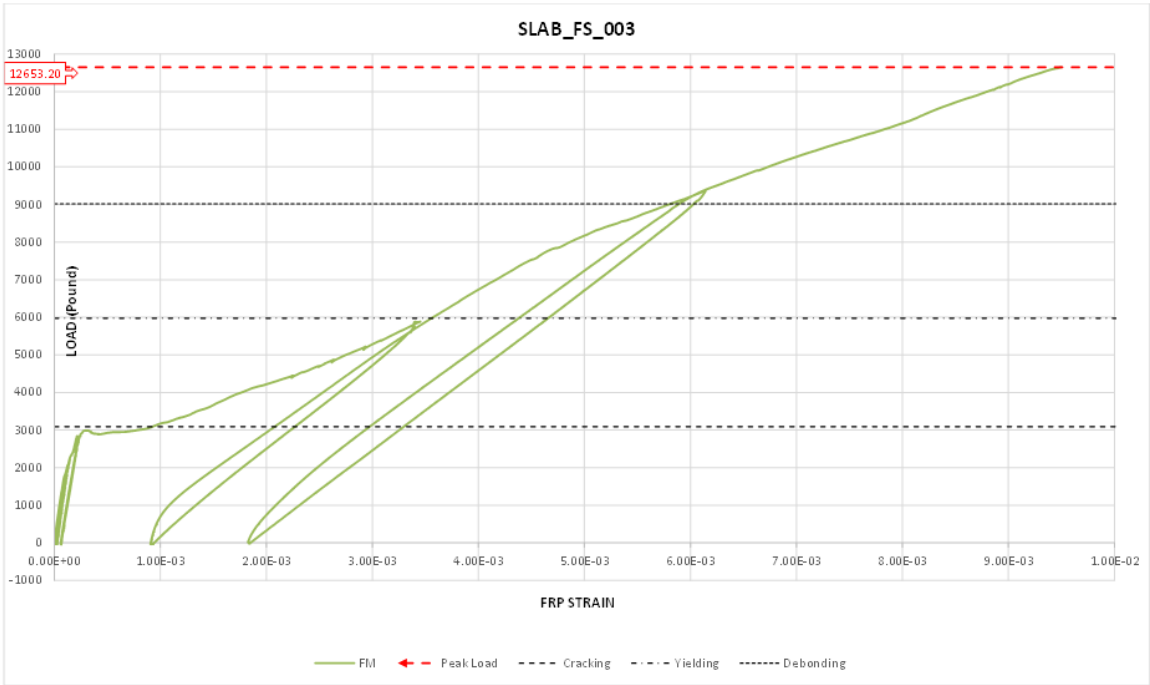

Figure 6.38 - Slab 003 load vs FM FRP strain diagram

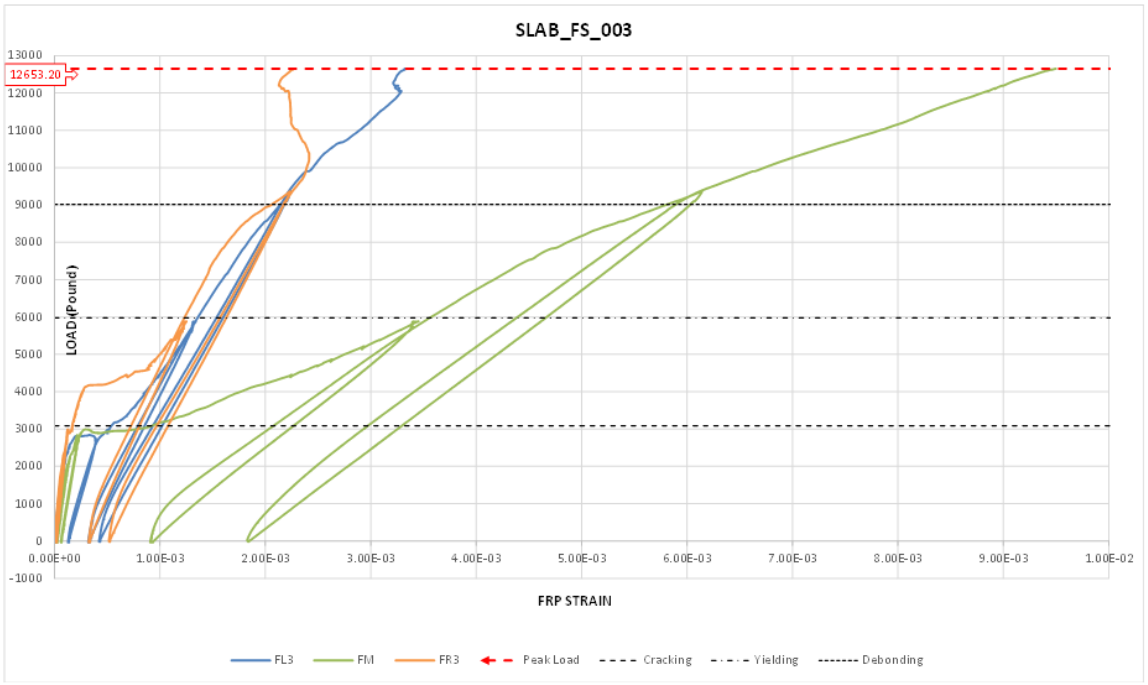

Figure 6.39 - Slab 003 load vs FL3, FM & FR3 FRP strain diagram

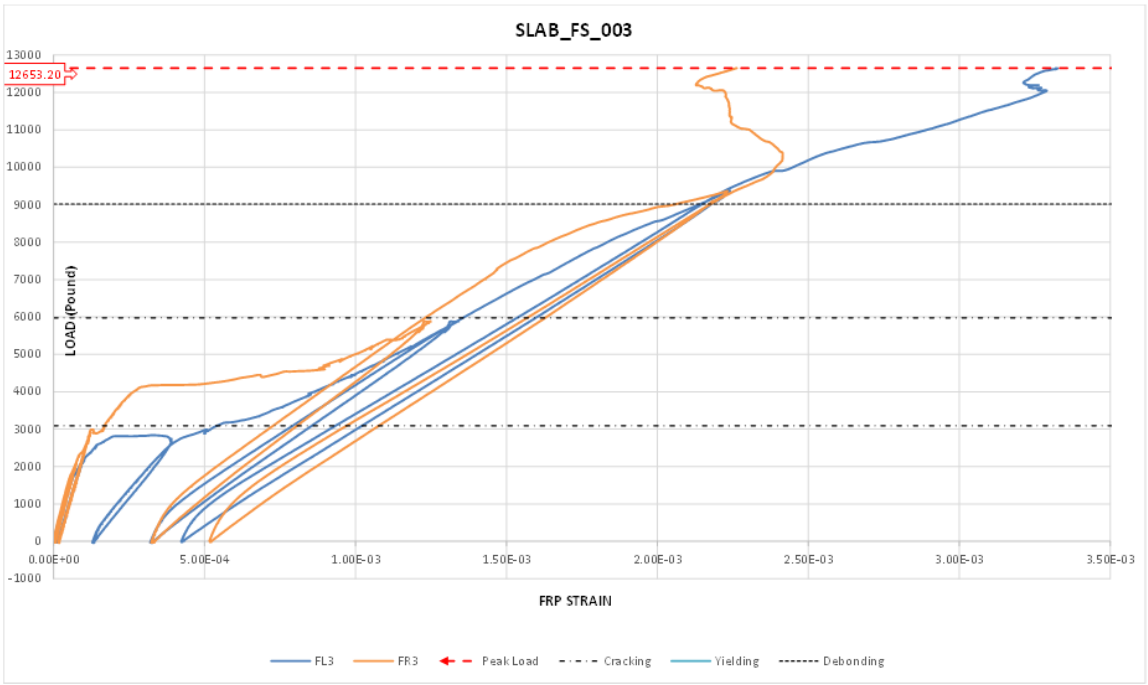

Figure 6.40 - Slab 003 load vs FL3 & FR3 FRP strain diagram

Analyzing the specimen's failure, the left anchors positioned at L/3 caused cracks propagation up to failure. To be noticed that also in this case, all anchors did not break, pointing out again the strength of this new anchorage system.

All the cracks were marked during the test, with different colors to identify the different phases (cracking, yielding, debonding, until collapse).

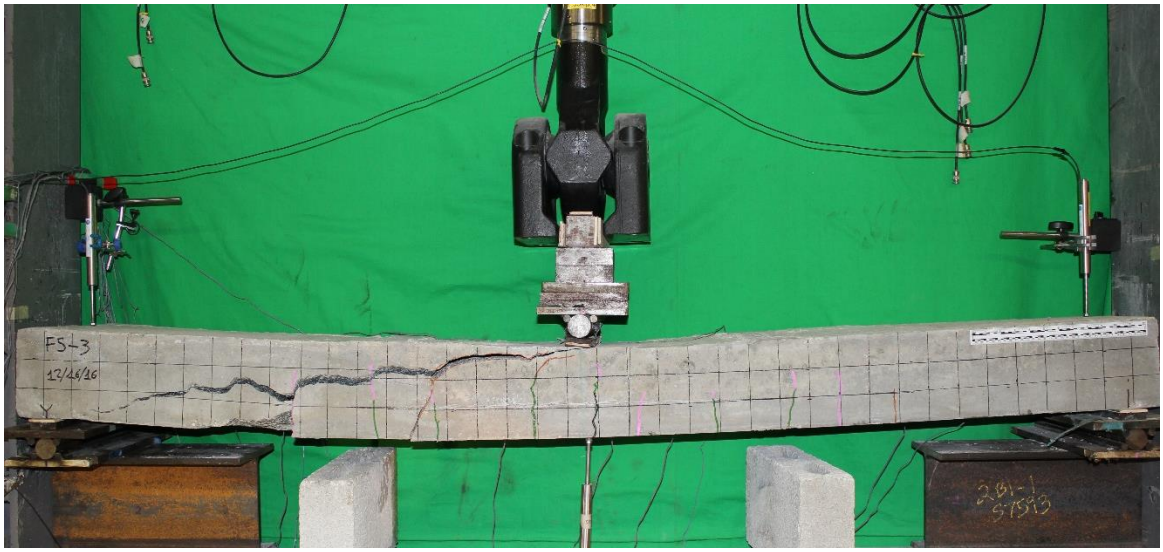

Figure 6.41 - Slab 003 failure at the end of the test

Figure 6.42 - Slab 003 failure details

6.5 Results Discussion

In this section, a brief comparison between the performance of the new anchorage system used as the purpose of this research and old anchor systems used in previous researches in terms of peak load and strains distribution is provided in order to highlight the improvement reached in this most recent research the author carried out.

Table 6.13 presents a comparison in terms of peak load, deflection and FRP strains between different anchorage systems on slabs studied at the University of Miami so far.

Anchor's Type	Anchor's Configuration	Peak Load [Kip]	Peak Load [KN]	Ultimate Deflection at Mid-span [in]	Ultimate Deflection at Mid-span [mm]	FRP Ultimate Strain at Mid-span [%]
Unreinforced Sample (C-C)	No FRP, No Anchors	4.49	19.97	0.56	14.00	-
Control Sample (C-FRP)	No Anchors (only FRP)	9.33	41.50	0.82	21.00	0.660
Spikes Anchors	60x2 (ends)	12.09	53.78	1.90	48.00	0.790
	90x2 (ends)	13.37	59.47	2.18	55.00	0.770
	90x2 (L/4)	12.80	56.94	2.54	64.52	1.080
	90x2 (L/3)	11.83	52.62	1.10	28.00	0.770
	90x3	12.67	56.36	1.99	51.00	0.660
	Sx 2-1	12.40	55.16	2.74	70.00	0.880
	Sx 2-2	13.28	59.07	2.50	64.00	1.060
Flat Staple anchors (new)	**Configuration 1 (ends)**	**10.86**	**48.30**	**2.85**	**72.39**	**0.65**
	Configuration 2 (L/3)	**12.93**	**57.51**	**2.15**	**54.61**	**0.95**

Rossini, 2016

Girotti, 2017

Table 6.13 – Slab's test results summary

The following Figure 6.43 shows a comparison in terms of peak load between all the anchorage system studied both in this research as well as in previous researches.

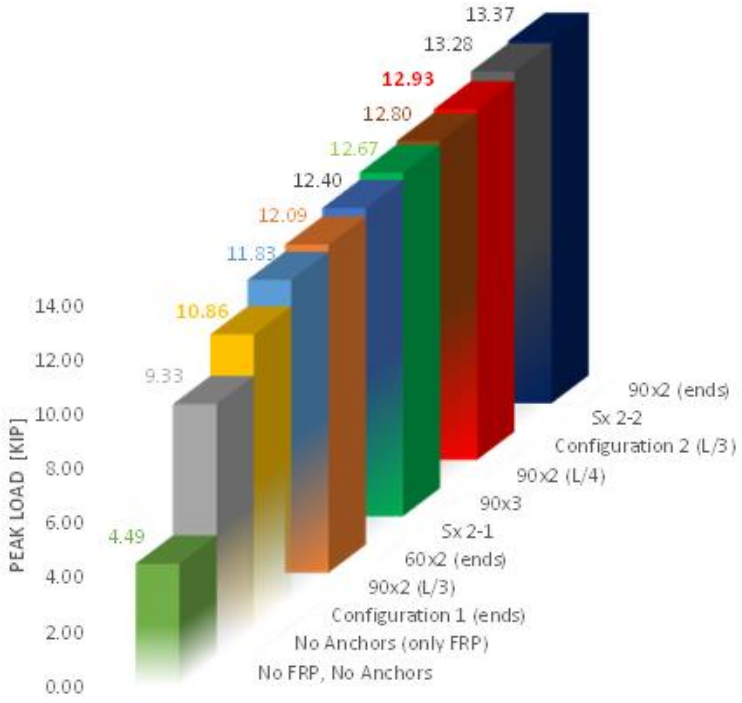

Figure 6.43 - Peak Loads comparison

The reader can easily understand, from the following Figure 6.44, how much effective is the presence of the externally bonded reinforcement; in fact, it gives an increase in terms of peak load more than 100% if compared with an unreinforced sample. Moreover, the presence of an anchorage system, aimed to avoid the well-known debonding problem, is even able to almost double the slab capacity.

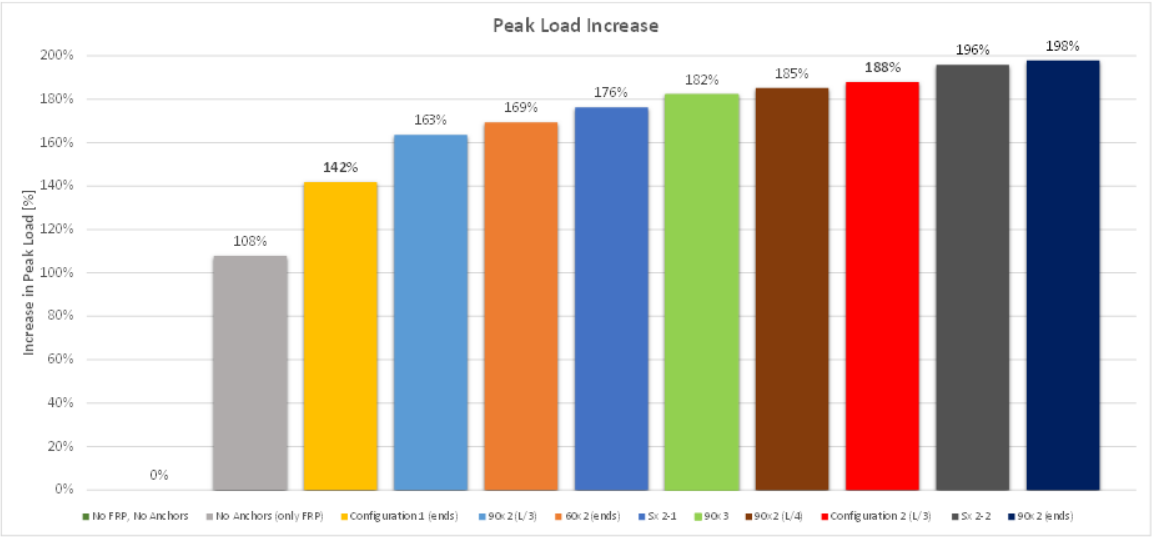

Figure 6.44 - Peak Loads Increase Comparison respect to the unreinforced sample

Regarding the strains, the only meaningful comparison that is reliable to make is comparing strains at mid-span, in fact, the different installation process, anchorage systems and strain gauges 'location do not allow us to entering more into detail comparing strains coming from different researches.

Figure 6.45 shows the strain at the peak load recorded by the strain gauges positioned at mid-span over the laminate. The anchor's configurations that take more advantage of the laminate, developing more strain (~ 1%) are the 90x2 (L/4), Sx 2-2 and the slabs in configuration 2 (L/3).

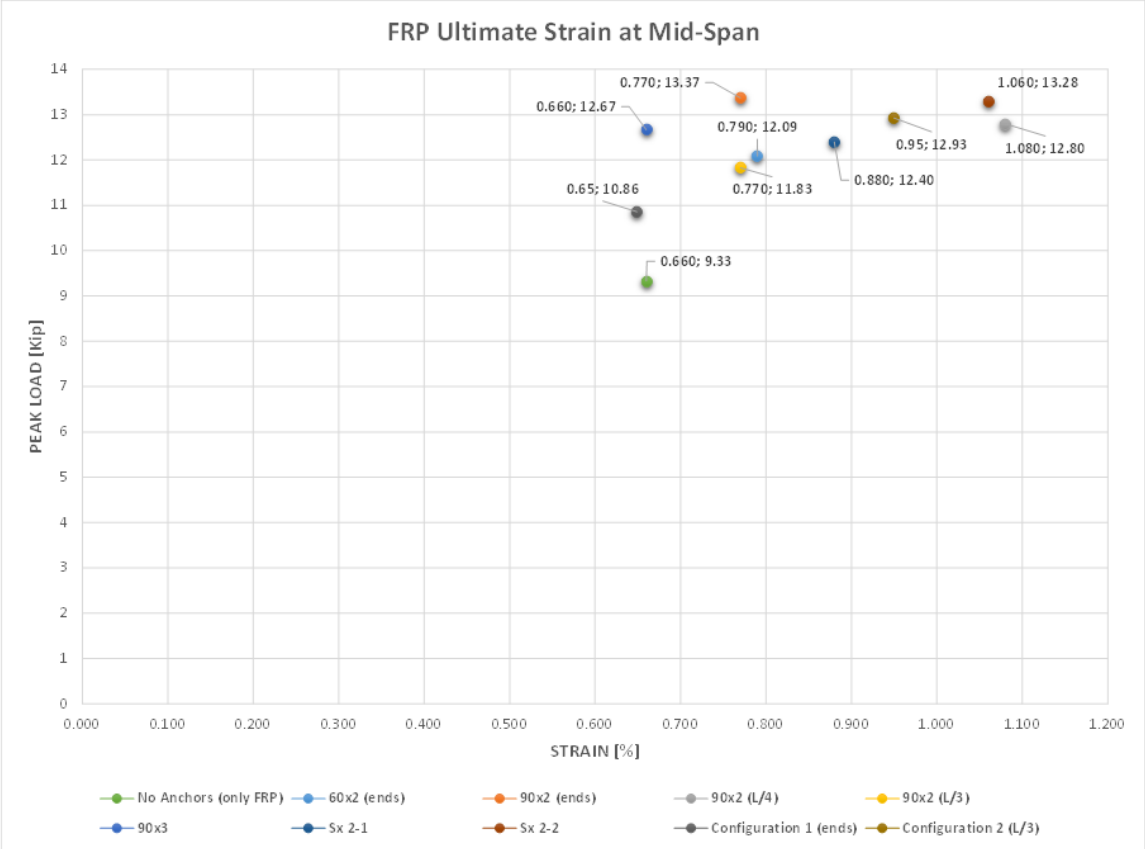

Figure 6.45 - Strain at laminate mid-span (FM) comparison

It is important, again, remarking that, as widely studied, the staple anchors distribute better the stresses. In fact, for the spike anchors, the strains were concentrated in front of the anchor (and that covered area was not along the entire FRP sheet width). Staple anchors,

instead, distribute better the strains over the entire area of the FRP, since they literally cover all the entire FRP laminate width of 6 inches, used for this study.

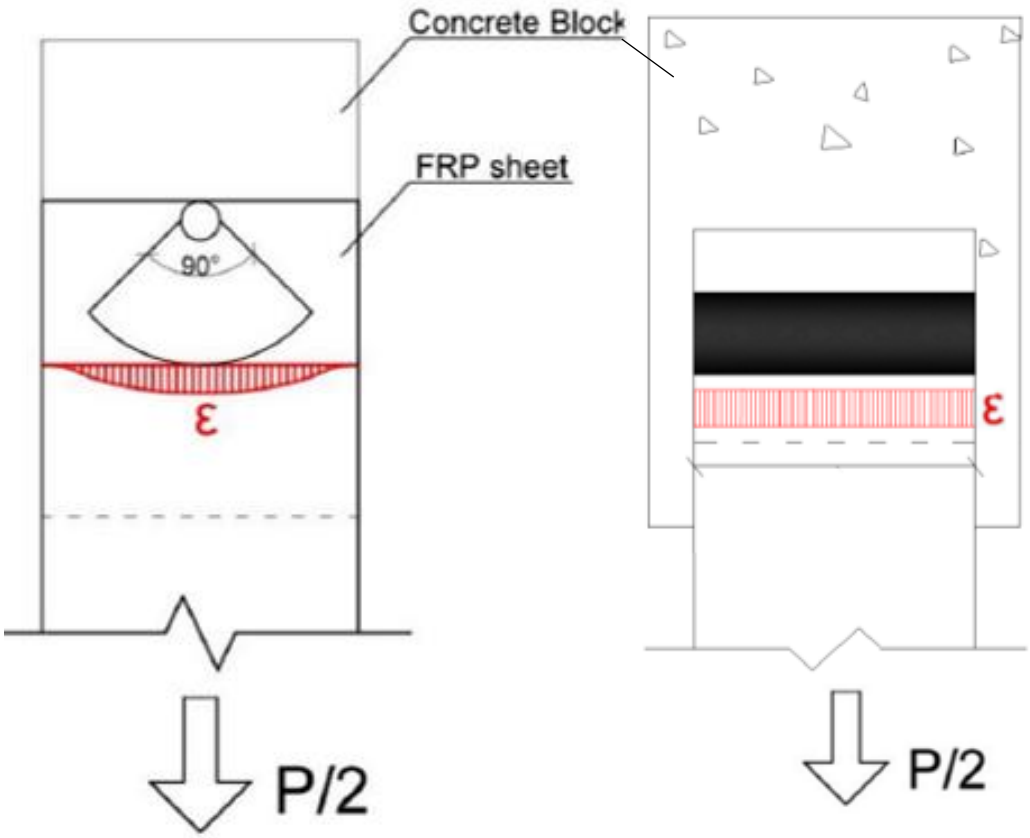

Figure 6.46 - Strain distribution on Spike (Berneschi, 2015) and on Staple anchors (Cadenazzi, 2016)

Strains are also more evenly well distributed in the specimens tested during this research considering the CFRP patch applied, that not only contributes to a better force transferring from the CFRP sheet to the anchor, but, being this patch oriented with fibers in the same direction of the fibers of the flexural sheet allows the development of higher stresses and strains (higher values of stresses and strains are obviously preferred).

Focusing on the slabs tested in this research, Figure 6.47 illustrates a load vs displacement diagram comparing all the four slabs tested. Also, a comparison in terms of energy is provided. As it is possible to see, the curve envelope between slabs 001 & 002, as well as between slabs 003 & 004, are very similar each other. The same, can be said comparing

energies, showing that each slab's configuration behaved in the same way, as meaning of consistent results.

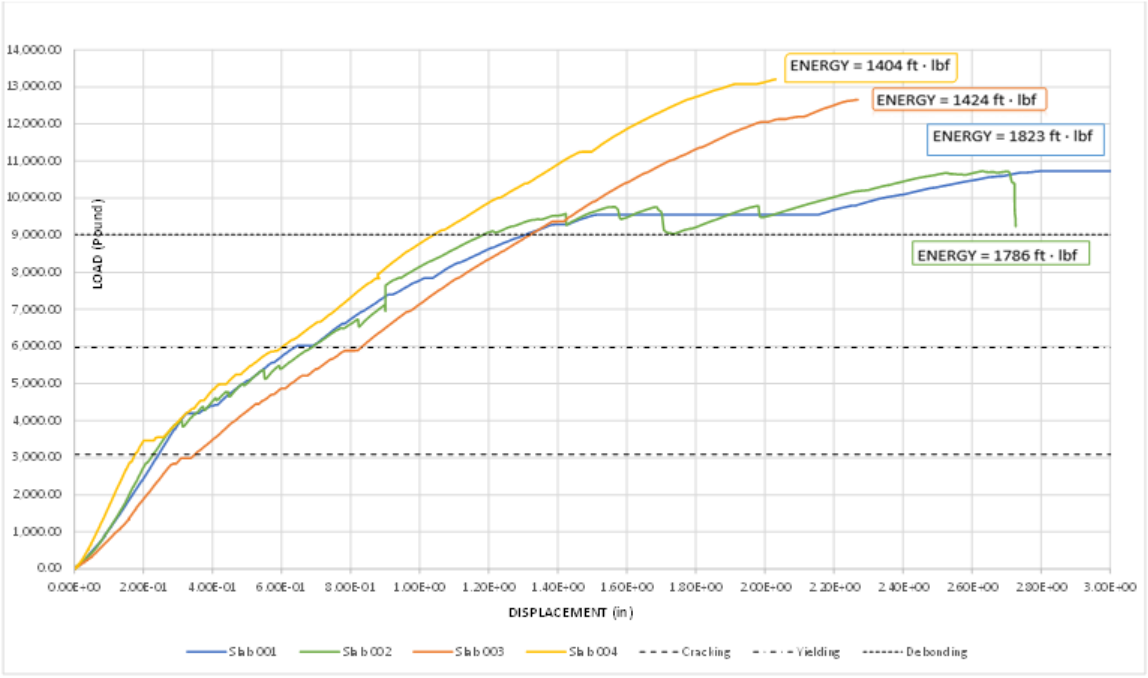

Figure 6.47 - Energy comparison diagram

Figure 6.48 shows how mid-span (FM) strain gauges developed over the time. All the slabs present a similar behavior, confirming again a good consistency on the results.

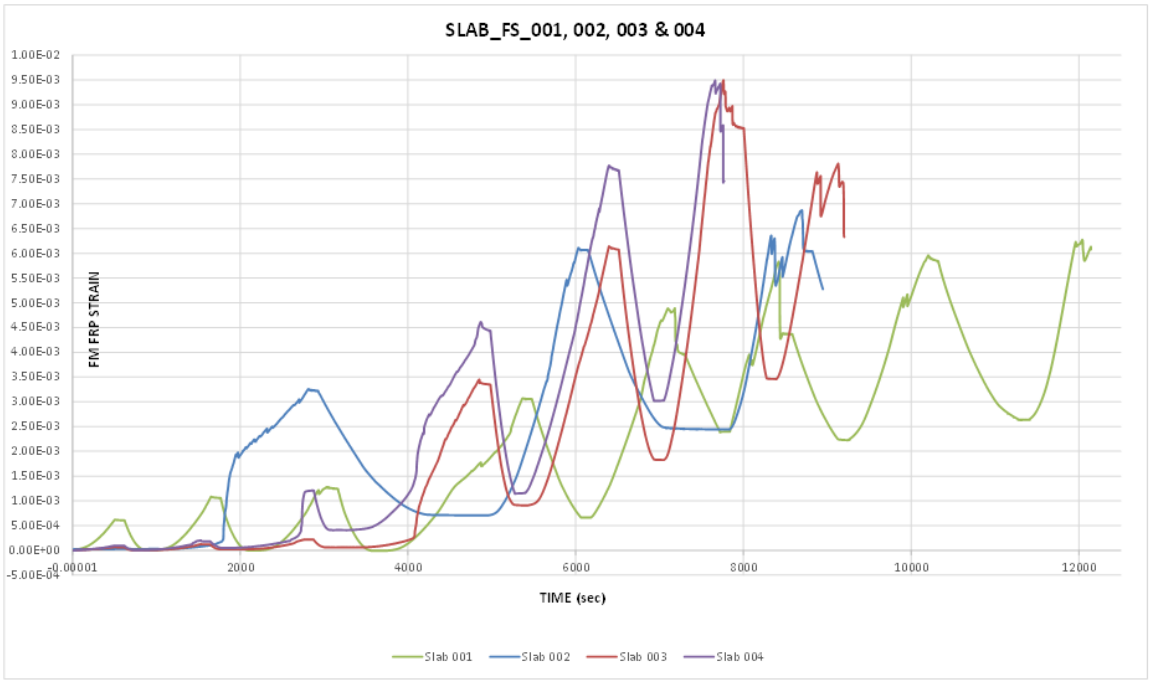

Figure 6.48 - FM FRP Strain evolution over the time

Again, the following figures illustrate that the mid-span strains evolution are very similar between the specimens 001 & 002, as well as the specimens 003 & 004.

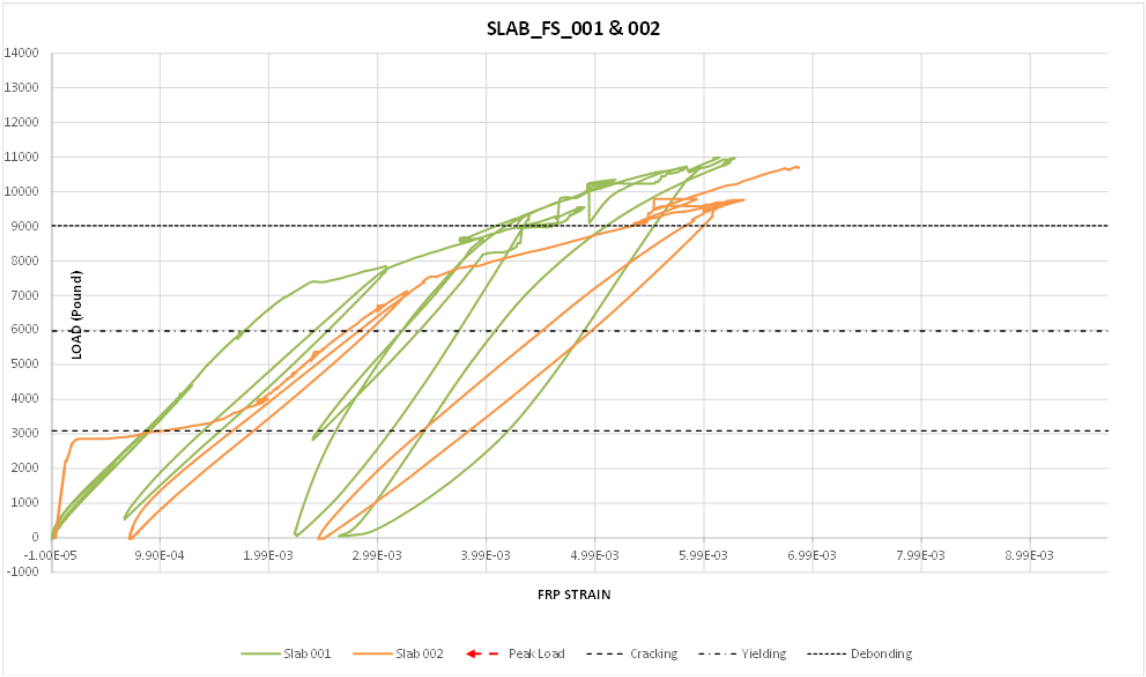

Figure 6.49 - Slab 001 & 002 - FM FRP strain vs load

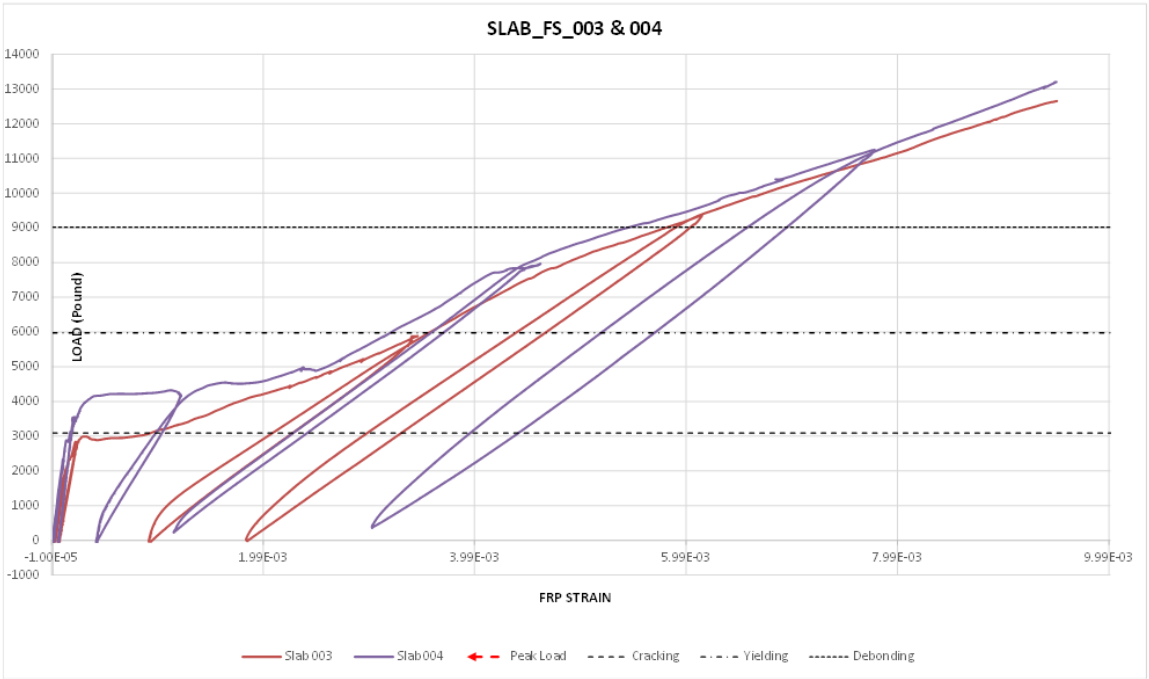

Figure 6.50 - Slab 003 & 004 - FM FRP strain vs load

In conclusion, based on the results obtained in this research, we can say that:

- *Regarding the Staple anchorage system in **configuration 1 (specimens 001 & 002)**:* the main goal is to increase the ultimate capacity allowing the slab carrying more load when catastrophic events happen. The ends-anchors' presence has no influence on the value of intermediate debonding load, suggesting end anchors do not provide any intermediate bonding improvement at serviceability, while provide a relevant strength and ductility increment at ultimate limit state. The failure mode was due to anchor's pull out, caused by mid-span debonding transferring all the stresses on the end-anchor. So, when anchors are located at the very end of the laminate, the observed behavior is in line with what other authors reported (Piyong et al. 2003) (Smith et al. 2011, 2013). The anchor's ultimate load very close to the theoretical one confirms that specimens' preparation, anchors' installation and test procedure were well performed, giving consistency on the test's results.

- *Regarding the Staple anchorage system in **configuration 2 (specimens 003 & 004)**:* the main goal is to improve the performance in terms of strains and load, engaging more of the FRP capacity and, so, allowing the system to sustain higher peak load and strains. The 4-anchors specimens showed a peak load higher than end-anchors specimens, as expected, comparable to the best spikes' anchorage system. Also, an evenly strain distribution can be spotted. The main advantage of Flat Staple anchorage system is in the installation process, easier than spikes anchors, keeping almost the same peak load and good strain distribution. Moreover, unlike the spikes' anchorage system studied in the past, where the failure mode was due to the slipping of the CFRP laminate, the failure mode here was due to a premature shear concrete failure; in fact, the whole anchorage system was still performing well, without getting broken. The anchor positioned at L/3 induced the premature failure, consequently the system does not have sufficient capacity to develop the full strength of the anchorage system. It seems very well plausible that, if the concrete-failure would have not happened, the slab would have just continued up to anchors' failure at a higher ultimate load.

A suggestion for further studies is to perform tests with different staple anchors' configuration in order to get a wider complete analysis of the flat staple anchorage system, allowing the creation of a standard and reliable design guidelines.

CHAPTER 7

Conclusions

The first part of this thesis pointed out the lack of a reliable characterization model for Staple anchors, forcing to rely on an experimental solution. The research presented in this thesis wants to be a full-study analysis on CFRP Staple anchorage system, starting from the characterization to the testing of them applied on R/C slabs.

All the information regarding the background of the composite materials, materials used, installation process, data analysis, and results discussion were provided.

Understanding the strengths, weaknesses, opportunities, and issues of externally-bonded FRP systems reveals that to advance the use of composite systems within the construction industry it is necessary to research new combinations of materials. To this extent, the experimental programs presented are unique activities to advance knowledge and understanding of CFRP anchorage systems. This thesis determined the anchors' effectiveness through an innovative installation process meant to be reliable, repeatable, and easy to perform. A total of two experimental campaigns were carried out:

1) Since the anchors are more subjected to shear forces rather than pullout forces, the standard characterization method for FRP anchors carried out on the ***first*** experimental program is a double shear test, providing a very reliable strength measurement and strain readings needed to fully understand the behavior of this anchorage system. In particular, two series of double shear tests over five specimens each were performed: five specimens were prepared with ***Flat*** staple anchors and other five with ***Round*** staple anchors. The new installation method using the CFRP patch gives a big improvement both in terms of peak load and strains compared with old anchorage systems. Regarding the *Flat* staple anchors as shown analyzing the failure modes, the rupture of the concrete substrate *without* the rupture of the anchor was the most common failure type, as meaning that the maximum shear capacity of the non-reinforced concrete was reached, consequently it does not have sufficient capacity to develop the full strength of the anchorage system. A suggestion for further studies is to create bigger blocks and test again the flat staple anchors, carefully positioning them far away from the edges in order to engage more concrete. Regarding the ***Round*** staple anchors unlike the new Flat staple anchorage system, the rupture of the concrete substrate and the rupture of the anchor was the most common failure type; anchors got broken on their edges and strengthening improvements are required before performing new tests.

2) After having characterized CFRP staple anchors finding out the Flat staples as the best anchorage system to apply so far, a 3-point bending test over R/C slabs was carried out on the second experimental program. The aim of this experimental campaign was to investigate the improvement in terms of resistance and strain distribution provided by the new anchors. This investigation was based on experimental work on RC slabs strengthened with FRP sheets connected to the concrete via carbon Flat staple anchors improved with a "FRP patch" as a new installation process tested in the previous experimental program (Chapter 3). In particular, a series of 3-point bending tests were performed: four specimens were prepared with Flat staple anchors installed with the innovative installation procedure already discussed, which gives successful and consistency results through a more reliable set-up of the test. Regarding the Staple anchorage system in ***configuration 1 (specimens 001 & 002)***, the main goal was to increase the ultimate capacity allowing the slab carrying more load when catastrophic events happen. The ends-anchors 'presence had no influence on the value of intermediate debonding load, suggesting end anchors do not provide any intermediate bonding improvement at serviceability, while provide a relevant strength and ductility increment at ultimate limit state. Regarding the Staple anchorage system in ***configuration 2 (specimens 003 & 004)***, the main goal was to improve the performance in terms of strains and load, engaging more of the FRP capacity and, so, allowing the system to sustain higher peak load and strains. The 4-anchors specimens, in fact, showed a peak load higher than end-anchors specimens, as expected, comparable to the best spikes' anchorage system. The maximum shear capacity of the R/C slab was reached, consequently it did not have sufficient capacity to develop the full strength of the anchorage system in fact, the whole anchorage system was still performing well, without getting broken. It seems very well plausible that, if the concrete-failure would have not happened, the slab would have just continued up to anchors' failure at a higher ultimate load. A suggestion for further studies is to perform tests with different staple anchors' configuration in order to do a wider analysis.

Also, comparisons between the performances of the old anchorage systems and the new ones studied in this experimental research were provided in order to show the main differences and, eventually, the enhancements made by this new anchorage system.

The author wants to point out how all the conclusions of this thesis are to be verified through a wider testing campaign before proceeding to any field application. In conclusion, further researches are surely needed to fully understand the behavior of this anchorage system in order to create standard and reliable design guidelines since the lack of a full-scale analysis did not allow, so far, to address it.

APPENDIX A

Units Conversion Table

Conversion Factors U.S. to Metric

A U.S. Customary	B Metric	Multiply by factor to convert from: A to B		B to A	
Length or thickness					
mil (0.001 in.)	micrometer (μm)	25.4	(25)*	0.03937	(0.04)
microinch (μin.)	micrometer (μm)	0.0254	(0.025)	39.37	(40)
inch (in.)	centimeter (cm) †	2.54	(2.5)	0.3937	(0.4)
foot (ft)	meter (m)	0.3048	(0.3)	3.281	(3.3)
angstrom unit	nanometer (nm)	0.1		10	
millimicron (mμ)	nanometer (nm)	1		1	
Area					
square inch ($in.^2$)	square centimeter (cm^2)	6.452	(6.5)	0.1550	(0.15)
square foot (ft^2)	square meter (m^2)	0.09290	(0.1)	10.76	(10)
Volume					
cubic inch ($in.^3$)	cubic centimeter (cm^3)	16.39	(16)	0.06102	(0.06)
cubic foot (ft^3)	cubic meter (m^3)	0.02832	(0.03)	35.31	(35)
gallon, U.S. liquid (gal)	milliliter (mL)	3.785	(4)	0.2642	(0.25)
1000 gallons	cubic meter (m^3)	3.785	(4)	0.2642	(0.25)
fluid ounce (fl oz)	milliliter (mL)	29.57	(30)	0.03381	(0.034)
Mass (weight)					
grain (gr)	milligram (mg)	64.80	(65)	0.01543	(0.015)
ounce, avoirdupois (oz)	gram (g)	28.35	(28)	0.03527	(0.035)
ounce, troy (troy oz)	gram (g)	31.10	(30)	0.03215	(0.03)
pound, avoirdupois (lb)	kilogram (kg)	0.4536	(0.45)	2.205	(2.2)
Weight (mass) per unit area					
$mg/in.^2$	g/m^2	1.550	(1.5)	0.6451	(0.65)
$mg/in.^2$	mg/cm^2 †	0.1550	(0.15)	6.451	(6.5)
$oz/in.^2$	kg/m^2	43.95	(44)	0.02275	(0.023)
$oz/in.^2$	g/cm^2 †	4.395	(4.4)	0.2275	(0.23)
oz/ft^2	kg/m^2	0.3052	(0.3)	3.277	(3.3)
oz/ft^2	mg/cm^2 †	305.2	(300)	0.003277	(0.003)

A U.S. Customary	B Metric	Multiply by factor to convert from: A to B		B to A	
Weight (mass) per unit volume					
oz/gal	g/L	7.490	(7.5)	0.1335	(0.13)
oz/gal	kg/m^3	7.490	(7.5)	0.1335	(0.13)
lb/100 gal	kg/m^3	1.198	(1.2)	0.8347	(0.8)
fl oz/gal	cm^3/m^3 †	7812	(8000)	0.0001280	(0.00013)
fl oz/gal	mL/L	7.812	(8)	0.1280	(0.13)
Current density					
A/ft^2	A/m^2	10.76	(10)	0.09290	(0.1)
A/ft^2	mA/cm^2 †	1.076	(1)	0.9290	(1)
A/ft^2	A/dm^2 †	0.1076	(0.1)	9.290	(10)
$A/in.^2$	kA/m^2	1.550	(1.5)	0.6451	(0.65)
$A/in.^2$	mA/cm^2 †	155.00	(150)	0.006451	(0.0065)
Energy					
calorie (cal)	joule (J)	4.19	(4)	0.239	(0.25)
kilowatt-hour (kWh)	megajoule (MJ)	3.600	(exact)	0.2778	(0.3)
Pressure					
$lb/in.^2$ (psi)	pascal (Pa)	6895	(7000)	0.0001450	(0.00015)
1000 psi	megapascal (MPa)	6.895	(7)	0.145	(0.15)
kilogram-force/mm^2 (kgf/mm^2)	megapascal (MPa)	9.806	(10)	0.1020	(0.1)
Quantity of electricity to plate unit thickness					
$A\text{-}h/ft^2$ for 1 mil	C/m^2 for μm	1530	(1500)	0.0006535	(0.00065)
$A\text{-}h/ft^2$ for 1 mil	$A\text{-}h/m^2$ for 1 μm	0.4236	(0.4)	2.361	(2.4)
$A\text{-}h/ft^2$ for 1 mil	$mA\text{-}h/cm^2$ or 1 μm	0.04236	(0.04)	23.61	(24)
Temperature					
$°F = 9/5°C + 32$	°F = Fahrenheit temperature				
$°C = 5/9 (°F - 32)$	°C = Celsius (centigrade) temperature				
$t\,°C = t_K - 273.15$	t_K = kelvins				

Table A - Unit Conversion Table

APPENDIX B

Block’s Geometry and Strain Gauges

Figure A shows the geometry of the blocks used for the ***first*** experimental program.

Figure A - Experimental Program 1 - Block's geometry

Figure B shows the strain gauges' location blocks used for the ***first*** experimental program.

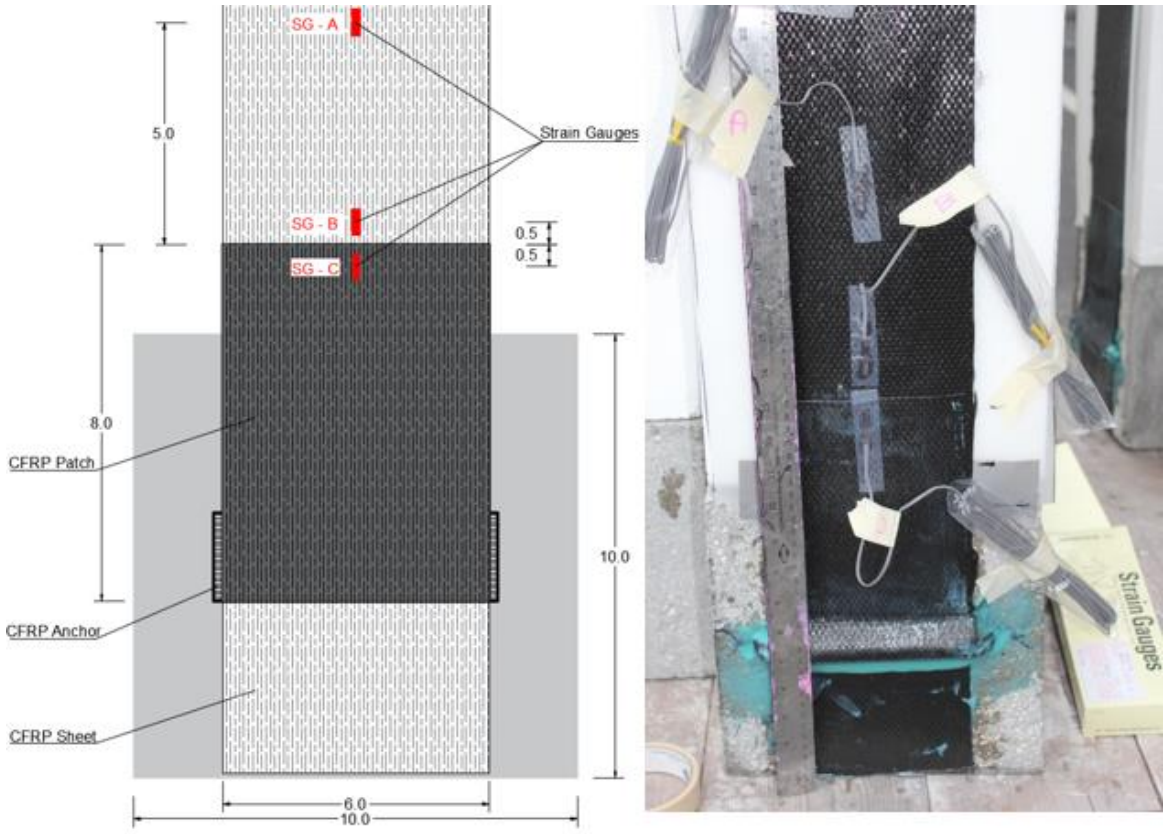

Figure B - Experimental Program 1 - Strain Gauge's position

APPENDIX C

Slab's Geometry

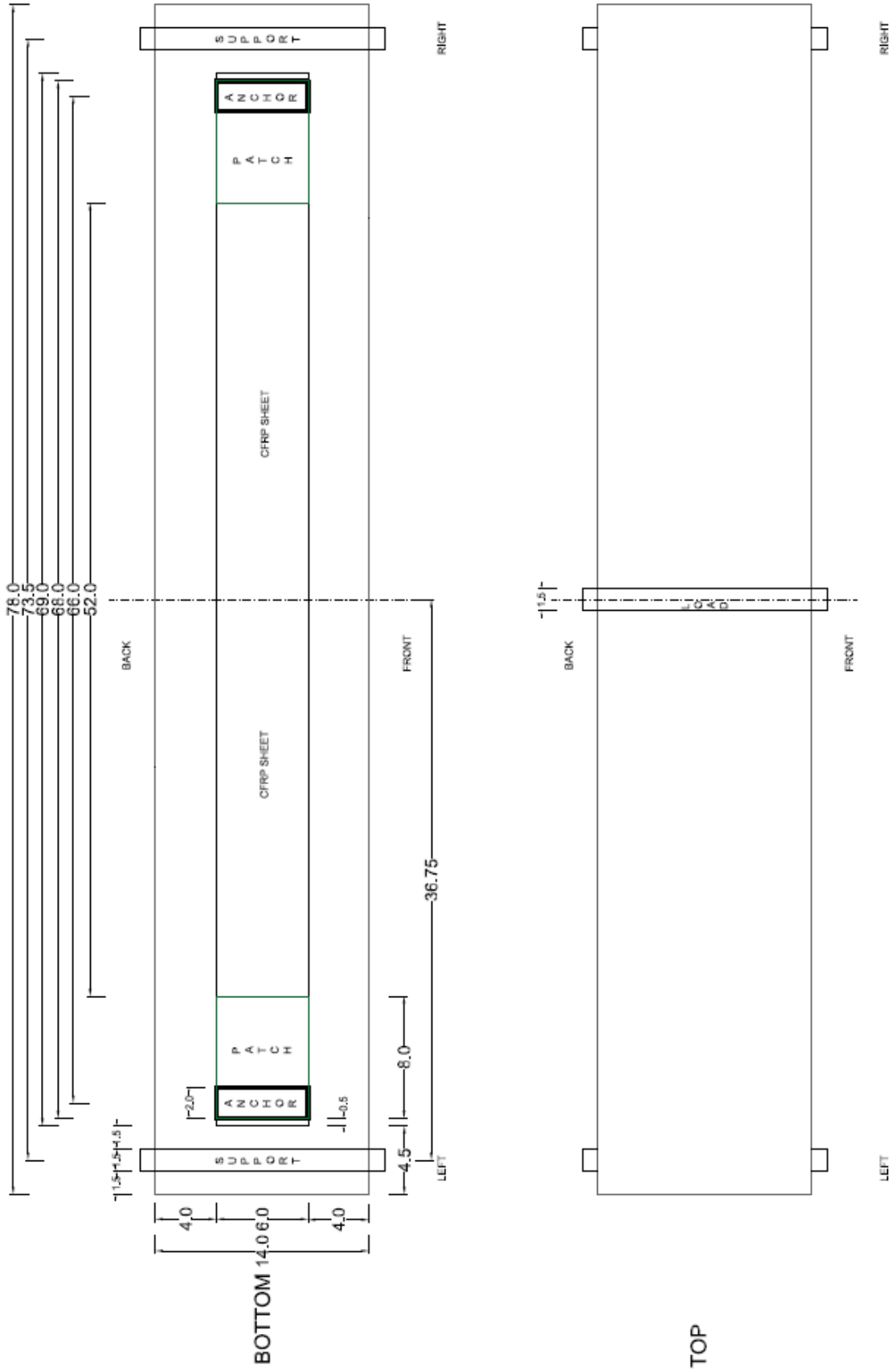

Figure C - Experimental Program 2 - Geometry - Slabs 001 & 002

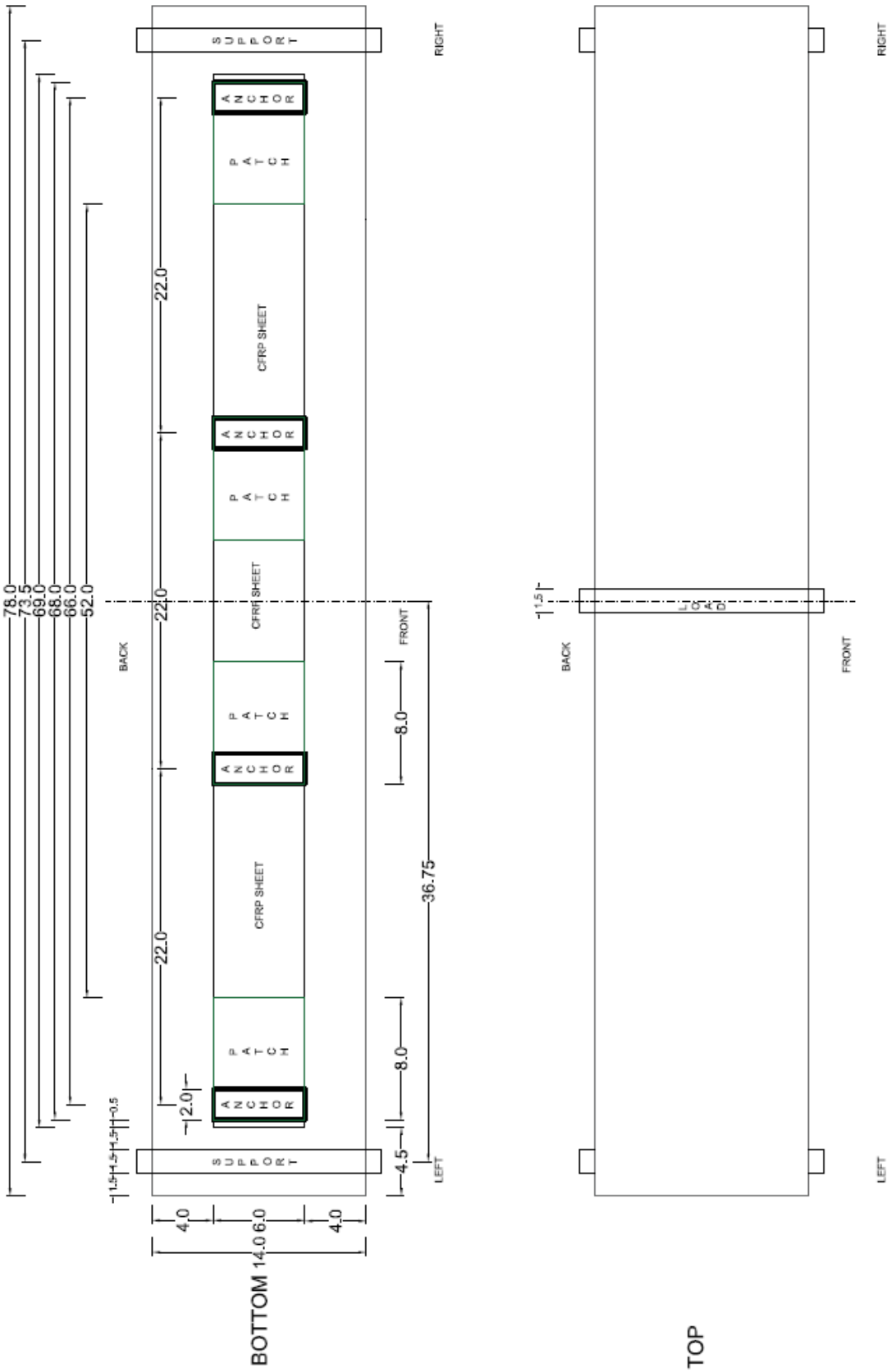

Figure D - Experimental Program 2 - Geometry - Slabs 003 & 004

APPENDIX D

Slab’s Strain Gauges

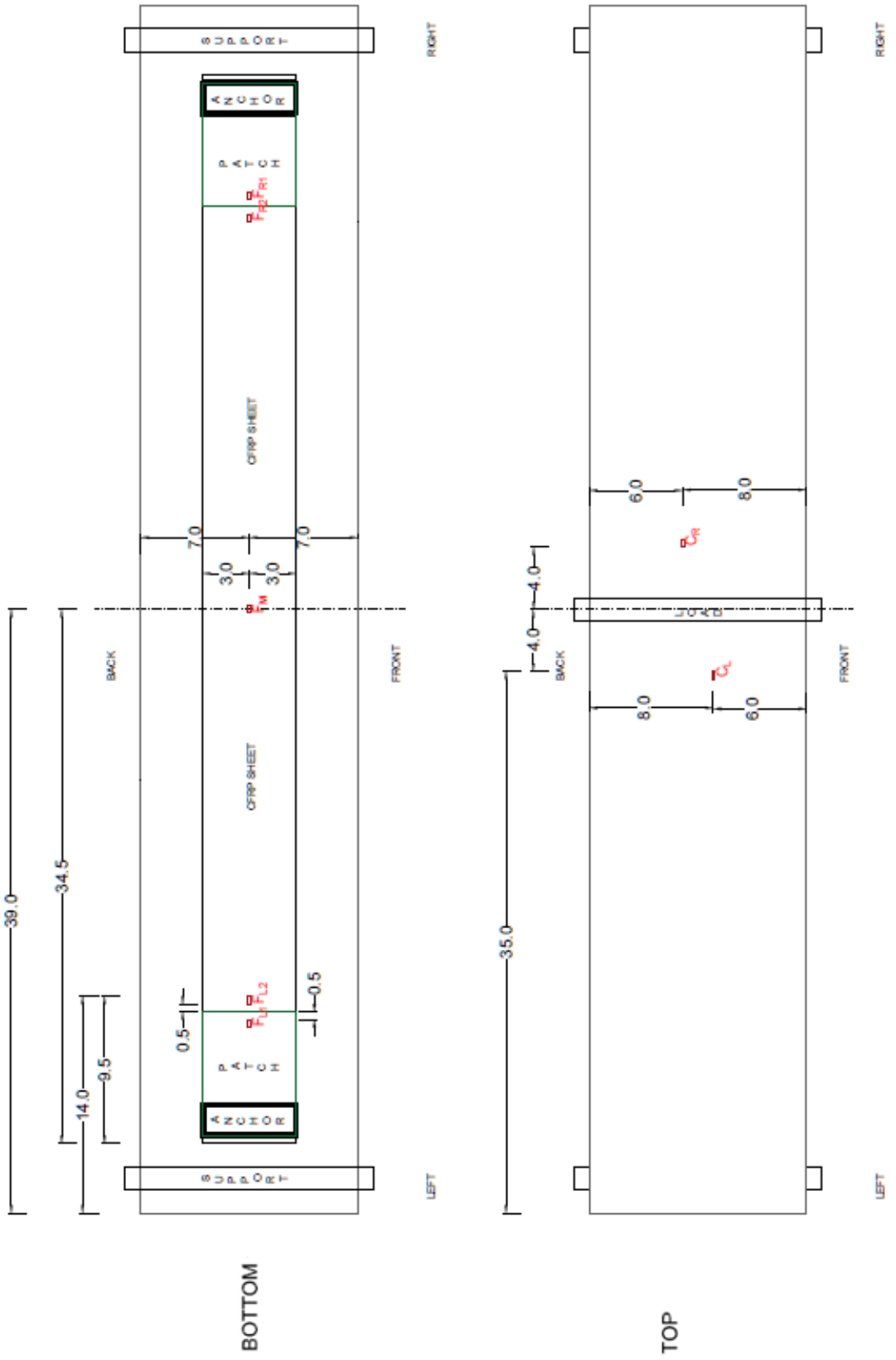

Figure E - Experimental Program 2 - Strain Gauges - Slab 001 & 002

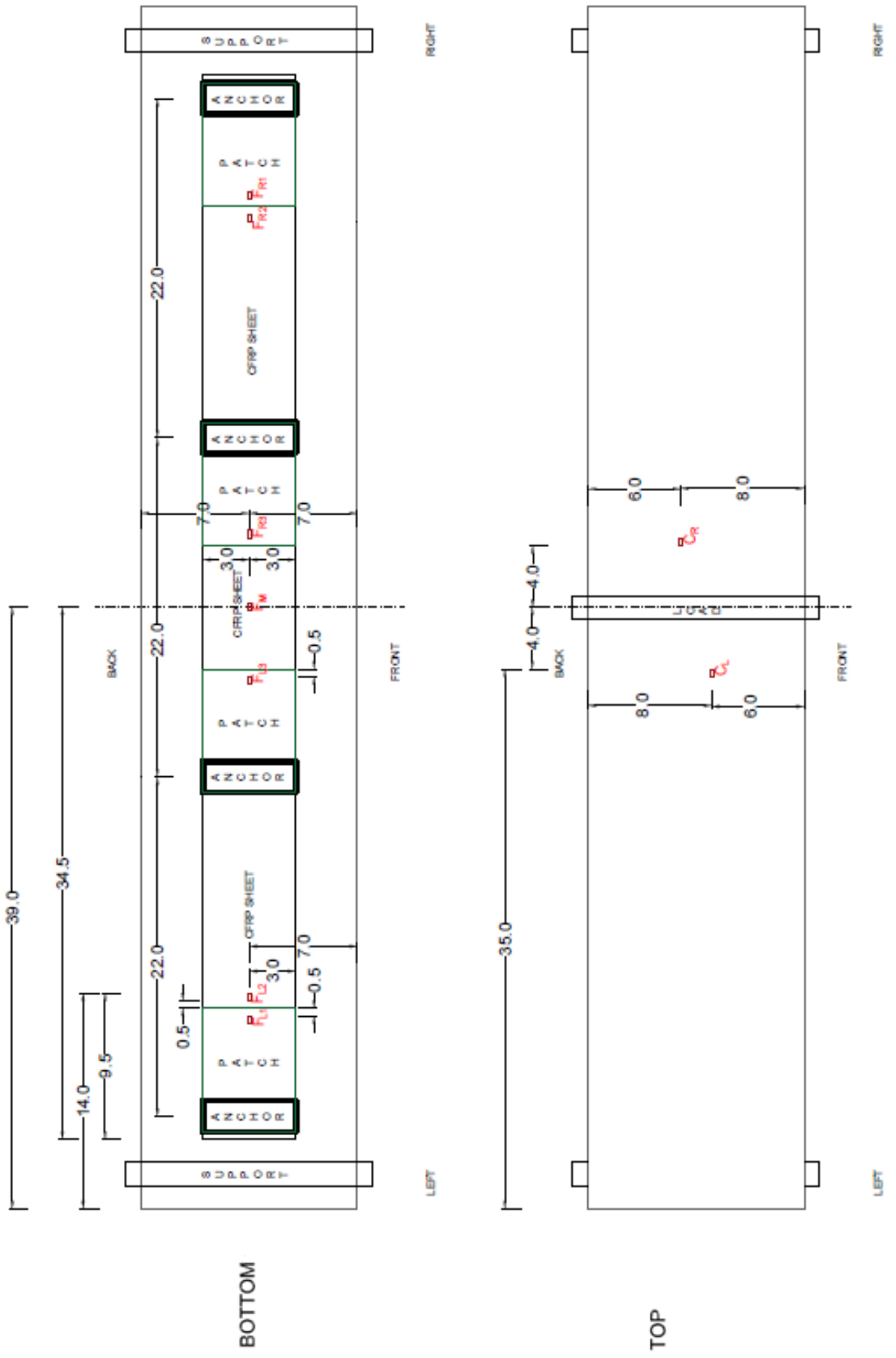

Figure F - Experimental Program 2 - Strain Gauges - Slab 003 & 004

APPENDIX E

Slab’s Test Results

For sake of completeness hereinafter all the slab's test results obtained and analyzed from the 3-point bending test performed on slabs are provided.

FLAT STAPLE 2" - Configuration 1 (ends) - TEST RESULTS - Slab 001

	US					SI				
	Load [Kip]	Deflection δ [in]	FRP Strain[%]	Concrete Strain[%]	x [in]	Load [KN]	Deflection δ [mm]	FRP Strain[%]	Concrete Strain[%]	x [mm]
Elastic	1.541	0.140	0.035	0.007	2.950	6.855	3.556	0.035	0.007	74.930
Cracking	4.197	0.324	0.122	0.018	0.949	18.669	8.230	0.122	0.018	24.098
Yielding Start	5.938	0.680	0.176	0.048	0.883	26.414	17.278	0.176	0.048	22.428
Debonding	9.846	1.532	0.448	0.070	0.707	43.797	38.907	0.448	0.070	17.963
Ultimate	10.986	3.069	0.613	0.062	0.681	48.868	77.948	0.613	0.062	17.289

FLAT STAPLE 2" - Configuration 1 (ends) - TEST RESULTS - Slab 002

	US					SI				
	Load [Kip]	Deflection δ [in]	FRP Strain[%]	Concrete Strain[%]	x [in]	Load [KN]	Deflection δ [mm]	FRP Strain[%]	Concrete Strain[%]	x [mm]
Elastic	1.542	0.131	0.009	0.006	2.867	6.858	3.334	0.009	0.006	72.823
Cracking	4.088	0.338	0.196	0.016	0.877	18.184	8.579	0.196	0.016	22.278
Yielding Start	5.481	0.593	0.250	0.039	0.936	24.382	15.050	0.250	0.039	23.769
Debonding	9.210	1.257	0.548	0.077	0.828	40.967	31.927	0.548	0.077	21.034
Ultimate	10.730	2.631	0.685	0.085	0.717	47.729	66.831	0.685	0.085	18.217

FLAT STAPLE 2" - Configuration 2 (L/3) - TEST RESULTS - Slab 003

	US					SI				
	Load [Kip]	Deflection δ [in]	FRP Strain[%]	Concrete Strain[%]	x [in]	Load [KN]	Deflection δ [mm]	FRP Strain[%]	Concrete Strain[%]	x [mm]
Elastic	1.543	0.172	0.008	0.007	2.956	6.863	4.363	0.008	0.007	75.082
Cracked	2.989	0.311	0.030	0.017	0.933	13.297	7.896	0.030	0.017	23.694
Yielding Start	5.752	0.798	0.340	0.042	0.848	25.587	20.278	0.340	0.042	21.543
Debonding	9.226	1.384	0.611	0.068	0.750	41.040	35.162	0.611	0.068	19.050
Ultimate	12.653	2.269	0.950	0.095	0.667	56.284	57.622	0.950	0.095	16.936

FLAT STAPLE 2" - Configuration 2 (L/3) - TEST RESULTS - Slab 004

	US					SI				
	Load [Kip]	Deflection δ [in]	FRP Strain[%]	Concrete Strain[%]	x [in]	Load [KN]	Deflection δ [mm]	FRP Strain[%]	Concrete Strain[%]	x [mm]
Elastic	1.546	0.119	0.012	0.007	3.010	6.879	3.013	0.012	0.007	76.454
Cracked	3.552	0.239	0.013	0.038	0.907	15.801	6.083	0.013	0.038	23.048
Yielding Start	5.885	0.581	0.314	0.041	0.826	26.177	14.769	0.314	0.041	20.988
Debonding	9.138	1.065	0.561	0.067	0.739	40.648	27.053	0.561	0.067	18.766
Ultimate	13.205	2.031	0.949	0.093	0.657	58.738	51.589	0.949	0.093	16.678

Table B - Slabs 001, 002, 003 & 004 test results

The following tables show the matching between the experimental results obtained from the 3-point bending test on slabs and the theoretical results coming from the preliminary design explained in Appendix F.

FLAT STAPLE 2" - Configuration 1 (ends) - EXPERIMENTAL MATCHING [US] - Slab 001

	Load [kip]			Displacement [in]			FRP Strain[%]			x [in]		
	Exp.	Th.	Δ [%]	Exp.	Th.	Δ [%]	Exp.	Th.	Δ [%]	Exp.	Th.	Δ [%]
Elastic	1.541	-	-	0.140	-	-	0.035	-	-	2.950	3.044	-3.10%
Cracking	4.197	3.090	35.83%	0.324	0.213	51.88%	0.122	0.133	-8.39%	0.949	1.004	-5.48%
Yielding Start	5.938	5.976	-0.64%	0.680	0.460	47.87%	0.176	0.292	-39.77%	0.883	0.849	3.98%
Debonding	9.846	9.018	9.18%	1.532	1.020	50.24%	0.448	0.658	-31.97%	0.707	0.710	-0.38%
Ultimate	10.986	9.561	14.91%	3.069	1.171	162.11%	0.613	0.724	-15.25%	0.681	0.700	-2.82%

FLAT STAPLE 2" - Configuration 1 (ends) - EXPERIMENTAL MATCHING [SI] - Slab 001

	Load [KN]			Displacement [mm]			FRP Strain[%]			x [mm]		
	Exp.	Th.	Δ [%]	Exp.	Th.	Δ [%]	Exp.	Th.	Δ [%]	Exp.	Th.	Δ [%]
Elastic	6.855	-	-	3.556	-	-	0.035	-	-	74.930	77.330	-3.10%
Cracking	18.669	13.744	35.83%	8.230	5.419	51.88%	0.122	0.133	-8.39%	24.098	25.494	-5.48%
Yielding Start	26.414	26.583	-0.64%	17.278	11.684	47.87%	0.176	0.292	-39.77%	22.428	21.570	3.98%
Debonding	43.797	40.116	9.18%	38.907	25.897	50.24%	0.448	0.658	-31.97%	17.963	18.032	-0.38%
Ultimate	48.868	42.528	14.91%	77.948	29.739	162.11%	0.613	0.724	-15.25%	17.289	17.790	-2.82%

FLAT STAPLE 2" - Configuration 1 (ends) - EXPERIMENTAL MATCHING [US] - Slab 002

	Load [kip]			Displacement [in]			FRP Strain[%]			x [in]		
	Exp.	Th.	Δ [%]	Exp.	Th.	Δ [%]	Exp.	Th.	Δ [%]	Exp.	Th.	Δ [%]
Elastic	1.542	-	-	0.131	-	-	0.009	-	-	2.867	3.044	-5.83%
Cracking	4.088	3.090	32.31%	0.338	0.213	58.33%	0.196	0.133	47.42%	0.877	1.004	-12.62%
Yielding Start	5.481	5.976	-8.28%	0.593	0.460	28.80%	0.250	0.292	-14.35%	0.936	0.849	10.19%
Debonding	9.210	9.018	2.12%	1.257	1.020	23.28%	0.548	0.658	-16.69%	0.828	0.710	16.65%
Ultimate	10.730	9.561	12.23%	2.631	1.171	124.73%	0.685	0.724	-5.38%	0.717	0.700	2.40%

FLAT STAPLE 2" - Configuration 1 (ends) - EXPERIMENTAL MATCHING [SI] - Slab 002

	Load [KN]			Displacement [mm]			FRP Strain[%]			x [mm]		
	Exp.	Th.	Δ [%]	Exp.	Th.	Δ [%]	Exp.	Th.	Δ [%]	Exp.	Th.	Δ [%]
Elastic	6.858	-	-	3.334	-	-	0.009	-	-	72.823	77.330	-5.83%
Cracking	18.184	13.744	32.31%	8.579	5.419	58.33%	0.196	0.133	47.42%	22.278	25.494	-12.62%
Yielding Start	24.382	26.583	-8.28%	15.050	11.684	28.80%	0.250	0.292	-14.35%	23.769	21.570	10.19%
Debonding	40.967	40.116	2.12%	31.927	25.897	23.28%	0.548	0.658	-16.69%	21.034	18.032	16.65%
Ultimate	47.729	42.528	12.23%	66.831	29.739	124.73%	0.685	0.724	-5.38%	18.217	17.790	2.40%

Table C - Slab 001 & 002 experimental matching (Exp.= experimental; Th.= theoretical)

FLAT STAPLE 2" - Configuration 2 (L/3) - EXPERIMENTAL MATCHING [US] - Slab 003

	Load [kip]			Displacement [in]			FRP Strain[%]			x [in]		
	Exp.	Th.	Δ [%]	Exp.	Th.	Δ [%]	Exp.	Th.	Δ [%]	Exp.	Th.	Δ [%]
Elastic	1.543	-	-	0.172	-	-	0.008	-	-	2.956	3.044	-2.91%
Cracked	2.989	3.090	-3.25%	0.311	0.213	45.73%	0.030	0.133	-77.74%	0.933	1.004	-7.06%
Yielding Start	5.752	5.976	-3.75%	0.798	0.460	73.54%	0.340	0.292	16.52%	0.848	0.849	-0.13%
Debonding	9.226	9.018	2.30%	1.384	1.020	35.78%	0.611	0.658	-7.10%	0.750	0.710	5.65%
Ultimate	12.653	15.452	-18.12%	2.269	1.258	80.38%	0.950	1.447	-34.38%	0.667	0.700	-4.80%

FLAT STAPLE 2" - Configuration 2 (L/3) - EXPERIMENTAL MATCHING [SI] - Slab 003

	Load [KN]			Displacement [mm]			FRP Strain[%]			x [mm]		
	Exp.	Th.	Δ [%]	Exp.	Th.	Δ [%]	Exp.	Th.	Δ [%]	Exp.	Th.	Δ [%]
Elastic	6.863	-	-	4.363	-	-	0.008	-	-	75.082	-	-
Cracked	13.297	13.744	-3.25%	7.896	5.419	45.73%	0.030	0.133	-77.74%	23.694	25.494	-7.06%
Yielding Start	25.587	26.583	-3.75%	20.278	11.684	73.54%	0.340	0.292	16.52%	21.543	21.570	-0.13%
Debonding	41.040	40.116	2.30%	35.162	25.897	35.78%	0.611	0.658	-7.10%	19.050	18.032	5.65%
Ultimate	56.284	68.736	-18.12%	57.622	31.945	80.38%	0.950	1.447	-34.38%	16.936	17.790	-4.80%

FLAT STAPLE 2" - Configuration 2 (L/3) - EXPERIMENTAL MATCHING [US] - Slab 004

	Load [kip]			Displacement [in]			FRP Strain[%]			x [in]		
	Exp.	Th.	Δ [%]	Exp.	Th.	Δ [%]	Exp.	Th.	Δ [%]	Exp.	Th.	Δ [%]
Elastic	1.546	-	-	0.119	-	-	0.012	-	-	3.010	3.044	-1.13%
Cracked	3.552	3.090	14.97%	0.239	0.213	12.26%	0.013	0.133	-90.07%	0.907	1.004	-9.59%
Yielding Start	5.885	5.976	-1.53%	0.581	0.460	26.39%	0.314	0.292	7.64%	0.826	0.849	-2.70%
Debonding	9.138	9.018	1.33%	1.065	1.020	4.46%	0.561	0.658	-14.76%	0.739	0.710	4.07%
Ultimate	13.205	15.452	-14.55%	2.031	1.258	61.49%	0.949	1.447	-34.41%	0.657	0.700	-6.25%

FLAT STAPLE 2" - Configuration 2 (L/3) - EXPERIMENTAL MATCHING [SI] - Slab 004

	Load [KN]			Displacement [mm]			FRP Strain[%]			x [mm]		
	Exp.	Th.	Δ [%]	Exp.	Th.	Δ [%]	Exp.	Th.	Δ [%]	Exp.	Th.	Δ [%]
Elastic		-	-		-	-		-	-	76.454	-	-
Cracked	15.801	13.744	14.97%	6.083	5.419	12.26%	0.013	0.133	-90.07%	23.048	25.494	-9.59%
Yielding Start	26.177	26.583	-1.53%	14.769	11.684	26.39%	0.314	0.292	7.64%	20.988	21.570	-2.70%
Debonding	40.648	40.116	1.33%	27.053	25.897	4.46%	0.561	0.658	-14.76%	18.766	18.032	4.07%
Ultimate	58.738	68.736	-14.55%		31.945	-100.00%	0.949	1.447	-34.41%	16.678	17.790	-6.25%

Table D - Slab 003 & 004 experimental matching (Exp.= experimental; Th.= theoretical)

APPENDIX F

Preliminary Design

Engineers designing CFRP strengthening systems require analytical methods that accurately predicts the main parameters involved.

Although if, is not the main goal of this dissertation, because the author adopted the same analytical models used in previous investigations to be consistent, in this section, general information recap about the analytical models used to carry out the two experimental programs aim of this research are provided. A complete preliminary design analysis and analytical models can be found in dissertations realized in previous years (Berneschi, 2015; Cadenazzi, 2016; Rossini, 2016).

The force transfer between FRP plate and concrete substrate takes place primarily through shear stresses and thus, shear tests are commonly adopted to determine the maximum debonding force. Despite that, comparisons of different set-ups show that, in general, shear tests offer lower bond strength than bending tests. Also, their simplicity makes them popular for laboratory investigations of FRP to concrete bond behavior. It is important to remark that the double-shear test is generally preferred over the single shear test, due to symmetry and for better control of induced normal stresses. However, it should be kept in mind that in flexural elements, peeling stresses also develop along the FRP-concrete interface and their interaction with shear stresses can lead to a reduction in the bond strength of the strengthening system.

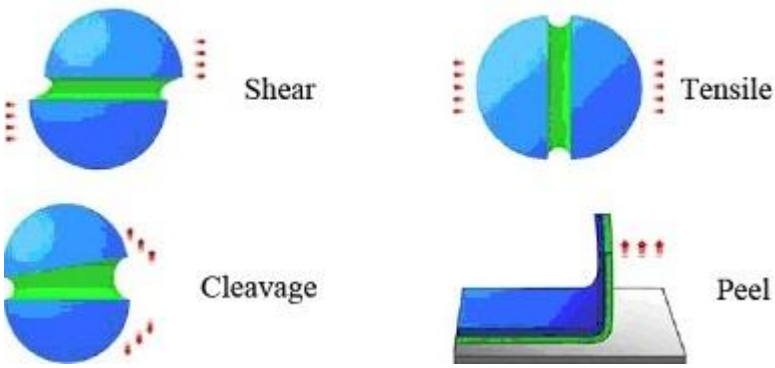

The bond system is fundamental because is responsible to transfer the load from the concrete to the FRP flexural element. The bond behavior between FRP and concrete is associated with the interfacial stress diffusion, which is correlated to mechanical characteristics, such as the geometry or the properties of the materials.

The Optimal Bond Length is the minimum bonded length that ensures the transmission of the bonding force and any longer bonded length does not produce any force increase.

According to the ACI formulation the optimal bond length is rigorously a function of the sheet properties only, the CNR formulation corrects the value accounting for the concrete element geometry. Both CNR and ACI formulation will be computed, referring to 5% design values for CNR formulation, and choosing the biggest one as design parameter, willing to stay on the safe side against end debonding.

The CNR-DT-200 (2013) and the ACI provide the following expressions for it:

$$l_{ed}^{CNR} = \frac{\pi s_u}{2 \gamma Rd} \cdot \sqrt{\frac{FC}{2 K_b K_g} \frac{E_f t_f}{\sqrt{f_{cm} f_{ctm}}}} \leq 200\ mm$$

$$l_{ed}^{ACI} = 0.057 \cdot \sqrt{\frac{E_f t_f}{\sqrt{f'_c}}}$$

Optimal Development length

	US [in]	SI [mm]
CNR (Average)	2.14	54.43
CNR (5%)	3.09	78.51
ACI	3.89	98.83

Tensions were taken as positive, both for stresses and strains, according to the following sketch (adapted from CNR 2013 & EC2 2008). In sectional analysis, the section's extrados is assumed as reference axis.

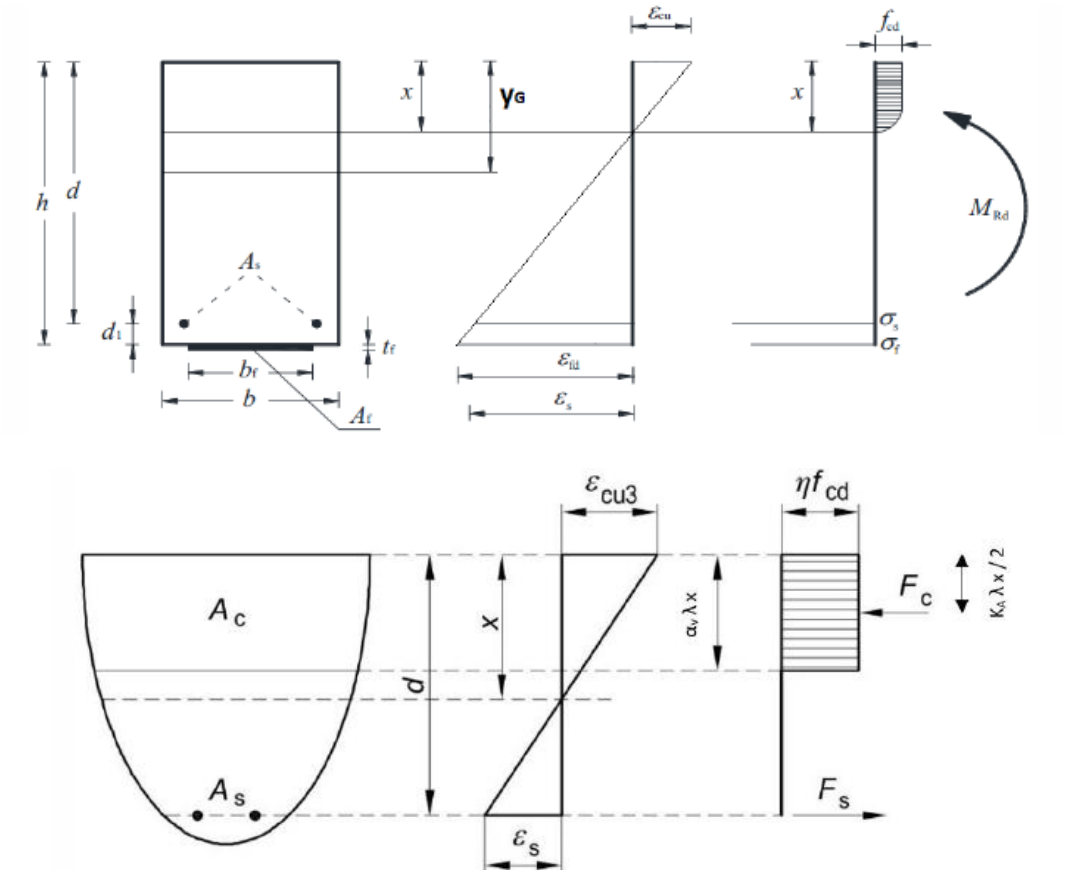

According to the standard R/C theory, a bended element undergoes three different stages before reaching collapse: (I) an initial elastic phase in which the concrete is working in tension and the element is rigorously an elastic prism, (II) a cracked elastic phase in which the tensioned concrete is assumed not working, but all the materials still show a perfectly elastic behavior, (III) a cracked plastic phase in which the materials, at increasing load, cease to behave elastically, until one of them reach its ultimate strain, defining the section's ultimate limit state.

Depending on the stage the section is undergoing, different mechanical models are required to define its strength and stiffness, based on different assumption. In order to extend the standard sectional model to externally reinforced applications, some addenda to the standard assumptions should be made (CNR, 2014):

II a. Perfect FRP – concrete bond up to failure

III a. FRP behaves elastically up to failure

The perfect-bond-up-to-failure assumption does not mean that the debonding failure mechanism should be disregarded, on the contrary debonding will generally control the element strength, determining its failure; but debonding can be very well modelled as a brittle mechanism, not preceded by any significant slipping between concrete and FRP. The same assumptions are considered valid to proceed to sectional design of anchored FRP applications, as suggested by Lam & Teng (2001).

Along with the design-assumption-addenda discussed, the critical phases of an externally reinforced anchored element would undergo and the different failures it can experience are here defined and summed up:

1. Cracking
2. Yielding
3. Intermediate Debonding
4. Anchors Failure
5. Sheet Rupture
6. Concrete Rupture
7. Steel Rupture

Each one of these stages is defined by a value of strain defining the cracking, yielding or failure of one of the material making the section.

The order can vary depending on the element's geometry and material properties, though the proposed one well define what experimentally experienced. End debonding and shear failure can be experienced as well and their occurrence should be checked.

Sectional Properties - Phase I - Uncracked Elastic Section

	US			SI		
	Virgin	FRP-Reinforced	[ ]	Virgin	FRP-Reinforced	[ ]
x_I	-	0.00	[in]	0.00	0.00	[mm]
$y_{G,I}$	3.03	3.04	[in]	76.91	77.33	[mm]
A_I	85.15	85.62	[in^2]	54934.30	55241.82	[mm^2]
I_{xI}	256.84	261.06	[in^4]	106905987.44	108662589.53	[mm^4]

Sectional Properties - Phase II - Cracked Elastic Section

	US			SI		
	Virgin	FRP-Reinforced	[ ]	Virgin	FRP-Reinforced	[ ]
x_{II}	0.83	1.00	[in]	21.16	25.49	[mm]
$y_{G,II}$	0.83	1.00	[in]	21.16	25.49	[mm]
A_{II}	12.81	15.68	[in^2]	8264.48	10114.07	[mm^2]
I_{xII}	23.24	35.63	[in^4]	9673049.43	14830562.25	[mm^4]

Cracking - EC2 & ACI - NO FRP

	US			SI		
	EC2	ACI	[]	EC2	ACI	[]
fctm(EC2), fr(ACI)	-0.596	-0.697	[Ksi]	-4.11	-4.8032	[MPa]
εCr	-0.00011	-0.00013250	[/]	-0.00011	-0.00013	[/]
Ecm(EC2), Ec(ACI)	5,447.88	5,257.60	[Ksi]	37,562.07	36,250.11	[MPa]
y_g	3.028	3.028	[in]	76.91	76.91	[mm]
I_{gross}	256.84	256.84	[in^4]	106,905,987	106,905,987	[mm^4]
M	51.51	60.20	[Kip in]	5,819.75	6,801.79	[KN mm]
P	2.54	3.02	[Kip]	11.32	13.42	[KN]
x	3.028	3.03	[in]	76.91	76.91	[mm]
IG_elastic_crack	256.84	256.84	[in^4]	106,905,987	106,905,987	[mm^4]
A*_elastic_crack	70.00	70.00	[in^2]	45,161.20	45,161.20	[mm^2]
fw, bernoulli, I	0.00191	0.00198	[in]	0.0486217	0.0504	[mm]
fp, bernoulli, I	0.01504	0.01848	[in]	0.382038654	0.47	[mm]
ft, timoshenko, II	0.000633	0.00074	[in]	0.016087271	0.02	[mm]
f2, strain based	0.01696	0.02047	[in]	0.430660378	0.52	[mm]
f1 tot	0.01759	0.02121	[in]	0.446747649	0.54	[mm]
f2 tot	0.01759	0.02121	[in]	0.446747649	0.54	[mm]
εFRP	-0.00011015	-0.00013339	[/]	-0.0001101	-0.00013	[/]

Cracking - EC2 & ACI - FRP

	US			SI		
	EC2	ACI	[]	EC2	ACI	[]
fctm(EC2), fr(ACI)	-0.596	-0.697	[Ksi]	-4.11	-4.8032	[MPa]
εCr	-0.00011	-0.00013250	[/]	-0.00011	-0.00013	[/]
Ecm(EC2), Ec(ACI)	5,447.88	5,257.60	[Ksi]	37,562.07	36,250.11	[MPa]
y_g	3.044	3.044	[in]	77.33	77.33	[mm]
I_{gross}	261.06	261.06	[in^4]	108,662,590	108,662,589.53	[mm^4]
M	52.65	61.53	[Kip in]	5,948.71	6,952.52	[KN mm]
P	2.61	3.09	[Kip]	11.59	13.74	[KN]
x	3.044	3.044	[in]	77.33	77.33	[mm]
IG_elastic_crack	261.06	261.06	[in^4]	108,662,590	108,662,589.53	[mm^4]
A*_elastic_crack	70.00	70.00	[in^2]	45,161.20	45,161.20	[mm^2]
fw, bernoulli, I	0.00188	0.00195	[in]	0.0478357	0.0496	[mm]
fp, bernoulli, I	0.01516	0.01862	[in]	0.38503981	0.47	[mm]
ft, timoshenko, II	0.000648	0.00076	[in]	0.016452192	0.02	[mm]
f2, strain based	0.01704	0.02057	[in]	0.432875532	0.52	[mm]
f1 tot	0.01769	0.02133	[in]	0.449327723	0.54	[mm]
f2 tot	0.01769	0.02133	[in]	0.449327723	0.54	[mm]
εFRP	-0.00011015	-0.00013295	[/]	-0.0001102	-0.00013	[/]

Balanced Section - NO FRP

	US		SI	
	ACI	[]	EC2	[]
εC	0.0030	[/]	0.0034	[/]
εS	-0.0024	[/]	-0.0024	[/]
x	2.8253	[in]	75.4223	[mm]
C	144.1856	[Kip]	1,260,985.1547	[N]
As balanced	2.143	[in^2]	2,718.412	[mm^2]
ρ	10.31	[%]	5.24	[%]
M		[Kip in]	114.59	[KN m]

Balanced Section - FRP min

	US		SI	
	ACI	[]	EC2	[]
εC	0.0030	[/]	0.0034	[/]
εF	-0.0066	[/]	-0.0066	[/]
x	1.8855	[in]	51.7988	[mm]
εS	-0.0051	[/]	-0.0050	[/]
C	96.226	[kip]	866,024.370	[N]
S	-14.86	[Kip]	-66,106.57	[N]
Af balanced	1.14	[in^2]	1,630.03	[mm^2]
n° ply	2.381598	[/]	5.26364518	[/]
ρ	20.99431	[%]	9.49912052	[%]

Shear ULS - EC2

	SI		
	NO FRP	FRP	[]
Ac	45,726	54,193	[mm^2]
k	2.000	2.000	[/]
ρl	0.0031	0.0026	[/]
CRd,c	0.018	0.018	[/]
k1	0.15	0.15	[/]
v min	0.71	0.71	[/]
VRd,c	32.481	38.495	[KN]
P	62.66	74.69	[KN]

Shear ULS - ACI

	US		
	NO FRP	FRP	[]
Ac	71	84	[in^2]
λ	1.000	1.000	[/]
ρw	0.0031	0.0026	[/]
Vca	13.061	15.377	[Kip]
Vcb	23.04	27.31	[kip]
Vc1	13.17	15.60	[Kip]
Vc2	13.061	15.377	[kip]
Vc	13.06	15.38	[Kip]
P	25.86	30.49	[kip]
ϕ	0.750	0.750	[/]
ϕP	19.40	22.87	[kip]

The load cycles, here reported for the sake of completeness, were defined, and normalized to be used in this investigation, according to the calculations and considerations reported on the previous research (Rossini, 2016).

The results obtained from the experimental research were compared with those obtained from existing analytical models in order to have a validation of the test results.

To be noticed that a Euler-based approach provides an underestimated deflection prediction. A strain-based approach, though being consistent with the sectional equilibrium assumptions, tends to provide underestimated results as well. The strain-based approach tends to be even less conservative than the Euler-based one at low level of load, while providing larger results at increasing load and strains; considering how both the proposed approaches are finally under-estimative, the larger value among the two, at each step, will be assumed as expected deflection.

The load levels here reported should be considered as indicative and subject to variation, as a function of the actual slabs' behavior.

Load Phases - Unreinforced (NO FRP)

		US					SI				
		Load [Kip]	δ [in]	Steel Strain[%]	Moment [Kip in]	x [in]	Load [KN]	δ [mm]	Steel Strain[%]	Moment [KN m]	x [mm]
Cracking	(EC2)	2.544	0.018	0.011	51.509	3.028	11.317	0.447	0.011	5.820	76.907
	(ACI)	3.017	0.021	0.013	60.201	3.028	13.421	0.539	0.013	6.802	76.907
Yielding		3.651	0.295	0.238	71.851	0.697	16.241	7.482	0.238	8.118	17.712
Concrete Collapse		3.785	0.377	9.230	74.312	0.159	16.837	9.568	9.230	8.396	4.048
Steel Rupture		3.785	9.359	10.000	74.317	0.157	16.838	237.712	10.000	8.397	3.979

Load Phases - Reinforced (FRP)

		US					SI				
		Load [Kip]	δ [in]	FRP Strain[%]	Moment [Kip in]	x [in]	Load [KN]	δ [mm]	FRP Strain[%]	Moment [KN m]	x [mm]
Cracking	(EC2)	2.606	0.177	0.110	52.651	3.044	11.593	0.449	0.110	5.949	77.330
	(ACI)	3.090	0.213	0.133	61.535	3.044	13.744	0.542	0.133	6.953	77.330
Yielding		5.976	0.460	0.292	114.560	0.849	26.581	11.684	0.292	12.944	21.570
Intermediate Debonding		9.018	1.020	0.658	170.474	0.710	40.116	25.897	0.658	19.261	18.032
Anchor's Failure	config.1	9.561	1.171	0.724	180.436	0.700	42.528	29.739	0.724	20.386	17.790
	config.2	15.452	1.258	1.447	288.699	0.683	68.736	31.945	1.447	32.619	17.352
Sheet Rupture		18.259	1.568	1.800	340.262	0.710	81.218	39.816	1.800	38.444	18.045
Concrete Collapse		22.066	2.010	2.289	410.230	0.773	98.156	51.042	2.289	46.350	19.622
Steel Rupture		92.013	18.800	13.985	1,695.491	2.660	409.292	477.509	13.985	191.565	67.564

APPENDIX G

Virtual Reality

The author used a 360° camera to record all the process, from the specimen's preparation to the test.

Having any kind of VR goggles, you can virtually "enter" to the Structures and Materials Laboratory at the University of Miami to see how the specimens were prepared and tested, simply following these steps:

1) From your smartphone, open YouTube on this link (https://www.youtube.com/channel/UCUUv1s5Zz7Vv0iwAh90-YXw) and play one of the two 360 video regarding either experimental program 1 (CFRP Staple anchors on concrete blocks) or experimental program 2 (CFRP Staple anchors on R/C slabs).
2) Once the video started click on the goggles icon located at the bottom right

3) Put your smartphone inside the goggles.

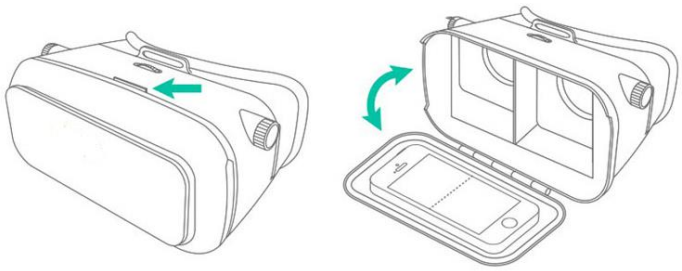

4) Enjoy.

REFERENCES

AASHTO-2012 “Guide Specification for Design of Bonded FRP Systems for Repair and Strengthening of Concrete Bridge Elements”. American Association of State Highway and Transportation Officials (AASHTO) 2012.Washington, DC.

AC125. (2012). Acceptance criteria for concrete and reinforced and unreinforced masonry strengthening using externally bonded fiber reinforced polymer (FRP) composite systems. International Code Council Evaluation Service.

ACI 440.2R-08. (2008). Guide for the Design and Construction of Externally Bonded FRP Systems for Strengthening Concrete Structures. American Concrete Institute (ACI).

ACI 440.3R-12. (2012). Guide Test Methods for Fiber-Reinforced Polymer (FRP) Composites for Reinforcing or Strengthening Concrete and Masonry Structures. American Concrete Institute (ACI).

ASTM C143/143M-12. (2012). Standard Test Method for Slump of Hydraulic-Cement Concrete. American Society for Testing and Materials (ASTM) .

ASTM C31/C31M-12. (2012). Standard Practice for Making and Curing Concrete Test Specimens in the Field. American Society for Testing and Materials (ASTM).

ASTM C39/C39M-14. (2014). Standard Test Method for Compressive Strength of Cylindrical Concrete Specimens. American Society for Testing and Materials (ASTM).

ASTM D3039/D3039M-08. (2008). Standard Tests Method for Tensile Properties of Polymer Matrix Composite Materials. American Society for Testing and Materials (ASTM).

ASTM E488/E488M – 10 “Standard Test Methods for Strength of Anchor in Concrete Elements”. American Society for Testing and Materials (ASTM) 2010

Brena S.F. and McGuirk G.N. “Advanced on the behavior characterization of FRPanchored carbon fiber-reinforced polymer sheets used to strengthen concrete elements”, International Journal of Concrete Structures and Materials, March 2013, Vol.7, No.1.

Cadenazzi, T. (2016). Study of an experimental anchor system ("staple" anchors) for externally bonded FRP laminates used for the consolidation and retrofitting if reinforce concrete structures, through an innovative double shear test method, Master's Thesis, in Preparation. Milano, Italy: Politecnico di Milano.

Campilhoa, De Mouraa, Dominguesb (2008). Using a cohesive damage model to predict the tensile behaviour of CFRP single-strap repairs. International Journal of Solids and Structures

Berneschi, A. (2015). Enhancing the use of externally bonded FRP laminates with FRP anchor spikes, Master's Thesis. Milano, Italy: Politecnico di Milano.

CNR DT-200 R1/2013. (2014). Guide for the Design and Construction of Externally Bonded FRP Systems for Strengthening Existing Structures. Roma, Italy: National Research Council, Advisory Committee on Technical Recommendations for Construction (CNR).

CNR-Advisory Committee on Technical Recommendations for Construction. "Guide for the Design and Construction of Externally Bonded FRP Systems for Strengthening Existing Structures". Materials, RC and PC structures, masonry structures. CNR-DT 200 R1/2013. Roma – 2013.

Grelle, S. & Sneed, L. (2013). Review of Anchorage Systems for Externally Bonded FRP Laminates. International Journal of Concrete Structures and Materials.

Meier, U., Deuring, M., Meier, H., & Schwegler. (1992). Strengthening of structures with CFRP Laminates: Research and applications in Switzerland. Advanced composite materials in bridges and structures.

Nanni, A. (1995). Concrete repair with externally bonded FRP reinforcement. Concrete International, 22-26.

Nanni, A. (1997). Carbon FRP Strengthening: New Technology Becomes Mainstream. Concrete International: Design and Construction, Vol. 19, No. 6, pp. 19-23.

Nanni, A. (1999). Composites: Coming on Strong. Concrete Construction, vol. 44, 120.

Nanni, A. (2000). Carbon Fibers in Civil Structures: Rehabilitation and New Construction. The Global Outlook for Carbon Fiber, Intertech. San Antonio, Texas.

Nanni, A. (2004). Fiber Reinforced Polymer Composites for Infrastructure Strengthening - From Research to Practice.

Niemitz, C. W., Ryan, J., & Brena, S. F. (2010). Experimental Behavior of Carbon Fiber-Reinforced Polymer (CFRP) Sheets Attached to Concrete Surfaces Using CFRP Anchors. ASCE Journal of Composites for Construction.

Obaidat, Y. T. (2011). Structural Retrofitting of Concrete Beams Using FRP - Debonding Issues. Lund, Sweden: Lund University.

Hu, F.Z. & Soutis, C. (2000). Strength prediction of patch-repaired CFRP laminates loaded in compression. Researchgate.net publication.

Haifeng Fan, Anastasios P. Vassilopoulos and Thomas Keller (2016). Pull-out behavior of CFRP single-strap ground anchors. ECCM17 - 17th European Conference on Composite Materials Munich, Germany

Hollaway, L.C (1999). Strengthening of Reinforced Concrete Structures - Using Externally-Bonded FRP Composites in Structural and Civil Engineering

Rossini, M. (2016). FRP Anchors for External Reinforcement of Concrete Structural Elements, Master's Thesis. Milano, Italy: Politecnico di Milano.

Seracino, R. (2004) FRP Composites in Civil Engineering - CICE 2004: Proceedings of the 2nd International Conference on FRP Composites in Civil Engineering - CICE 2004, Adelaide, Australia

Serbescu A., Guadagnini M., Pilakoutas K. “Standardised double-shear test for determining bond of the FRP to concrete and corresponding model development” Elsevier Ltd, 2013.

Tatar, J. & Hamilton, R. (2016). Bond Durability Factor for Externally Bonded CFRP Systems in Concrete Structures. ASCE Journal of Composites for Construction.

Teng J. G. Smith S. T. Yao J. and Chean J. F. “Intermediate Crack Induced Debonding in RC Beams and Slabs”,Construction and Building Materials, 2001, V. 17, No. 6-7 pp 447-462.

ONLINE REFERENCES

https://www.structuraltechnologies.com/sites/default/files/structuraltech/datasheet/TD-VWrap-C200H.pdf

http://www.fortressstabilization.com/specs.php

https://www.structuraltechnologies.com/

http://www.forconstructionpros.com/product/12261989/fortec-stabilization-systems-fortec-stabilization-systems-introduces-the-carbon-staple-anchor

http://www.fortecstabilization.com/datasheets/countersunk_specs.pdf

https://en.wikipedia.org/wiki/Composite_material

https://en.wikipedia.org/wiki/Carbon_fibers